A TRIBOLOGICAL STUDY OF THE DESIGN AND PERFORMANCE OF AUTOMOTIVE CAMS

by

Andrew D. Ball B.Sc.

Thesis Submitted to the University of Leeds

for the Degree of Doctor of Philosophy

Institute of Tribology
Department of Mechanical Engineering
The University of Leeds

November, 1988

PAGE NUMBERS ARE CLOSE TO THE EDGE OF THE PAGE.

SOME ARE CUT OFF

ABSTRACT

A Tribological Study of the Design and Performance of Automotive Cams

Andrew D. Ball B.Sc.

Thesis Submitted for the Degree of Doctor of Philosophy

November, 1988

Analytical methods to enable the evaluation of important lubrication operational parameters at the contact between any cam and follower mechanism (excluding valve trains incorporating rolling element followers or hydraulic lash adjusters) have been collated, critically assessed and developed. A robust and user friendly computer program, which incorporated these methods, was written in order that the tribological conditions existing at the cam/follower interface of any type of valve train in common use in today's internal combustion engines could be studied. The output from the program included graphical displays of frictional torque, minimum lubricant film thickness and Hertzian stress around the cam cycle. Such studies were performed on a cam and flat faced follower system, a cam and centrally pivoted follower system, a cam and end pivoted follower system and a desmodromic system (comprising a conventional cam and centrally pivoted system and a desmodromic cam and end pivoted follower system).

The computer program also allowed parametric studies to be carried out on valve train mechanisms. Parametric studies of three different valve trains, including the valve trains from the Rover 2300 and the Ford 2.0 litre Pinto engines, have been presented, the results being presented in graphical and tabular form.

The loadings, orbits, and power losses associated with the camshaft bearings of the Ford 2.0 litre Pinto engine were evaluated using existing dynamically loaded bearing analysis techniques. The total frictional power loss predicted for the three camshaft bearings was found to be equal to approximately one fifth of that calculated for all of the cam/follower interfaces throughout the operational speed range of the engine.

An experimental single valve desmodromic valve train apparatus was designed and commissioned to test the accuracy of the valve train lubrication analysis computer program. The apparatus allowed studies to be made of the running-in of valve trains operating at lubricant temperatures of 40C, 60C and 80C, by applying the electriacl resistivity technique. Analytical models used to predict which cam/follower pair was in control of the valve at any point around the cam cycle were tested using an electrical continuity technique and were found to show good agreement with practice. Good agreement was also found between the theoretically predicted and measured torque and power required to drive the valve train.

Acknowledgements

Thanks are due to a great number of people who have helped towards the completion of this thesis.

I am greatly indebted to Professor Duncan Dowson and Dr Chris Taylor whose guidance, enthusiasm and example have been inspirational - it has been a source of great pleasure to work under the supervision of two such distinguished scholars.

The friendship and assistance of my fellow students and members of staff have also been greatly valued. Special thanks are due to Dr Richard Chittenden for his advice and unselfish provision of time and effort during the coding of the computer programs. The excellent work (and constant encouragement) of Mr Ron Harding during the designing and commissioning of the experimental apparatus is also gratefully acknowledged as is the vast amount of work carried out by the laboratory technicians Mr Luciano Bellon, Mr Balbir Randowa, Mr Alan Bartlet and Mr Alan Heald. I am also very grateful for the help of Dr Rosemary Creasey in the printing of this thesis.

Thanks are due to Mr Nigel Weaver of the Ford Motor Co. Ltd. for his practical advice and help in procuring parts for the experimental apparatus. The financial and technical support of the Ford Motor Co. Ltd. is also gratefully acknowledged as is the funding of the project by the Science and Engineering Research Council.

Finally, I wish to thank my parents for their love and support throughout my education, and my wife, Helen for being by my side at times of crisis. I hope that the completion of this work will in some way help to repay them for the many sacrifices they have made.

CONTENTS

NOMENCLATURE

A	distance between the centre of rotation of the follower and the centre of curvature of the follower face in contact with the cam
2b	width of Hertzian contact
b	bearing length (chapter (6))
B	distance between the centre of rotation of the follower and the centre of curvature of the follower face in contact with the valve
c	radial clearance
C_d	diametral clearance
C_p, C_q, C_r, C_s	four power lift polynomial coefficients
D	distance between centre of rotation of follower and centre of rotation of cam
D	diameter of bearing (Chapter (6))
e	journal eccentricity
E_1, E_2	elastic modulus of solids in contact
E'	equivalent elastic modulus, $\dfrac{2E_1E_2}{(1-\nu_1'^2)E_2 + (1-\nu_2'^2)E_1}$
F	frictional force
F_X, F_Y	bearing loads (Chapter (6))

G	dimensionless materials parameter, $\alpha E'$
H	power loss
h	lubricant film thickness
h_{cen}	central lubricant film thickness
h_{min}	minimum lubricant film thickness
l_c	cam lift
l_{cmax}	maximum cam lift
l_v	valve lift
L	cam lobe width
M	reciprocating mass
M	mobility (Chapter (6))
M_f	equivalent reciprocating mass of follower
M_1	equivalent reciprocating mass on camshaft side of rocker arm for a pushrod valve train
M_2	equivalent reciprocating mass on valve side of rocker arm for a pushrod valve train
p	pressure
p_{max}	maximum Hertzian pressure
P_c	film load (Chapter (6))
r	radius of bearing

r_B	base circle radius of cam
r_c	radius of curvature of cam at point of contact
r_f	radius of curvature of follower face in contact with the cam
R	equivalent radius of curvature
RR	rocker ratio
s	displacement of the point of contact along the follower face referred to the position of maximum lift as zero
t	time
U	dimensionless speed parameter, $\frac{\eta_o V_c}{E' R}$
V_c	velocity of the point of contact relative to the cam
V_e	mean entrainment velocity, $\frac{1}{2}(V_c + V_f)$
V_f	velocity of the point of contact relative to the follower
V_s	sliding velocity, $(V_c - V_f)$
W'	dimensionless load parameter, $\frac{W}{E' R L}$
W	load
x,y	coordinate system
x_1, y_1	co-ordinates of the point of contact between the cam and follower

Z	$l_v + r_B + r_f$
α	pressure-viscosity coefficient
γ	variable angle between lines joining the centre of rotation of the follower to the centre of rotation of the camshaft and to the centre of curvature of the follower face in contact with the valve
η	dynamic viscosity
η_0	reference viscosity (at inlet)
ν_1', ν_2'	Poisson's ratio of solids in contact
λ	fixed angle between lines joining the centre of rotation of the follower to the centres of curvature of the follower faces in contact with the cam and the valve respectively
μ	coefficient of friction
ν	variable angle between the common normal at the point of contact between cam and follower and the line joining the centre of rotation of the follower with the centre of curvature of the follower face in contact with the cam
ϕ	cam anglular rotation (measured from maximum lift position)
ϕ	angular coordinate measured from the point of maximum film thickness on the lines of centres in the direction of rotation (Chapter (6))
ϕ'	the variable angle between the x-axis and the

line joining the centres of rotation of the cam and the follower, $\phi + \phi_0'$

κ fixed angle between the direction of valve motion and the line joining the centres of rotation of the cam and of the follower

ψ variable angle between the x-axis and the common tangent at the point of contact between cam and follower

ψ attitude angle (Chapter (6))

θ angular coordinate measured from the line of centres (Chapter (6))

τ shear stress

ω camshaft angular speed (rad/s), $\frac{d\phi}{dt}$

ω rotational speed of journal centre about bearing centre (rad/s) (Chapter (6))

$\bar{\omega}$ $\frac{\Omega_B + \Omega_S}{2}$

Ω_B angular velocity of bearing (rad/s)

Ω_S angular velocity of journal (rad/s)

Subscripts

B base circle

c cam

f follower

o	top of lift
v	valve

Other variables may be defined in the text where necessary.

CHAPTER 1

INTRODUCTION

1.1 The Need to Consider Tribology in the Design of Valve Trains

1.2 A Summary of the Aims and Contributions of This Work

1.1 The Need to Consider Tribology in the Design of Valve Trains.

In the 1970's the western world became increasingly aware of the fact that the earth's reserves of fossil fuels were not limitless. Political pressures from environmental groups and, much more significantly, the pressures brought about by the Middle Eastern countries upon the economies of their consumers during the 'Oil Crisis', caused many governments to campaign for the merits of saving energy. In Britain the motorist was subjected to spiralling petrol prices and even the threat of rationing. The motor manufacturers were put under increasing pressure from the consumer to design vehicles that not only cost less than their competitors for a similar specification, but also returned better fuel consumption figures.

Coincidently, around this time the use of an overhead camshaft (OHC) using pivoting followers to drive two banks of valves had just become very popular within the motor industry. The design was favoured as it allowed the cylinder head to be assembled separately from the block (good from a production point of view), it operated better at high speeds than other single camshaft designs driving two banks of valves (as it was more rigid) and it utilised fewer components and was therefore cheaper. Unfortunately the design was found to be inherently poor from a tribological view-point - many manufacturers suffering from early failures of their (OHC) valve train sytems due to excessive wear of the cams and followers.

The problem was therefore defined; the designer was required to design valve trains that had very small frictional losses and that would not wear out within the life of the rest of the vehicle. Regrettably the tools that the designer needed to fulfil the task were not available and similar types of design kept emerging. As the cost of warranty claims and lost sales rose into the millions, calls were made from within the industry for theoretical studies to fill these gaps within the knowledge.

Much work has been carried out upon ways in which the efficiency of the internal combustion engine could be increased. Many workers investigated the sources of losses within the internal combustion engine and ways in which they could be reduced (for example Parker and Adams (1982), Hoshi (1984) and Martin (1985)). Although the

majority of the losses were found to be due to thermal inefficiencies, there are still large benefits to be gained from reducing the mechanical losses which account for approximately 15% of the total fuel energy input. Figure (1.1) shows the breakdown of the total engine friction losses according to Hoshi (1985). It can be seen that the valve train frictional losses account for between 7.5% - 21% of the total engine frictional loss, and so there is still a large scope for improvement.

Whilst there have been major developments in the tribological understanding of the behaviour of many of the engine components, such as the dynamically loaded bearings (main bearings, little-end bearings and big end bearings) and the piston assemblies (piston pads and rings) the amount of work upon the valve train has been relatively small. This may be due to the complexity of the problem as the cam and follower operate in the most arduous tribological conditions within the internal combustion engine. They are subjected to dynamically changing loads, high contact stresses, high sliding speeds and poor lubrication. If a plentiful supply of lubricant can be offered to the region of the cam/follower contact, it is often very hot (temperatures exceeding 120 C are not uncommon) and entrainment into the contact is usually poor due to unfavourable surface velocities of the components.

There is still the need for theoretical studies of the cam and follower contact to be undertaken, for the tribology of such contacts is still far from being fully understood. There is also an increasing need for existing knowledge to be put into a form that can be used by designers within industry.

1.2 A Summary of the Aims and Contributions of This Work.

The aims and contributions of the present study were:

(i) To build upon existing models to study the kinematics of cams acting against flat faced followers and cams acting against pivoted followers and to extend them to cover any type of sliding contact valve train in commmon use today.

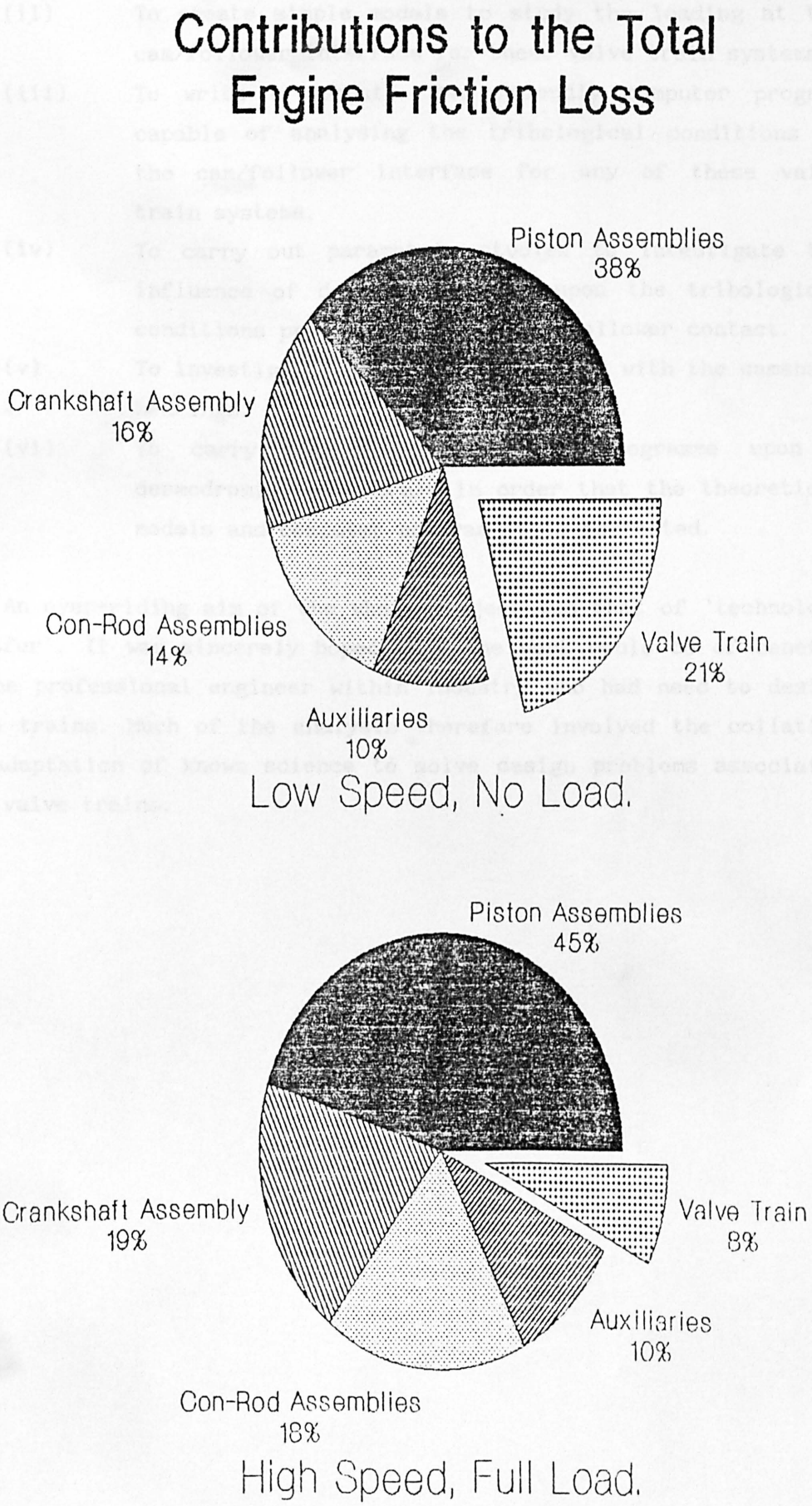

Figure (1.1) Contributions to the Total Engine Friction Loss. Hoshi (1985).

(ii) To create simple models to study the loading at the cam/follower interface for these valve train systems.

(iii) To write a robust, user friendly computer program capable of analysing the tribological conditions at the cam/follower interface for any of these valve train systems.

(iv) To carry out parametric studies to investigate the influence of design variables upon the tribological conditions prevailing at the cam/follower contact.

(v) To investigate the losses associated with the camshaft bearings.

(vi) To carry out an experimental programme upon a desmodromic valve train in order that the theoretical models and computer program could be tested.

An over-riding aim of the whole project was that of 'technology transfer'. It was sincerely hoped that the work would be of benefit to the professional engineer within industry who had need to design valve trains. Much of the analysis therefore involved the collation and adaptation of known science to solve design problems associated with valve trains.

CHAPTER 2

THE DESIGN OF VALVE TRAIN SYSTEMS

2.1 Introduction.

Valve train design philosophy has been changing rapidly over the past decade. This has been due mainly to research carried out after many manufacturers experienced serious valve train wear problems with new engines in service. The cost of research therefore paled into insignificance compared with the cost of warranty claims and the loss of sales.

This chapter addresses many of the problems that the designer faces when creating a new valve train. It starts, however, with a description of many of the terms commonly used to describe valve train systems and a brief history of developments in valve train design.

2.2 Valve Train Nomenclature.

There follows a description of many of the commonly used terms in valve train design.

2.2.1 Cam Follower.

The cam follower is the part of the valve train mechanism that is in contact with the cam and follows its profile. The follower may take many forms. Some of the most commonly used followers are shown in Figure (2.1). It can be seen that the follower bears either directly upon the valve or via a pivoting mechanism. A comparison of the merits of these different designs is given in section (2.4).

2.2.2 Cam Profile.

The cam profile obviously determines the motion of the valve. Figure (2.2) shows a typical cam profile and the various portions of the lift cycle. The cam nose is the portion of the cam across which the valve acceleration is approximately constant, and corresponds to the area around the maximum lift position. The cam flanks are responsible for the rapid acceleration and deceleration of the valve.

a) centre-pivoted follower (OHC)

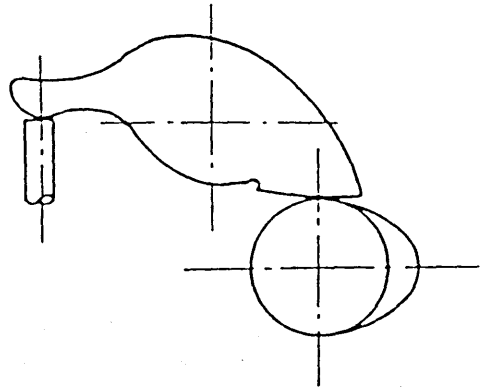

b) finger follower (OHC)

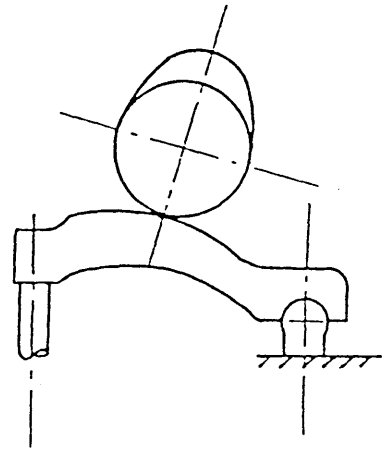

c) pushrod operated

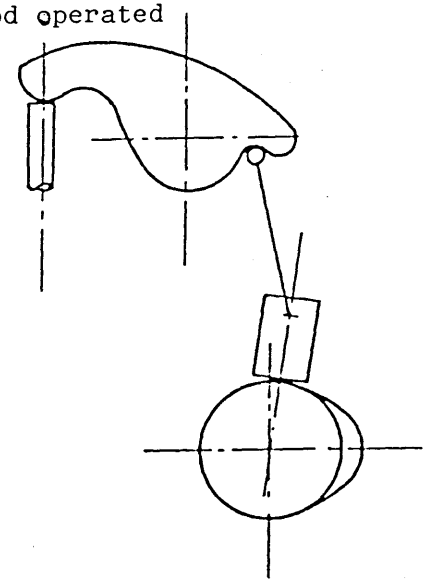

d) direct acting (OHC)

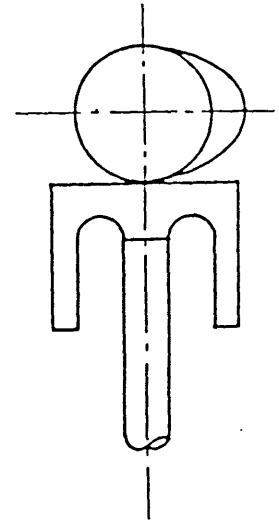

Figure (2.1) Valve Train Systems In Common Use.

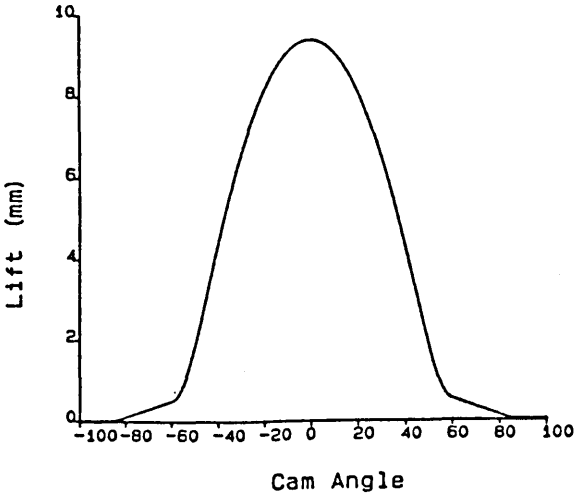

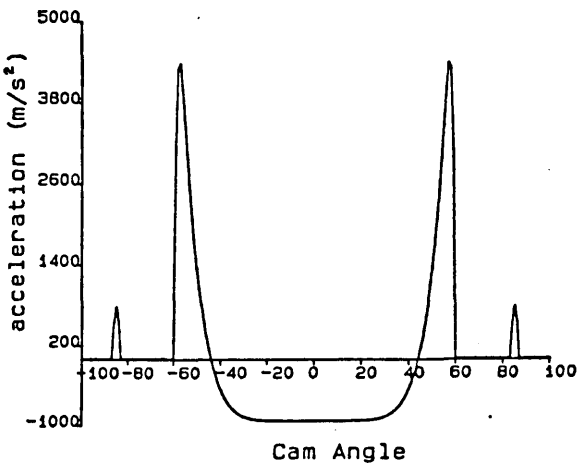

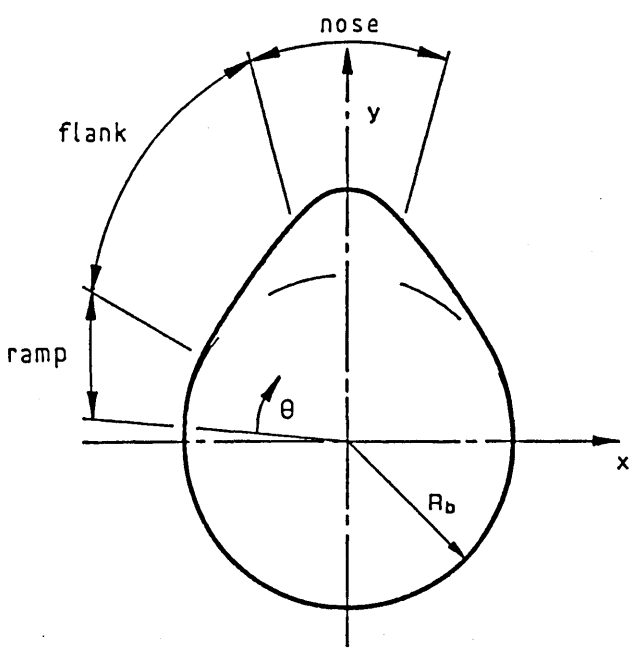

Figure (2.2) Typical Cam Profile and Lift Characteristics.

The cam base circle radius is the portion of the cam across which there is no valve lift, i.e. the valve is closed. The cam ramps serve the purpose of taking up the clearance between the cam and follower at each end of the lift cycle. These ramps are usually of a constant velocity type, where for a constant camshaft rotational speed the velocity of the valve is constant. The cam ramps are usually fairly long in order to seat and lift the valve gently.

2.2.3 Lift Curve Definition.

It is important that the motion of the valve is always controlled by the cam. For this reason dynamic effects are kept to a minimum by careful consideration of the cam profile and the lift it will provide to the valve. Great care is taken that the valve lift and its first, second and third derivatives with respect to cam angle (valve velocity, acceleration and jerk respectively) are smooth. This ensures that the valve motion is largely unaffected by dynamic effects.

Modern cam profiles are usually defined by polynomials which ensure smooth profiles. The most common form is the four power polynomial. An example of such a polynomial is given below:

$$l_c = Y_R + l_{cmax} + C_p\left[\frac{\phi}{\phi_T}\right]^p + C_q\left[\frac{\phi}{\phi_T}\right]^q + C_r\left[\frac{\phi}{\phi_T}\right]^r + C_s\left[\frac{\phi}{\phi_T}\right]^s$$

where

Y_R = the height of the ramp,
l_{cmax} = the maximum lift,
ϕ_T = the cam half period.

C_p, C_q, C_r, and C_s can be derived from the values of p, q, r, and s, which are selected by exponent manipulation to give the desired cam characteristics.

A relatively new method of defining a cam profile is by the use of a multipol. A multipol defines the lift characteristics of a cam by a series of polynomials, each defining a different portion of the cam. The lift, velocity, acceleration and jerk at the intersection of two adjoining polynomials are the same. The advantage of using a multipol to define the lift of a cam is that the area under the lift curve can be maximised to give optimum engine breathing.

2.2.4 Cam Duration.

The duration of a cam is equal to the angle through which the crankshaft turns between the valve opening and closing. (This is equal to twice the angle through which the camshaft turns).

2.2.5 Cam Timing.

The timing of a cam is quoted in crankshaft degrees. Two angles are quoted; the angle at which the valve opens and the angle at which the valve closes. It is usual that the overall timing of the engine is quoted i.e. the timing of the inlet valve and the exhaust valve. A typical production engine timing is 20°-50°/50°-20°. This means that the inlet valve opens 20° before crank top dead centre and closes 50° after crank bottom dead centre and the exhaust valve opens 20° before bottom dead centre and closes 50° after top dead centre (Bell (1981)).

2.2.6 Overlap.

The overlap is the angle in degrees of crankshaft rotation during which both the inlet and exhaust valves of a cylinder are open.

2.2.7 Spring Cover.

The spring cover is the amount by which the spring force at a given valve lift exceeds the inertia force of the reciprocating mass.

2.2.8 Symmetry.

If a pivoted cam follower is used then a symmetrical cam form will not give a symmetrical valve lift. It is desirable that the valve lift be as near symmetrical as possible as this allows the optimum spring choice to be made (the spring cover is optimal on both

the rising and falling flanks of the cam). It is also desirable that the cam profile be as near symmetrical as possible for ease of manufacture. In designing a cam profile it is usual to adopt a symmetrical valve lift curve and allow the cam profile to become slightly asymmetric.

2.2.9 Cam Concavity.

In order that high valve accelerations and decelerations are attained when overhead cams are used with pivoted followers it is often necessary that the profile of the cam flanks needs to be concave. The maximum allowable cam concavity (and hence valve acceleration) is limited by the minimum size of grinding wheel used to machine the cam profile. To a large extent the performance of pivoted follower systems is limited by the available grinding technology.

2.3 History of Valve Train Design.

Although throughout this century various different types of engine valving have been tried, the poppet valve has been almost universally adopted by the major automobile manufacturers. Other types of valving such as sleeve or rotary valves have been deemed to have lubrication difficulties, allow excessive engine oil consumption, provide poor sealing and have excessive frictional losses (Buuck (1982)).

Over the years there has been a demand for ever increasing engine speeds in the search for more energy efficient engines. This has caused the rise in popularity of overhead camshaft mechanisms (OHC) at the expense of push-rod systems. The push-rod system had been favoured in the past due to its many virtues; ease of adjustment, the availability of the camshaft to drive accessories such as the oil pump and distributor, and good lubrication and wear characteristics. As the camshaft is located close to the sump it receives a plentiful supply of oil in the form of oil mist and splash from the crankshaft. Also the tappets are free to rotate, thus improving lubricant entrainment and decreasing wear by ensuring that

any two points on the cam and tappet surfaces do not continually meet cycle after cycle.

The main disadvantage of push-rod systems is their flexibility brought about by the use of long thin push-rods. This makes them unsuitable for use in very high speed engines. OHC mechanisms are inherently much stiffer. Modern production techniques have also added to the decline in popularity of the push-rod system. OHC mechanisms utilise fewer parts and allow the cylinder head assembly to be built up as a separate unit. Production engineers see these as great advantages (Polak and Letts (1987)). OHC mechanisms appear in two basic forms; either direct acting or via a pivoted follower. One of the major manufacturing and assembly problems with these systems is in the alignment of the camshaft and followers. If the cam lobes and followers are not properly aligned then severe edge loading can occur resulting in damage to the contacting parts. Mercedes patented a novel solution to this problem in 1959. Their design utilised end pivoted followers which pivoted upon spherical ended posts rather than the more conventional rocker shaft. This allowed the followers to self align.

Whilst direct acting OHC mechanisms have proved to be very successful both from a performance and wear point of view, the same cannot be said of pivoted OHC mechanisms. Many manufacturers have experienced major wear problems with these types of valve trains. This has been attributed to many causes. One suggested cause is the higher temperatures seen in the cylinder heads of modern engines due to the adoption of thermostatically controlled electric fans and the use of more selective coolant channels through the whole of the engine. These higher temperatures not only increase the bulk temperature of the contacting parts, thus increasing the probability of scuffing (Dyson and Naylor (1960)), but also serve to lower the viscosity of the lubricant. As the followers do not run in bores they have limited means of conducting away heat generated in the contact region - this again leads to high bulk temperatures in the followers. As the camshaft is at the very top of the engine in an OHC arrangement it is also at the end of the lubricant feed path. In many early OHC designs the cam and follower contact had to rely upon oil splashed from the camshaft bearings to provide adequate amounts of lubricant. Other reasons suggested for the untimely demise of such

systems have been fuel dilution of the lubricant and oil starvation at engine start up.

Most manufacturers have solved the problem of excessive wear in pivoted OHC systems by the adoption of high specification materials and the use of spray bars and even holes in the cam lobes to supply sufficient lubricant to the contact region. The additional lubricant supply not only serves to lubricate the contact but also acts as a coolant. One manufacturer has reverted to the use of manual chokes which perhaps suggests that they blamed fuel dilution for their problems. It is the belief of the author that if attention were to be directed towards the geometry and kinematics of such systems significant gains in lubricant entrainment could be achieved. This point is illustrated in Chapter (5) by the use of parametric studies.

In the quest for higher engine speeds and better valve control, some manufacturers have shown an interest in desmodromic valve trains. In a desmodromic system the valve is opened in the conventional manner by a cam and a follower but closed by using a second cam and follower rather than a spring. Ducati motor cycles utilised desmodromic valve gear in their successful race engines and later in their production machines. By using desmodromic valve gear they were able to increase the power band of the engine by over 600 rpm by eliminating the effects of valve bounce.

Probably the most famous use of desmodromic valve trains was by Mercedes in their 300 SLR sports and Grand Prix racing cars. In 1954 Mercedes Grand Prix cars were producing in excess of 100 b.h.p. per litre - a figure few manufacturers were achieving even five years later. Mercedes did not see any benefits in using the desmodromic valve train to increase the engine speed as the maximum engine speed was dictated by maximum piston acceleration. Mercedes used desmodromics to control the valve in such a way as to fill the combustion chamber in a much more efficient manner than was possible with a sprung valve train system. Mercedes engineers calculated that they were able to utilise valve accelerations 128% higher than considered feasible when using valve springs. This produced a smooth engine power curve with excellent torque characteristics (Mundy (1961)).

It is generally felt that desmodromic valve trains will never see use in mass produced engines due to the complexity of the mechanism plus their noisy operation due to the large clearances needed between the cams and followers. It appears then that the engines of the future, if they are internal combustion engines, will utilise OHC mechanisms due to their ease of assembly and manufacture.

OHC mechanisms do, however, have several drawbacks apart from their frequently poor wear characteristics. The camshaft is often used to drive auxiliaries such as the fuel and oil pump and the distributor. This means that these components must be mounted very high on the engine if they are to be driven from the camshaft. It is therefore often necessary when using an OHC valve train to drive the oil pump from the crankshaft so as to keep the distance from the pump to the sump as small as possible. This unfortunately aggravates overall engine length and may also lead to lubricant aeration problems. The majority of the flexing of the valve train system takes place in the camshaft in an OHC system, which can cause serious ignition timing problems if the distributor is driven from the camshaft.

It can be seen that the choice of a valve train is very complex and that many other engine components and characteristics must be taken into account when making a choice. It is apparent that the valve train designer cannot be isolated from the overall design of the engine. This is becoming more and more apparent as engine specifications improve and engine speeds increase.

2.4 Valve Train Design Philosophy.

Several design parameters have usually been decided upon before the valve train of an engine is designed: the engine's displacement, bore and stroke, the overall engine height, the maximum allowable manufacturing and assembly cost, the desired engine performance, etc. These parameters set restraints upon the final choice and design of valve train.

The performance of the engine is closely related to how efficiently the charge of air and fuel can be drawn into the

combustion chamber and how efficiently the exhaust gases can be expelled after combustion. In order to admit and expel the various gases effectively, great care is taken over the design of the combustion chamber and the valve lift curve, and the choice of the number of valves per cylinder and their angle of entry into the combustion chamber. The choice of valve train can often be virtually dictated by these conditions.

If, for example, the performance requirement for an engine dictates that the valve must be opened and closed very rapidly this implies that very high accelerations are required along the cam flanks. It is certain that push-rod systems would be eliminated from the choice of available mechanisms at this point due to their flexibility. OHC pivoted followers may also be eliminated from the choice as the maximum allowable flank acceleration is limited by the allowable concavity of the cam flanks. This may leave a direct acting OHC mechanism as the only choice. The designer must then decide whether the large diameter followers required for this type of system can be fitted into the space available, and whether the luxury of two camshafts can be afforded if the valves are not in line.

The different types of valve train mechanisms obviously have differing advantages and disadvantages and the designer must weight the requirements of his design in order of preference in order to get the right compromise. Figures (2.3), (2.4), and (2.5) summarise many of the good and bad points of the various valve train mechanisms.

Once the type of mechanism has been decided upon the geometry of the system must be calculated. If a direct acting OHC system is used then the geometry can be readily decided. The diameter of the follower is dictated by the maximum eccentricity of the cam during the operating cycle. The maximum eccentricity is given directly by the maximum valve velocity (see Dyson and Naylor (1960)). The designer can then calculate whether there is enough space between the valves to accommodate the followers. Once the followers have been sized, an approximate value for the equivalent reciprocating mass of the valve train components can be calculated. This, along with the maximum required engine speed and valve acceleration, gives the minimum allowable spring stiffness to prevent valve bounce at the maximum rated engine speed. The spring stiffness is then chosen by

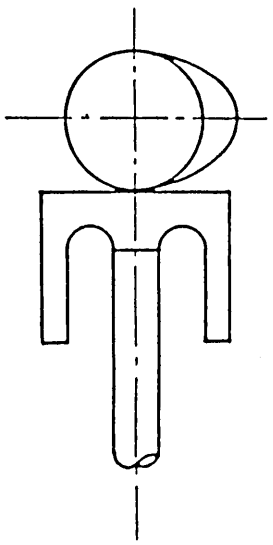

- Good engine breathing as valve train is very rigid and therefore high valve accelerations and operating speeds are possible.
- Symmetrical cam profiles give symmetrical lift curves.
- Good lubrication conditions - low wear.
- If the valves are not in line then two camshafts are required unless a direct acting cam and follower are used in conjunction with a cam and pivoted follower.
- The cam lobes for a direct acting system are much larger than any other OHC system. This necessitates the use of large camshaft bearings.

Figure (2.3) Advantages and Disadvantages of Direct Acting OHC Valve Train Systems.

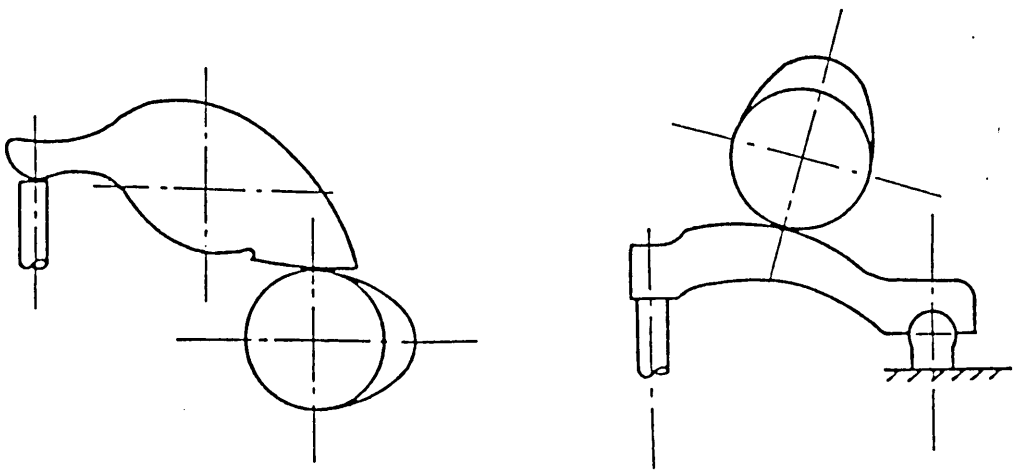

- Not as stiff as direct acting OHC mechanisms. This along with cam profile limitations due to cam concavity necessitates the use of modest valve accelerations. These restraints obviously limit the engine breathing. Maximum operating speed is less than that for direct acting OHC.

- Poor wear characteristics.

- Allows the use of only one camshaft even when there are two banks of valves.

- The cam lobes are smaller than those of a direct acting system as a mechanical advantage can be used by having rocker ratios greater than unity. This allows smaller camshaft bearings to be used.

- Adjustment is usually very easy.

Figure (2.4) Advantages and Disadvantages of Pivoted Follower OHC Valve Train Systems.

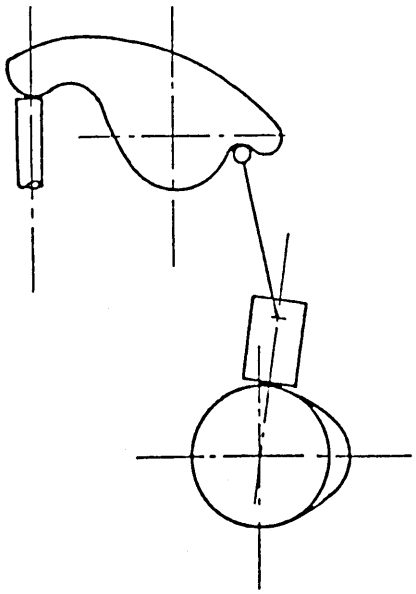

- Very flexible. This allows only very low valve accelerations to be used thus limiting engine breathing. The low rigidity also limits the maximum allowable operating speeds.

- Low wear. The cam and followers receive a plentiful supply of lubricant mist and splash from the main engine bearings due to their close proximity to the sump.

- A mechanical advantage may be used by employing a rocker ratio of greater than unity. This leads to small cam lobes.

- Easy adjustment.

- Engine auxiliaries driven by the camshaft suffer less detrimental effects than with any other system.

Figure (2.5) Advantages and Disadvantages of Push-rod Valve Train Systems.

allowing a given amount of spring cover across the nose region of the cam. The actual valve spring dimensions and number of coils are decided by available standard wire diameters, space limitations, an acceptable number of working coils, satisfactory fatigue life, and dynamic considerations. Valve spring design is discussed in greater detail by Beard and Hempson (1962).

The cam size is chosen by satisfying the requirements of maximum allowable Hertzian stress, engine height, sliding speed at the contact, cam bearing diameter, and also, hopefully, by studying the lubrication conditions around the cam cycle for the range of operating speeds. It will be shown in Chapter (5) how parametric studies can be used to help the designer to arrive at a satisfactory solution to his design problems by considering the prevailing tribological conditions at the cam/follower contact.

If a pivoted follower system is chosen the decision processes are similar but with additional variables, such as rocker ratios and symmetry to be considered. Again parametric studies may be used to great advantage.

Having chosen a particular valve train the designer must then choose the correct materials for the contacting parts. This must be done with a knowledge of the stressing of the components and the sliding speeds and lubrication conditions expected at the contact. The choice of materials for cam and follower pairs is a complex subject worthy of study in its own right, and indeed many learned papers have been written on the subject. The materials aspects of cam and follower design are considered to be beyond the scope of the present study.

2.5 Conclusions.

It is apparent that the demand for automotive engines which produce more power with greater economy is presenting engineers with immense challenges. The problems faced are not insurmountable, but will require the use of sophisticated analytical models and computer aided design techniques. In the following chapters, analyses will be presented which allow the tribological behaviour of valve train

designs to be studied. The models and parametric studies presented in these chapters provide a basis for a general design philosophy which includes tribological considerations - considerations, which in the past, have been overlooked, with costly consequences!

CHAPTER 3

THE KINEMATICS AND LOADING OF THE CAM AND FOLLOWER INTERFACE

3.1 Introduction.

Over the past decade modern production techniques and the ever increasing engine speeds of passenger cars have led to an almost universal adoption of overhead camshaft (OHC) systems rather than conventional push-rod/rocker arm arrangements. It has been found in service that certain of these designs, namely the pivoted OHC mechanisms, are more prone to wear than others (Polak and Letts (1987)).

In the past lubrication difficulties in cam and follower systems have often been seen purely as boundary lubrication problems and cam profiles were designed by a process of limiting the Hertzian stress at the cam nose. Difficulties of valve train wear with an engine in service would often be diagnosed entirely as a materials specification problem, or as a rheology problem to be resolved by using a superior material or a suitable antiwear additive. In an excellent paper Beard and Hempson (1962) summed up the design philosophy of that period,

"... it has been found that cams wear in a number of different ways, the most frequent being pitting, scuffing, and 'polish' wear.

Each of these forms of wear is affected not only by the load and the radii of curvature but also by the hardness, surface finish, and metallurgy, including the method of hardening of the cam and tappet; and by the temperature, viscosity, and type of oil, including additives, used. In spite of its shortcomings, the figure for Hertzian stress is the only practical means by which the designer can assess the likely behavior of a new design while it is still on the drawing board."

It was not until Muller (1966) showed that hydrodynamic lubrication was important that another means of assessing the likely behaviour of a new design became available. Muller reported that of two different cam designs, the one giving the higher Hertzian stresses but the higher values of hydrodynamic entrainment velocity (the algebraic sum of the cam and follower surface velocities relative to their common point of contact) gave the lower wear. In more recent years Dyson ((1977) and (1980)), Harrison (1985) and

Dowson et al (1985) have given consideration to the choice of design parameters and their effects upon elastohydrodynamic film thickness and Hertzian stress around the cam cycle, and have drawn conclusions in agreement with Muller. It has therefore become apparent that a compromise between maximum Hertzian stress and the lubricant film thickness around the cam cycle is required if a successful design is to be achieved.

This chapter will show that by considering the kinematics and geometry of a valve train it is possible to predict the lubricant entrainment velocity and Hertzian stress at any point around the cam throughout its range of operating conditions.

3.2 Kinematic Analysis of Cam/Follower Pairs.

The kinematic velocities of the various components in a valve train can be found by adaptation of the analysis presented in ESDU item number ME2 (1981). This document whilst being very rigorous in its treatment of the relative motions between cams and followers can be very cumbersome to use. It is far better to break automotive cam/follower systems into two basic categories and examine each separately. The two categories are:

(i) Cams acting against translating followers, comprising domed followers/tappets (from push-rod systems) and flat faced followers.

(ii) Cams acting against pivoted followers, comprising centrally pivoted followers and end pivoted followers.

3.2.1 The Kinematics of a Cam Acting Against a Translating Follower.

It is not intended to present the analysis of these systems here. A very thorough treatment of the analysis of the kinematics of cams acting against domed and flat faced follower systems can be found in Dyson and Naylor (1960). The authors show that by expanding the results for a cam and domed follower of radius (r_f) as a series in terms of ($1/r_f$) the equivalent results for a cam acting against a flat faced follower may be obtained by letting (r_f) tend to infinity.

The important surface velocities and equivalent radii of curvature of domed and flat faced follower systems are given below. It should be noted that the results shown below are for a cam acting against a non-rotating follower.

3.2.1.1 Surface Velocities and Equivalent Radius of Curvature For a Cam and Domed Follower System.

The velocity of the point of contact relative to the cam, (V_c), is given by:

$$V_c = \omega \left[Z^2 + \left(\frac{dZ}{d\phi}\right)^2 - \frac{r_f \left\{ Z^2 + 2\left(\frac{dZ}{d\phi}\right)^2 - Z\frac{d^2Z}{d\phi^2} \right\}}{Z^2 + \left(\frac{dZ}{d\phi}\right)^2} \right] \qquad (3.1)$$

the velocity of the point of contact relative to the follower, (V_f), is given by:

$$V_f = \omega \left[r_f \frac{\left\{ Z\frac{d^2Z}{d\phi^2} - \left(\frac{dZ}{d\phi}\right)^2 \right\}}{Z^2 + \left(\frac{dZ}{d\phi}\right)^2} \right] \qquad (3.2)$$

and the equivalent radius of curvature at the contact, (R), is given by:

$$R = \frac{r_f^2 \left[Z^2 + 2\left(\frac{dZ}{d\phi}\right)^2 - Z\frac{d^2Z}{d^2\phi} \right]}{\left[Z^2 + \left(\frac{dZ}{d\phi}\right)^2 \right]^{\frac{3}{2}}} \qquad (3.3)$$

where

$$Z = l_v + r_B + r_f$$

3.2.1.2 Surface Velocities and Equivalent Radius of Curvature of a Cam and Flat Faced Follower System.

The velocity of the point of contact relative to the cam, (V_c), is given by:

$$V_c = \omega \left[\frac{d^2 l_v}{d\phi^2} + l_v + r_B \right] \qquad (3.4)$$

the velocity of the point of contact relative to the follower, (V_f), is given by:

$$V_f = \omega \frac{d^2 l_v}{d\phi^2} \qquad (3.5)$$

and the equivalent radius of curvature at the contact is given by:

$$R = \frac{d^2 l_v}{d\phi^2} + l_v + r_B \qquad (3.6)$$

3.2.2 The Kinematics of a Cam Acting Against a Pivoted Follower.

Two different methods of obtaining the kinematic velocities of a cam/pivoted follower pair have been proposed by Dyson (1980) and Bell et al (1985). The method proposed by Dyson is an extension of the analysis used to describe the kinematics of a cam acting against a translating follower (Dyson (1977)). The method proposed by Bell et al differs from that of Dyson and claims to offer certain advantages over the latter's method.

Dyson's analysis requires that both the first and second derivatives of lift with respect to cam angle be known. This is acceptable if the lift curve is defined by a polynomial and exact values for these derivatives can be found. It is also acceptable if a series of lift against cam angle figures are available and are known to be exact as numerical differentiation can be used with little loss of accuracy. If however the lift figures are found by measurement, say, then serious errors can occur in the second order numerical differential required to obtain the valve acceleration.

The method proposed by Bell et al claims to require only the first order differential of lift with respect to cam angle and a further first order differential, the slope of the cam surface, which is obtained numerically. Closer examination of the method reveals that a cubic (or other) spline fit to the lift data is required, which necessitates a numerical differentiation. This spline function is then differentiated again to find the slope of the cam surface, hence a second order numerical differentiation is used. The method requires that numerical differentiation be used regardless of whether the lift data is given as a polynomial or data points. It can be seen that the results presented by Bell et al suffer from numerical errors introduced by the numerical differentiation and splining of data points.

It is for the above reasons that the analysis adopted in this work follows that proposed by Dyson. The analysis of a cam acting against a pivoted follower system is presented in Appendix (A).

3.2.3 The Kinematics of a Desmodromic Cam and Follower System.

A desmodromic valve train uses a cam/follower pair to close the valve rather than a spring. The valve is opened utilising a cam and follower in the same way as a conventional system incorporating a return spring. This type of valve train system has advantages over conventional valve train systems in that cam/follower contact stresses are reduced and the motion of the valve is more controlled at higher speeds. Figure (3.1) shows an example of a typical desmodromically operated valve train.

In analysing the kinematics of a desmodromic valve train the opening cam/follower pair are treated just as a conventional cam/follower pair. The closing cam/follower pair can be treated similarly but with two minor changes; as the lift of the closing cam is negative, the valve lift and its first derivative with respect to cam angle must be negated in the analysis.

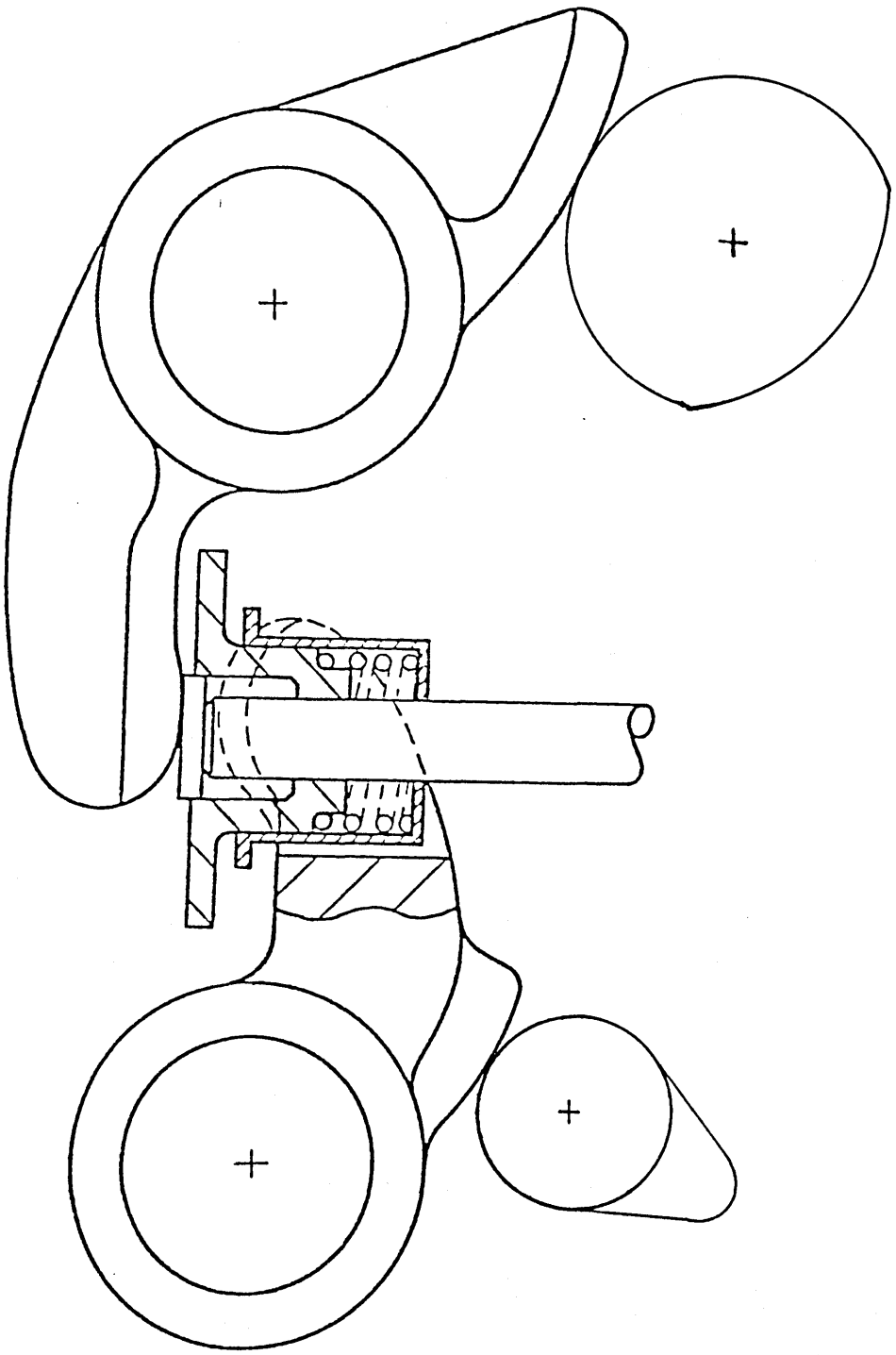

Figure (3.1) Typical Desmodromically Operated Valve Train.

3.3 The Contact Loading and Hertzian Stress at the Cam/Follower Interface.

The maximum Hertzian stress at the cam/follower interface is an important design parameter. If modes of failure such as pitting are to be avoided then the maximum Hertzian stress at the contact must be limited. To evaluate the Hertzian stress the load and equivalent radius of curvature at the contact must be known. It has been shown in the previous sections how the equivalent radius of curvature at the contact can be evaluated. The proceeding sections will show how the contact loading and consequently the maximum Hertzian stress at the contact can be calculated.

It is assumed throughout this analysis that the valve train is rigid. This assumption is obviously more valid for certain types of valve trains than others; push-rod systems, for example, are much more flexible than direct acting flat faced follower valve trains. Modern OHC valve trains are designed to be as rigid as possible and utilise cam profiles evolved especially to maintain smooth valve acceleration. It is therefore assumed in the analysis that the dynamic effects of loading and valve train stiffness and damping are negligible. The effects of the elastic deflections and damping characteristics associated with the camshaft and follower are discussed in great detail by Chen (1982) and in many other learned papers (see, for example, Barken (1953), Beard and Hempson (1962), Sakai and Tsuda (1970), Kenesa et al (1977) and Akiba et al (1981)).

3.3.1 The Loading at the Cam/Follower Interface.

Again this is best treated in two parts; the loading of a cam acting against a translating follower and a cam acting against a pivoted follower. The analyses of these two categories of valve trains are given in Appendices (B) and (C) respectively. The loading at the cam/follower interface for the two categories, accepting the assumptions given in the text, are given in Table (3.1). The special case of the loading of an example desmodromic valve train is investigated in Appendix (D).

	Load (W)
Translating Domed Follower System	$r_f \left\{ \dfrac{M_1\omega^2\dfrac{d^2 l_c}{d\phi'^2} + M_2 RR^2\omega^2\dfrac{d\, l_c^2}{d\phi'^2} + RR.k(l_c RR + \delta)}{\left\{ r_f^2 + \left[\dfrac{d^2 l_c}{d\phi'^2} \right]^2 \right\}^{\frac{1}{2}}} \right\}$
Flat Faced Follower System	$k(l_v + \delta) + M\omega^2\dfrac{d^2 l_v}{d\phi'^2}$
Centrally Pivoted Follower System	$\dfrac{\left[M\dfrac{d^2 l_v}{d\phi'^2}\omega^2 + k(\delta + l_v) \right] B\cos\left[\dfrac{-3.\pi}{2} + \kappa + \gamma \right] + M_f\dfrac{d^2\gamma}{d\phi'^2}\omega^2 B^2}{A\cos\left[\dfrac{3.\pi}{2} - \nu \right] - \mu\left[r_f + A\sin\left[\dfrac{3.\pi}{2} - \nu \right] \right]}$
End Pivoted Follower System	$\dfrac{\left[M\dfrac{d^2 l_v}{d\phi'^2}\omega + k(\delta + l_v) \right] B\cos\left[\dfrac{\pi}{2} - \kappa - \gamma \right] + M\dfrac{d^2 l_v}{d\phi'^2}\omega^2 B^2}{A\sin\nu + \mu\left[r_f - A\cos\nu \right]}$

Table (3.1) Summary of Cam/Follower Interface Load for Various Valve Train Systems.

3.3.2 The Hertzian Stress at the Cam/Follower Interface.

The interaction between a cam and domed follower results in an elliptical contact area between the two components, whilst that between a cam and a flat faced follower or a cam and a pivoted follower results in a line contact area. Great care is taken during the design and manufacture of systems that are in line contact that the cam and follower contact faces are aligned to within very tight tolerances to avoid edge loading situations.

The theory used to determine the contact stresses was established by Hertz (1881). He considered the contact and elastic deformation between two elastic, smooth solids. Once the dimensions of the contact zone and the pressure distribution normal to the applied load are known, the stresses between the two bodies can be found.

3.3.2.1 The Hertzian Stress at an Elliptical Contact.

The contact between a cam and a domed follower can be shown to be geometrically equivalent to an ellipsoid, with principal radii of curvature (R_x) and (R_y), in contact with a plane. Figure (3.2) shows the contact between an ellipsoid and a plane with a Hertzian contact patch.

On the assumption that;

(i) the bodies are elastic in accordance with Hooke's Law,

(ii) the contact area is small with respect to the radius of curvature of the undeformed cylinder, and,

(iii) only normal pressures are considered,

Hertz showed the following results;

(a) The pressure distribution between the bodies, for an elliptical contact, is semi-elliptical on the contact patch,

(b) The maximum Hertzian stress (p_{max}) is given by the expression;

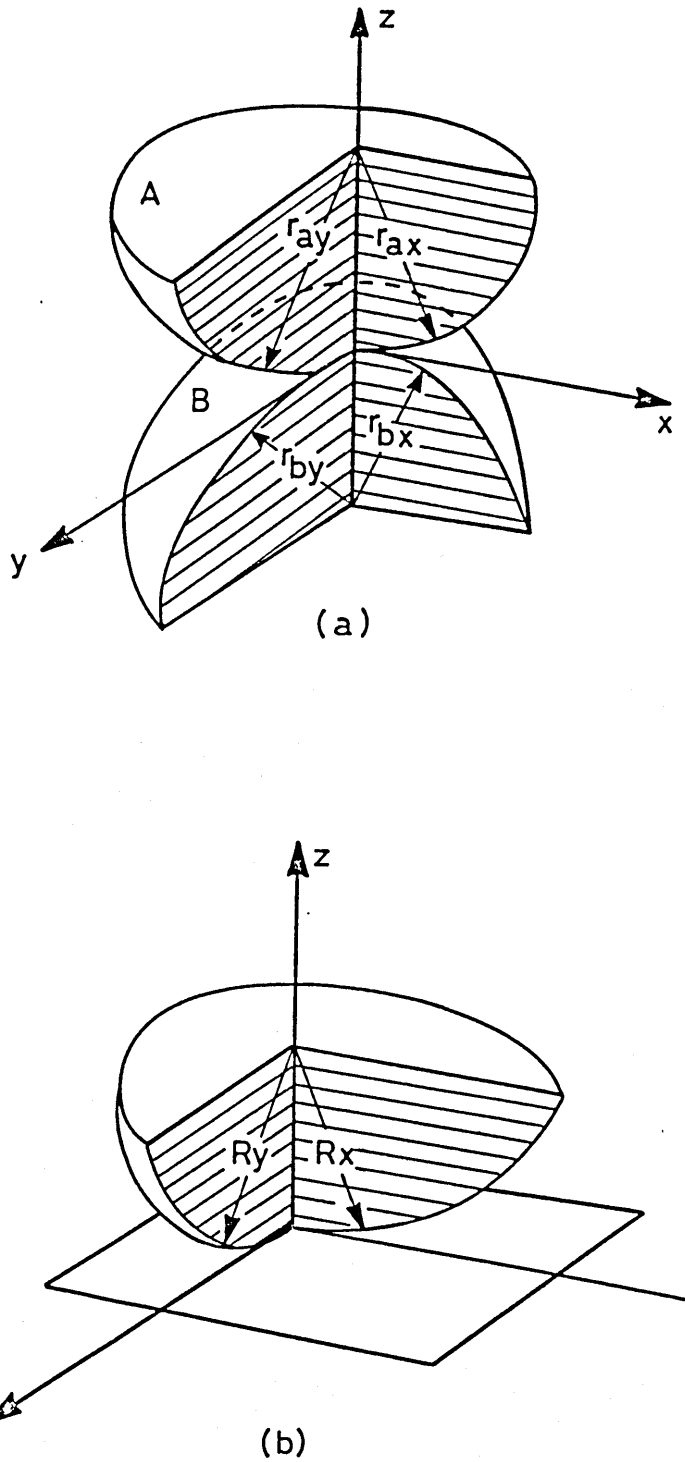

Figure (3.2) Geometry of Point Contacts
(a) Contact Between Two Ellipsoidal Solids
(b) Equivalent Geometry

$$p_{max} = \frac{E'}{2\pi}\left[\frac{3W}{E'R^2}\right]^{\frac{1}{3}} \tag{3.7}$$

where

$$\frac{1}{R} = \frac{1}{R_x} + \frac{1}{R_y}$$

and

$$\frac{1}{R_x} = \frac{1}{r_f}$$

and

$$\frac{1}{R_x} = \frac{1}{r_f} + \frac{1}{r_c}$$

3.3.2.2 The Hertzian Stress at a Line Contact.

It can be shown that the contact between a cam and a flat faced follower or a cam and a pivoted follower is geometrically equivalent to the contact of a cylinder, of length (L) and radius (R), against a plane. Figure (3.3) shows the contact between a cylinder and a plane with a Hertzian contact patch.

Adopting the same assumptions as the previous section Hertz showed that;

(i) The pressure distribution between the bodies, for a line contact, is semi-elliptical.

(ii) The pressure distribution is given by;

$$p = p_{max}\left[1 - \frac{x^2}{b^2}\right]^{\frac{1}{2}} \tag{3.8}$$

where (b) the contact half width is given by;

$$b = \left[\frac{8WR}{\pi LE'}\right]^{\frac{1}{2}} \tag{3.9}$$

where

$$\frac{1}{R} = \frac{1}{r_c} + \frac{1}{r_f}$$

The follower radius of curvature, (r_f), takes the value of infinity for a flat faced follower, hence the term ($1/r_f$) disappears.

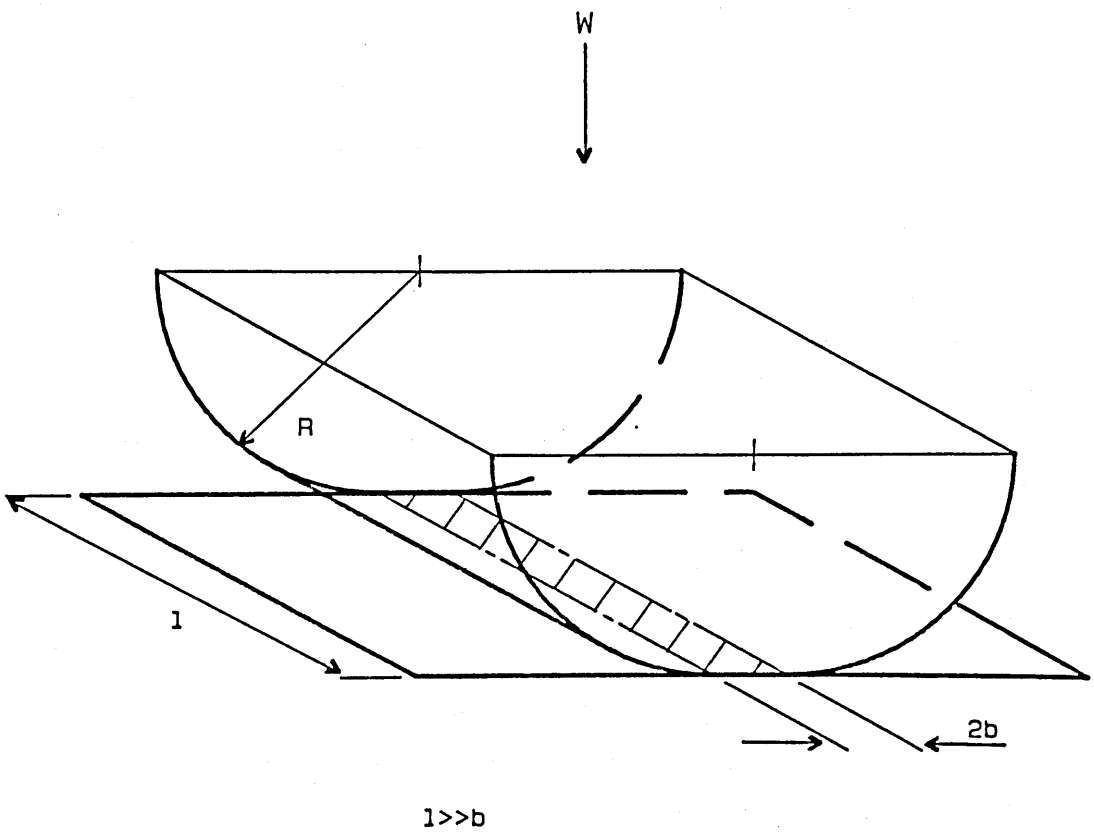

Figure (3.3) The Contact Between a Cylinder and a Plane With a Hertzian Contact Patch.

The maximum Hertzian stress is given by;

$$p_{max} = \frac{2W}{\pi Lb} \qquad (3.10)$$

3.4 Discussion.

Figure (3.4) shows how the velocities (V_c), (V_f), ($V_c + V_f$), and ($V_c - V_f$), equivalent radius of curvature, load, and Hertzian stress vary around the cam cycle for a typical cam acting against a flat faced follower at a camshaft speed of 25Hz (1500rpm). It can be seen that the Hertzian stress is at its largest around the cam nose corresponding to the largest values of load and smallest values of equivalent radius of curvature.

It can also be seen how the velocity of the point of contact with respect to the cam (V_c) is always in the same direction, whereas this is not true for the velocity of the point of contact with respect to the follower (V_f). This is illustrated in Figure (3.5). It can be seen how the point of contact moves to the extreme of its travel in one direction and then back to its base circle position at maximum lift, and then to its extreme of travel in the opposite direction and once again back to its base circle position.

It can be seen (Figure (3.4)) that because (V_c) and (V_f) vary by similar magnitudes throughout the cam cycle the sliding velocity ($V_c - V_f$) remains approximately constant. The sliding velocity is of interest to designers as it influences the amount of heat generated at the contact and hence the bulk temperature of the interacting solids. The entrainment velocity ($V_c + V_f$) is also of interest to designers as it is very important to the lubrication of the contact. It should be noted that the entrainment of lubricant into the contact region falls to zero at two points around the cam cycle; this is typical of many cam and follower pairs and is of obvious concern to designers. These parameters and their sensitivity to changes in design variables will be discussed in much more detail in Chapter (5).

Figure (3.6) shows how the velocities (V_c), (V_f), ($V_c + V_f$) and

CAM AND FLAT FACED FOLLOWER

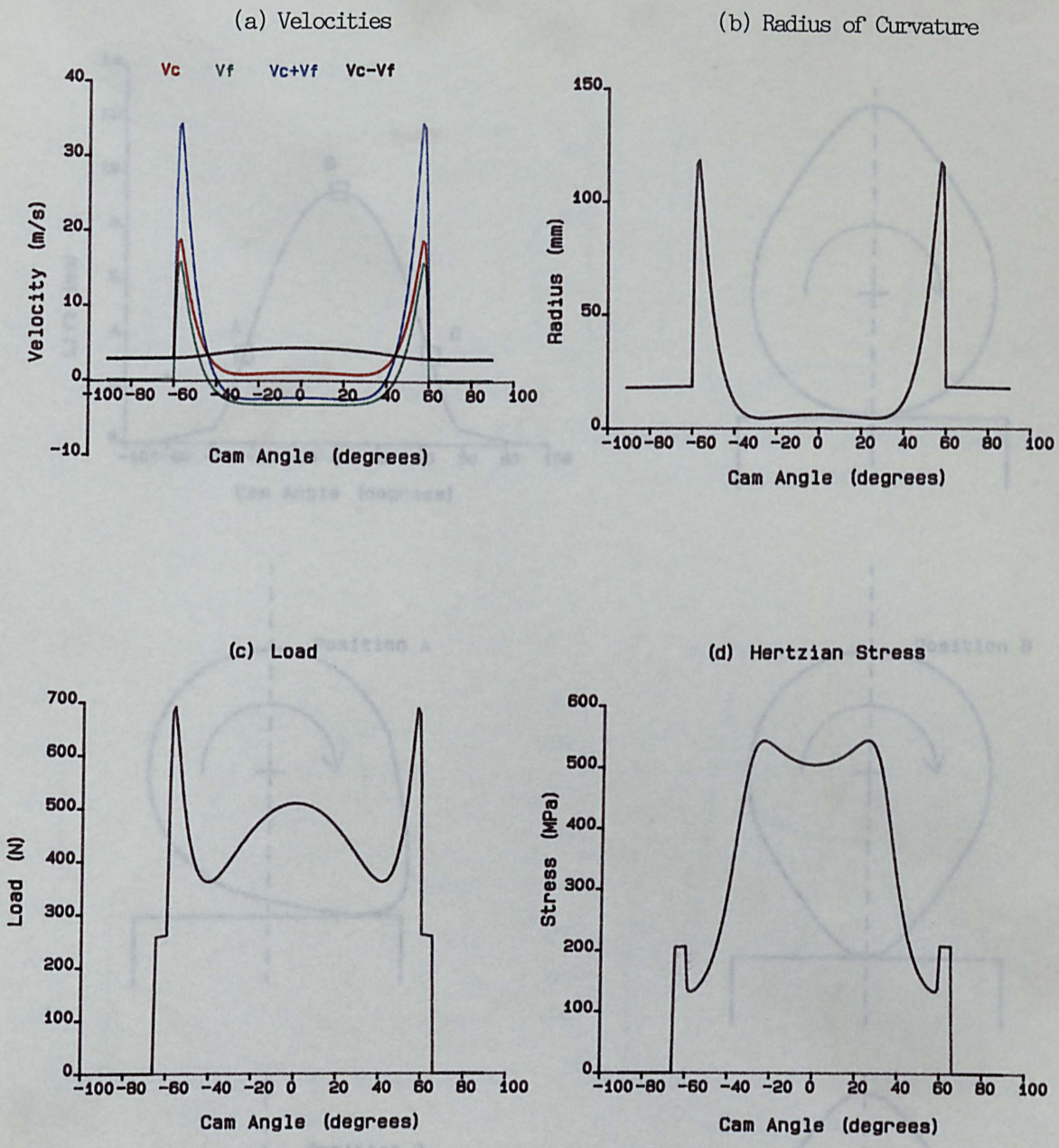

Figure (3.4) The Variation of Important Kinematic Velocities, Radius of Curvature, Load and Hertzian Stress Around the Cam Cycle at a Camshaft Rotational Speed of 25 Hz.

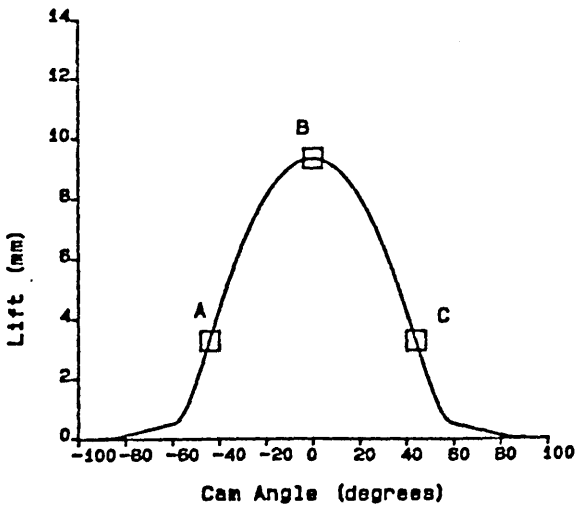

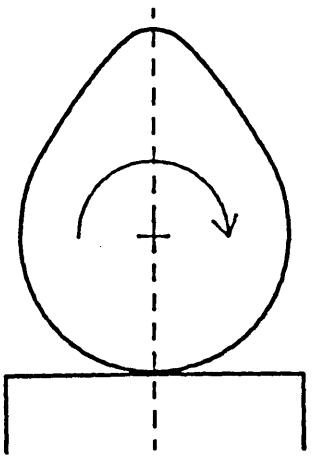

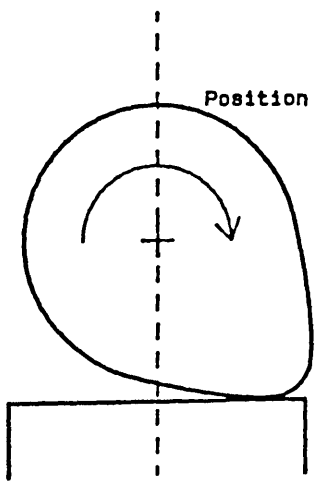

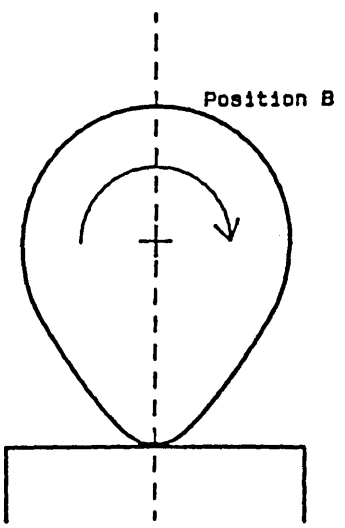

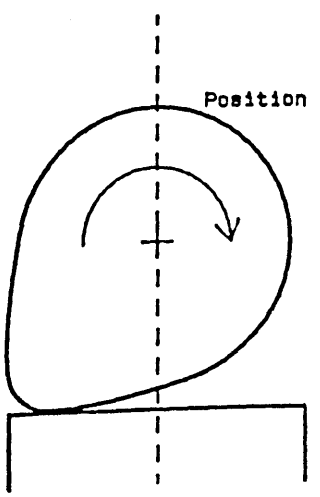

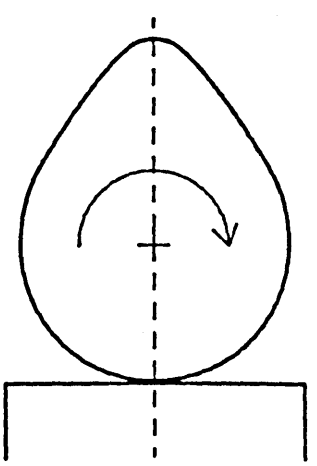

Figure (3.5) Movement of the Point of Contact Around the Cam Cycle.

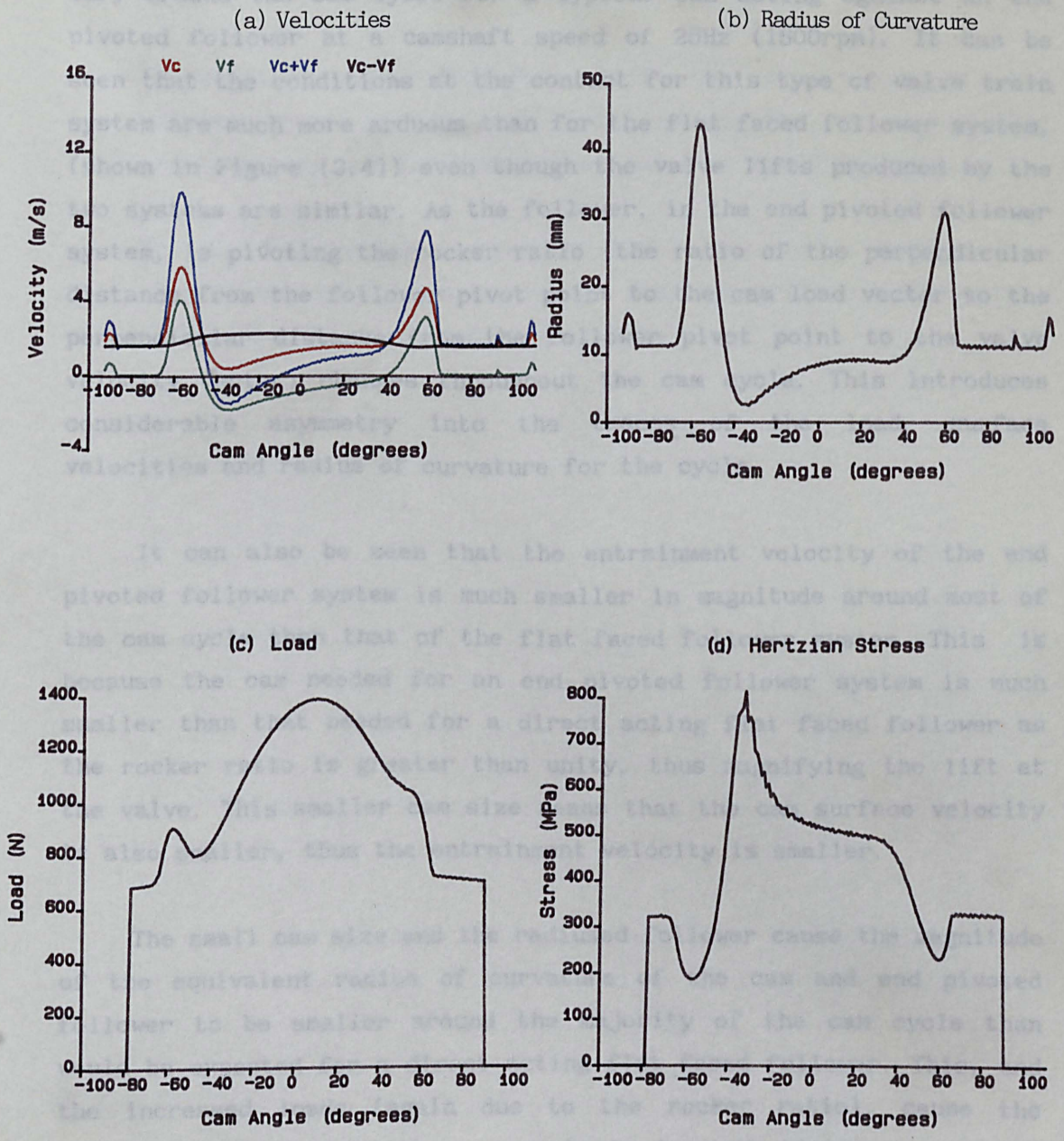

Figure (3.6) The Variation of Important Kinematic Velocities, Radius of Curvature, Load and Hertzian Stress Around the Cam Cycle at a Camshaft Rotational Speed of 25Hz.

($V_c - V_f$), equivalent radius of curvature, load, and Hertzian stress vary around the cam cycle for a typical cam acting against an end pivoted follower at a camshaft speed of 25Hz (1500rpm). It can be seen that the conditions at the contact for this type of valve train system are much more arduous than for the flat faced follower system, (shown in Figure (3.4)) even though the valve lifts produced by the two systems are similar. As the follower, in the end pivoted follower system, is pivoting the rocker ratio (the ratio of the perpendicular distance from the follower pivot point to the cam load vector to the perpendicular distance from the follower pivot point to the valve velocity vector) changes throughout the cam cycle. This introduces considerable asymmetry into the traces of the load, surface velocities and radius of curvature for the cycle.

It can also be seen that the entrainment velocity of the end pivoted follower system is much smaller in magnitude around most of the cam cycle than that of the flat faced follower system. This is because the cam needed for an end pivoted follower system is much smaller than that needed for a direct acting flat faced follower as the rocker ratio is greater than unity, thus magnifying the lift at the valve. This smaller cam size means that the cam surface velocity is also smaller, thus the entrainment velocity is smaller.

The small cam size and the radiused follower cause the magnitude of the equivalent radius of curvature of the cam and end pivoted follower to be smaller around the majority of the cam cycle than would be expected for a direct acting flat faced follower. This, and the increased loads (again due to the rocker ratio), cause the Hertzian stress around the cam cycle to be much higher for an end pivoted follower system than for a direct acting flat faced follower system.

3.5 Conclusions.

It has been shown that the kinematics of a cam and follower system can be evaluated utilising standard differential geometry. It has also been demonstrated how the loading and Hertzian stress at the cam/follower interface can be calculated. All valve train systems in common use in passenger car engines have been considered namely cams

acting against flat faced followers, against domed followers, against centrally pivoted followers, and against end pivoted followers.

Calculations have indicated that the conditions at the cam/follower interface are much more arduous for an end pivoted follower than they are for a direct acting flat faced follower.

The following chapter shows how the relationships developed in this chapter can be introduced into a computer program to produce a powerful aid to the design of valve trains.

CHAPTER 4

A COMPUTER PROGRAM FOR VALVE TRAIN LUBRICATION ANALYSIS

4.1 Introduction.

Many parameters are at the disposal of the designer when creating a valve train system. There is, unfortunately, never a clear cut optimal solution to the design problem and experience of acceptable levels of Hertzian stress and minimum lubricant film thickness still plays a vital role in the design process. The interactions of design parameters upon each other and upon the tribological performance of the valve train are very complex, and are often not fully appreciated by engineers. It was therefore apparent that a design aid was needed which would reveal how the various parameters affect the performance of the camshaft and its followers.

Digital computers are now extremely fast in their operation and solutions to complex problems can be achieved both quickly and (often more importantly in a commercial environment) cheaply. As time passes they will become even faster and cheaper. It was therefore decided that a computer program should be written that would act as a design aid. Such a program would need to be very easy to use, and would have to be capable of presenting the data to the user in an efficient and easily understood manner.

Such a program has been developed and coded, in a structured manner, on an Amdahl 580 series mainframe computer. The program is capable of analysing the kinematics and tribological performance of all types of cam and follower combinations in common use in automobile engines. The program is described in the following text.

4.2 A Description of the Program.

A flow diagram of the computer program is shown in Figures (4.1), (4.2), (4.3) and (4.4). Each of the Figures relates to a particular part of the program:

(i) Figure (4.1) relates to the section of the program that handles the input data, processing it into a form that can be used by subsequent parts of the program.

(ii) Figure (4.2) relates to the kinematic analysis.

(iii) Figure (4.3) relates to the section of the program that calculates the load, the lubrication conditions at the

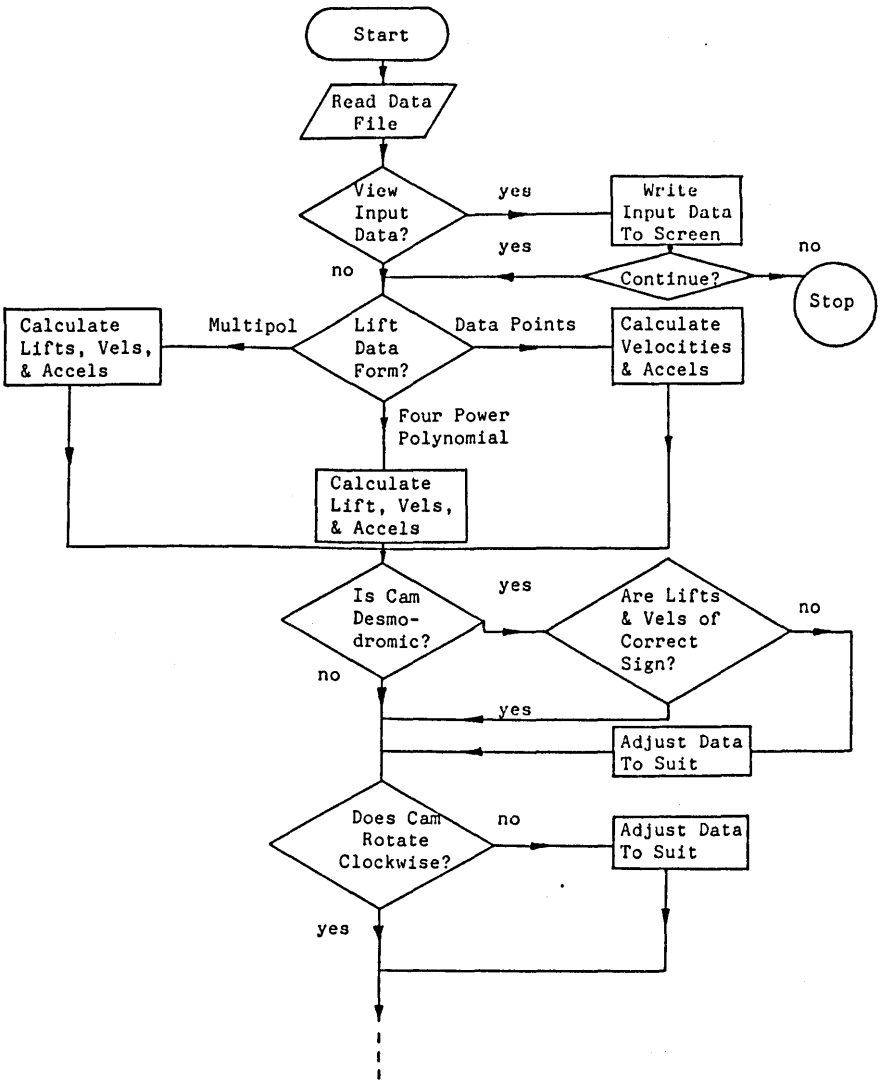

Figure (4.1) Flow Diagram for the Valve Train Lubrication Analysis Computer Program.

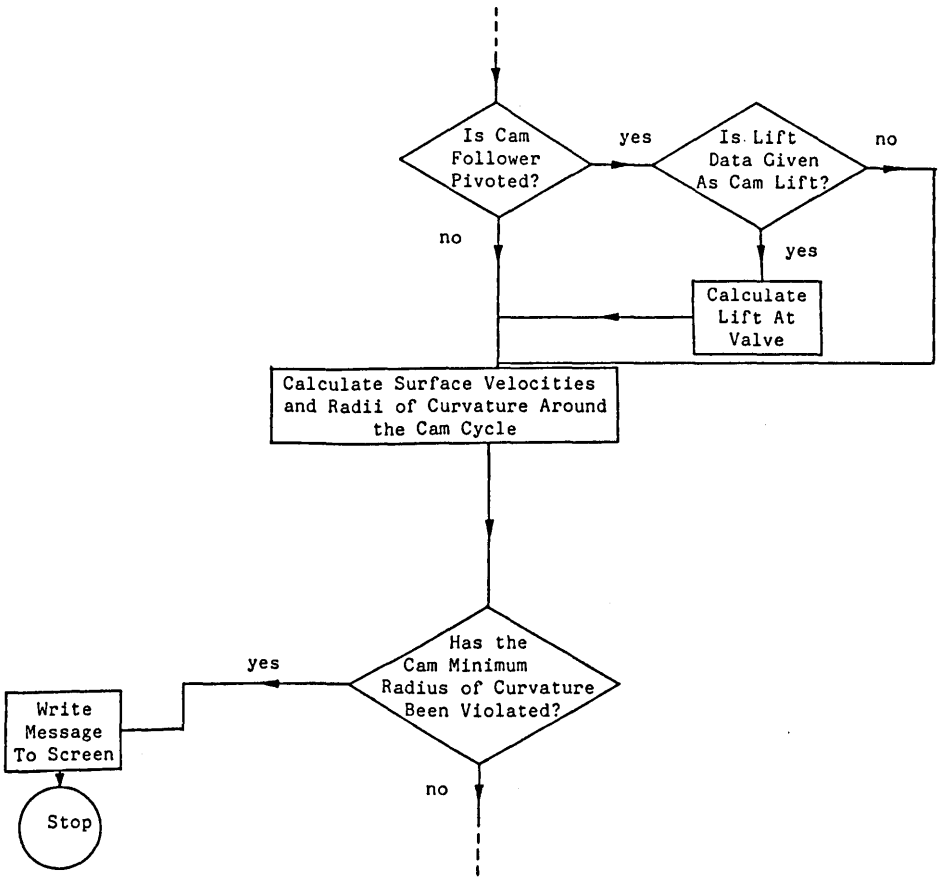

Figure (4.2) Flow Diagram for the Valve Train Lubrication Analysis Computer Program.

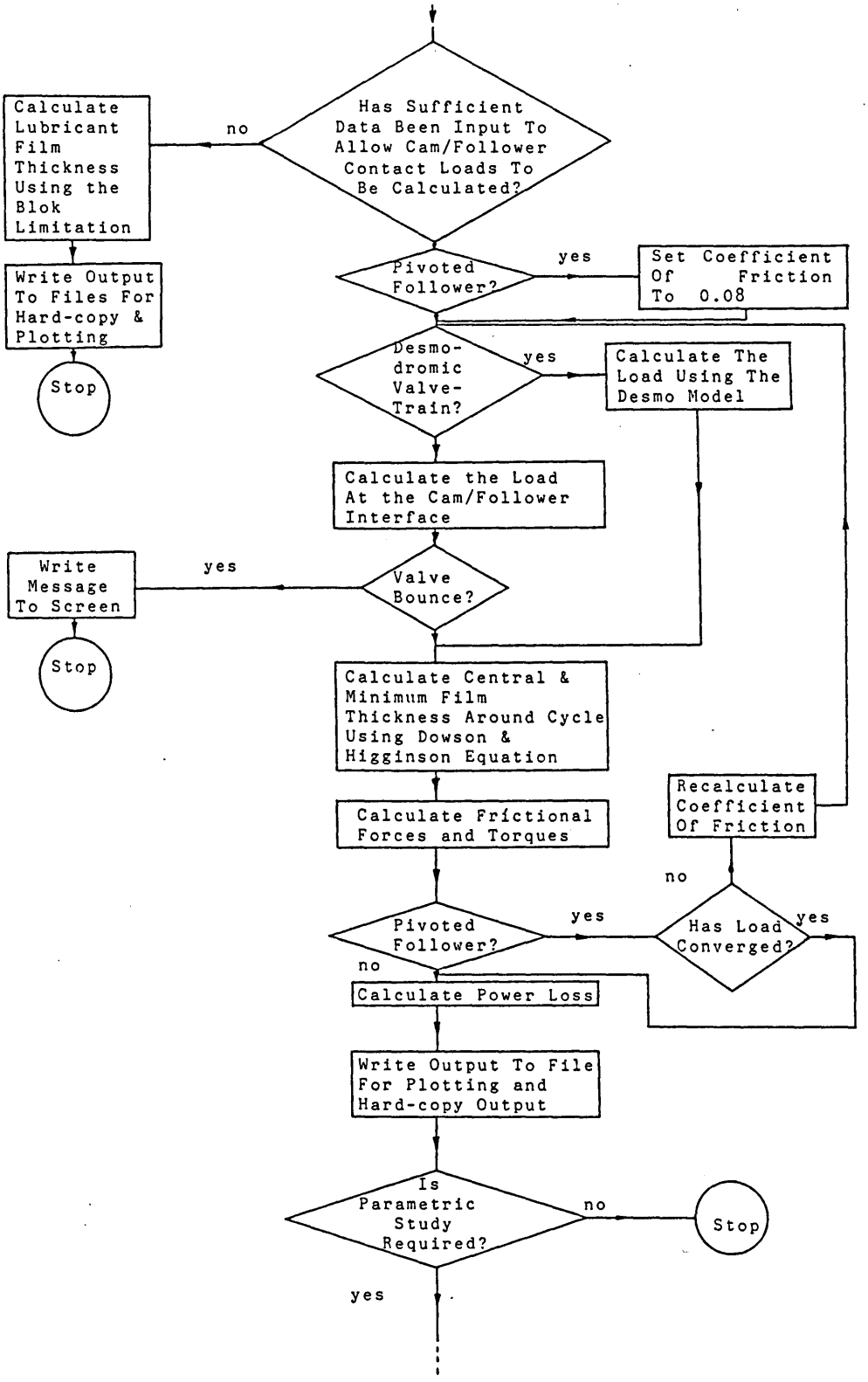

Figure (4.3) Flow Diagram for the Valve Train Lubrication Analysis Computer Program.

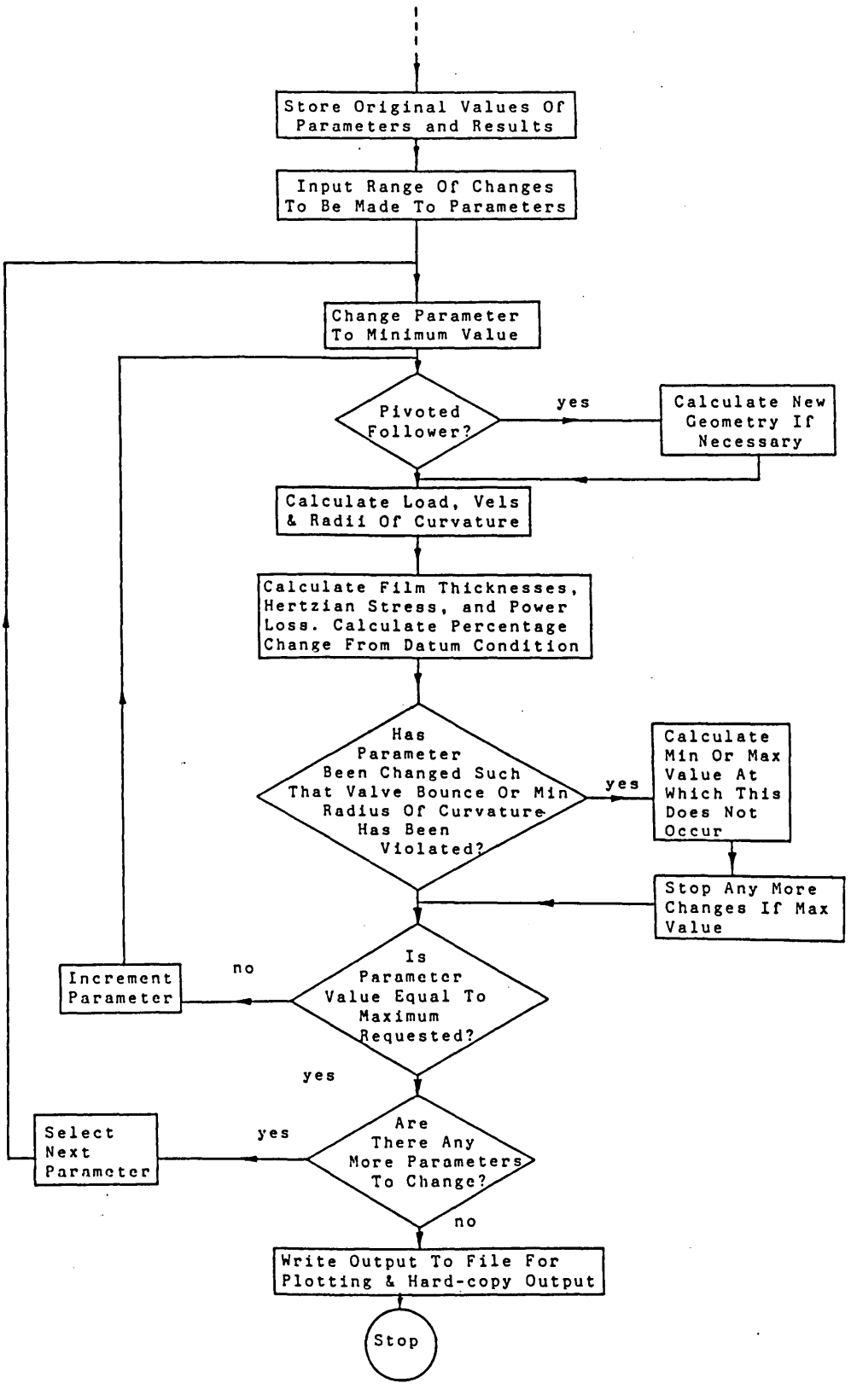

Figure (4.4) Flow Diagram for the Valve Train Lubrication Analysis Computer Program.

cam/follower contact, the frictional torque and the frictional power loss.

(iv) Figure (4.4) shows the flow diagram for the part of the program that carries out a parametric study of a given design of valve train.

Each of these parts of the program will be discussed in the following sections.

4.2.1 Input of Data to the Program and Handling of this Data.

The valve train data is introduced to the program via an input file. This file is created by editing a standard data file, or template, using the computer's screen editing facility. Such a file is shown in Figure (4.5). The input file was designed to be read easily and to be as helpful as possible to the new user. It can be seen that the user is led through the file being asked to respond to prompts for data. Many of the data lines are already complete and hold default responses which may be over-written by the user if so wished. All of the data is introduced to the program in SI units unless the template requests otherwise (for example initial spring compression is asked for in units of mm). The section of the data file requesting data for pivoted follower systems uses the notation of Dyson (1980).

The kinematic analysis subroutines require the valve lift and its first and second derivatives with respect to cam angle. The lift data may be input in various forms; as discrete data points, as a four-power polynomial or as a multipol, the program user being led to the appropriate section of the input file by prompts in the template. If the valve train is a pivoted follower type, the lift may be given as lift at the valve or as lift at the cam (acting upon an inspection follower of a given diameter). This is discussed in the next section.

Lift data described by either a multipol or a four-power polynomial is evaluated at a requested number of points. The first and second derivatives of lift with respect to cam angle are given by polynomials obtained by differentiation of the original polynomial(s).

```
THIS IS A DATA FILE FOR THE VALVE TRAIN ANALYSIS PROGRAM
,,,,,,,,,,,,,,,,,,,,,,,,,,,,,,,,,,,,,,,,,,,,,,,,,,,,,,,,

EXPRESS FORTRAN
,,,,,,,,,,,,,,,

ALL DATA TO BE IN S.I. UNITS UNLESS OTHERWISE STATED
,,,,,,,,,,,,,,,,,,,,,,,,,,,,,,,,,,,,,,,,,,,,,,,,,,,,

INPUT VALVE TRAIN NAME ON NEXT LINE (UPTO 20 CHARACTERS):-
,,,,,,,,,,,,,,,,,,,,,,,,,,,,,,,,,,,,,,,,,,,,,,,,,,,,,,,,,,

CAM & FLAT FACED FOLLOWER


DATE (DD MM YY)
,,,,,,,,,,,,,,,

02 08 88


VALVE TRAIN TYPE
,,,,,,,,,,,,,,,,

FLAT FACED FOLLOWER          = 1
DOMED TAPPET                 = 2
FINGER FOLLOWER              = 3
CENTRALLY PIVOTED FOLLOWER = 4


INPUT TYPE ON NEXT LINE:-
1
FOR A DOMED TAPPET INPUT RADIUS OF TAPPET FACE (mm):-


CAM TYPE
,,,,,,,,

CONVENTIONAL = 0
DESMODROMIC  = 1


INPUT CAM TYPE ON NEXT LINE:-
0


IS CAM PART OF A DESMO PAIR 1=YES, 0=NO:-
0
```

Figure (4.5a) An Example Input Data File for the Valve Train Analysis Program. (continued ...)

```
LUBRICANT PROPERTIES
,,,,,,,,,,,,,,,,,,,,
INPUT PRESSURE VISCOSITY COEFFICIENT ON NEXT LINE:-
0.22E-7
INPUT VISCOSITY AT AMBIENT PRESSURE AND TEMPERATURE ON NEXT LINE:-
0.050

LOAD DATA
,,,,,,,,,
IF THESE ARE NOT KNOWN PUT VALUE AS 0
EQUIVALENT MASS OF VALVE,SPRING AND RETAINERS (Mv + Mr + 1/3Ms):-
0
INITIAL SPRING COMPRESSION (mm):-
0
SPRING RATE:-
0
PIVOTED FOLLOWER MOMENT OF INERTIA:-
0
FOLLOWER EQUIVALENT MASS:-
0
CAM WIDTH (mm):-
0
YOUNG'S MODULUS OF CAM (GN/m**2)
207
YOUNG'S MODULUS OF FOLLOWER (GN/m**2)
207
POISSON'S RATIO OF CAM
0.29
POISSON'S RATIO OF FOLLOWER
0.29
VALVE CLEARANCE AT BASE CIRCLE POSITION
0.4
```

Figure (4.5b) An Example Input Data File for the Valve Train Analysis Program. (continued ...)

VALVE TRAIN GEOMETRY DETAILS (FOR A PIVOTED FOLLOWER - OTHERWISE GOTO $$$$

,,

A (mm):-

B (mm):-

D (mm):-

R1 (mm):-

RB (mm):-

CHI (degrees):-

LAMBDA (degrees):-

MINIMUM CAM CONCAVITY (MAXIMUM GRINDING WHEEL RADIUS) (mm):-

DIRECTION OF CAM ROTATION 1=CLOCKWISE (AS DYSON OR LIM) -1=ANTICLOCKWISE

$$$$

GEOMETRY DETAILS FOR A DOMED OR FLAT FACED FOLLOWER

,,

BASE CIRCLE RADIUS OF CAM (mm):-

18

CAMSHAFT ROTATIONAL SPEED (r.p.m.):-

,,,,,,,,,,,,,,,,,,,,,,,,,,,,,,,,,,,,,,

1500

Figure (4.5c) An Example Input Data File for the Valve Train Analysis Program. (continued ...)

```
VALVE OR CAM LIFT?
,,,,,,,,,,,,,,,,,,

CAM LIFT   = 0
VALVE LIFT = 1

INPUT ON NEXT LINE:-
1
IF CAM LIFT IS USED INPUT THE RADIUS OF THE INSPECTION
FOLLOWER THAT WAS USED (NOT APPLICABLE TO FLAT FACED FOLLOWER)(mm):-


LIFT DATA
,,,,,,,,,

DATA POINTS           = 0
FOUR POWER POLYNOMIAL = 1
MULTIPOL              = 2

INPUT TYPE ON NEXT LINE:-
1

IS THE LIFT CURVE SYMMETRICAL (EXCLUDING RAMPS):-
YES = 1
NO  = 0
ENTER 0 OR 1 ON NEXT LINE:-
1

INPUT NUMBER OF DATA POINTS TO BE USED FOR ANALYSIS:-
180
```

Figure (4.5d) An Example Input Data File for the Valve Train Analysis Program. (continued ...)

```
IF A MULTIPOL IS TO BE USED FILL THE TABLE BELOW:-OTHERWISE GOTO ####
,,,,,,,,,,,,,,,,,,,,,,,,,,,,,,,,,,,,,,,,,,,,,,,,,,,,,,,,,,,,,,,,,,,,,,,,
----------------------------------------------------------------------------
SEGMENT            1            2            3            4            5
LENGTH(deg)     00.00000000  00.00000000  00.00000000  00.00000000  00.0000000
COEFFICIENT1    00.00000000  00.00000000  00.00000000  00.00000000  00.0000000
COEFFICIENT2    00.00000000  00.00000000  00.00000000  00.00000000  00.0000000
COEFFICIENT3    00.00000000  00.00000000  00.00000000  00.00000000  00.0000000
COEFFICIENT4    00.00000000  00.00000000  00.00000000  00.00000000  00.0000000
COEFFICIENTS5   00.00000000  00.00000000  00.00000000  00.00000000  00.0000000
----------------------------------------------------------------------------

INPUT OPENING RAMP HEIGHT(mm):-

INPUT OPENING RAMP LENGTH(deg):-

INPUT CLOSING RAMP HEIGHT(mm):-

INPUT CLOSING RAMP LENGTH(deg):-

INPUT NUMBER OF SEGMENTS USED:-

INPUT MAXIMUM ORDER OF POLYNOMIALS:-

#### END OF DATA FILE IF LIFT IS GIVEN BY MULTIPOL!!!!
```

Figure (4.5e) An Example Input Data File for the Valve Train Analysis Program. (continued ...)

```
IF A FOUR POWER POLYNOMIAL IS TO BE USED:- OTHERWISE GOTO ****
,,,,,,,,,,,,,,,,,,,,,,,,,,,,,,,,,,,,,,,,,,,,,,,,,,,,,,,,,,,,,
CAM HALF PERIOD (deg):-
60.0
MAXIMUM LIFT (mm):-
8.9000
p:-
2
q:-
9
r:-
78
s:-
80
Cp:-
-11.692
Cq:-
2.8499
Cr:-
-0.58946
Cs:-
0.53140
INPUT OPENING RAMP HEIGHT (mm):-
0.50
INPUT OPENING RAMP LENGTH (deg):-
25
INPUT CLOSING RAMP HEIGHT (mm):-
0.50
INPUT CLOSING RAMP LENGTH (deg):-
25
**** END OF DATA FILE IF LIFT IS GIVEN BY FOUR POWER POLYNOMIAL!!!!
```

Figure (4.5f) An Example Input Data File for the Valve Train Analysis Program. (continued ...)

```
IF DATA POINTS ARE TO BE USED:-
,,,,,,,,,,,,,,,,,,,,,,,,,,,,,,,,

CAM ANGLES IN DEGREES = 0
CAM ANGLES IN RADIANS = 1

INPUT ON NEXT LINE:-


CAM ANGLE            LIFT(mm)
,,,,,,,,,,,,,,,,,,,,,,,,,,,,,,,,
```

Figure (4.5g) An Example Input Data File for the Valve Train Analysis Program.

Lift data given by discrete data points is numerically differentiated with respect to cam angle to obtain the first and second derivatives. This is done using the central difference formula. This is reasonable only as long as the lift data is accurate as the second derivative is very sensitive to errors. Lim et al (1983) suggested a method whereby a function of the form

$$l_v = \exp(a_0 + a_1\phi + a_2\phi^2 + a_3\phi^3 + \ldots + a_m\phi^m)$$

was fitted to the lift data. This function could then be differentiated to give the required derivatives. A test was performed on this method using data for which the first and second derivatives were known (from a four power polynomial lift definition). Whilst the method appeared to give stable results for the case studied by Lim and his co-workers, it was found that in practice that curve fitting introduced significant errors.

If the cam is a desmodromic closing cam the lift data is checked to ensure that the lift is negative throughout the cycle. If it is not, the lift is negated and the sign of the velocity data is changed to suit. In this way the desmodromic cam and follower can be treated just as a conventional cam and follower within the kinematic analysis subroutines.

The kinematic analysis for a cam acting against a pivoted follower (which is described in the previous chapter) assumes that the cam rotates clockwise when viewed with the pivot centre to the right of the cam centre of rotation. If the cam rotates anticlockwise then the data is adjusted. This is done by reordering the arrays containing lift, velocity and acceleration in reverse order. The array containing the valve lift velocities has all its elements changed in sign. After all the lubrication analysis has been carried out, these arrays (along with the arrays containing Hertzian stress, frictional torque, and film thickness results) are rearranged.

At this stage in the program all the data has been processed into a form that is acceptable for the next group of subroutines dealing with the kinematic analysis of the valve train.

4.2.2 Kinematic Analysis.

In order to assess the tribological performance of the cam and follower several parameters are required. These will be discussed in more depth in section 4.2.3 of this chapter. Amongst these parameters are the equivalent radius of curvature of the contact and the surface velocities of the cam and follower relative to their point of contact.

The analysis relating to the evaluation of these parameters was presented in the previous chapter. To enable the calculation of the parameters the program requires the lift data, evaluated in the previous part of the program, and the valve train geometry which is given in the input data file. The lift data may have been given as cam or valve lift for a pivoted follower system. The analysis requires that the data be in the form of valve lift. Any data given as cam lift is therefore translated to lift at the valve.

The kinematic velocities and radii of curvature are calculated and stored in arrays in readiness for the next section of the program which calculates the lubrication conditions at the cam/follower interface. During the calculations checks are made to ensure that the cam profile does not become too concave. The maximum allowable cam concavity is dictated by the type of valve train (the cam obviously cannot be concave in a flat faced follower system) and the minimum grinding wheel diameter allowable during the cam machining process. If the cam does become too concave a warning is printed to the terminal screen and the program ends.

4.2.3 Evaluation of Tribological Performance.

At this stage of the program the analysis can take one of two directions dependent upon whether or not sufficient data has been supplied to allow the load at the cam/follower interface to be calculated. If the load can be evaluated the lubricant film thickness at the cam/follower interface is predicted using the Dowson and Higginson (1977) formula (see below), otherwise the Blok limitation (Dowson et al (1983)) is used (again, see below). If the load at the interface is available, then the Hertzian stress and the frictional

torque arising from the contact can be evaluated. This then allows a prediction of the power loss due to friction to be made.

4.2.3.1 Evaluation of the Lubricant Film Thickness Between the Cam and Follower.

The conditions at the cam and follower contact are very severe. Assuming an adequate supply of lubricant reaches the contact, full separation of the cam and follower around all of the lift cycle is not guaranteed. If the camshaft rotational velocity is high enough then the contact around the cam flanks (where the lubricant entrainment velocity is at its highest) may enjoy elastohydrodynamic lubrication (EHL), otherwise the contact will operate in the mixed lubrication regime. Around the nose of the cam, where the lubricant entrainment is small, some elememt of boundary lubrication can almost always be anticipated.

EHL occurs between lubricated non-conformal contacts. The geometry of the contact is such that very high pressures are generated, leading to elastic deformation of the interacting solids. The pressure generated within the lubricant film may be of the order of hundreds of mega-pascals, which leads to dramatic changes in the lubricant properties. The viscosity of the lubricant increases rapidly with pressure (indeed exponentially according to the Barus relationship, ($\eta=\eta_0 e^{\alpha p}$)), and at high pressures exhibits almost solid like characteristics. Dowson and Higginson (1977) presented a formula for the minimum lubricant film thickness between two cylinders in line contact:

$$\frac{h_{min}}{R} = 2.65\ U^{0.70}\ G^{0.54}\ W'^{-0.13} \qquad (4.1)$$

Dowson and Toyoda (1978) presented a similar formula for the film thickness at the centre of the contact:

$$\frac{h_{cen}}{R} = 3.06\ U^{0.69}\ G^{0.56}\ W'^{-0.10} \qquad (4.2)$$

For fully developed EHL an acceptable approximation to the lubricant film thickness may be obtained from the condition that the

maximum hydrodynamic pressure tends to infinity for the film shape determined by the undeformed surfaces - i.e a rigid-peizoviscous solution (Dowson et al (1983)). For this condition the film thickness is given by:

$$h_{min} = 1.666\ (\eta V_e \alpha)^{\frac{2}{3}}\ R^{\frac{1}{3}} \qquad (4.3)$$

It can be seen that this relationship is independent of the load at the contact. It can therefore be used to predict the lubricant film thickness at the cam/follower interface in cases where the load is unknown.

These formulae are obviously not strictly accurate for the situations found in cam/follower contacts, in which the action of squeeze will be very important around the areas where the entrainment of the lubricant into the contact is very small. They are, however, felt to be adequate to allow qualitative judgements of the merits of valve train designs to be made.

Boundary lubrication occurs between two interacting solids when some asperity contact or interaction between surface films takes place as the lubricant film thickness falls to a value less than the composite surface roughness of their surfaces. In such conditions the contact must rely upon the ability of the lubricant and solids to form surface reaction layers in order to prevent severe wear taking place. In boundary lubrication the laws of dry friction apply since the coefficient of friction is independent of load, speed, and apparent ares of contact. This regime of lubrication can almost certainly be expected around the nose of the cam. The transition from boundary lubrication to full EHL does not take place instantaneously. As the load and entrainment velocity at the cam/follower interface become more favourable larger proportions of the load are carried by the pressure of the lubricant within the contact, with less and less of the load being borne by surface asperities.

4.2.3.2 Evaluation of the Load at the Cam/Follower Interface.

An analysis for the determination of the loading at the cam/follower interface for the various types of valve train has been given in Chapter (3). The program identifies the valve train type and then, if sufficient data has been supplied, calculates the load using the appropriate analysis.

The analysis for the loading at the cam/follower interface for a centrally or end pivoted follower requires that the coefficient of friction at the contact be known. This obviously cannot be calculated without the load at the contact being known. A coefficient of friction of 0.08 is therefore assumed to allow the load to be calculated. This allows the frictional traction at the contact to be determined (see below). The coefficient of friction can then be recalculated and a new load assessed. This procedure is repeated until the loading around the cycle converges. Convergence is very rapid, usually taking only three iterations.

Throughout the load calculation procedures checks are performed to ensure that the load on the cam and follower never falls to zero. If it does, then the cam is no longer controlling the motions of the follower or valve, and valve bounce is occurring. In such cases a warning is written to the terminal screen and the program stops.

4.2.3.3 Evaluation of the Hertzian Stress at the Contact.

Once the load at the cam/follower interface has been evaluated then the maximum Hertzian stress at the contact can be found. This also allows the dimensions of the contact zone to be calculated according to the theory of Hertz (1882) (see 3.3.2).

4.2.3.4 Frictional Traction.

In fully lubricated contacts the frictional forces acting upon the interacting components are a function of the velocity gradients across the contact zone. The frictional force consists of contributions due to rolling and sliding of the components. In the

contact between cams and followers much shearing of the lubricant film takes place due to the sliding action of the cam and follower. This would, in reality, lead to a lowering of the lubricant viscosity due to the associated temperature rise. The model used in the present study, however, assumes that isothermal conditions exists within the contact region.

As the elastic deformation of the cam and follower is large in comparison to the lubricant film thickness, the contact can be approximated by a lubricated Hertzian contact as shown in Figure (4.6). At the inlet to the contact the frictional force arises almost entirely due to the rolling of the components. In the long parallel zone the contribution of rolling is negligible, especially when the sliding speeds encountered with cams and followers are taken into account. Thus, the frictional traction calculations are restricted to the sliding contribution from the 'Hertzian' region taking the Hertz pressure distribution.

The shear stress acting upon the solid boundaries is given by:

$$\tau = \eta \frac{du}{dy} \tag{4.4}$$

where (du/dy) is the velocity gradient across the lubricant film thickness. Substituting the Barus relationship for the viscosity term and V_s/h_{cen} for the velocity gradient, we obtain

$$F = \int \frac{\eta_0 V_s e^{\alpha p}}{h_{cen}} dx \tag{4.5}$$

upon integrating the shear stress along the length of the contact.

From (3.3.2) the Hertzian pressure distribution across the contact is given by:

$$p = p_{max}\left[1 - \frac{x^2}{b^2}\right]^{\frac{1}{2}} \tag{4.6}$$

Therefore,

$$F = \frac{\eta_0 V_s e^{\alpha p_{max}}}{h_{cen}} \int e^{(1-x^2/b^2)^{\frac{1}{2}}} . dx \tag{4.7}$$

Equation (4.7) is solved numerically using Simpson's rule to give the instantaneous frictional force at a given instant during the

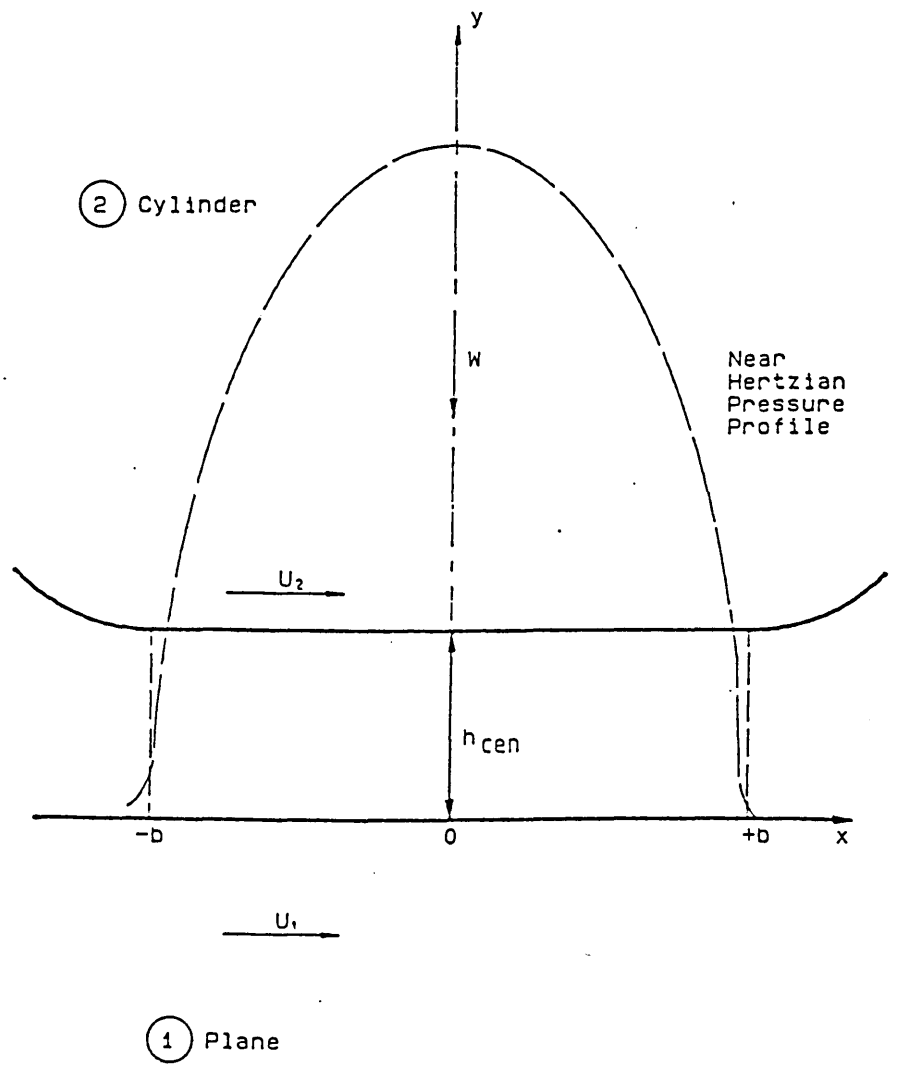

Figure (4.6) Hertzian Contact Assumed for Friction Force Calculation.

cam cycle.

As the Barus viscosity relationship is exponential, the viscosity term in Equation (4.7) can become very large at high pressures. This leads to very high frictional forces being predicted. The model, therefore, calculates a boundary friction value taking a limiting friction coefficient:

$$F = \mu W$$

The value of the coefficient of friction (μ) was taken to be 0.08. Experimental evidence (Zhu (1988)) and work on piston rings at the University of Leeds show this value to be reasonable. If the frictional force predicted by the boundary lubrication model was less than that predicted by the lubricant shearing model then the former was taken as the frictional force arising at the interface.

Another approach used to assess which friction model should be employed is to use the ratio of the lubricant film thickness to the composite surface roughness of the contacting surfaces. Once this ratio falls to a value below unity, boundary lubrication can be said to be occurring. A reasonable surface roughness value for a run-in cam and follower pair is 0.2 μm (Harrison (1985)). The results obtained using this model are very similar to those from the limiting oil shear friction model. The reason for the similarity can be seen by referring to the parametric studies presented in Chapter (5). Figure (5.7) shows how the coefficient of friction varies throughout the cam cycle using the limiting coefficient of friction model. From Figure (5.1f) it can be seen that with a surface roughness of 0.2 μm, the ratio of oil film thickness to average asperity height would cause the limiting coefficient of friction, (0.08), to be invoked around the very same portions of the cam cycle.

4.2.3.5 Power Loss.

The instantaneous power loss due to friction is given by

$$H = Fr\omega \qquad (4.8)$$

where (r) is the perpendicular distance from the cam centre of rotation to the frictional load vector. This can be integrated around the cam lift cycle (using Simpson's rule) to give an average power

loss:

$$H = \frac{1}{2\pi} \int_0^{2\pi} Fr\omega \, d\phi \qquad (4.9)$$

4.2.4 Parametric Study Routines.

In order to enable the effects of changes in various of the design parameters be investigated, a series of parametric study subroutines was built into the program. These enabled the value of the cam base circle radius, the cam width, the spring stiffness, the camshaft speed, the follower radius of curvature, the lubricant viscosity and the equivalent mass at the valve to be changed. The effect of changes in these values upon Hertzian stress at the contact, minimum lubricant film thickness, and power loss could then be studied. Examples of parametric studies are given in Chapter (5).

4.2.5 Output.

It was felt important that the output from the program should be easily understood by a competent professional engineer. The output was therefore both graphical and numerical. The graphical output is arranged in a concise manner such that the trends in important tribological parameters, and their interaction upon each other, can be easily assimilated. Examples of the graphical output are presented in the next chapter and in the next section. The numerical data output shows the same information as the graphical output in a tabular form.

4.3 An Example Program Run.

In this section the reader will be led through a typical session using the valve train lubrication analysis program.

Firstly the input data file is created using the screen editing facility on the mainframe computer. A cam acting against a flat faced follower will be used for this an example, the lift data being given as a four power polynomial, and loading data being neglected. The data file, called FLAT is shown in Figure (4.5). The program is run,

for convenience, using an execution (exec) file named 'FR'. The format for the exec being:

FR file_1 file_2 file_3 file_4 file_5 ...

where

file_1 is the fortran file to be run,
file_2 is the input data file (assigned to channel 1),
file_3 is an output data file (assigned to channel 2),
file_4 is a file (assigned to channel 10),
file_5 is a file (assigned to channel 11), etc, etc.

If any file in the string prior to the last defined input or output channel is not used then it is replaced in the string by a full-stop (.). The valve train analysis program is called EXPRESS and is a fortran file. The program reads the input data from channel 1 and writes an output data file for a hard-copy to channel 2. If a pivoted follower is used data concerning the geometrical variables is written to channel 10. All of the program variables are written to a data file assigned to channel 12 in a format which can be read by a graphs program. Hence to run the program the user in this example types:

FR EXPRESS FLAT A . PICTURE

where

FLAT is the input data file (shown in Figure (4.5),
A is the hard-copy output data file,
a '.' is used as the follower is not pivoted,
and PICTURE is the data file for the graphics program.

Figure (4.7a) shows the computer terminal response when the program is executed (note that the exec, fr, is not case sensitive). The user is shown an introductory page and is given the option to view a summary of the data that has been introduced to the program by FLAT. In this example the option to view the data is accepted and the data summary is printed to the terminal (Figure (4.7b). Having viewed the data the operator is given the choice of continuing the run, or, if the input data is not correct, of aborting the run. If the run is continued then a further option is given which allows the user to opt for a parametric study to be carried out upon the valve train (Figure 4.7c). In this example this option is not taken and the program ends by reminding the user of the names of the output data files and gives instructions upon how hard-copies and graphical output may be obtained.

```
.fr express flat a . picture
Execution begins...

                    Cam and follower analysis
                    =========================

                                        Andrew Ball
                                        Dept of Mech. Eng.
                                        University of Leeds.
                                        April 1987

          This program analyses the kinematics and the
     lubrication of the point of contact of various
     cam/follower pairs. The analysis is based upon the
     technique developed by Dyson that is outlined in the
     following:-

          Dyson, A. Kinematics and wear patterns of cam
          and finger follower automotive valve gear,
          Tribology International, June 1980 pp 121-132.

          Dyson, A., Naylor, H., Application of the flash
          temperature concept to cam and tappet wear
          problems. Proc. I. Mech. E. 1961.

 DO YOU WISH TO SEE THE INPUT DATA? Y/N <N>
.y
```

Figure (4.7a) Computer Terminal Responses During a Typical Run of the Valve Train Analysis Program. (continued ...)

```
CAM & FLAT FACED FOLLOWER
Created on  2:08:88

                INPUT DATA
                ----------

Cam acting against a flat faced follower
Lubricant viscosity ..............  0.050 Ns/m(sqd)
Pressure viscosity coefficient ....  0.220E-07 m(sqd)/N
Cam rotational speed .............  1500.0 rpm
Cam Base Circle Radius ...........  18.00 mm

*** HIT RETURN KEY TO CONTINUE ***

Lift input as valve lift
Lift has been input as a four power polynomial ...

        Data For Four Power Polynomial
        ------------------------------
        Action Period =   60.00 deg
        Ramp Height   =    0.50 mm
        Max Lift      =    8.90 mm

        Powers are:-
            p = 2    q = 9
            r =78    s =80

        Coefficients are:-
           Cp =   -11.69200  Cq =     2.84990
           Cr =    -0.58946  Cs =     0.53140

Lift curve is symmetrical

Contact Loading Data
--------------------
No Load Data Supplied
Film thicknesses calculated using the Blok Limitation
```

Figure (4.7b) Computer Terminal Responses During a Typical Run of the Valve Train Analysis Program. (continued ...)

```
DO YOU WISH TO CONTINUE? Y/N <Y>
.y
 ********** OK PROGRAM IS RUNNING

DO YOU WANT A PARAMETRIC STUDY TO BE CARRIED OUT? Y/N <N>
.n


Hard copy of output data may be obtained by typing PR A DATA (CC

Graphical output can be obtained by typing FR GRAFIT PICTURE

Ready; T=0.79/0.99 11:39:21
```

Figure (4.7c) Computer Terminal Responses During a Typical Run of the Valve Train Analysis Program.

The graphical output, which may be directed to a graphics terminal or to a plotter, is obtained by running another program called GRAFIT. Figure (4.8) shows the graphical output obtained from the example above. In this case the output is contained on two sheets of A4 plotter output (if loading data had been supplied then a third would have been obtained). The output offers information to the user in a concise and easily assimilated format, showing the variation of the important lubrication parameters around the cam cycle (V_e, V_s, R, etc) and the lubricant film thickness plotted against cam rotational angle and against eccentricity. The final sheet shows the cam profile with the predicted lubricant film thickness superimposed upon it.

4.4 Conclusion.

A user friendly computer program which, it is felt, could be used by any competent professional engineer has been developed to analyse the tribological operation of all types of cam and follower arrangements in common use in today's automobile engines. The program has expanded previous design programs available at the University of Leeds, the previous program being non-user-friendly and being capable only of analysing cam and flat faced follower systems with the lift data being presented in the form of a four power polynomial. It is felt that the program is well structured and robust, and gives clear, easily assimilated output data.

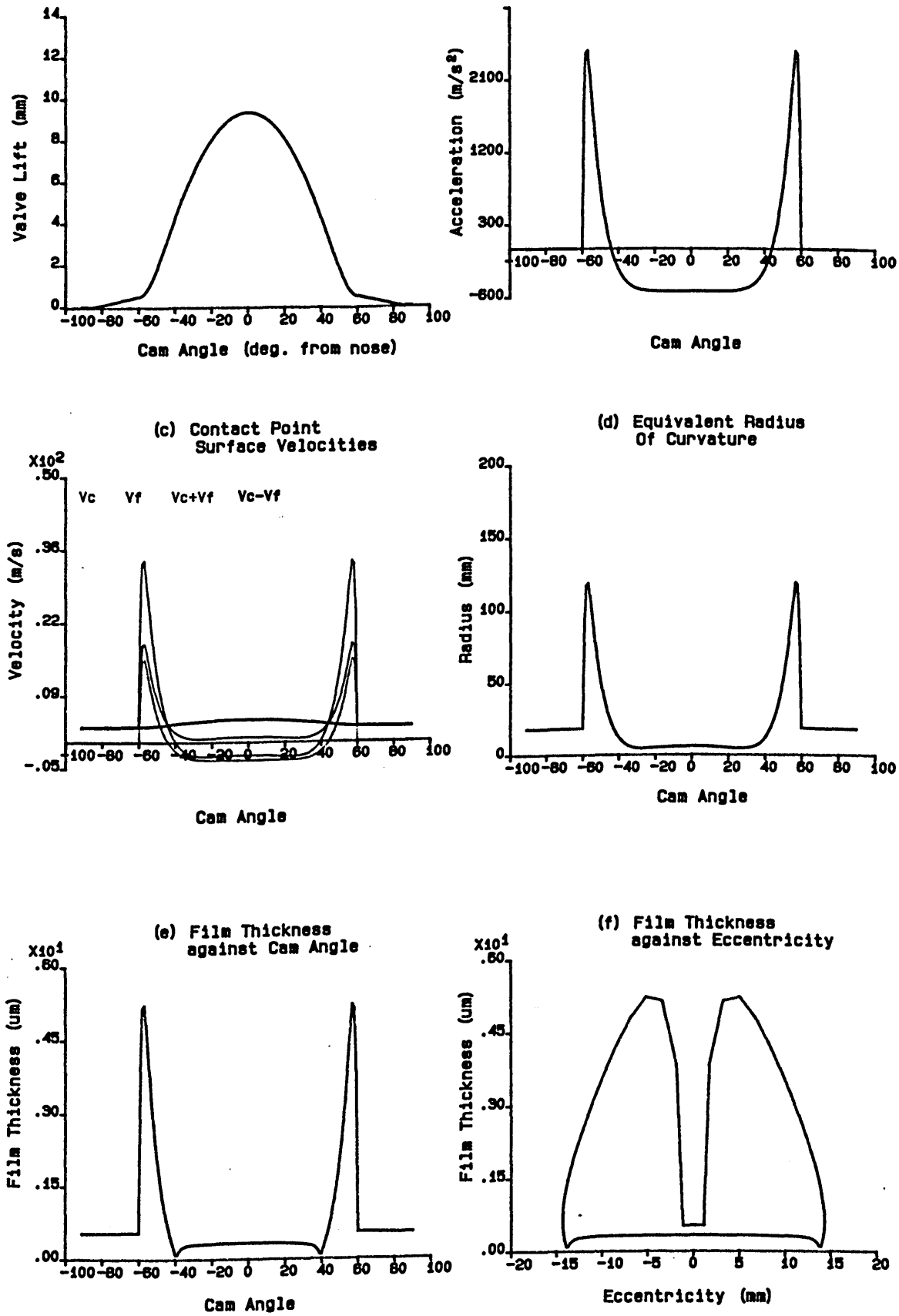

Figure (4.8a) Graphical Output from the Computer Program.

Cam Base Circle Radius (mm)	=	18.00
Lubricant Viscosity (Ns/m²)	=	.050
Press. Visc. Coeff. (/Pa)	=	22.0E-9
Cam Rotational Speed (rpm)	=	1500.0

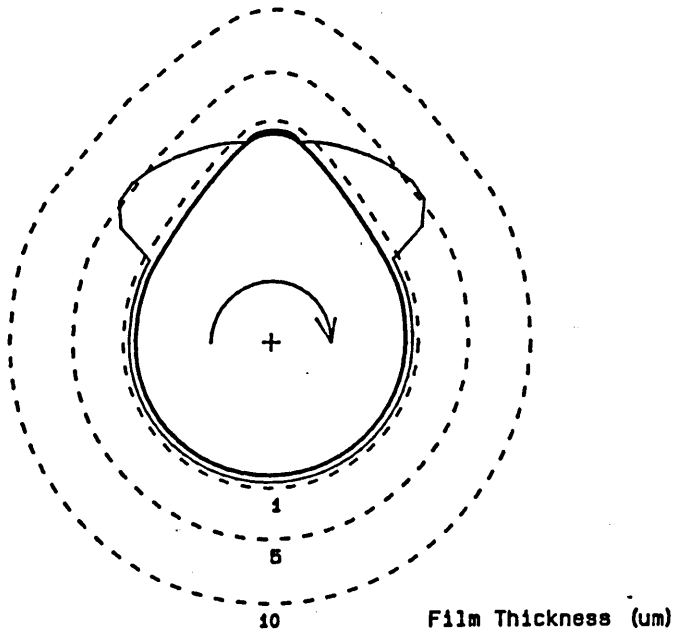

Figure (4.8b) Graphical Output From the Computer Program.

CHAPTER 5

PARAMETRIC STUDIES OF THREE VALVE TRAIN SYSTEMS

5.1 Introduction.

The successful design of a valve train system requires a skilful compromise between various parameters. Very little work has been done to determine which factors most affect the performance of the cam mechanism, and so the designer often has to resort to 'rule of thumb'. The design philosophy involved in the creation of a valve train is discussed at length in Chapter (2).

Muller (1966) was the first to show that, theoretically, the shape of the cam profile could affect not only the Hertzian Stress but also the lubricant film thickness at the cam/follower interface. It therefore became apparent that if a cam mechanism was to work satisfactorily attention should be paid to limiting the Hertzian stress whilst sustaining an adequate lubricant film. Dyson (1977) showed how both the equivalent radius of curvature and the lubricant film thickness at the contact varied as several important design parameters were changed for a cam acting against a domed follower. He then showed (1980) how this theoretical work could be extended to a cam and end pivoted follower system. Harrison (1985) carried out a comprehensive parametric study of a cam and flat faced follower system and showed how the frictional power loss, lubricant film thickness at the cam nose and Hertzian stress at the cam nose varied as several design parameters were altered. Dowson, Harrison and Taylor (1985) produced a table explaining and summarising the important findings of this study - a most useful aid for anyone wishing to design a cam and flat faced follower mechanism.

In this chapter parametric studies of three valve train systems will be presented and the results summarised in tabular form. The valve train systems are: a cam and flat faced follower mechanism (identical to that used by Harrison (1985)), a cam and centrally pivoted follower mechanism, and finally a cam and an end pivoted follower mechanism. The parametric studies were carried out using the computer program described in the previous chapter. It will be shown, using the cam and end pivoted follower mechanism, how a parametric study can reveal that small changes in a design may produce significant benefits in the performance of a cam and follower system.

5.2 A Parametric Study of a Cam and Flat Faced Follower System.

The cam and follower pair used in this study is identical to that investigated by Harrison (1985). Data relating to the system is listed below and is taken as the datum condition:

Cam base circle radius = 18.00 mm
Cam width = 12.00 mm
Spring stiffness = 38254 N/m
Initial spring displacement = 6.40 mm
Equivalent mass at valve = 0.172 kg
Young's modulus of cam and follower = 207 GN/m^2
Poisson's ratio of cam and follower = 0.29
Lubricant viscosity = 0.050 Ns/m^2
Lubricant pressure-viscosity coefficient = 22.0×10^{-9} m^2/N

The valve lift is described by a four-power polynomial:

$$l = Y_r + l_{cmax} + C_p\left[\frac{\phi}{\phi_T}\right]^p + C_q\left[\frac{\phi}{\phi_T}\right]^q + C_r\left[\frac{\phi}{\phi_T}\right]^r + C_s\left[\frac{\phi}{\phi_T}\right]^s$$

where

$p = 2,\ q = 9,\ r = 78,\ s = 80,$

and

$C_p = -11.6918407$ mm, $C_q = 2.8498942$ mm,

$C_r = -0.5894568$ mm, $C_s = 0.5314033$ mm,

$Y_r = 0.50$ mm, $l_{cmax} = 9.40$ mm, $\phi_T = 60^\circ$.

Each design parameter was changed from its datum, whilst the others remained constant, and the effect upon the pridicted frictional power loss, lubricant film thickness at the cam nose and Hertzian stress at the cam nose was studied. The parameters changed were:

(a) Cam base circle radius,
(b) Cam width,
(c) Equivalent mass at the valve,
(d) Camshaft speed,
(e) Valve spring rate, and
(f) Lubricant viscosity.

Figure (5.1) shows the cam operating characteristics at the

CAM OPERATING CHARACTERISTICS
PAUL HARRISON'S DATA - 2500 rpm

Cam Base Radius (mm)	=	18.00
Maximum Valve Lift (mm)	=	9.40
Cam Width (mm)	=	12.00
Rotational Speed (rpm)	=	2500.0
Spring Stiffness (kN/m)	=	38.254
Initial Spring Disp. (mm)	=	6.4
Equiv. Mass At Valve (kg)	=	.172
Lubricant Viscosity (Ns/m^2)	=	.050
Press. Visc. Coeff. (/Pa)	=	22.0E-9
Youngs Mod. (Cam) (GPa)	=	207.0
Youngs Mod. (Foll.) (GPa)	=	207.0
Poissons Ratio (Cam)	=	.29
Poissons Ratio (Foll.)	=	.29
Frictional Power Loss (W)	=	48.50

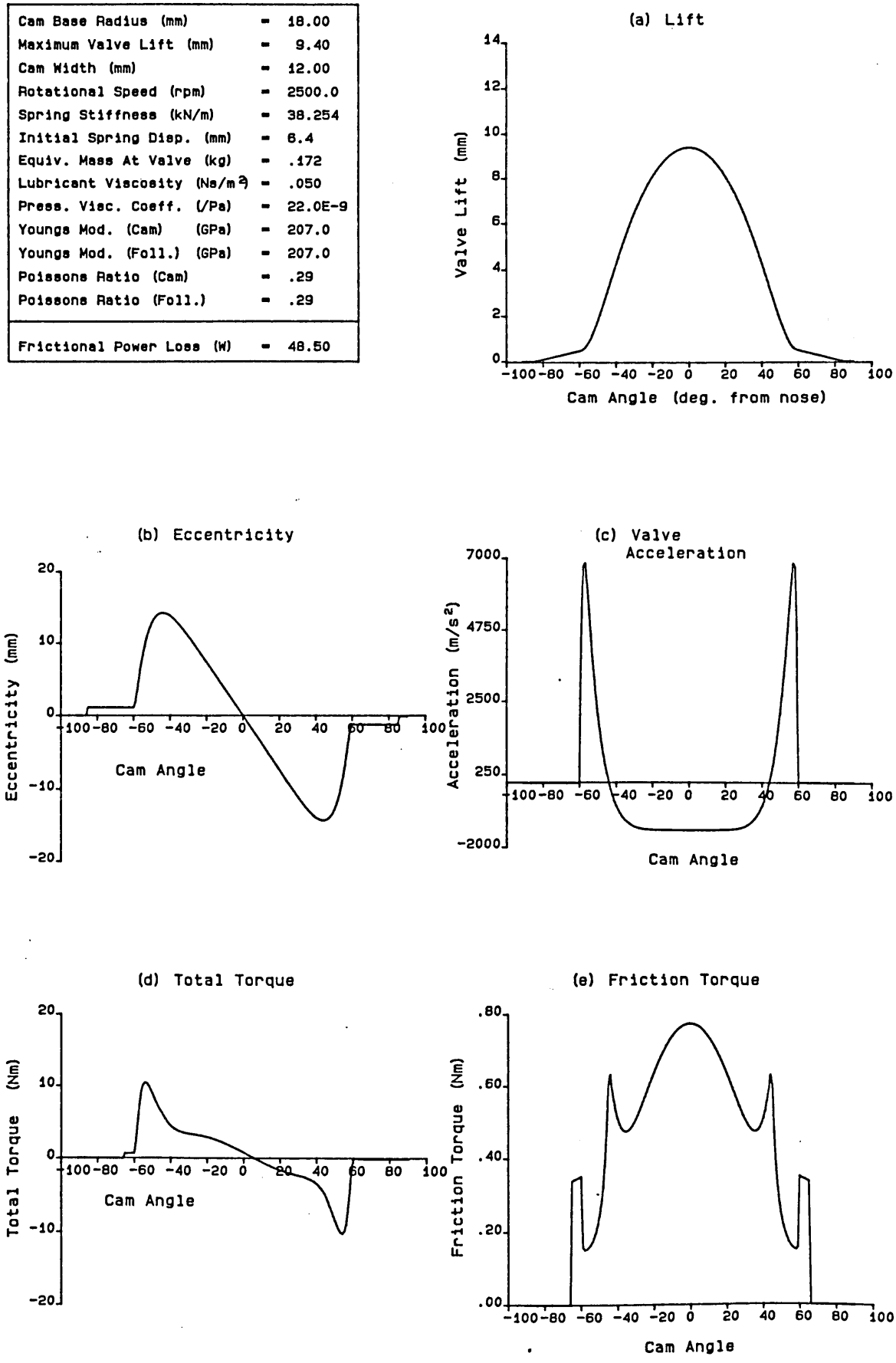

Figure (5.1) Cam and Flat Faced Follower Operating Characteristics at the Datum Condition (Camshaft Rotational Speed = 41.67 Hz).

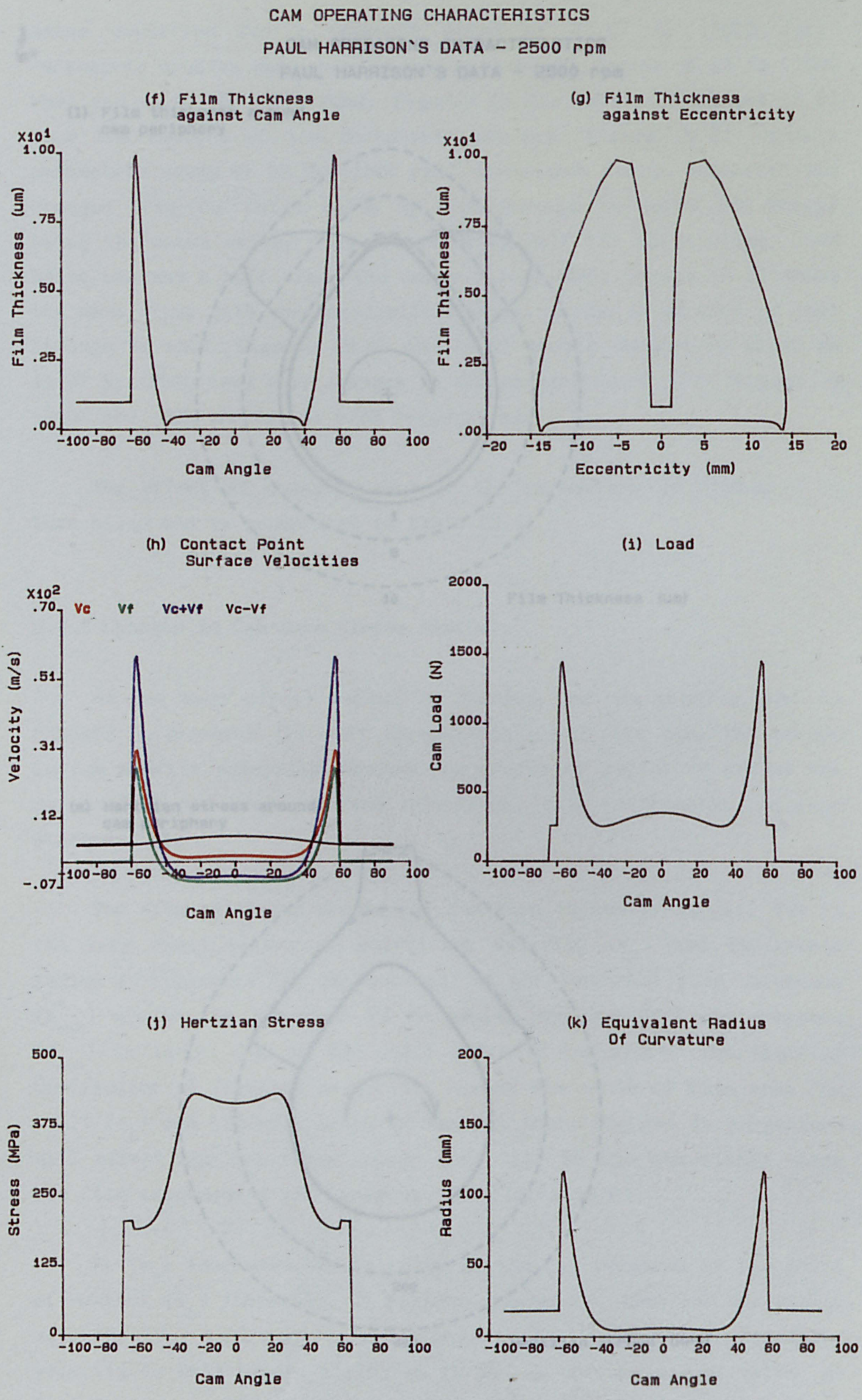

Figure (5.1 continued).

CAM OPERATING CHARACTERISTICS
PAUL HARRISON'S DATA - 2500 rpm

(l) Film thickness around cam periphery

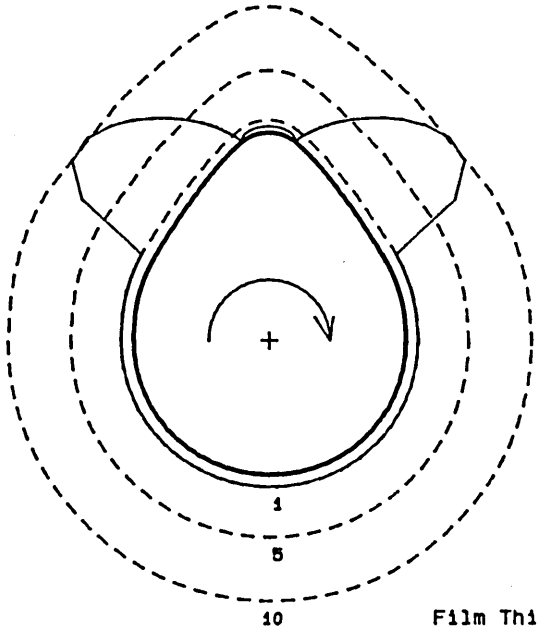

(m) Hertzian stress around cam periphery

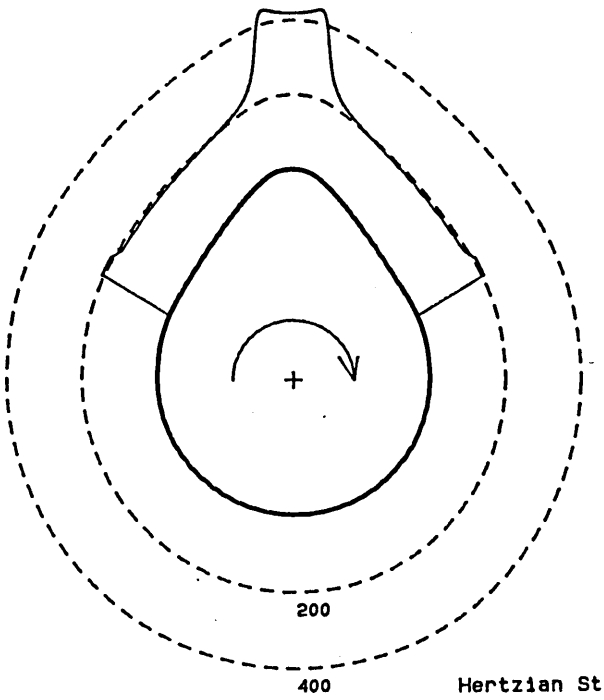

Figure (5.1 continued).

datum condition for a camshaft speed of 41.67 Hz (2500 rpm). Parametric studies were carried out at camshaft speeds of 25 Hz (1500 rpm) and 41.67 Hz (2500 rpm). Figures (5.2), (5.3), (5.4) and (5.5) show the results of the parametric studies. Figure (5.2) shows a parametric study at 25 Hz (1500 rpm) where each design parameter was changed from its datum value by -70% through to +300% (0% change being the datum value, -50% change being half the datum value, +50% being one and a half times the datum value, etc). Figure (5.3) shows the same study with more realistic changes in the parameters of -25% through to +25%. Figures (5.4) and (5.5) show a parametric study at 41.67 Hz (2500 rpm) with changes in the parameters of -70% through to +300% and -25% through to +25% respectively.

The effect of changing each of the parameters is discussed in turn below and is summarised in Table (5.1).

5.2.1 Changes in Cam Base Circle Radius.

As the base circle radius is changed the cam profile must be changed to preserve the lift characteristics of the cam. The change in cam profile naturally changes the radius of curvature around the cam surface and hence surface velocities, film thicknesses, surface stresses, etc.

The film thickness around the cam nose is small, largely due to the very small values of entraining velocity (V_e) and equivalent radius of curvature (R) encountered. As the lubricant film thickness (h_{cen}) around the cam nose is so small, and the Hertzian pressure (p_{max}) is large, due to the small radii of curvature, the limiting coefficient of friction is applied around the whole of this area for small (r_B) and the only areas of the cam where changes in parameters will affect the frictional power loss will be the cam flanks where the film thicknesses are generous (see Figure (5.6)).

As (r_B) increases the velocity of the cam relative to the point of contact (V_c) increases. It follows, therefore, that the entraining velocity (V_e) is changed. An increase in (r_B) causes the entraining velocity to fall before rising as it passes through a zero value. As (r_B) increases (R), the equivalent radius of curvature, increases.

PARAMETRIC STUDY

PAUL HARRISON'S DATA - 1500 rpm

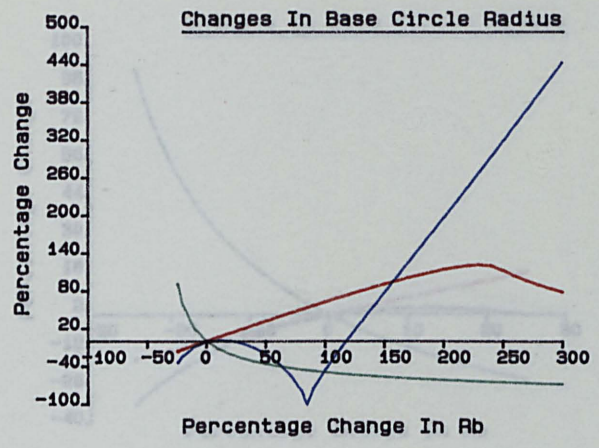

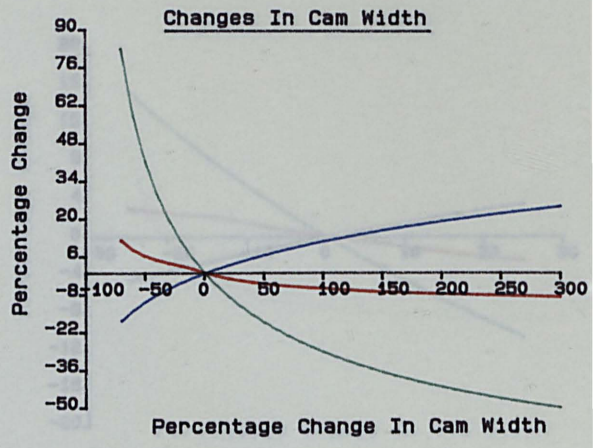

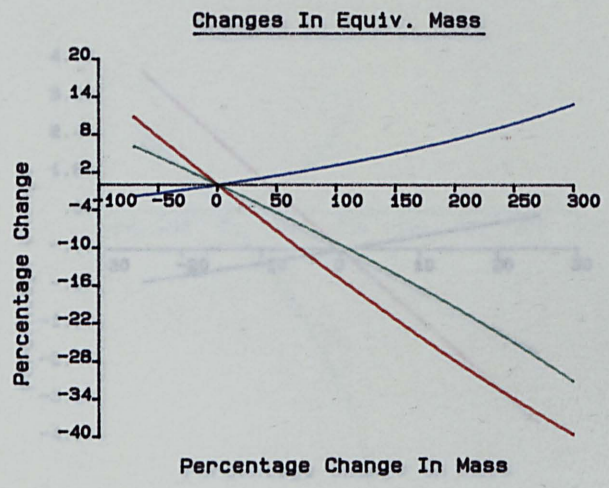

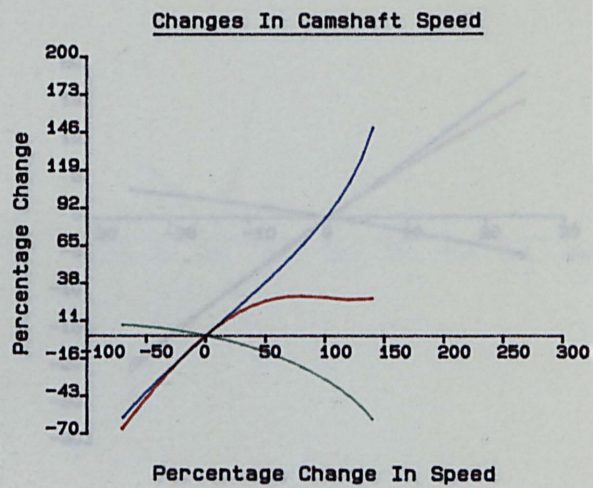

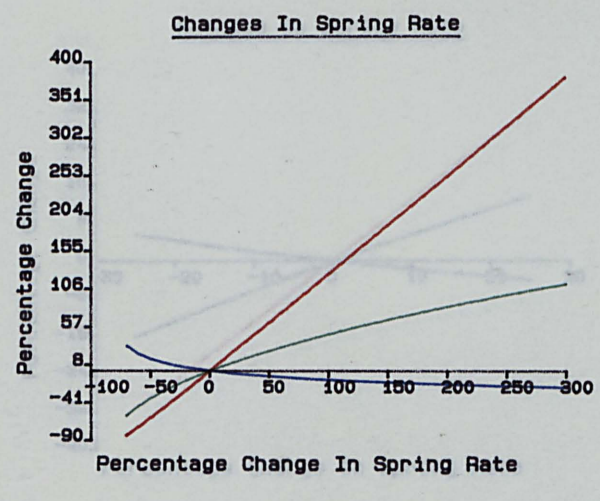

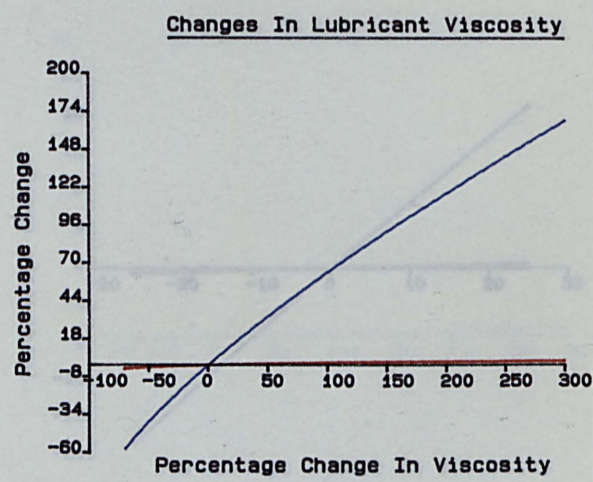

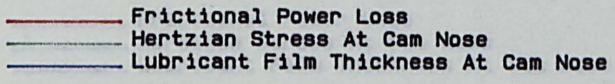

Figure (5.2) Parametric Study for Cam and Flat Faced Follower (25 Hz).

PARAMETRIC STUDY
PAUL HARRISON'S DATA - 1500 rpm

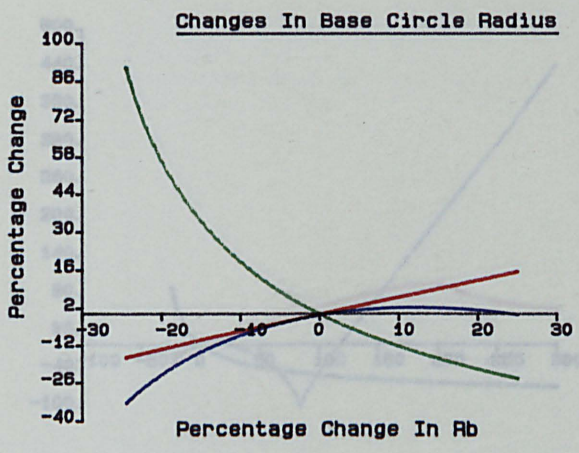

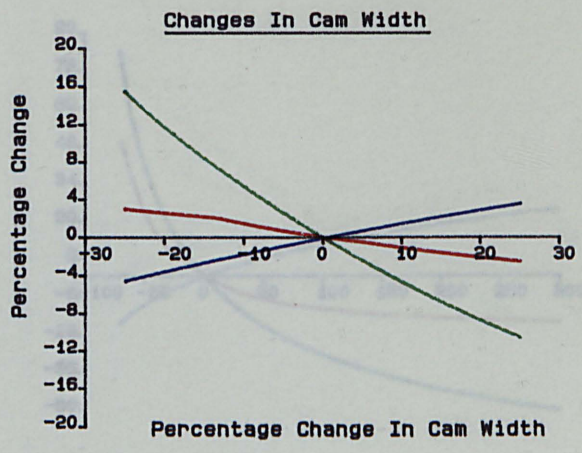

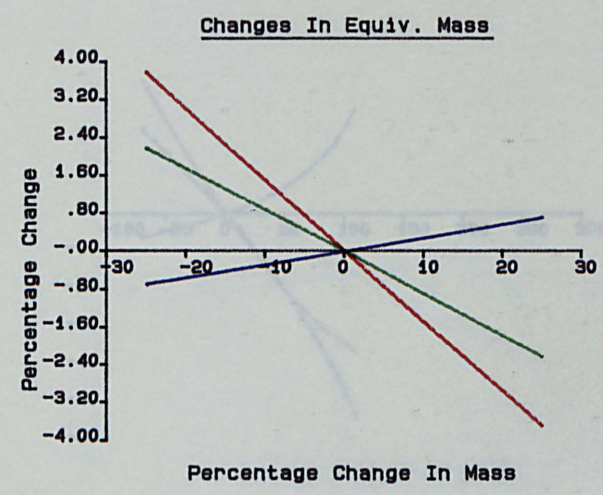

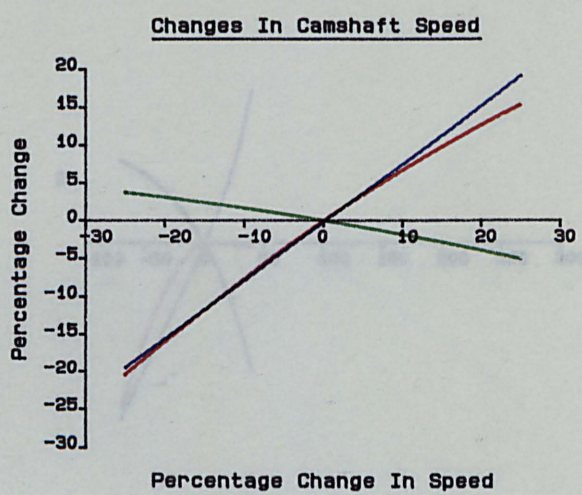

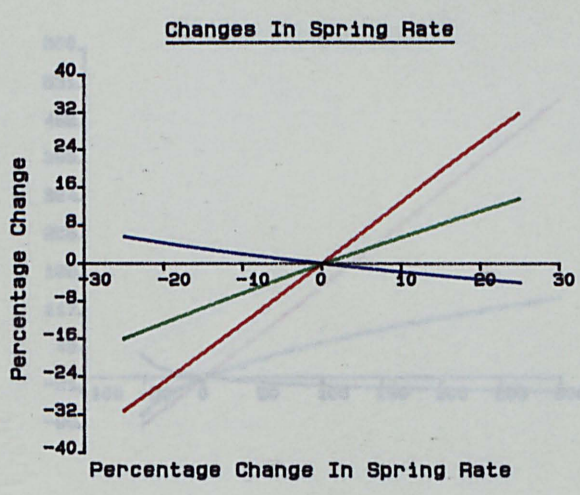

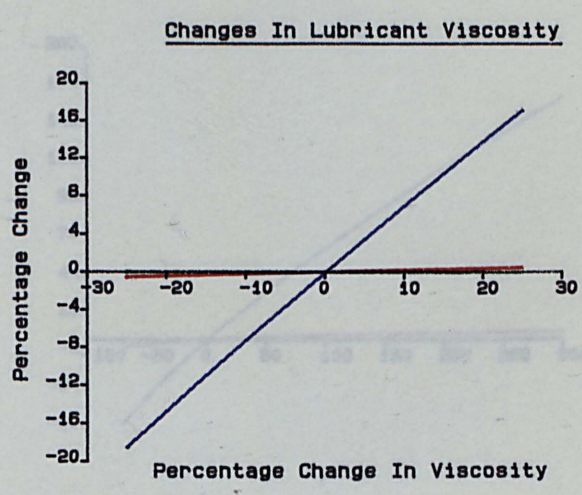

Frictional Power Loss
Hertzian Stress At Cam Nose
Lubricant Film Thickness At Cam Nose

Figure (5.3) Parametric Study for Cam and Flat Faced Follower (25 Hz).

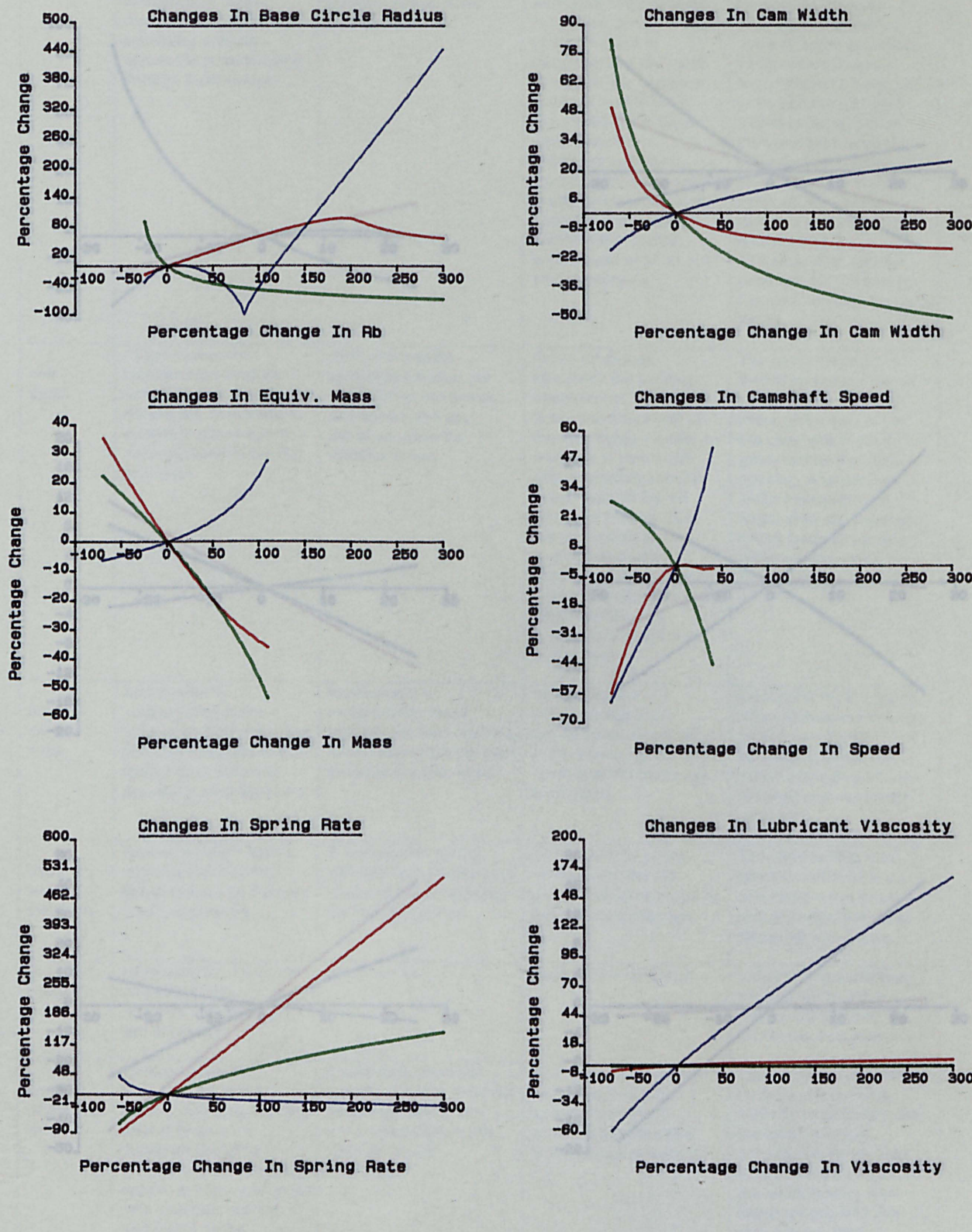

Figure (5.4) Parametric Study for Cam and Flat Faced Follower (41.67 Hz).

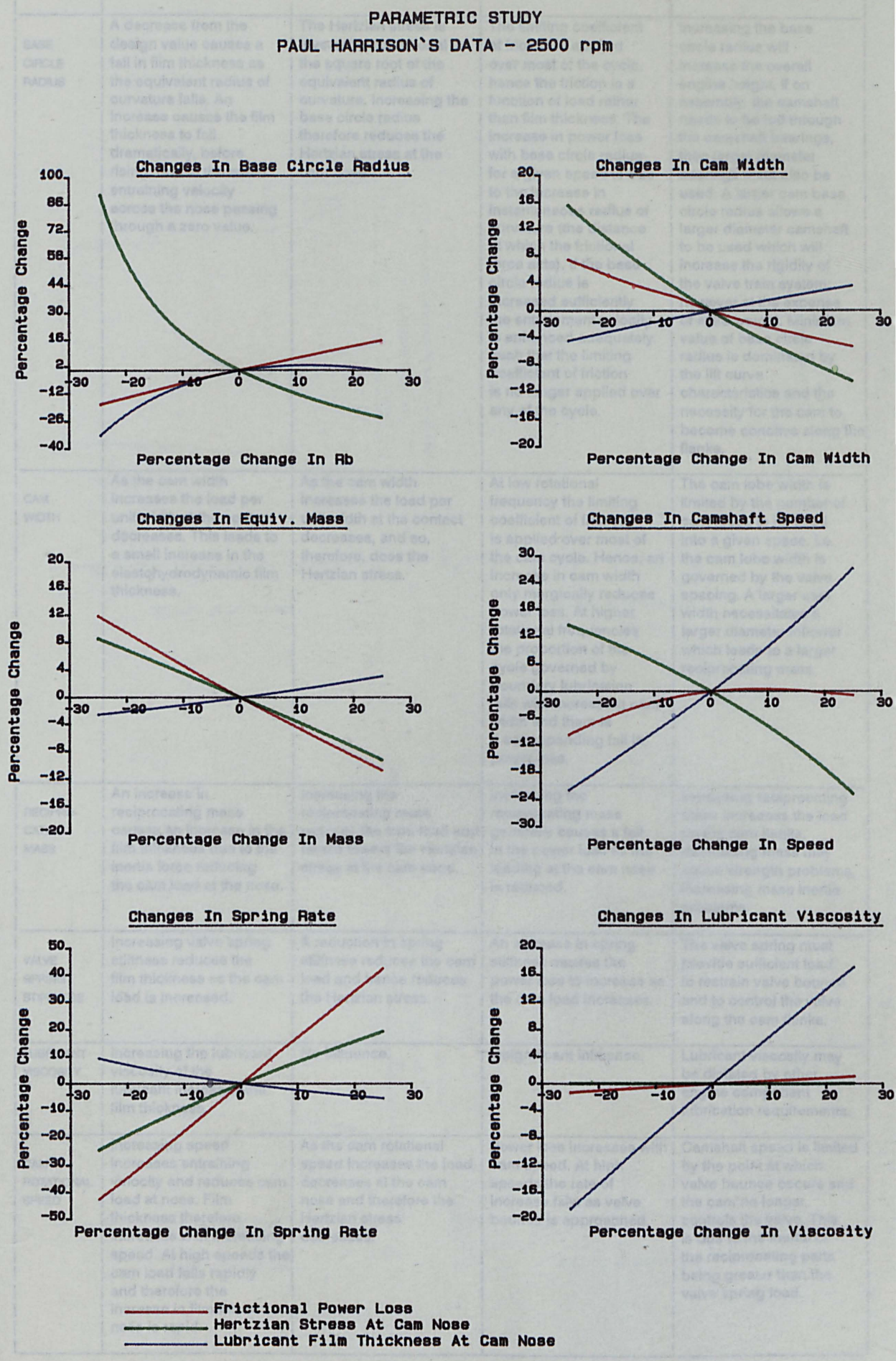

Figure (5.5) Parametric Study for Cam and Flat Faced Follower (41.67 Hz).

	MINIMUM FILM THICKNESS AT MAXIMUM LIFT POSITION	MAXIMUM HERTZIAN STRESS AT MAXIMUM LIFT POSITION	POWER LOSS	OTHER COMMENTS
BASE CIRCLE RADIUS	A decrease from the design value causes a fall in film thickness as the equivalent radius of curvature falls. An increase causes the film thickness to fall dramatically, before rising, due to the mean entraining velocity across the nose passing through a zero value.	The Hertzian stress is inversely proportional to the square root of the equivalent radius of curvature. Increasing the base circle radius therefore reduces the Hertzian stress at the cam nose.	The limiting coefficient of friction is applied over most of the cycle, hence the friction is a function of load rather than film thickness. The increase in power loss with base circle radius for a given speed is due to the increase in instantaneous radius of curvature (the distance at which the frictional force acts). If the base circle radius is increased sufficiently the entrainment velocity is enhanced adequately such that the limiting coefficient of friction is no longer applied over any of the cycle.	Increasing the base circle radius will increase the overall engine height. If on assembly, the camshaft needs to be fed through the camshaft bearings, then larger diameter bearings must also be used. A larger cam base circle radius allows a larger diameter camshaft to be used which will increase the rigidity of the valve train system; however at the expense of extra weight. Minimum value of base circle radius is dominated by the lift curve characteristics and the necessity for the cam to become concave along the flanks.
CAM WIDTH	As the cam width increases the load per unit width at the contact decreases. This leads to a small increase in the elastohydrodynamic film thickness.	As the cam width increases the load per unit width at the contact decreases, and so, therefore, does the Hertzian stress.	At low rotational frequency the limiting coefficient of friction is applied over most of the cam cycle. Hence, an increase in cam width only marginally reduces power loss. At higher rotational frequencies the proportion of the cycle governed by boundary lubrication falls with increasing cam width and there is a corresponding fall in power loss.	The cam lobe width is limited by the number of cam lobes to be fitted into a given space. i.e. the cam lobe width is governed by the valve spacing. A larger cam width necessitates a larger diameter follower which leads to a larger reciprocating mass.
RECIPRO-CATING MASS	An increase in reciprocating mass causes an increase in the film thickness due to the inertia force reducing the cam load at the nose.	Increasing the reciprocating mass reduces the cam load and hence lowers the Hertzian stress at the cam nose.	Increasing the reciprocating mass generally causes a fall in the power loss as the loading at the cam nose is reduced.	Increasing reciprocating mass increases the load on the cam flanks. decreasing mass may cause strength problems, increasing mass inertia problems.
VALVE SPRING STIFFNESS	Increasing valve spring stiffness reduces the film thickness as the cam load is increased.	A reduction in spring stiffness reduces the cam load and hence reduces the Hertzian stress.	An increase in spring stiffness causes the power loss to increase as the cam load increases.	The valve spring must provide sufficient load to restrain valve bounce and to control the valve along the cam flanks.
LUBRICANT VISCOSITY	Increasing the lubricant viscosity of the lubricant increases the film thickness.	No influence.	Insignificant influence.	Lubricant viscosity may be dictated by other engine component lubrication requirements.
CAM ROTATIONAL SPEED	Increasing speed increases entraining velocity and reduces cam load at nose. Film thickness therefore increases with increasing speed. At high speeds the cam load falls rapidly and therefore the increase in film thick-ness is rapid.	As the cam rotational speed increases the load decreases at the cam nose and therefore the Hertzian stress decreases.	Power loss increases with cam speed. At high speeds the rate of increase falls as valve bounce is approached.	Camshaft speed is limited by the point at which valve bounce occurs and the cam no longer controls the valve. This is due to the inertia of the reciprocating parts being greater than the valve spring load.

Table (5.1) Parametric Study Results Summary.

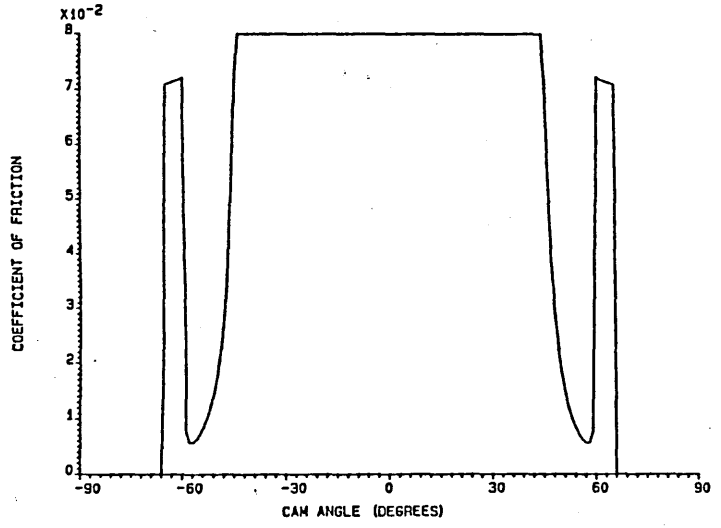

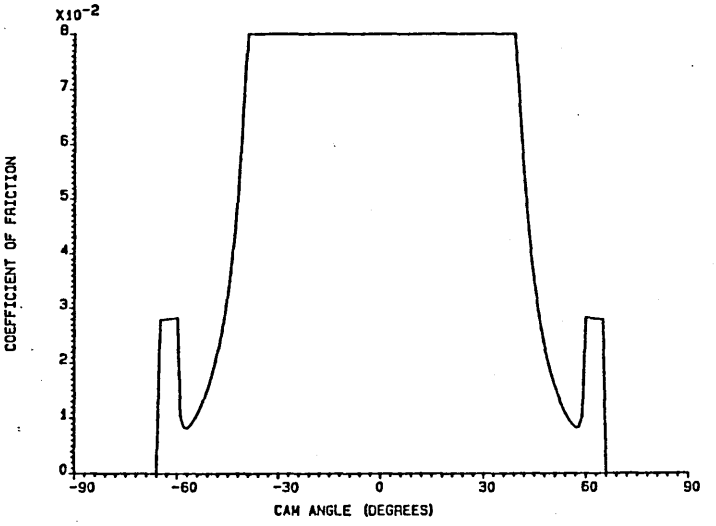

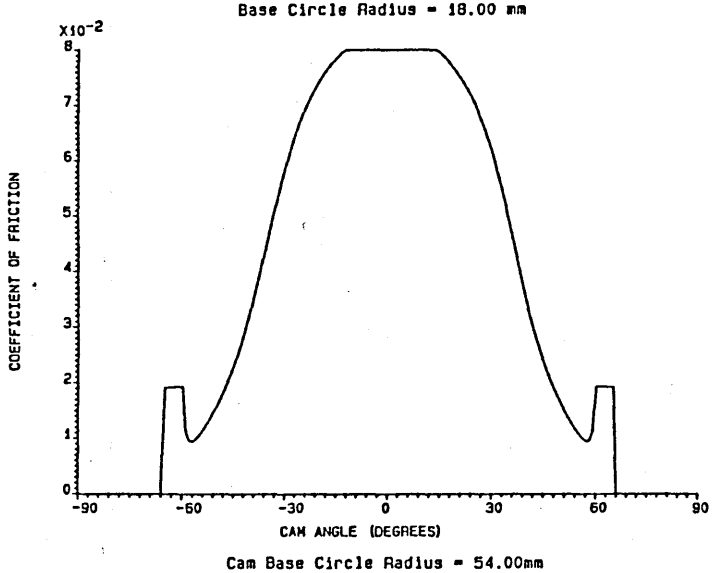

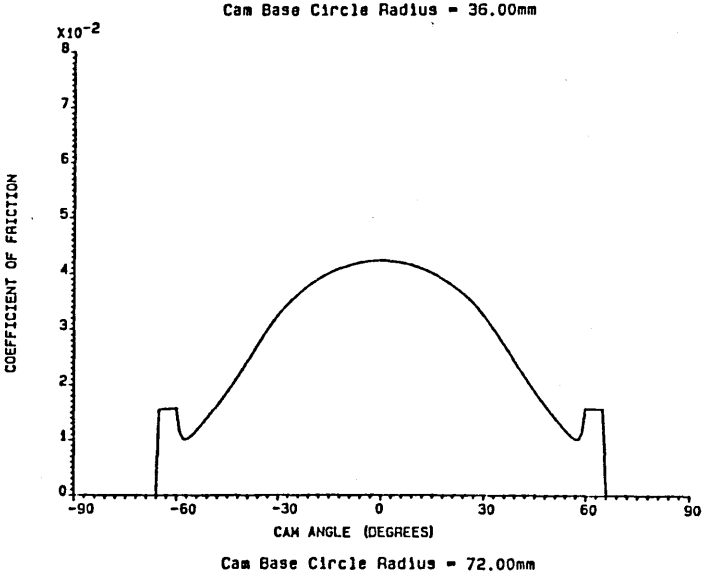

Figure (5.6) The Effect of Changes in Cam Base Circle Radius Upon the Coefficient of Friction.

Thus the minimum and central film thicknesses, (h_{min}) and (h_{cen}) respectively, fall dramatically before rising as (r_B) increases. This is due to their dependence upon (V_e). The sliding velocity (V_S) increases (as (V_C) is increased). The maximum Hertzian stress at the contact, (p_{max}), decreases as there is a decrease in (R).

The frictional traction (F) is proportional to (V_S), inversely proportional to (h_{cen}), and proportional to the viscosity of the lubricant (which is proportional to the exponential of (p_{max})). The maximum Hertzian stress, however, is proportional to the inverse of the square root of (r_B). The frictional torque is proportional to the frictional traction and to the perpendicular distance from the cam centre to the frictional force vector. This distance is equal to the cam lift plus the base circle radius and therefore increases as (r_B) increases.

Increasing (r_B) causes an increase in the frictional power loss up to a point where the lubricant film thickness at the cam nose becomes significant due to the increasing entraining velocities and a downward trend then occurs due to the limiting coefficient of friction no longer being applied (again see Figure (5.6)).

The lubricant film thickness at the cam nose can be forced to a zero value, due to the entraining velocity being zero. Figure (5.1h) showing the contact point surface velocities can be used to illustrate this point. The entraining velocity at the cam nose is usually negative (if a system is adopted whereby the entraining velocity is positive at the flanks), but as (r_B) is increased the entraining velocity around the whole cycle is increased and can reach a point where it is positive around the whole cycle. The entraining velocity at the cam nose is given by the expression

$$V_e = \omega(2\cdot\frac{d^2l}{d\phi^2} + l + r_B).$$

It can be seen that when

$$r_B = -(2\cdot\frac{d^2l}{d\phi^2} + l)$$

then

$$V_e = 0$$

and hence the lubricant film thickness at the nose is zero if squeeze film effects are neglected.

The film thickness at the cam nose decreases as (r_B) is increased up to the point at which the entraining velocity is positive for the whole cycle. It is worthwhile to note that if a large enough base circle is used then the points of theoretical zero film thickness do not occur. The physical size of the camshaft would however be prohibitive if this design was adopted.

It should be noted that the computer program used for the parametric studies searches for the minimum allowable value of (r_B) which occurs at a decrease of just over 20% from the datum value. The minimum value of (r_B) is limited by the cam radius of curvature required to attain the lift and acceleration characteristics of the cam. As (r_B) is decreased a point is reached at which the cam must be concave to attain the lift characteristics. This is clearly impossible for a flat faced follower.

5.2.2 Changes in Cam Lobe Width.

As would be expected the Hertzian stress at the cam nose will decrease as the cam lobe width is increased as the load per unit width of cam lobe decreases. The film thickness increases and the frictional power loss decreases as the cam lobe width is increased also as a direct result of this. The designer is limited in choice of cam width by the spacing between valves.

5.2.3 Changes in Reciprocating Mass.

As the reciprocating mass increases, the inertia of the system increases and hence the loading at the cam nose decreases. (It should be noted though that the loading on the flanks is increased). This decreased loading leads to a larger film thickness and obviously reduced Hertzian stress at the cam nose. On the flanks the film thickness is decreased due to the increased loading. As the film thickness is less sensitive to load than the power loss, the overall power loss is reduced.

5.2.4 Changes in Camshaft Speed.

As the camshaft speed is increased the loading on the cam nose becomes less due to the negative lift acceleration. It can be seen (Figure (5.4)) that valve bounce occurs at approximately 60 Hz (3600 rpm (7200 rpm crank)). (Again it should be noted that the loading on the flanks increases). This reduced loading leads to a larger film thickness and reduced Hertzian stress at the cam nose. The power loss increases as the cam speed increases as would be expected. At speeds approaching those at which valve bounce occurs the power loss starts to fall as the loading becomes so small on the cam nose. This then levels off as the coefficient of friction around the cam flanks approaches and then assumes the limiting value due to the increasing loads (see Figure (5.7)).

5.2.5 Changes in Spring Rate.

As the spring rate increases the Hertzian stress at the cam nose increases due to the load increasing. This increase in load also causes the film thickness to decrease but the changes are not large ((h_{min}) only being proportional to load raised to the power -0.13 in the Dowson and Higginson (1977) relationship). The frictional power loss increases as both (h_{cen}) and (p_{max}) increase. If the limiting coefficient of friction is applied throughout the majority of the cycle, then the change in frictional power loss would be expected to be almost linear with change in spring stiffness.

5.2.6 Changes in Lubricant Viscosity.

As would be expected the lubricant film thickness will be enhanced by a higher lubricant viscosity. The increase in viscosity will have no effect upon the Hertzian stress and little effect upon the power loss. The small changes in power loss are due to (h_{cen}) increasing proportionally to the viscosity to the power 0.72 (using the Dowson and Higginson equation). If we then note that the frictional power loss is proportional to the viscosity and inversely proportional to (h_{cen}) we can see that overall the power loss is proportional to the viscosity to the power 0.28.

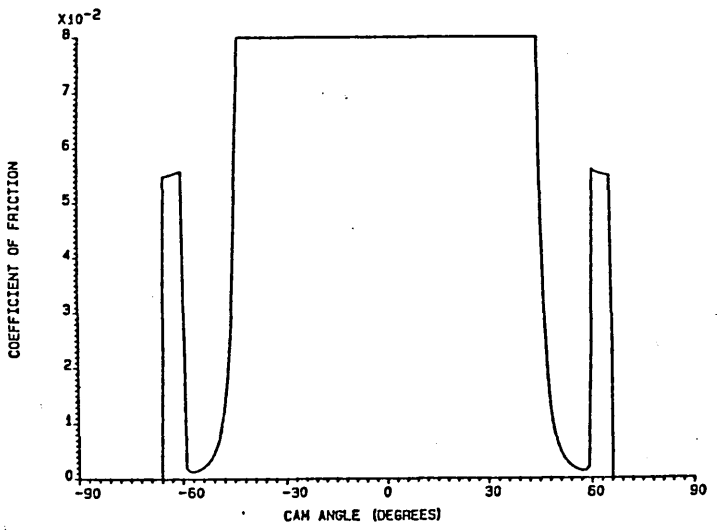

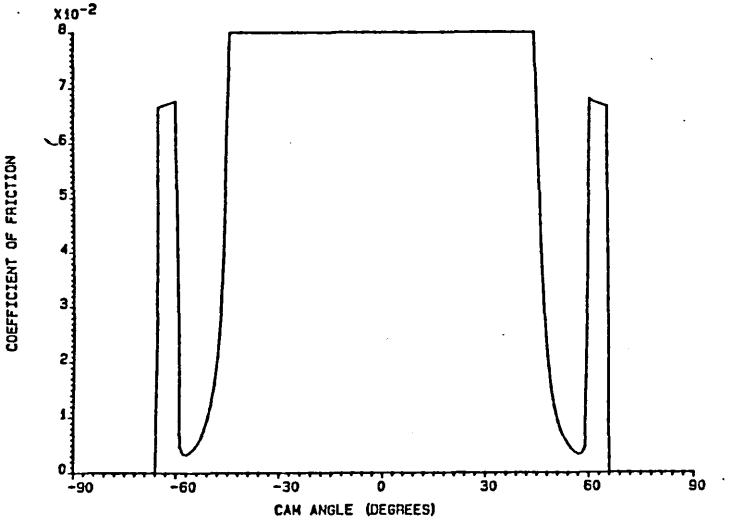

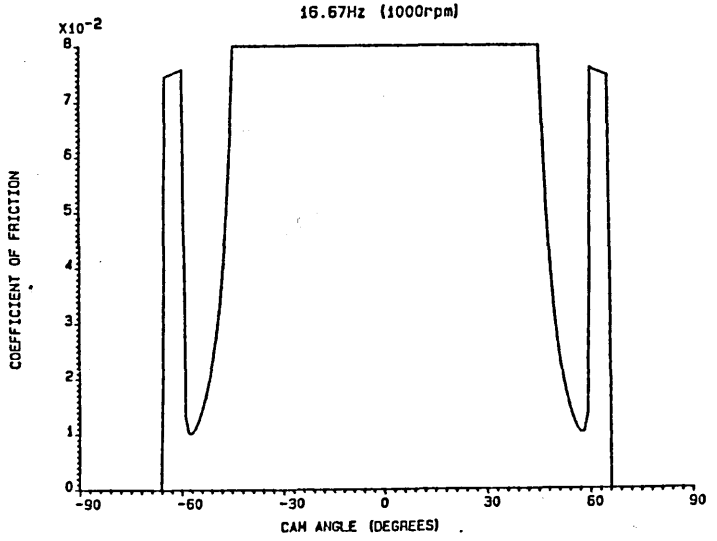

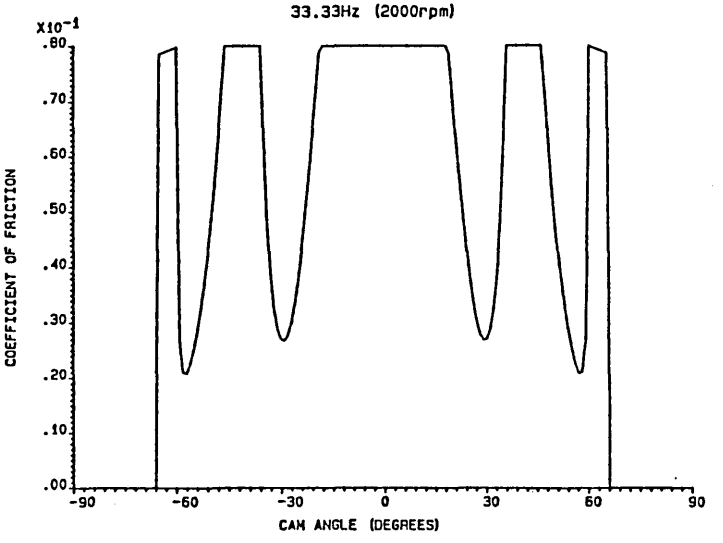

Figure (5.7) The Effect of Changes in Camshaft Rotational Speed Upon Coefficient of Friction.

5.3 A Parametric Study of a Cam and Centrally Pivoted Follower System.

The cam and follower adopted for this study are in use in a current engine (Rover 2600) and are the same as those studied by Lim et al (1983), the valve lift data being given as a fitted exponential function:

$$l_v = \exp\left[a + b\phi + c\phi^2 + d\phi^3 + e\phi^4 + f\phi^5 + g\phi^6\right]$$

where

$a = 2.317111$ $\quad b = -0.8104 \times 10^{-3}$

$c = -1.526837$ $\quad d = -0.1552985$

$e = -1.789897$ $\quad f = 0.1171634$

$g = -0.2422081$

The geometry of the system is shown in Figure (5.8). This is taken to be the datum condition. Each design parameter was changed from its datum, whilst the others remained constant, and the effect upon the frictional power loss, lubricant film thickness and Hertzian stress at the cam nose was studied. The parameters changed were:

(a) Cam base circle radius,
(b) Cam width,
(c) Equivalent mass at the valve,
(d) Camshaft speed,
(e) Spring rate, and
(f) Follower radius of curvature.

As the cam base circle radius is changed, the valve train geometry must be changed to take up the clearance between the cam and follower. This is done by moving the follower contact radius along the line between its centre of curvature and the cam centre of rotation. i.e.

$$\gamma_B + \kappa = \text{constant},$$

and,

$$\psi_B + \phi_B + \kappa = \text{constant}.$$

Similarly, as the follower radius of curvature is changed the position of its centre of curvature moves in the direction of the line from the cam centre of rotation to the follower contact face's centre of curvature. i.e. B, D, r_B, κ, and $(\psi_B + \phi_B)$ are constant.

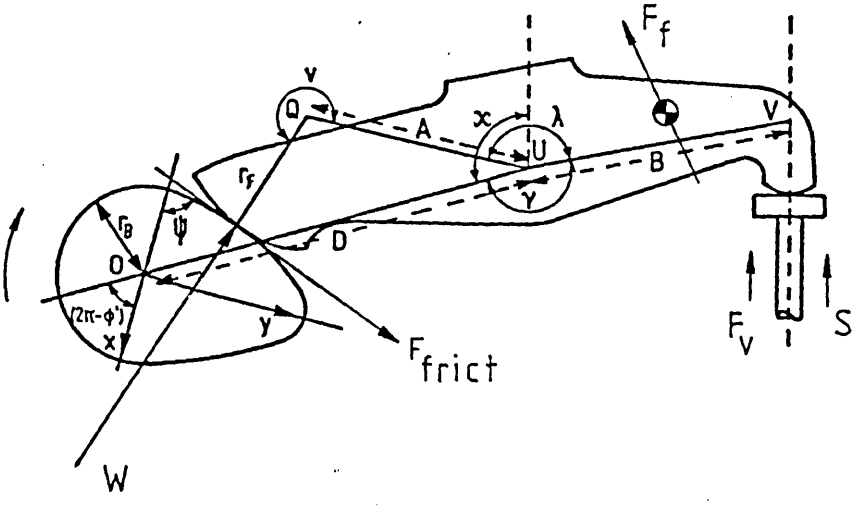

A = 50.06 mm		$\nu'_{follower}$	= 0.3
B = 54.00 mm		ν'_{cam}	= 0.3
D = 74.27 mm		$E_{follower}$	= 207 GNm^{-2}
r_f = 35.56 mm		E_{cam}	= 207 GNm^{-2}
r_B = 14.30 mm		α	= 15.0 nm^2N^{-1}
κ = 107.5°		η_0	= 0.013 Nsm^{-2}
λ = 140.0°		k	= 60.0 kN/m
L = 17.00 mm		M	= 0.10 kg
		δ	= 4.00 mm

Figure (5.8) Geometry of Rover 2300 Valve Train

Figure (5.9) shows the cam operating characteristics at the datum condition for a camshaft speed of 41.67 Hz (2500 rpm). A parametric study was carried out at 25 Hz (1500 rpm) and 41.67 Hz (2500 rpm). Figures (5.10), (5.11), (5.12) and (5.13) show the results of the parametric studies. Figure (5.10) shows a parametric study at 25 Hz (1500 rpm) where each design parameter was changed from its datum value by -70% through to +300% (0% change being the datum value, -50% change being half the datum value, +50% being one and a half times the datum value, etc). Figure (5.11) shows the same study with more realistic changes in the parameters of -25% through to +25%. Figures (5.12) and (5.13) show a parametric study at 41.67 Hz (2500 rpm) with changes in the parameters of -70% through to +300% and -25% through to +25% respectively.

The effect of changing each of the parameters is discussed in turn below and is summarised in Table (5.2).

5.3.1 Changes in Cam Base Circle Radius.

Figure (5.9h) shows how the surface velocities at the point of contact vary throughout the cam cycle. The curve describing the lubricant entrainment velocity ($V_c + V_f$) is of a typical shape for a centrally pivoted follower. It can be seen that the pivoting follower introduces a degree of asymmetry to the curve (compared to the symmetrical curve for a the flat faced follower system). This makes the interpretation of the results from the parametric study a little more difficult to interpret than those for the cam and flat faced follower where, for example the lubricant film thickness across the whole of the cam nose was almost constant. In the parametric studies the value of the film thickness at the position of maximum lift is taken to be indicative of the film thickness across the whole of the cam nose. Due to the asymmetry the film thickness is not constant across the nose, however, it can be seen from Figure (5.9f) that the lubricant film thickness at the maximum lift position gives a reasonable approximation to the mean value of the film thickness across the whole of the cam nose. It should be noted that the value for the Hertzian stress at the cam nose is not the maximum value across the nose (see Figure (5.9j).

CAM OPERATING CHARACTERISTICS

ROVER 2300 - 2500rpm

Cam Base Radius (mm)	=	14.30
Maximum Valve Lift (mm)	=	10.15
Cam Width (mm)	=	17.00
Rotational Speed (rpm)	=	2500.0
Spring Stiffness (kN/m)	=	60.000
Initial Spring Disp. (mm)	=	4.0
Equiv. Mass At Valve (kg)	=	.100
Lubricant Viscosity (Ns/m^2)	=	.013
Press. Visc. Coeff. (/Pa)	=	15.0E-9
Youngs Mod. (Cam) (GPa)	=	207.0
Youngs Mod. (Foll.) (GPa)	=	207.0
Poissons Ratio (Cam)	=	.30
Poissons Ratio (Foll.)	=	.30
Frictional Power Loss (W)	=	58.78

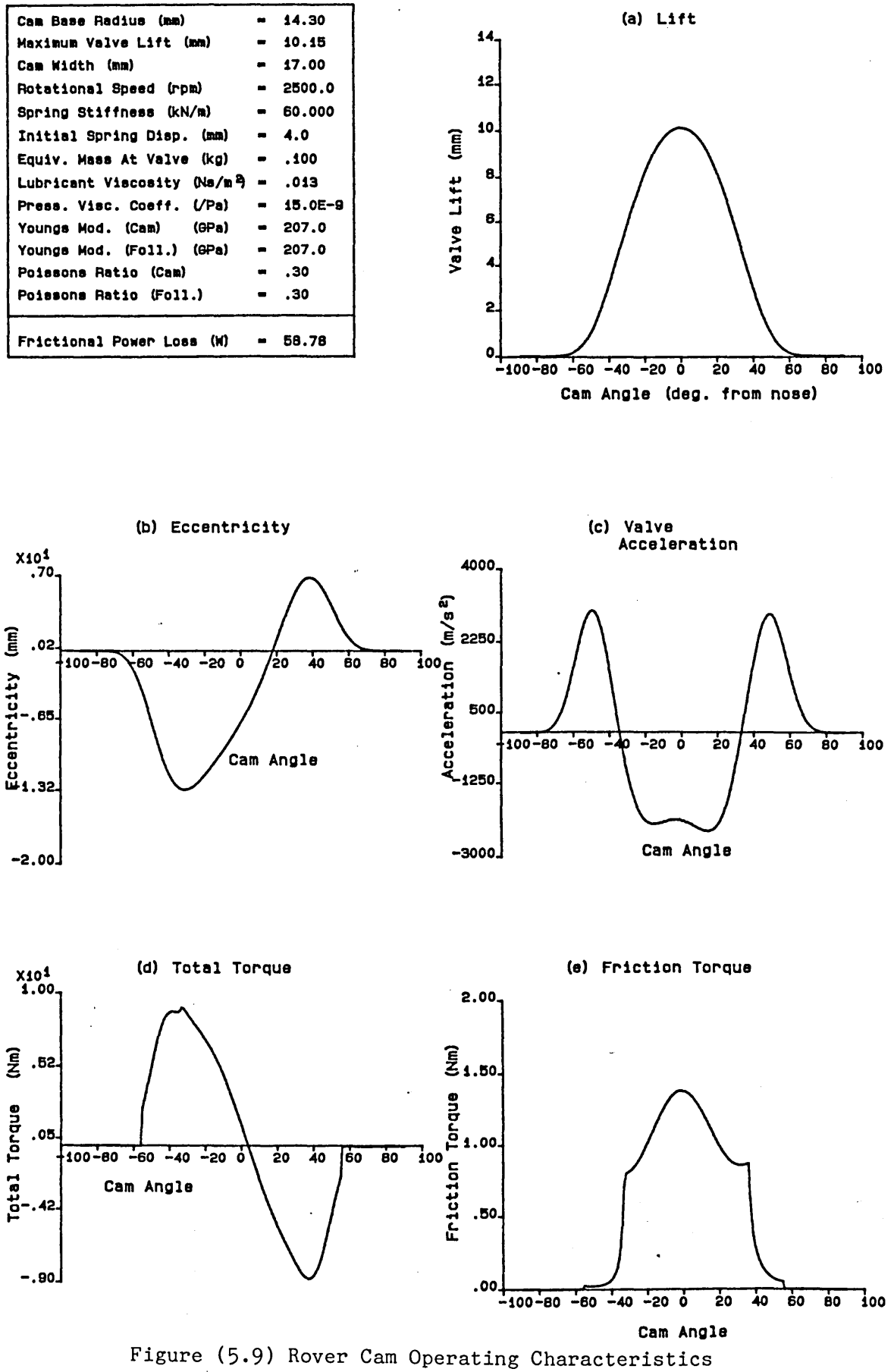

Figure (5.9) Rover Cam Operating Characteristics at the Datum Conditions (41.67 Hz).

(f) Film Thickness against Cam Angle

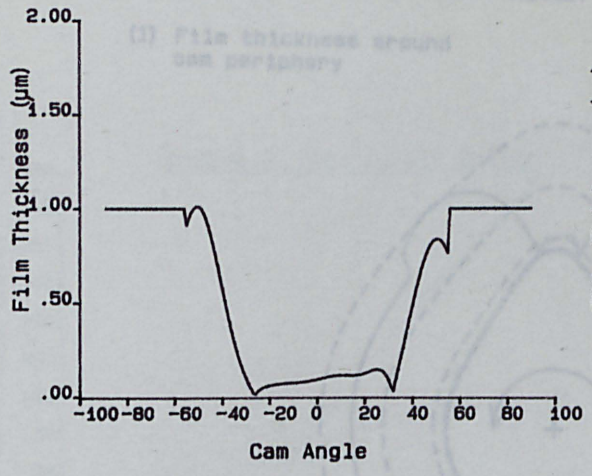

(g) Film Thickness against Eccentricity

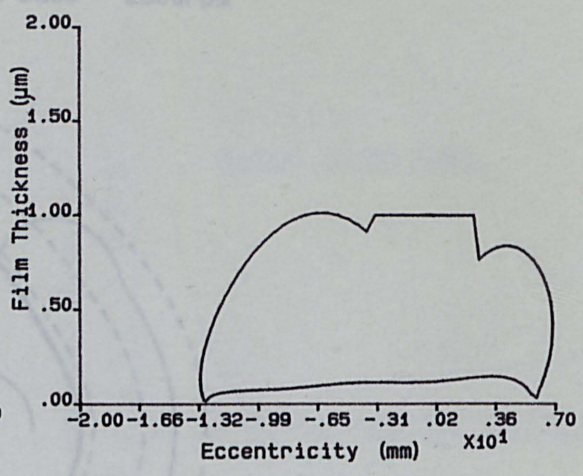

(h) Contact Point Surface Velocities

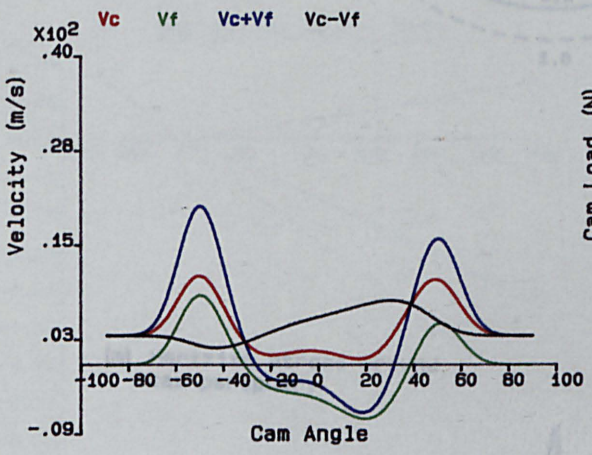

(i) Load

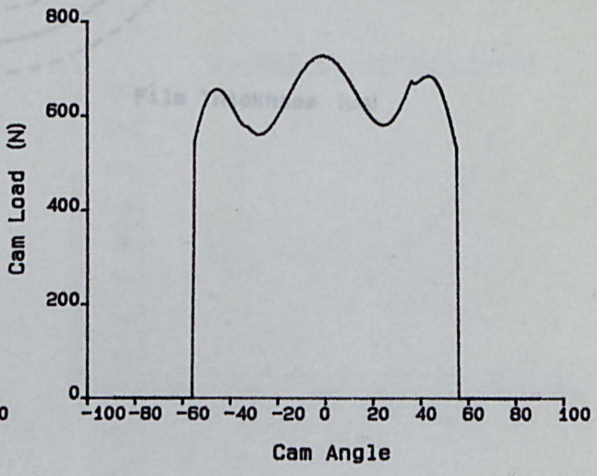

(j) Hertzian Stress

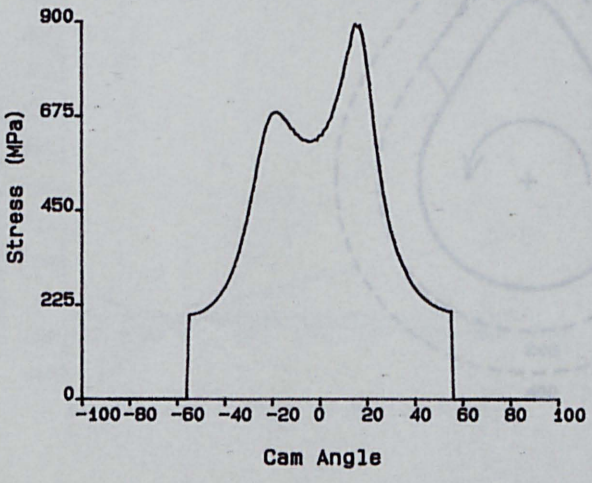

(k) Equivalent Radius Of Curvature

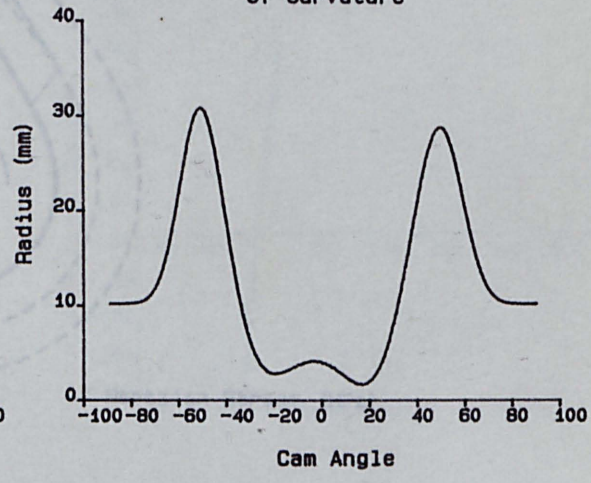

Figure (5.9 continued).

CAM OPERATING CHARACTERISTICS
ROVER 2300 - 2500rpm

(l) Film thickness around cam periphery

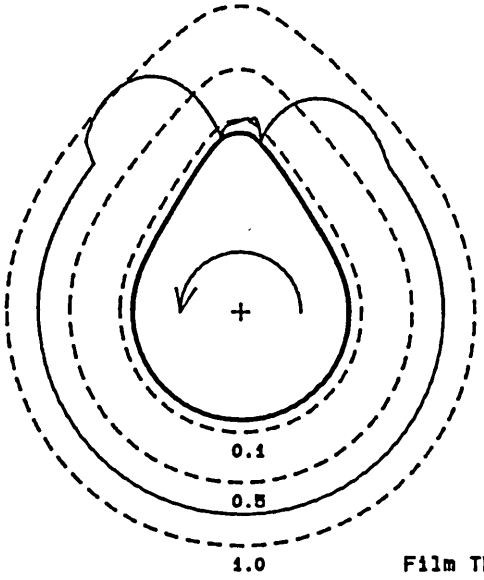

(m) Hertzian stress around cam periphery

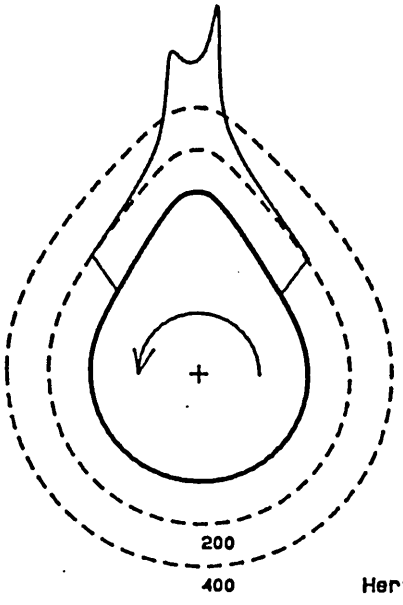

Figure (5.9 continued).

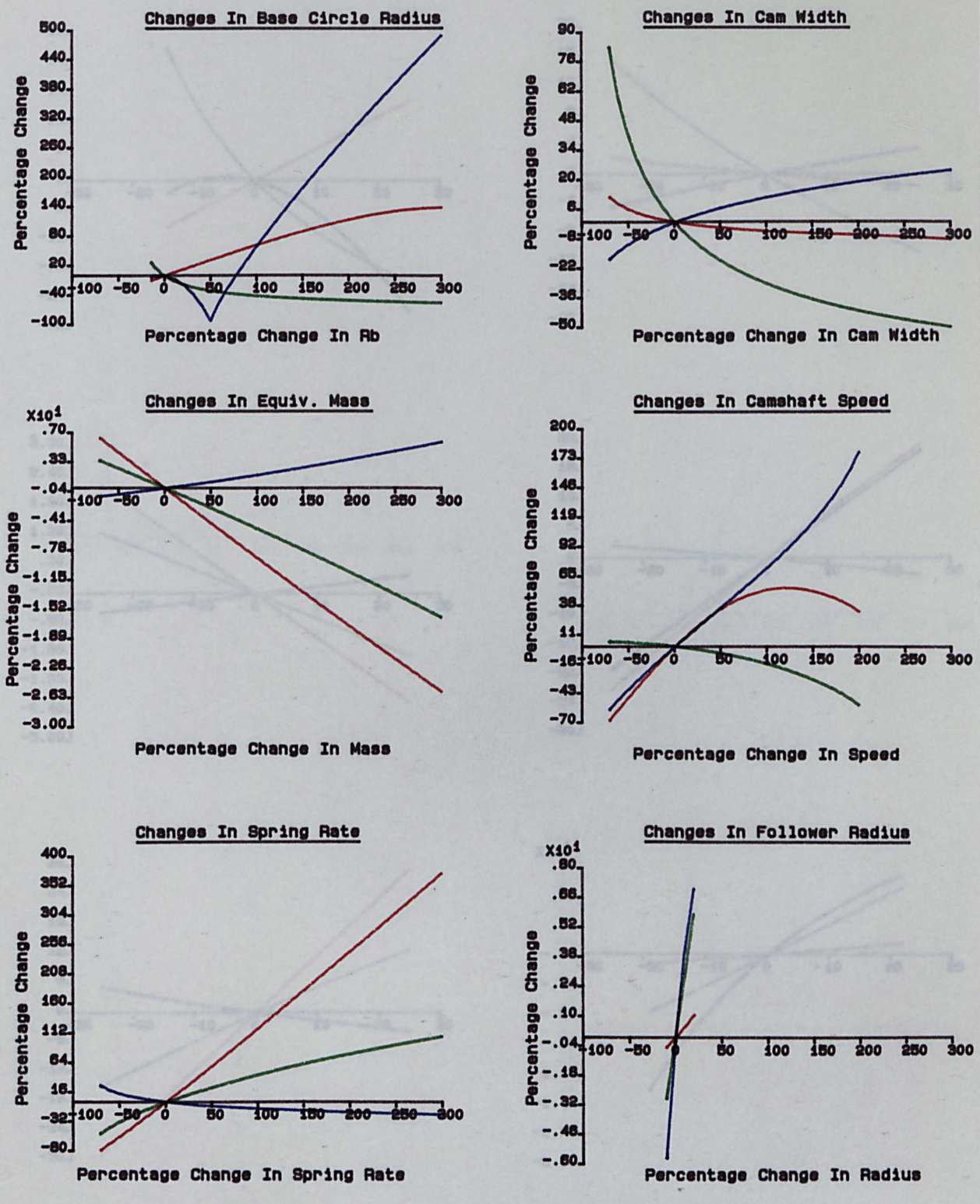

Figure (5.10) Parametric Study for Rover 2300 (25 Hz).

PARAMETRIC STUDY
ROVER 2300 - 1500rpm

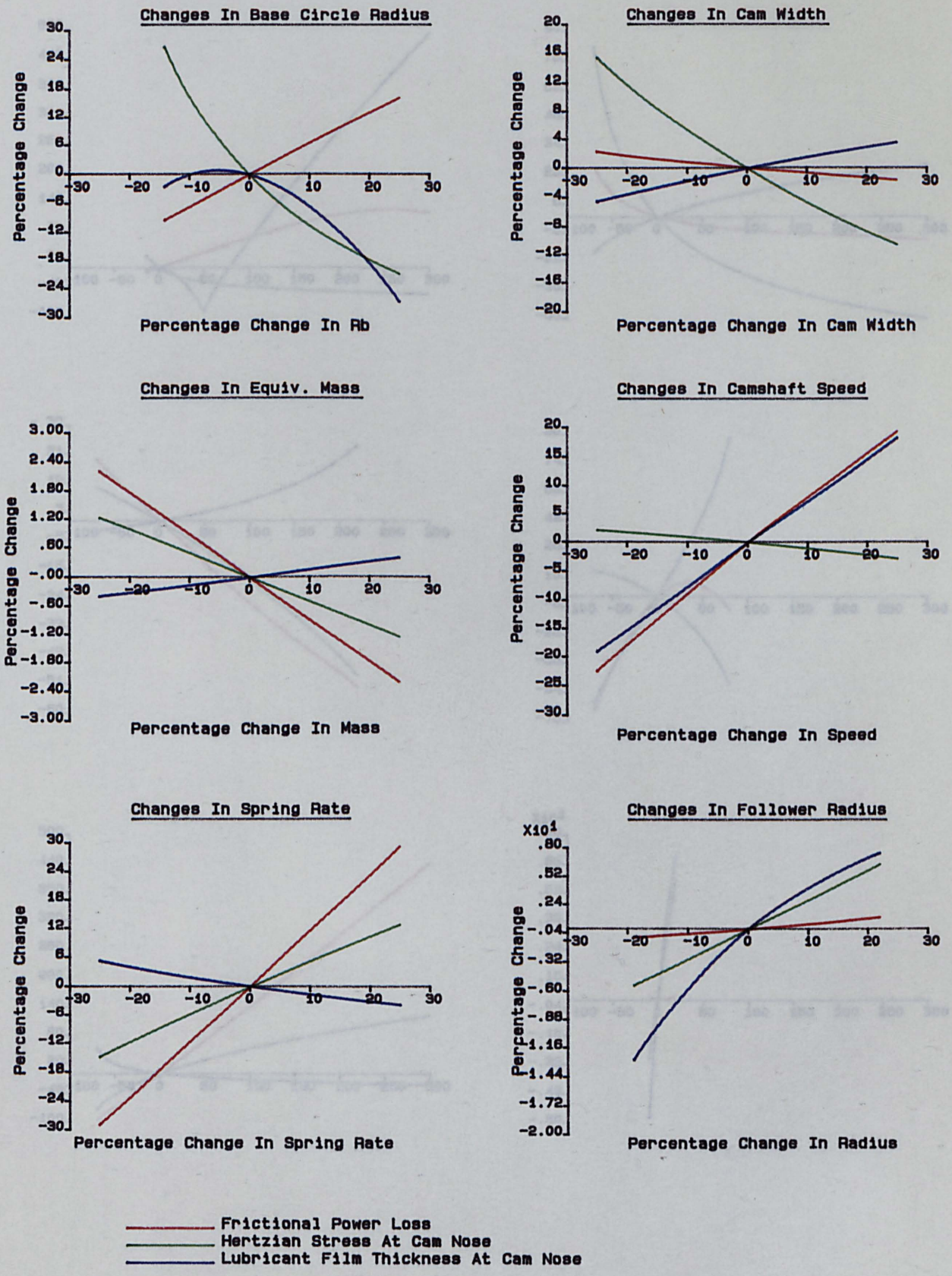

Figure (5.11) Parametric Study for Rover 2300
(25 Hz)

PARAMETRIC STUDY
ROVER 2300 - 2500rpm

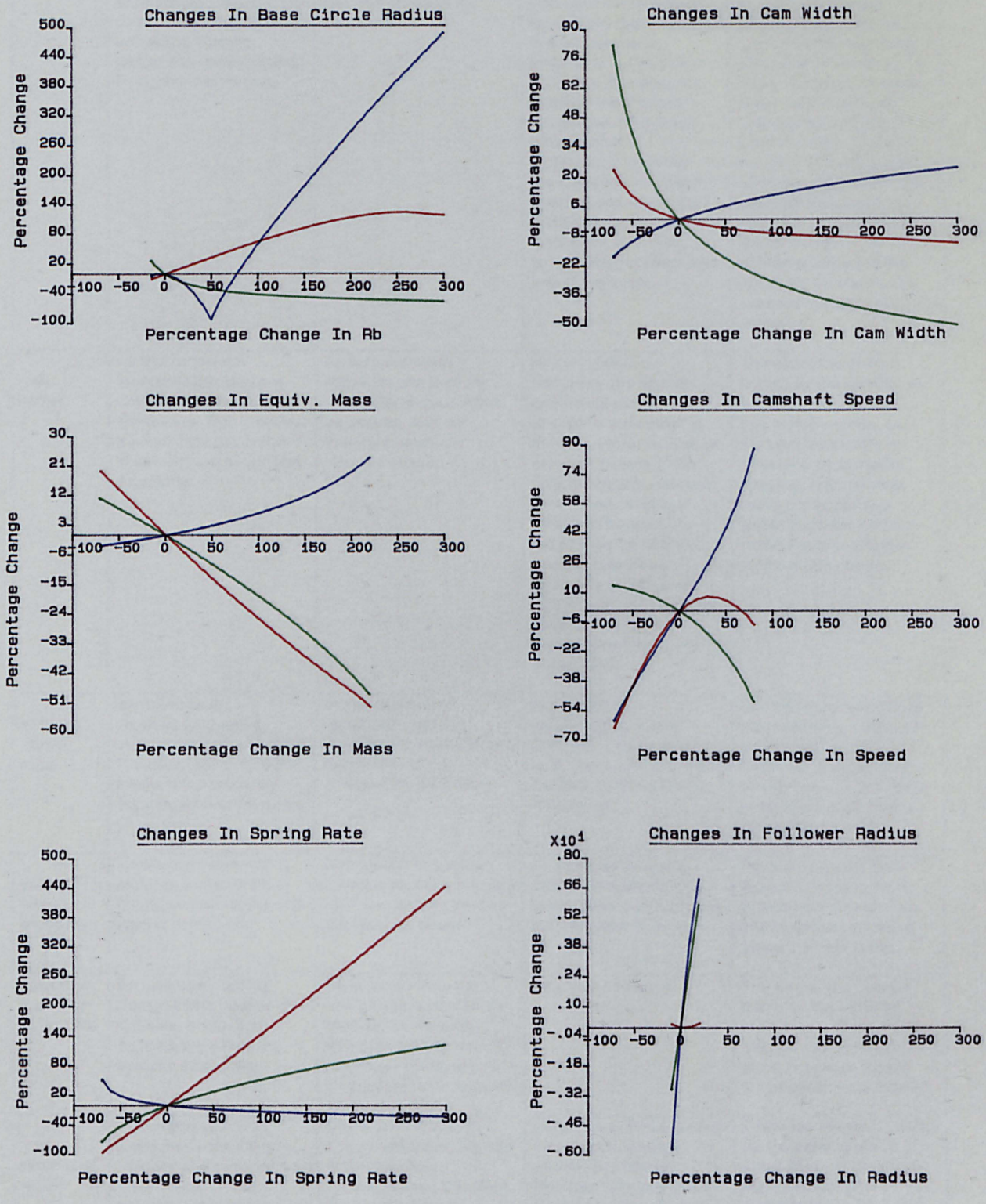

Figure (5.12) Parametric Study for Rover 2300 (41.67 Hz).

PARAMETRIC STUDY

ROVER 2300 - 2500rpm

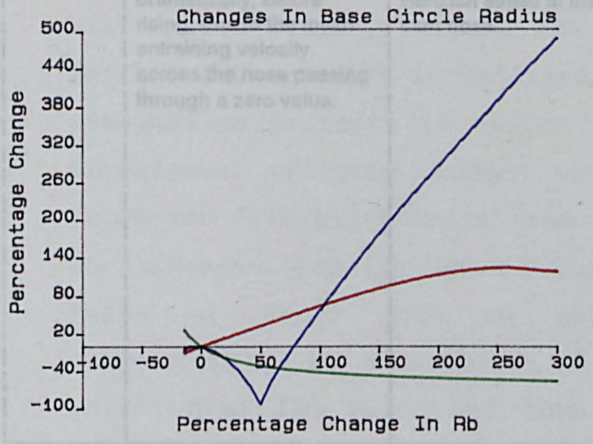

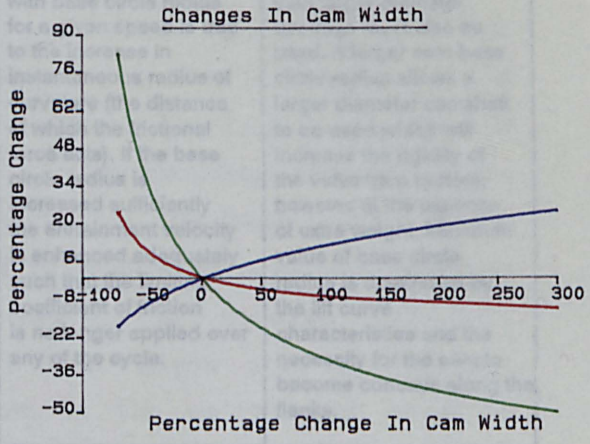

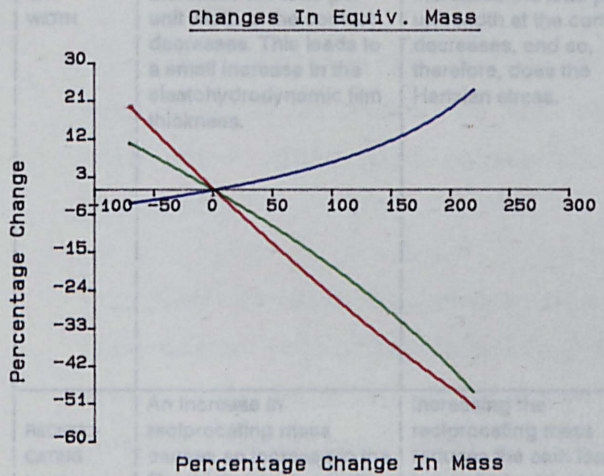

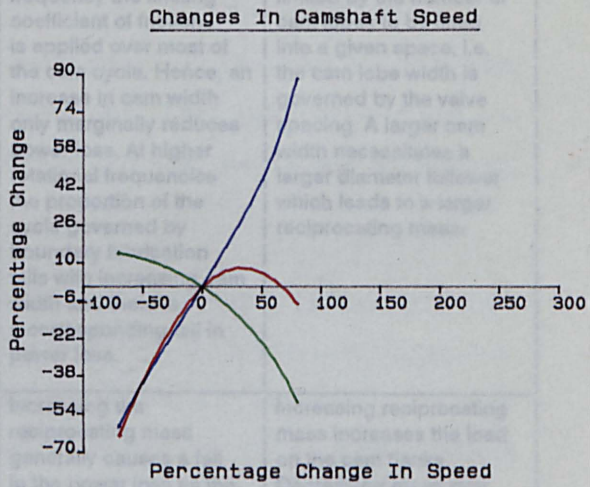

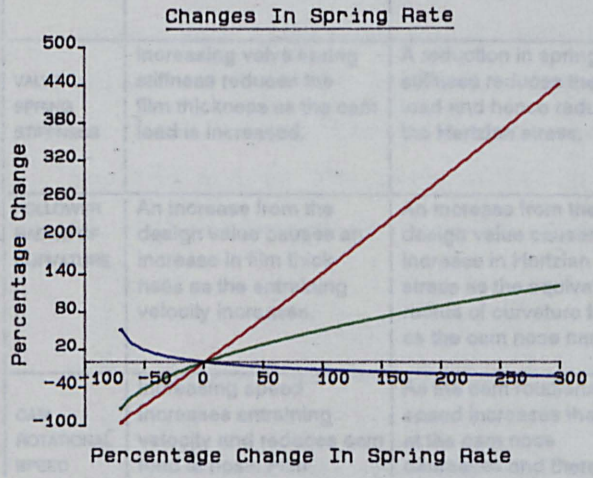

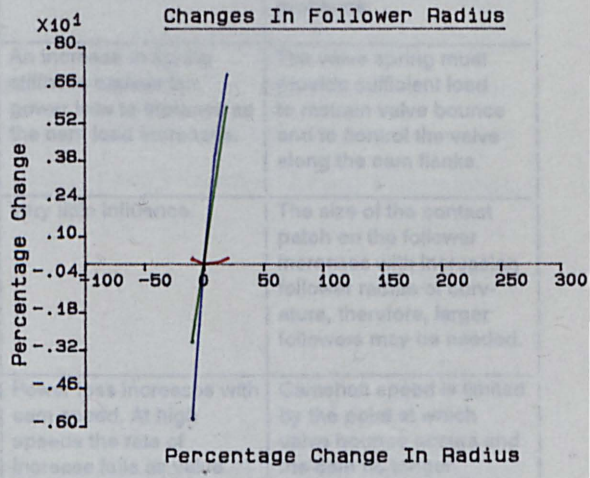

Frictional Power Loss
Hertzian Stress At Cam Nose
Lubricant Film Thickness At Cam Nose

Figure (5.13) Parametric Study for Rover 2300 (41.67 Hz).

	MINIMUM FILM THICKNESS AT MAXIMUM LIFT POSITION	MAXIMUM HERTZIAN STRESS AT MAXIMUM LIFT POSITION	POWER LOSS	OTHER COMMENTS
BASE CIRCLE RADIUS	A decrease from the design value causes a fall in film thickness as the equivalent radius of curvature falls. An increase causes the film thickness to fall dramatically, before rising, due to the mean entraining velocity across the nose passing through a zero value.	The Hertzian stress is inversely proportional to the square root of the equivalent radius of curvature. Increasing the base circle radius therefore reduces the Hertzian stress at the cam nose.	The limiting coefficient of friction is applied over most of the cycle, hence the friction is a function of load rather than film thickness. The increase in power loss with base circle radius for a given speed is due to the increase in instantaneous radius of curvature (the distance at which the frictional force acts). If the base circle radius is increased sufficiently the entrainment velocity is enhanced adequately such that the limiting coefficient of friction is no longer applied over any of the cycle.	Increasing the base circle radius will increase the overall engine height. If on assembly, the camshaft needs to be fed through the camshaft bearings, then larger diameter bearings must also be used. A larger cam base circle radius allows a larger diameter camshaft to be used which will increase the rigidity of the valve train system; however at the expense of extra weight. Minimum value of base circle radius is dominated by the lift curve characteristics and the necessity for the cam to become concave along the flanks.
CAM WIDTH	As the cam width increases the load per unit width at the contact decreases. This leads to a small increase in the elastohydrodynamic film thickness.	As the cam width increases the load per unit width at the contact decreases, and so, therefore, does the Hertzian stress.	At low rotational frequency the limiting coefficient of friction is applied over most of the cam cycle. Hence, an increase in cam width only marginally reduces power loss. At higher rotational frequencies the proportion of the cycle governed by boundary lubrication falls with increasing cam width and there is a corresponding fall in power loss.	The cam lobe width is limited by the number of cam lobes to be fitted into a given space. I.e. the cam lobe width is governed by the valve spacing. A larger cam width necessitates a larger diameter follower which leads to a larger reciprocating mass.
RECIPRO-CATING MASS	An increase in reciprocating mass causes an increase in the film thickness due to the inertia force reducing the cam load at the nose.	Increasing the reciprocating mass reduces the cam load and hence lowers the Hertzian stress at the cam nose.	Increasing the reciprocating mass generally causes a fall in the power loss as the loading at the cam nose is reduced.	Increasing reciprocating mass increases the load on the cam flanks. Decreasing mass may cause strength problems, increasing mass inertia problems.
VALVE SPRING STIFFNESS	Increasing valve spring stiffness reduces the film thickness as the cam load is increased.	A reduction in spring stiffness reduces the cam load and hence reduces the Hertzian stress.	An increase in spring stiffness causes the power loss to increase as the cam load increases.	The valve spring must provide sufficient load to restrain valve bounce and to control the valve along the cam flanks.
FOLLOWER RADIUS OF CURVATURE	An increase from the design value causes an increase in film thick-ness as the entraining velocity increases.	An increase from the design value causes an increase in Hertzian stress as the equivalent radius of curvature falls as the cam nose narrows.	Very little influence.	The size of the contact patch on the follower increases with increasing follower radius of curv-ature, therefore, larger followers may be needed.
CAM ROTATIONAL SPEED	Increasing speed increases entraining velocity and reduces cam load at nose. Film thickness therefore increases with increasing speed. At high speeds the cam load falls rapidly and therefore the increase in film thick-ness is rapid.	As the cam rotational speed increases the load at the cam nose decreases and therefore the Hertzian stress decreases.	Power loss increases with cam speed. At high speeds the rate of increase falls as valve bounce is approached.	Camshaft speed is limited by the point at which valve bounce occurs and the cam no longer controls the valve. This is due to the inertia of the reciprocating parts being greater than the valve spring load.

Table (5.2) Rover 2300 Parametric Study Results Summary.

As the base circle radius of the cam is increased from its datum value the cam radius of curvature increases and so the velocity of the point of contact relative to the cam surface (V_c) increases which leads to an increase in the entrainment velocity, in that the curve in Figure (5.9h) rises. This means that the magnitude of the entrainment velocity around the cam nose falls at first until the entrainment velocity is positive (i.e. in the same direction as the cam surface velocity (V_c)) for the whole of the cam cycle. As the entrainment velocity changes we see a corresponding change in the lubricant film thickness at the cam nose. As the base circle radius is increased from its datum value the film thickness at the cam nose falls at first down to zero (neglecting squeeze effects), corresponding to the value of (r_B) that gives zero entrainment velocity at the nose, and then rises as the entrainment velocity increases.

The increases in the radius of curvature of the cam at the cam nose also contributes to the enhancement of the lubricant film at this point. This also causes the decrease in the Hertzian stress at the nose.

The frictional power loss increases almost linearly with increasing (r_B). The limiting coefficient of friction is applied around the majority of the cam cycle at both 25 Hz and 41.67 Hz camshaft rotational speed with the datum value of (r_B). The loading at the contact does not change as (r_B) changes but the radius at which the frictional traction force is applied increases as (r_B) increases, thus the frictional power loss increases. At very high values of (r_B) the lubricant entrainment velocity is enhanced to such an extent that the limiting coefficient of friction is no longer applied and so the rate at which the frictional power loss increases as (r_B) increases levels off.

5.3.2 Changes in Cam Width.

As would be expected the Hertzian stress at the cam nose will decrease as the cam lobe width is increased because the load per unit width decreases. The film thickness at the cam nose and the frictional power loss decrease as a direct result of this.

5.3.3 Changes in Reciprocating Mass.

Increasing the reciprocating mass at the valve causes higher loads on the cam flanks but smaller loads at the cam nose. As the load at the cam nose decreases with increasing reciprocating mass the lubricant film thickness will increase and the Hertzian stress will decrease. The frictional power loss decreases due to the limiting coefficient of friction being applied around the cam nose and so the power loss is proportional to the normal load around this portion of the cam which represents the majority of the cam cycle (time wise).

5.3.4 Changes in Camshaft Speed.

The acceleration of the valve around the cam nose is negative. Therefore as the camshaft speed increases the valve acceleration becomes more negative and the contact load at the cam decreases. A point is reached as the speed is increased at which the inertia of the valve becomes so great that the cam and follower part and valve bounce occurs. (It should be noted that the loading on the cam flanks increases as the camshaft speed increases). This decrease in load at the cam nose leads to an increase in lubricant film thickness and a decrease in Hertzian stress. At lower camshaft speeds the frictional power loss increases with speed as would be expected. As the speed increases the loading on the cam nose becomes less and less until a point is reached at which the limiting coefficient of friction is no longer applied around the nose and so the power loss starts to fall with increasing speed. It should be noted that this relationship between the camshaft speed and frictional power loss is highly dependent upon the valve lift curve. A lift curve producing very high negative accelerations around the cam nose, as seen here, causes this portion of the lift curve to dominate the overall power loss around the cam cycle. If however a cam lift curve which produces relatively low negative accelerations around the cam nose is used then the contribution of the power loss at the cam flanks becomes more important as will be seen in the parametric studies in the next section.

5.3.5 Changes in Spring Rate.

As the spring rate is increased the loading at the cam/follower interface increases and so the Hertzian stress at the cam nose increases. This increase in load also causes the lubricant film thickness to decrease. The changes in lubricant film thickness are not large ((h_{min}) only being proportional to load to the power -0.13 (Dowson and Higginson (1977)). The frictional power loss increases as both (h_{cen}) and (p_{max}) increase. As the limiting coefficient of friction is applied throughout the majority of the cam cycle the change in frictional power loss with changing spring stiffness is almost linear.

5.3.6 Changes in Follower Radius of Curvature.

Changing the follower radius of curvature necessitates a change in the valve train geometry as explained earlier. This causes the cam profile to be changed, and so the radius of curvature of the cam also changes. As the follower radius of curvature is decreased the cam nose becomes broader and the cam flanks become flatter and flatter until they eventually become concave and finally the maximum cam concavity is reached (this is equal to the minimum allowable radius of the grinding wheel used to machine the cam). As the follower radius of curvature is increased the nose of the cam becomes narrower until it becomes a sharp edge with zero radius of curvature.

The Hertzian stress at the cam nose increases as the follower radius of curvature increases because the radius of curvature at the cam nose becomes smaller. The film thickness at the cam nose increases with increasing follower radius of curvature as the entrainment velocity is enhanced. The entrainment velocity increases as the velocity of the point of contact relative to the follower surface (V_f) is directly proportional to the follower radius of curvature. The frictional power loss changes very little with changing follower radius of curvature.

It should be noted that the extent of the cam's travel across the follower face increases proportionally to the follower radius of

curvature. This will require a larger area of the follower surface to be ground and may necessitate a larger follower.

5.4 A Parametric Study of a Cam and End Pivoted Follower System.

The cam and follower mechanism used in this study is in use in a current production car engine (the Ford 2.01 Pinto engine as fitted to certain of the Sierra and Granada range of cars). The engine is a four cylinder in-line engine using two valves per cylinder operated by a single overhead camshaft via finger followers. During its early years on the market it suffered badly from camshaft failures characterised by severe scuffing of the cam and followers. This situation was overcome to a satisfactory level by using better cam and follower materials and by increasing oil flow to the cam/follower contact by fitting a spray-bar. A redesign of the lubricant galleys also helped by feeding oil to the contact immediately at engine start up, the previous design having suffered from starvation at start up. The geometry of the system is shown in Figure (5.14). The cam lift data is given in Appendix (E).

The above data is taken as the datum condition. Again the effect of changing cam base circle radius, cam width, equivalent reciprocating mass, camshaft speed, spring rate and follower radius of curvature has been investigated. Each of the parameters was changed in turn whilst keeping the rest constant. The valve lift curve remained the same throughout; the cam profile being altered to effect this. Each parameter was changed from its datum value by decreasing its magnitude by 70% and observing the effects upon lubricant film thickness and Hertzian stress at the cam nose, and frictional power loss at intervals of 10% through to a 300% increase in the parameter magnitude from its datum value. Parametric studies were also undertaken using the more realistic changes of -25% and +25% at 1% intervals. Figure (5.15) shows the cam operating characteristics at the datum condition for a camshaft speed of 41.67 Hz (2500 rpm), whilst Figures (5.16) and (5.17) show the results of parametric studies carried out with a camshaft speed of 25 Hz (1500 rpm), and Figures (5.18) and (5.19) show the results of parametric studies carried out with a camshaft speed of 41.67 Hz (2500 rpm). As the value of base circle radius is changed the geometry must be

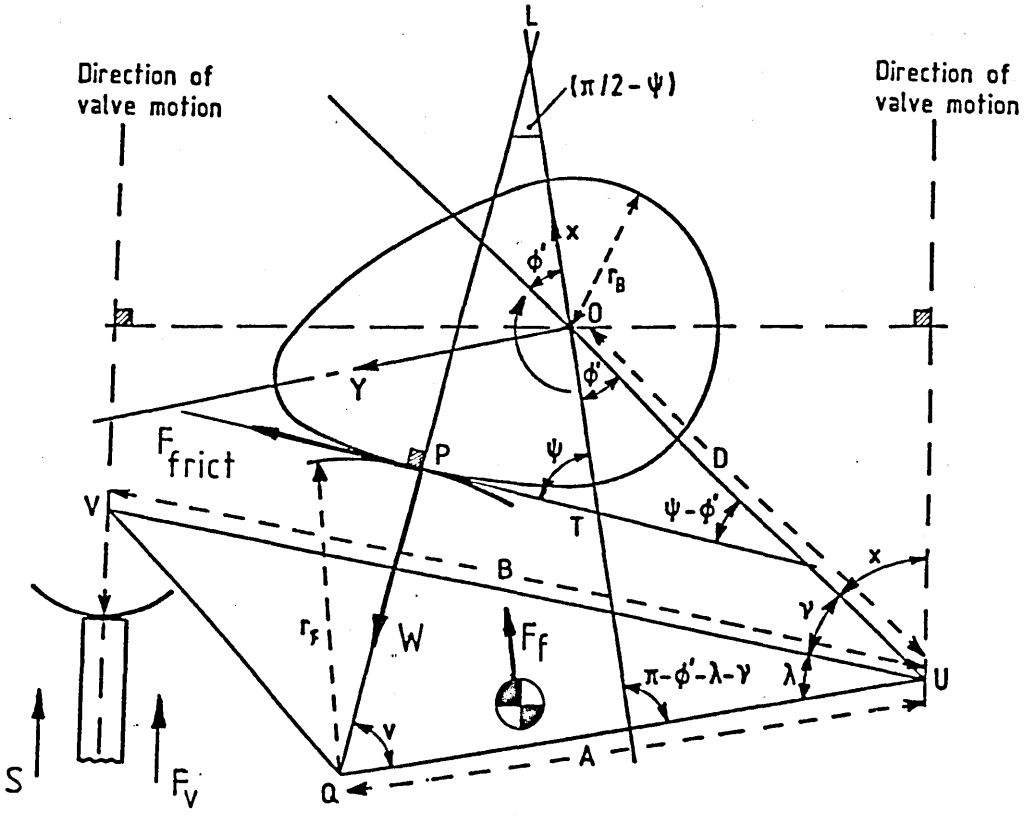

A = 51.80 mm		$\nu'_{follower}$	= 0.3
B = 61.80 mm		ν'_{cam}	= 0.3
D = 46.20 mm		$E_{follower}$	= 207 GNm^{-2}
r_f = 44.00 mm		E_{cam}	= 207 GNm^{-2}
r_B = 15.00 mm		α	= 22.0 nm^2N^{-1}
κ = 39.7°		η_0	= 0.013 Nsm^{-2}
λ = 31.9°		k	= 40.0 kN/m
L = 21.00 mm		M	= 0.15 kg
		δ	= 11.0 mm

Figure (5.14) Geometry of Ford 2.0 litre Pinto Valve Train

CAM OPERATING CHARACTERISTICS
SIERRA 2.0L - INLET: 2500 rpm

Cam Base Radius (mm)	=	15.00
Maximum Valve Lift (mm)	=	10.35
Cam Width (mm)	=	21.00
Rotational Speed (rpm)	=	2500.0
Spring Stiffness (kN/m)	=	40.000
Initial Spring Disp. (mm)	=	11.0
Equiv. Mass At Valve (kg)	=	.148
Lubricant Viscosity (Ns/m^2)	=	.013
Press. Visc. Coeff. (/Pa)	=	22.0E-9
Youngs Mod. (Cam) (GPa)	=	207.0
Youngs Mod. (Foll.) (GPa)	=	207.0
Poissons Ratio (Cam)	=	.29
Poissons Ratio (Foll.)	=	.29
Frictional Power Loss (W)	=	166.14

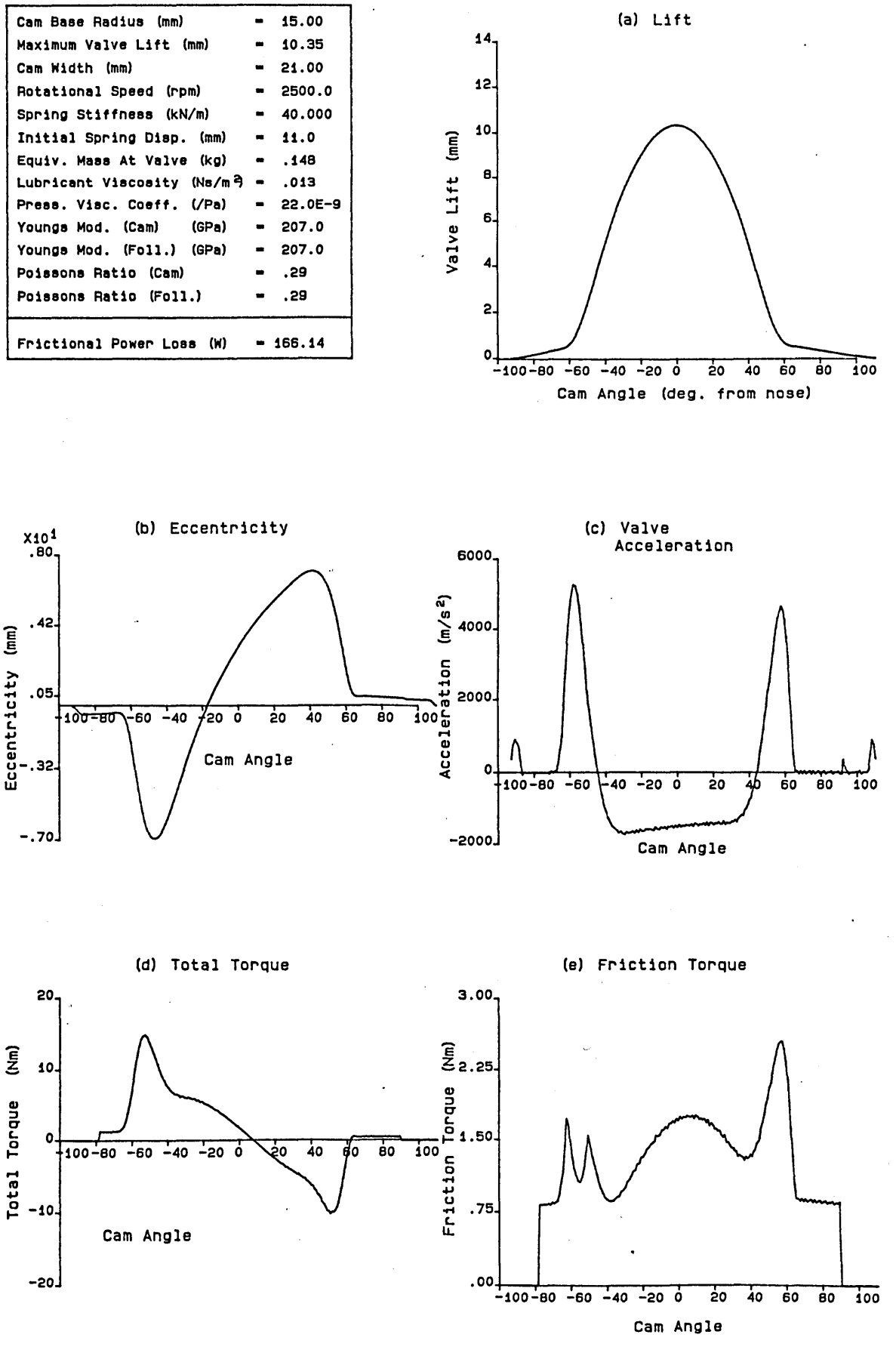

Figure (5.15) Ford 2.01 Pinto Cam Operating Characteristics at the Datum Conditions (41.67 Hz).

(f) Film Thickness against Cam Angle

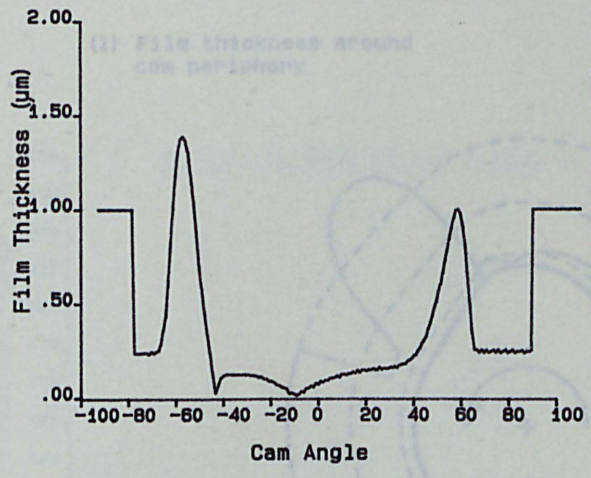

(g) Film Thickness against Eccentricity

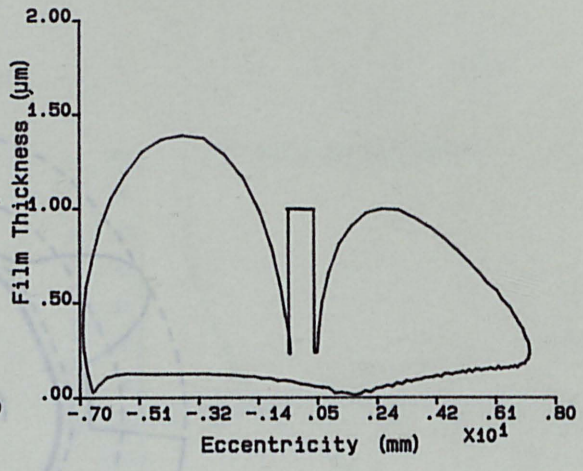

(h) Contact Point Surface Velocities

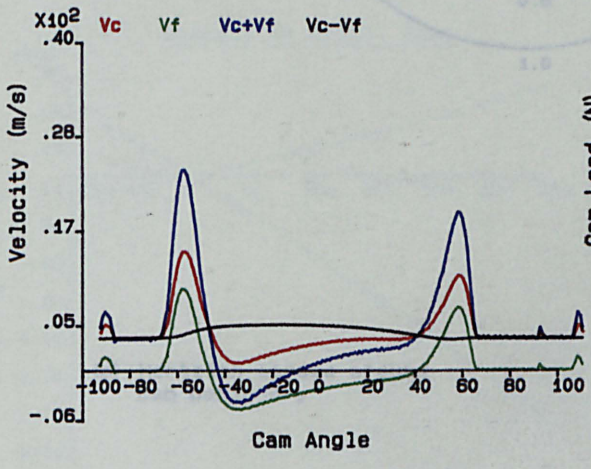

(i) Load

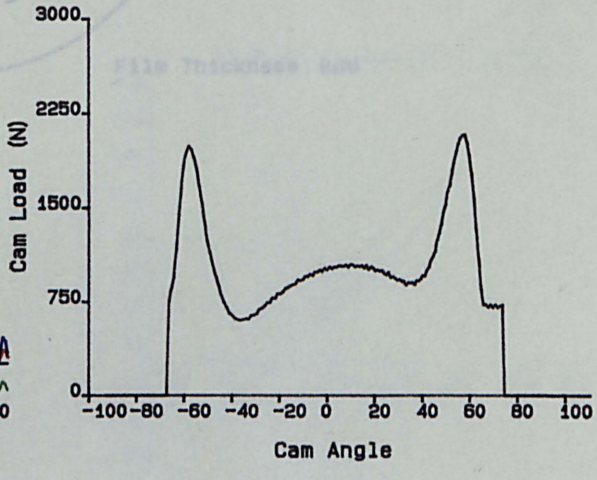

(j) Hertzian Stress

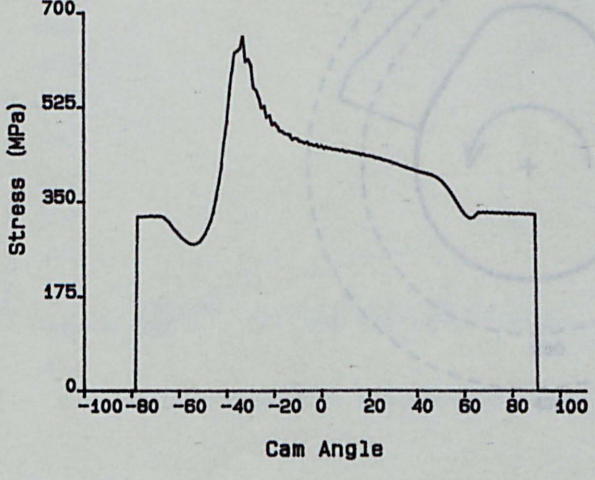

(k) Equivalent Radius Of Curvature

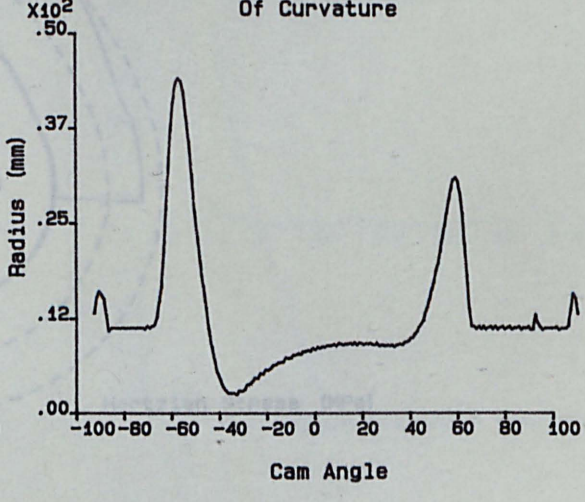

Figure (5.15 continued).

CAM OPERATING CHARACTERISTICS
SIERRA 2.0L - INLET: 2500 rpm

(l) Film thickness around cam periphery

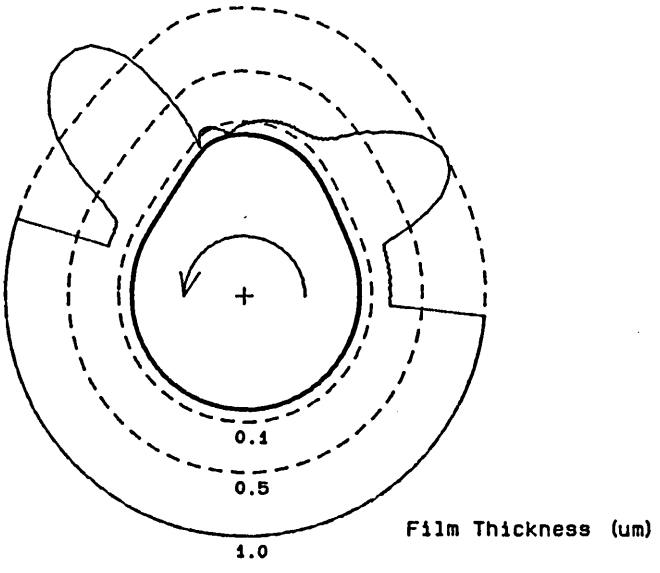

(m) Hertzian stress around cam periphery

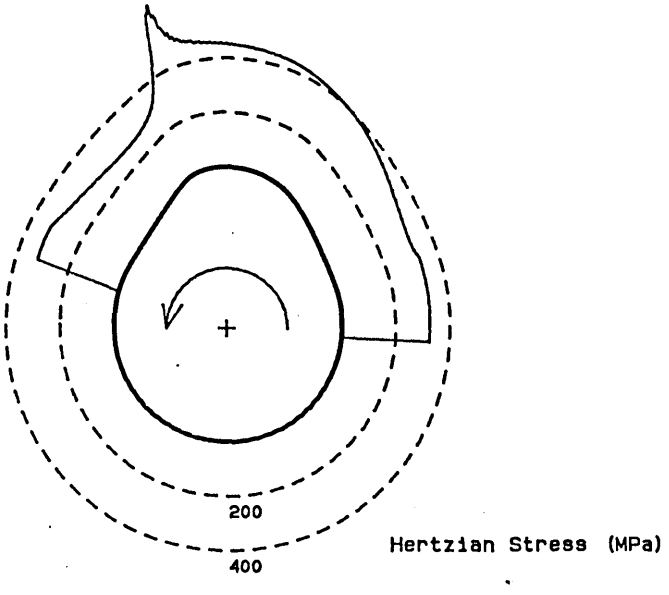

Figure (5.15 continued).

PARAMETRIC STUDY

SIERRA 2.0L - INLET: 1500 rpm

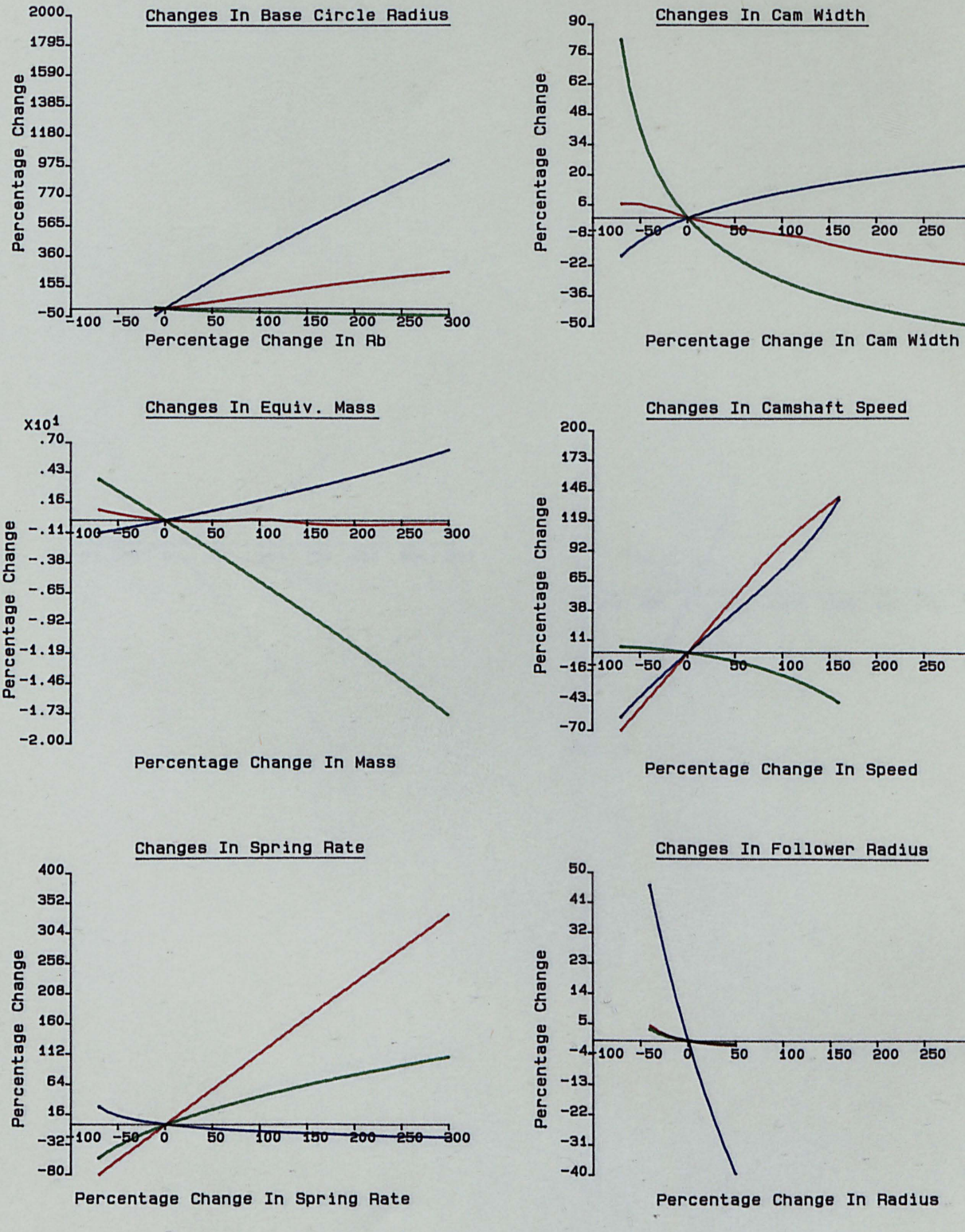

Figure (5.16) Parametric Study for Ford 2.01 Pinto (25 Hz).

PARAMETRIC STUDY
SIERRA 2.0L - INLET: 1500 rpm

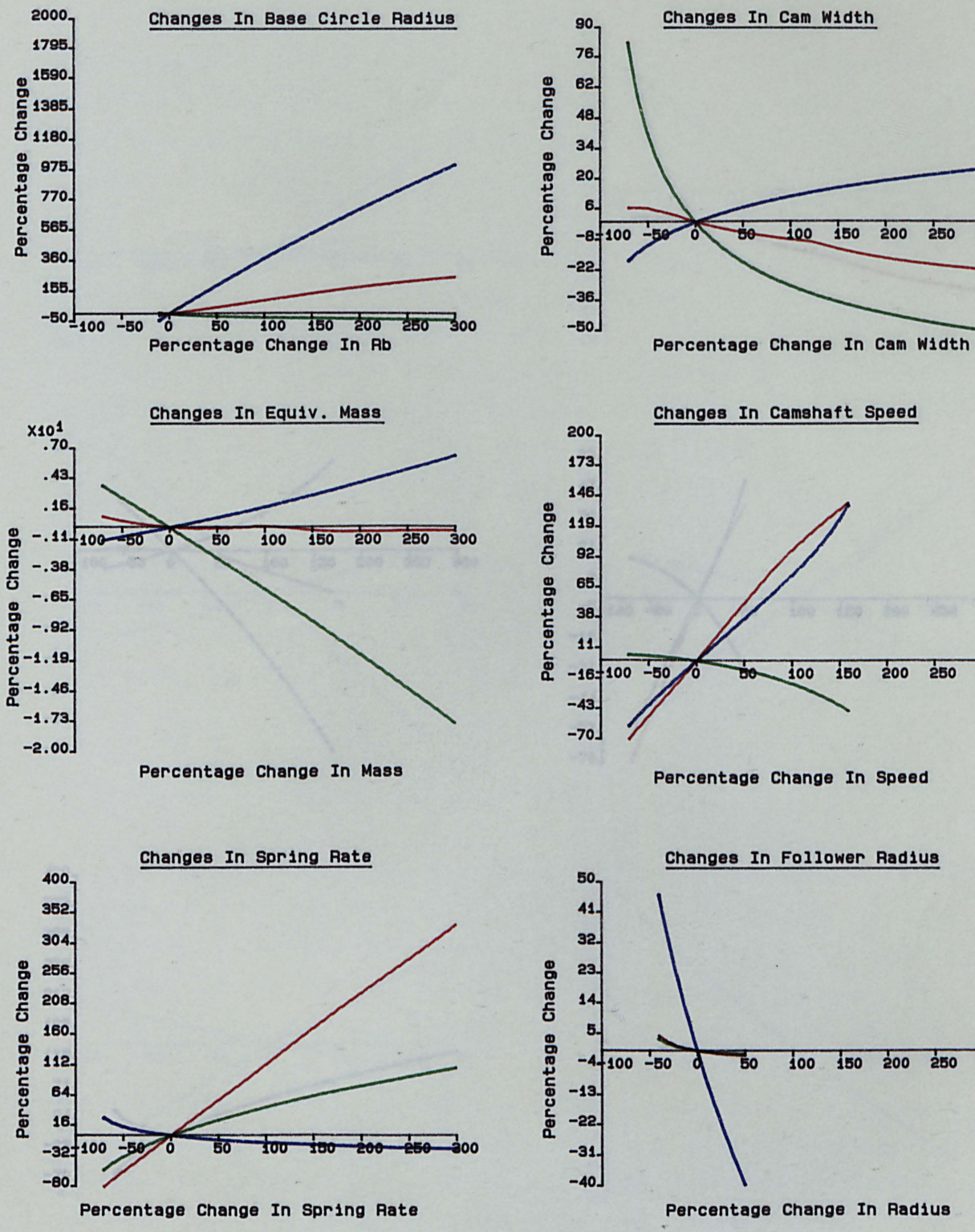

Figure (5.17) Parametric Study for Ford 2.0l Pinto (25 Hz).

PARAMETRIC STUDY

SIERRA 2.0L - INLET: 2500 rpm

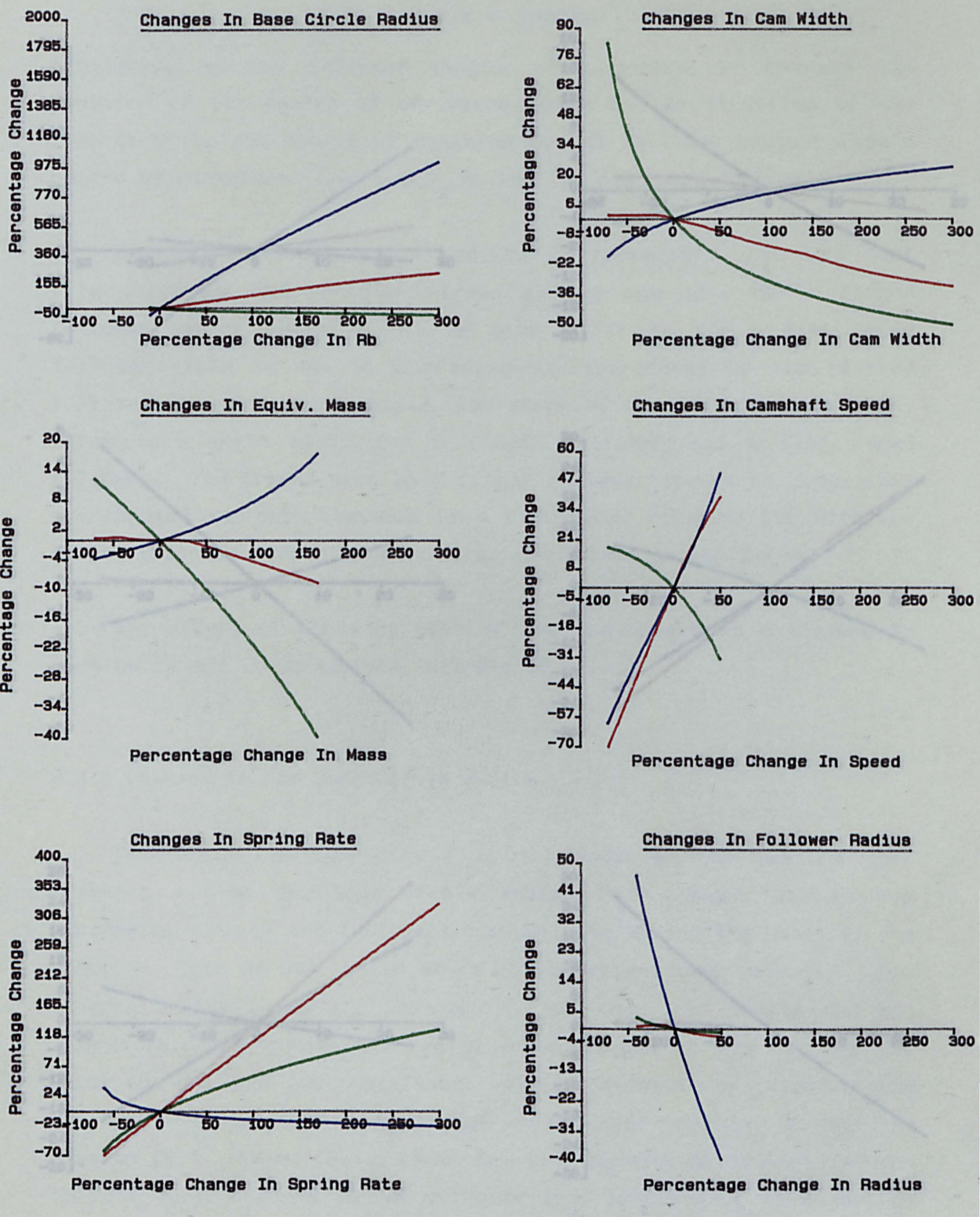

Figure (5.18) Parametric Study for Ford 2.0l Pinto (41.67 Hz).

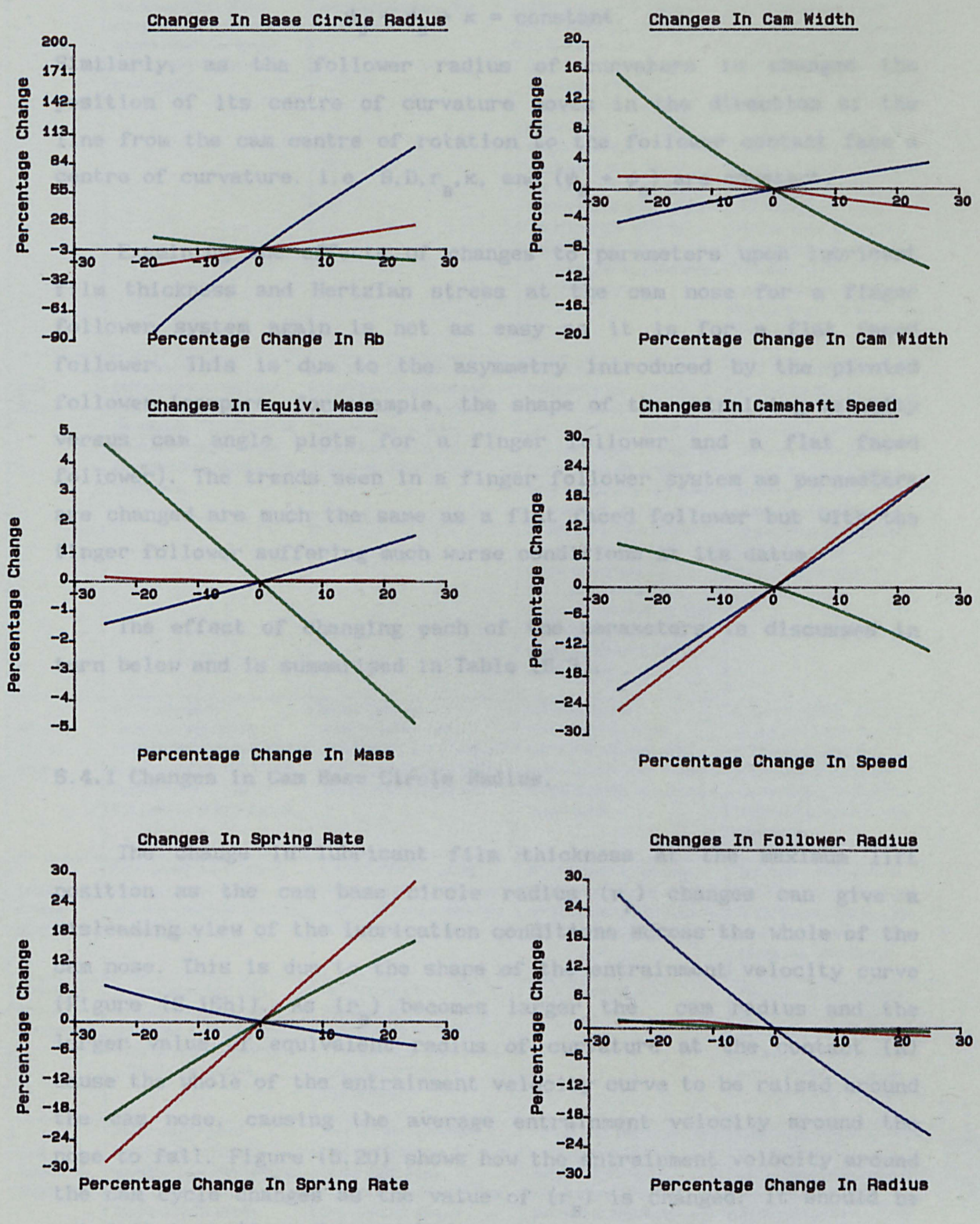

Figure (5.19) Parametric Study for Ford 2.01 Pinto (41.67 Hz).

changed to take up the clearance between the cam and follower. This is done by moving the follower contact radius along the line between its centre of curvature and the cam centre of rotation i.e.

$$\gamma_B + \kappa = \text{constant},$$

$$\psi_B + \phi_B + \kappa = \text{constant}.$$

Similarly, as the follower radius of curvature is changed the position of its centre of curvature moves in the direction of the line from the cam centre of rotation to the follower contact face's centre of curvature. i.e. B, D, r_B, κ, and $(\psi_B + \phi_B)$ are constant.

Examining the effects of changes to parameters upon lubricant film thickness and Hertzian stress at the cam nose for a finger follower system again is not as easy as it is for a flat faced follower. This is due to the asymmetry introduced by the pivoted follower (compare, for example, the shape of the entraining velocity versus cam angle plots for a finger follower and a flat faced follower). The trends seen in a finger follower system as parameters are changed are much the same as a flat faced follower but with the finger follower suffering much worse conditions at its datum.

The effect of changing each of the parameters is discussed in turn below and is summarised in Table (5.3).

5.4.1 Changes in Cam Base Circle Radius.

The change in lubricant film thickness at the maximum lift position as the cam base circle radius (r_B) changes can give a misleading view of the lubrication conditions across the whole of the cam nose. This is due to the shape of the entrainment velocity curve (Figure (5.15h)). As (r_B) becomes larger the cam radius and the larger value of equivalent radius of curvature at the contact (R) cause the whole of the entrainment velocity curve to be raised around the cam nose, causing the average entrainment velocity around the nose to fall. Figure (5.20) shows how the entrainment velocity around the cam cycle changes as the value of (r_B) is changed. It should be noted that as the value of (r_B) increases the positions of the two zeros of entrainment velocity get closer together which will not enhance the lubrication and life expectancy of the cam/follower pair

	MINIMUM FILM THICKNESS AT MAXIMUM LIFT POSITION	MAXIMUM HERTZIAN STRESS AT MAXIMUM LIFT POSITION	POWER LOSS	OTHER COMMENTS
BASE CIRCLE RADIUS	This should be chosen carefully using plots of entraining velocity as a guide. The value of film thickness at the maximum lift position does not give a true representation of the conditions across the whole nose due to the asymmetry of the valve train system.	The Hertzian stress is inversely proportional to the square root of the equivalent radius of curvature. Increasing the base circle radius therefore reduces the Hertzian stress at the cam nose.	The limiting coefficient of friction is applied over most of the cycle, hence the friction is a function of load rather than film thickness. The increase in power loss with base circle radius for a given speed is due to the increase in instantaneous radius of curvature (the distance at which the frictional force acts). If the base circle radius is increased sufficiently the entrainment velocity is enhanced adequately such that the limiting coefficient of friction is no longer applied over any of the cycle.	Increasing the base circle radius will increase the overall engine height. If on assembly, the camshaft needs to be fed through the camshaft bearings, then larger diameter bearings must also be used. A larger cam base circle radius allows a larger diameter camshaft to be used which will increase the rigidity of the valve train system; however at the expense of extra weight. Minimum value of base circle radius is dominated by the lift curve characteristics and the necessity for the cam to become concave along the flanks.
CAM WIDTH	As the cam width increases the load per unit width at the contact decreases. This leads to a small increase in the elastohydrodynamic film thickness.	As the cam width increases the load per unit width at the contact decreases, and so, therefore, does the Hertzian stress.	At low rotational frequency the limiting coefficient of friction is applied over most of the cam cycle. Hence, an increase in cam width only marginally reduces power loss. At higher rotational frequencies the proportion of the cycle governed by boundary lubrication falls with increasing cam width and there is a corresponding fall in power loss.	The cam lobe width is limited by the number of cam lobes to be fitted into a given space. i.e. the cam lobe width is governed by the valve spacing. A larger cam width necessitates a larger diameter follower which leads to a larger reciprocating mass.
RECIPRO-CATING MASS	An increase in reciprocating mass causes an increase in the film thickness due to the inertia force reducing the cam load at the nose.	Increasing the reciprocating mass reduces the cam load and hence lowers the Hertzian stress at the cam nose.	Increasing the reciprocating mass generally causes a fall in the power loss as the loading at the cam nose is reduced.	Increasing reciprocating mass increases the load on the cam flanks. Decreasing mass may cause strength problems, increasing mass inertia problems.
VALVE SPRING STIFFNESS	Increasing valve spring stiffness reduces the film thickness as the cam load is increased.	A reduction in spring stiffness reduces the cam load and hence reduces the Hertzian stress.	An increase in spring stiffness causes the power loss to increase as the cam load increases.	The valve spring must provide sufficient load to restrain valve bounce and to control the valve along the cam flanks.
FOLLOWER RADIUS OF CURVATURE	An increase from the design value causes a decrease in film thickness as the entraining velocity decreases.	An increase from the design value causes a decrease in Hertzian stress as the equivalent radius of curvature increases.	Very little influence.	The size of the contact patch on the follower increases with increasing follower radius of curvature, therefore, larger followers may be needed.
CAM ROTATIONAL SPEED	Increasing speed increases entraining velocity and reduces cam load at nose. Film thickness therefore increases with increasing speed. At high speeds the cam load falls rapidly and therefore the increase in film thickness is rapid.	As the cam rotational speed increases the load at the cam nose decreases and therefore the Hertzian stress decreases.	Power loss increases with cam speed. At high speeds the rate of increase falls as valve bounce is approached.	Camshaft speed is limited by the point at which valve bounce occurs and the cam no longer controls the valve. This is due to the inertia of the reciprocating parts being greater than the valve spring load.

Table (5.3) Ford Pinto Parametric Study Results Summary.

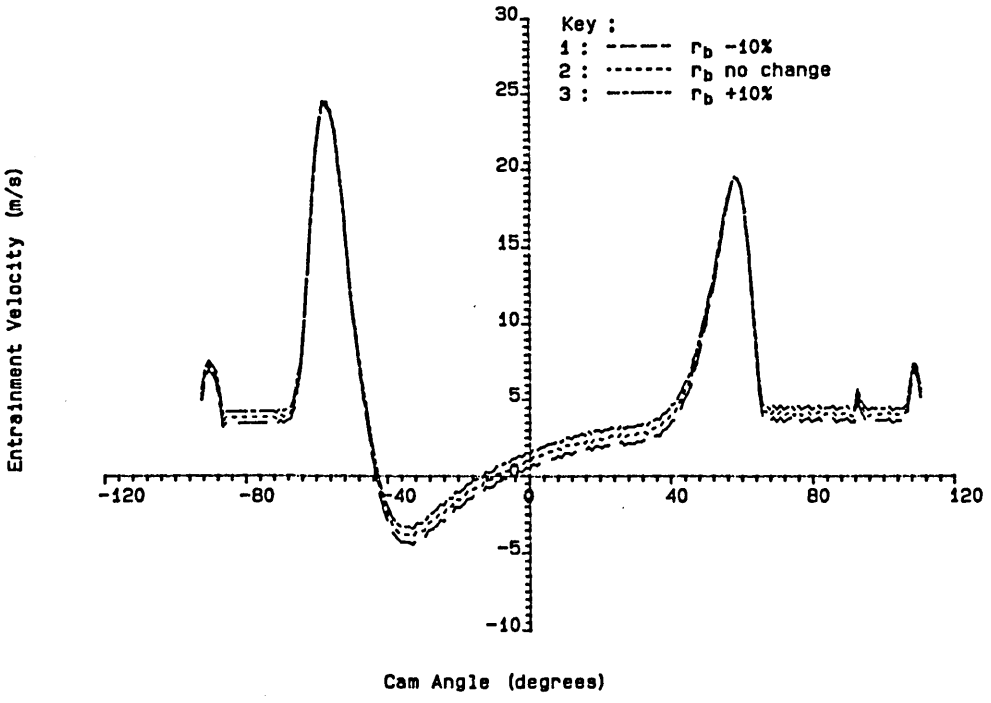

Figure (5.20) Effect of Changing r_b Upon Entrainment Velocity

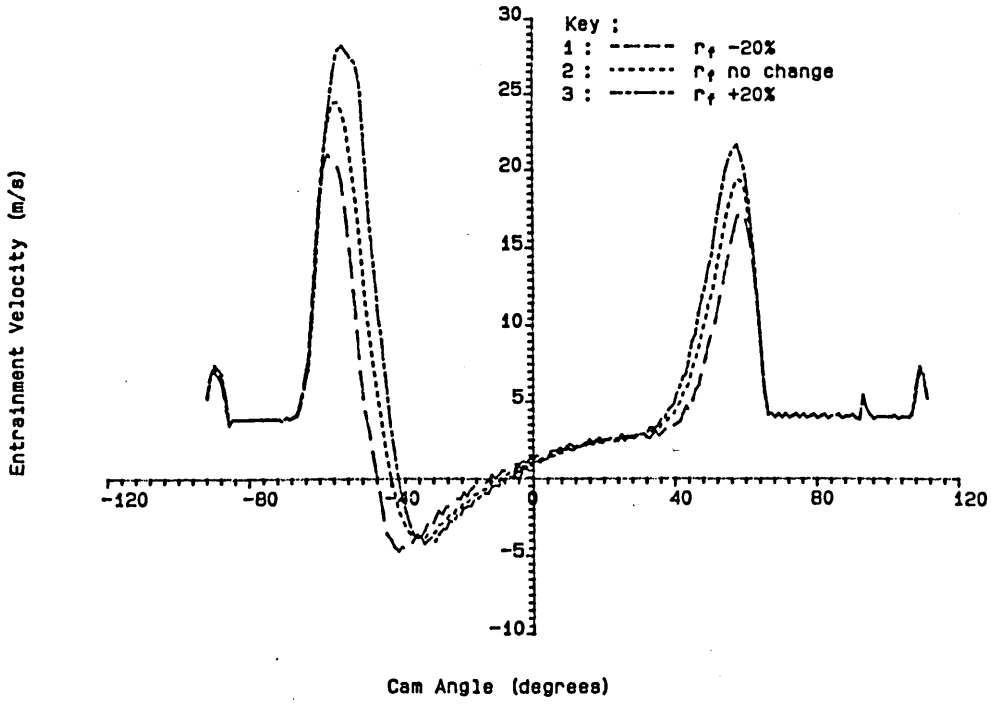

Figure (5.21) Effect of Changing r_f Upon Entrainment Velocity

(again see Figure (5.21)). The maximum allowable decrease in the cam base circle radius is limited by the permissible concavity of the cam flanks. The frictional power loss increases almost linearly with increase in (r_B). The limiting coefficient of friction is applied around the majority of the cam cycle at 25 Hz (1500 rpm) and at 41.67 Hz (2500 rpm) (this is similar to the centrally pivoted follower). The loading at the contact does not change as (r_B) changes but the radius at which the frictional traction force is applied increases as (r_B) increases, thus the frictional power loss increases.

5.4.2 Changes in Cam Width.

As would be expected the Hertzian stress at the cam nose will decrease as the cam lobe width is increased as the load per unit width decreases. The film thickness increases and the frictional power loss decreases as a direct result of this.

5.4.3 Changes in Reciprocating Mass.

Increasing the reciprocating mass at the valve causes higher loads on the flanks but smaller loads at the cam nose. As the load at the cam nose decreases with increasing reciprocating mass the lubricant film thickness will increase and the Hertzian stress will decrease. The frictional power loss decreases due to the load around the majority of the cycle decreasing. It can be seen in Figure (5.18) that when the reciprocating mass is increased, a point is reached where due to the increasing inertia of the system, the frictional power loss decreases more rapidly as the coefficient of friction at the cam nose becomes less than the limiting value. Figure (5.16) shows that at the lower camshaft speed the effect of increasing the equivalent mass at the valve is not significant. This is due to the limiting coefficient of friction being applied around the majority of the cam cycle even with the greatly reduced valve masses, therefore the effect of decreasing the load at the cam nose is offset by the effect of increasing the load at the flanks.

5.4.4 Changes in Camshaft Speed.

As the camshaft speed is increased the loading on the cam nose becomes less due to the negative lift acceleration. It can be seen that valve bounce occurs at approximately 67.5 Hz (3750 rpm (7500 rpm crank)). (Again it should be noted that the loading on the flanks increases). This reduced loading leads to a larger film thickness and reduced Hertzian stress at the cam nose. The power loss increases as the cam speed increases as would be expected. At speeds approaching valve bounce the rate at which the power loss increases starts to fall as the loading becomes so small on the cam nose.

5.4.5 Changes in Spring Rate.

As the spring rate increases the Hertzian stress (p_{max}) at the cam nose increases due to the load increasing. This increase in load also causes the film thickness to decrease but the changes are not large ((h_{min}) only being proportional to load raised to the power -0.13). The frictional power loss increases as both (h_{cen}) and (p_{max}) increase. As the limiting coefficient of friction is applied throughout the majority of the cycle then the change in frictional power loss is, as would be expected, almost linear.

5.4.6 Changes in Follower Radius.

As the radius of curvature of the follower is increased the cam nose becomes broader hence the radius of curvature of the cam becomes larger in this area. This leads to a fall in the maximum Hertzian stress at the cam nose. It can be seen from Figure (5.15i) that there is a point on the cam, at the transition from the rising flank to the nose, where the radius of curvature is small. This radius of curvature decreases as the follower radius of curvature increases and limits the amount by which the follower radius can be increased. Decreasing the radius of curvature of the follower causes the cam flanks to eventually become concave, therefore the maximum allowable decrease in follower radius of curvature is limited by the acceptable concavity of the cam flanks.

The change in the lubricant film thickness at the maximum lift position is very misleading. Although the lubricant film thickness is enhanced at the maximum lift position as the follower radius of curvature (r_f) is decreased the lubrication of the cam nose taken as a whole is much poorer. This is due to the shape of the entrainment velocity curve. Figure (5.21) illustrates the problems involved in choosing the correct follower radius of curvature. As (r_f) is decreased the entrainment velocity at the maximum lift position is greater but over the whole of the cam nose the entrainment velocity is very close to zero for the entire nose period. Also the points where the entrainment velocity passes through zero become closer, which is not advisable as it brings together two points of distress on the cam (and follower). It is therefore better to increase the follower radius of curvature to gain better lubrication conditions across the whole of the nose region.

The frictional power loss decreases as (r_f) increases due the better lubrication conditions at the cam flanks brought about through increased entrainment velocities (again see Figure (5.21)). The increase in radius of curvature at the cam nose causes the frictional power loss across this region to increase as the frictional traction force acts at a greater radius and so the frictional torque is increased. This effect is not as great as the decrease in power loss on the cam flanks as the changes in cam radius of curvature are small.

5.5 Enhancement of an End Pivoted Follower Design.

By using the information gathered by parametric studies it is possible to comment on valve train designs and to suggest possible improvements. By way of an example the end pivoted follower design used in the parametric study presented above was taken and the effect of changing several parameters at once was investigated.

It was found that because of the necessary geometry changes involved with changing the cam base circle radius and the follower radius of curvature the results of changing these parameters could not be investigated separately and then presumed to be additive. It was therefore necessary to chose these parameters together. Changes

to other parameters such as the spring stiffness could obviously be investigated separately. It was also necessary to use a good deal of compromise between the Hertzian stress at the cam nose and the lubricant film thickness across the nose.

It was decided to increase the follower radius of curvature in order to enhance the film thickness across the cam nose. This also had the added advantage of decreasing the Hertzian stress across the cam nose. Unfortunately it caused a dramatic increase in the Hertzian stress at the transition between the cam rising flank and nose where the radius of curvature was already very small. To counter this change it was necessary to increase the base circle radius of the cam. This change decreased the lubricant film thickness across the cam nose and brought the two zeros of entrainment velocity closer together requiring a further increase follower radius of curvature. This process was repeated until a satisfactory compromise was found.

An obvious change that brings improvements to both the Hertzian stress at the cam nose and the lubricant film thickness is a decrease in the valve spring stiffness.

The improved design shown was arrived at by decreasing the valve spring stiffness by 10%, increasing the follower radius of curvature by 20%, and increasing the cam base circle radius by 12%. The results of these changes can be seen in Figure (5.22). The resulting geometry is given below:

$A = 57.98$ mm

$B = 61.80$ mm

$D = 47.19$ mm

$r_f = 52.80$ mm

$r_B = 16.80$ mm

$\kappa = 37.86^\circ$

$\lambda = 38.45^\circ$

It can be seen that these changes significantly improve the distribution of Hertzian stress around the cam whilst also improving the lubrication of the cam. Also the two points where the lubricant film thickness falls to zero (if we neglect squeeze effects) are spread further apart. There is also a small decrease in the frictional power loss.

CAM OPERATING CHARACTERISTICS
SIERRA 2.0L - Improved Design

Cam Base Radius (mm)	=	16.80
Maximum Valve Lift (mm)	=	10.35
Cam Width (mm)	=	21.00
Rotational Speed (rpm)	=	2500.0
Spring Stiffness (kN/m)	=	36.000
Initial Spring Disp. (mm)	=	11.0
Equiv. Mass At Valve (kg)	=	.148
Lubricant Viscosity (Ns/m^2)	=	.013
Press. Visc. Coeff. (/Pa)	=	22.0E-9
Youngs Mod. (Cam) (GPa)	=	207.0
Youngs Mod. (Foll.) (GPa)	=	207.0
Poissons Ratio (Cam)	=	.29
Poissons Ratio (Foll.)	=	.29
Frictional Power Loss (W)	=	160.89

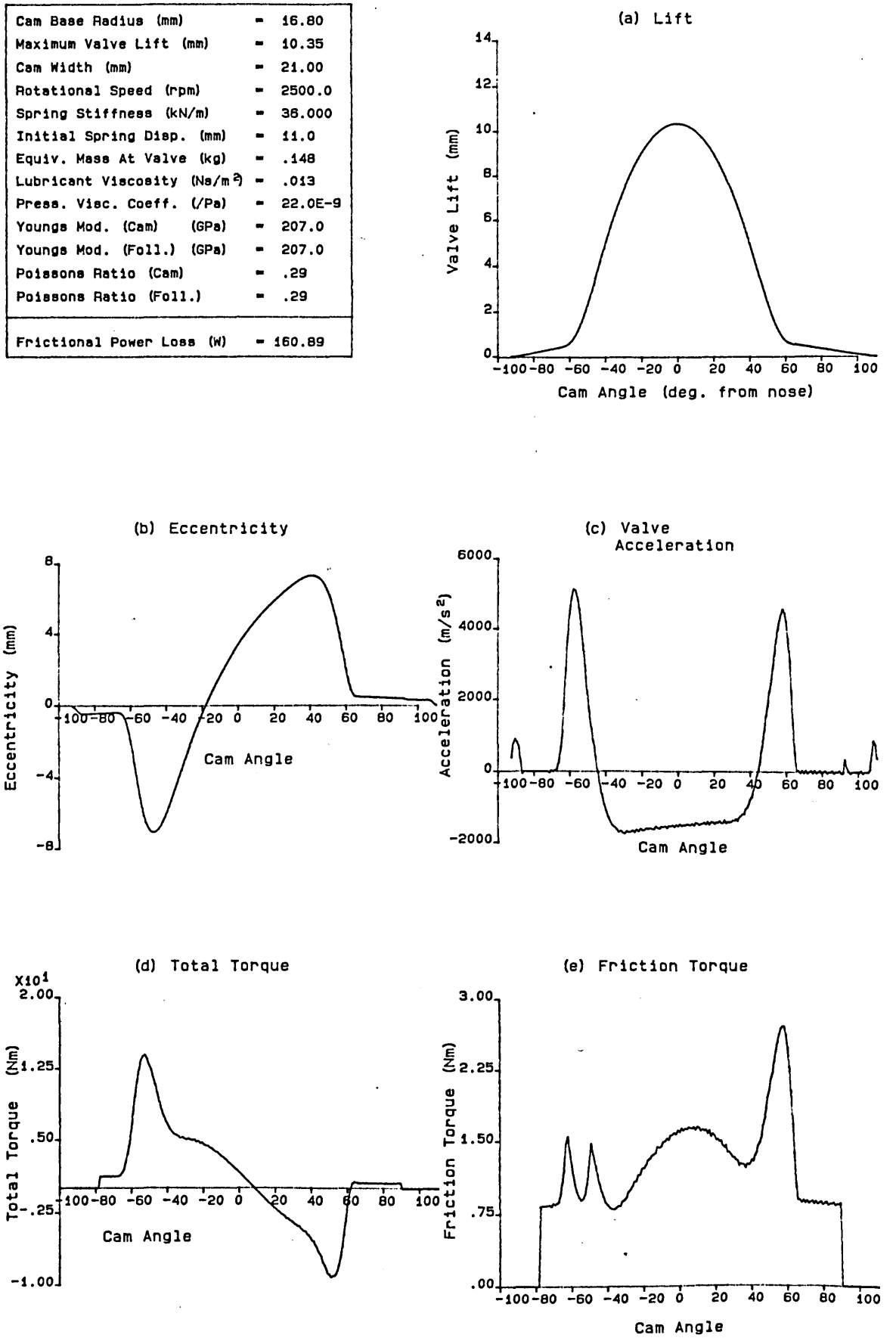

Figure (5.22) Cam Operating Characteristics for Improved Ford 2.01 Pinto (41.67.Hz).

CAM OPERATING CHARACTERISTICS

SIERRA 2.0L - Improved Design

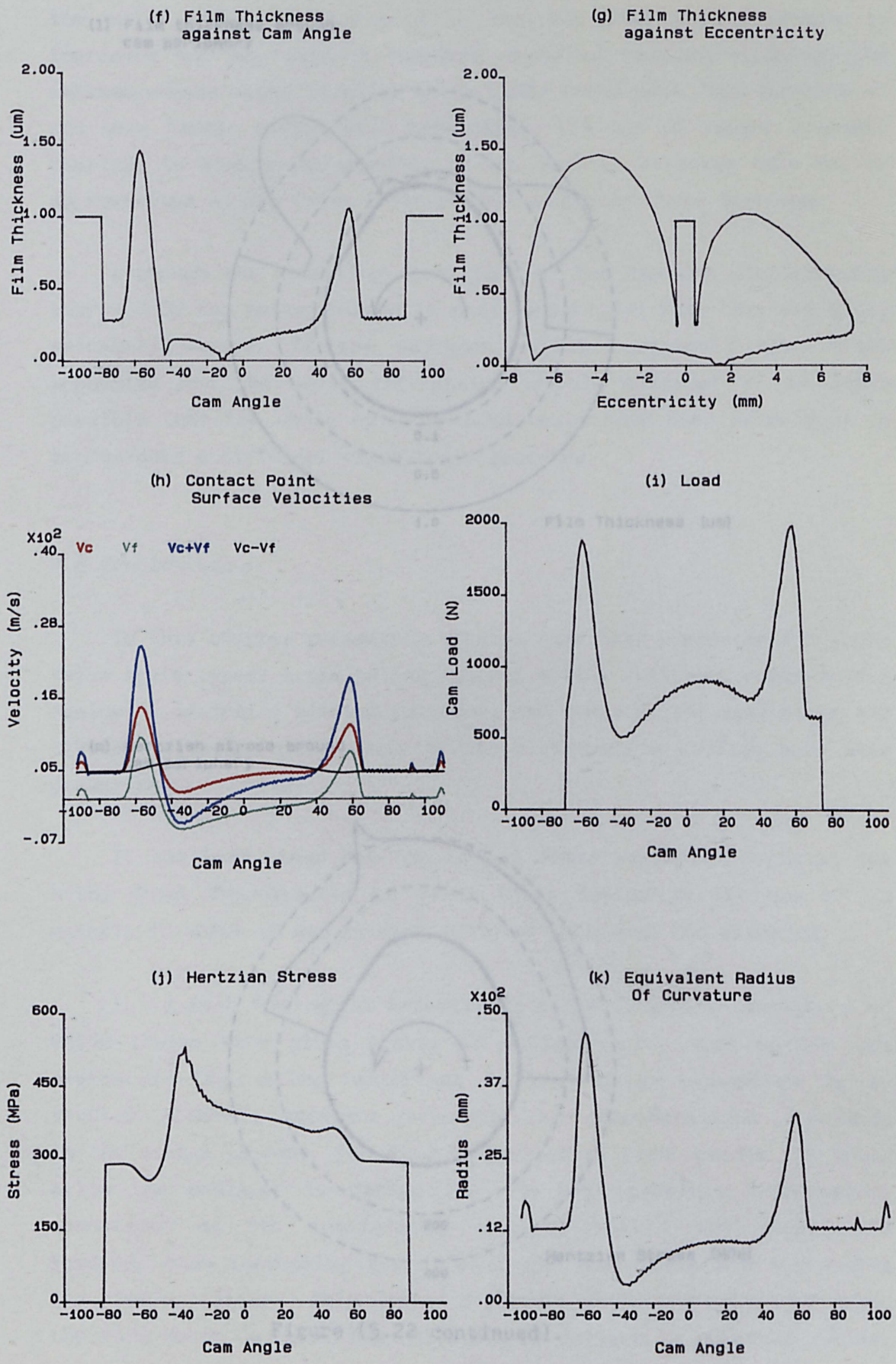

Figure (5.22 continued).

CAM OPERATING CHARACTERISTICS
SIERRA 2.0L - Improved Design

(l) Film thickness around cam periphery

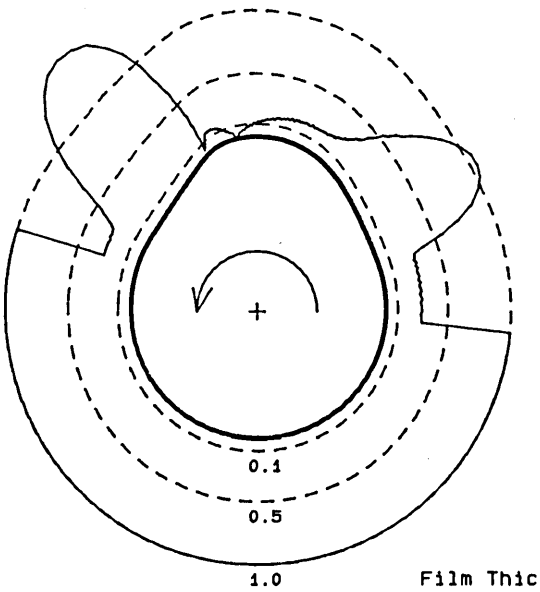

(m) Hertzian stress around cam periphery

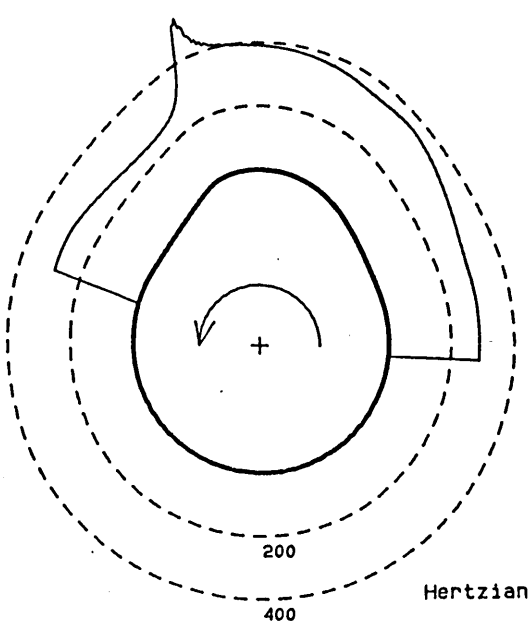

Figure (5.22 continued).

The disadvantages of the new design are that the overall size of the valve train is increased as the cam base circle radius is increased and the maximum camshaft speed is reduced, although the maximum engine speed is still above 110Hz (6600 rpm). The increase in cam base circle radius will necessitate the use of larger camshaft bearings to enable the assembly of the system, although this may be an advantage as the valve train relies upon only three bearings.

Although the operating conditions of the cam are significantly improved by the above changes it must be realised that they are still extremely severe. If the designer of the original valve train mechanism had the above information at his disposal it is quite possible that the whole cylinder head would have been redesigned to accommodate a different valve train geometry.

5.6 Conclusions.

In this chapter parametric studies have been presented for three valve train types; a cam acting against a flat follower, a cam acting against a centrally pivoted follower, and a cam acting against an end pivoted follower. The results of these parametric studies have been summarised in tables.

It has been shown how the use of these parametric studies can bring about improvements to valve train design by the use of an example in which an end pivoted follower mechanism was enhanced.

It is felt that great benefits could be reaped if designers of valve trains were given access to design tools, such as the one presented, that allow variations in the design parameters to be studied. Although there are obviously other considerations to be made in the design process, for example combustion requirements, it would allow the designer to design for the best possible tribological conditions at the cam/follower contact within the constraints imposed, thus increasing the life of the components and decreasing the risk of failure. This design procedure would probably have saved the Ford Motor Co. Ltd. many millions of dollars in warranty claims, lost sales and redesign costs, during its early years of production

of the 1.6 litre and 2.0 litre Pinto engines. Ford have learnt through their costly mistake of not making proper considerations of the tribological conditions at the cam/follower interface during the design of the valve-train - other manufacturers are still making the same mistake!

CHAPTER 6

A STUDY OF THE LOADING, JOURNAL ORBITS, AND POWER LOSSES OF THE CAMSHAFT BEARINGS IN THE FORD 2.01 PINTO ENGINE.

6.1 Introduction.

The energy losses associated with internal combustion engines have been the subject of many studies. Authors, such as Hoshi (1984) and Lang (1981), have split the losses into various categories and expressed them as a percentage of the total fuel chemical energy input to the engine. Figure (6.1) shows a typical energy distribution in an internal combustion engine.

The energy losses associated with the valve train have also been attributed values as proportions of total energy input by many authors. The energy dissipation within the valve train has not, however, received attention regarding the relative magnitudes of the losses associated with the friction at the cam/follower interface compared with the losses associated with the camshaft bearings. It was therefore decided that a study should be made of the frictional losses of the bearings of a typical automobile camshaft. These losses could then be compared with the energy required to overcome friction at the cam/follower interface.

A complete and rigorous study of this kind would be worthy of an extensive programme of work in itself. This study aims to give an indication of the order of magnitude of the power loss associated with the camshaft bearings. To this end the study comprises of:

(i) A model to estimate the loading on each of the bearings on a camshaft for a complete cycle,

(ii) The introduction of these loadings into available software for the prediction of journal orbits,

(iii) The input of these orbits into a model to predict the power losses within the bearings.

The study contains many simplifications, which will be introduced during the chapter. These simplifications will no doubt introduce errors into the power loss predictions. It is nevertheless felt that the results, even when these simplifications are taken into account, will give an idea of the relative importance of the losses associated with the bearings.

The camshaft chosen for the purpose of this study was that from the Ford 2.0l Pinto Sierra engine. This is shown schematically in

Typical Energy Distribution in a Petrol Automotive Engine (part open throttle)

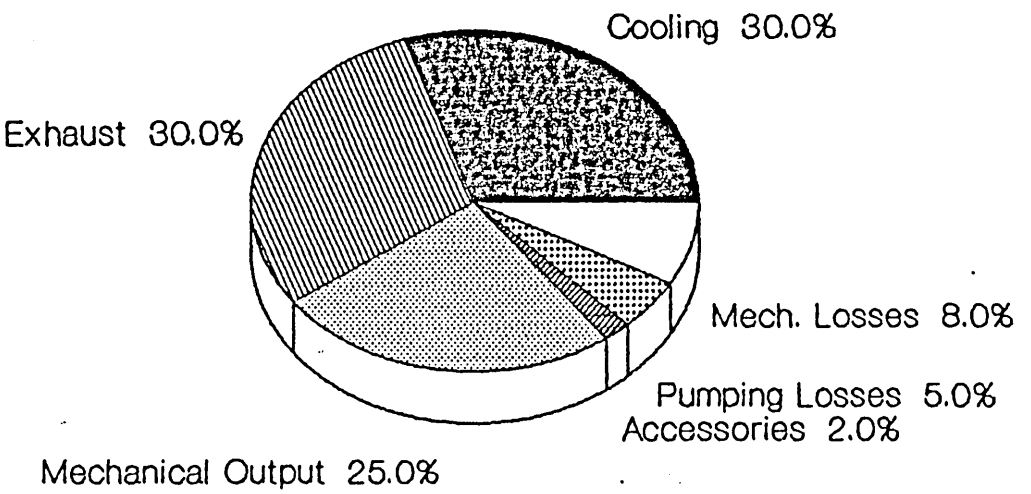

Figure (6.1) Typical Distribution of Fuel Energy Input in a Petrol Automotive Engine.

Figure (6.2). The camshaft has eight lobes, controlling eight valves via finger followers. There are three bearings, each neighbouring pair being separated by four cam lobes. The camshaft is driven by a toothed belt via a pulley located at one end of the camshaft.

6.2 A Brief Discussion Of Dynamically Loaded Journal Bearings.

Camshaft bearings have to support and locate the camshaft during its operation. The bearings are subjected to rapidly changing loads, both in magnitude and direction, and must therefore be treated as dynamically loaded bearings.

6.2.1 The Analysis of Dynamically Loaded Bearings.

The ratio of breadth to diameter of the bearings under consideration is of the order of 0.3 and the bearings can therefore be described as "short". The short journal bearing approximation assumes the circumferential pressure gradient is negligible as the pressure gradient along the bearing axis is of a much larger magnitude. Using the short bearing approximation and assuming that the lubricant viscosity is constant, it is possible to solve the Reynolds' equation to obtain the pressure distribution,

$$p = -\frac{6\eta}{h^3}\left[\frac{b^2}{4} - y^2\right]\left[\frac{\partial e}{\partial t}\cos\phi + e\sin\phi\left[\omega - \frac{\Omega_B + \Omega_S}{2}\right]\right] \qquad (6.1)$$

It can be seen that this relationship is made up of two parts:

(i) The part dependent upon $\frac{\partial e}{\partial t}.\cos\phi$ - the "squeeze term", and,

(ii) The part dependent upon $e.\sin\phi\left[\omega - \frac{\Omega_B + \Omega_S}{2}\right]$ - the "hydrodynamic wedge" term.

Referring to Figure (6.3) it can be seen that for a camshaft bearing the bush itself is stationary ($\Omega_B = 0$). It is apparent that if the journal centre rotates about the bearing centre at half the shaft rotational speed, i.e. $\omega = \frac{\Omega_S}{2}$, then the hydrodynamic wedge term is equal to zero. For this situation the load capacity of the bearing

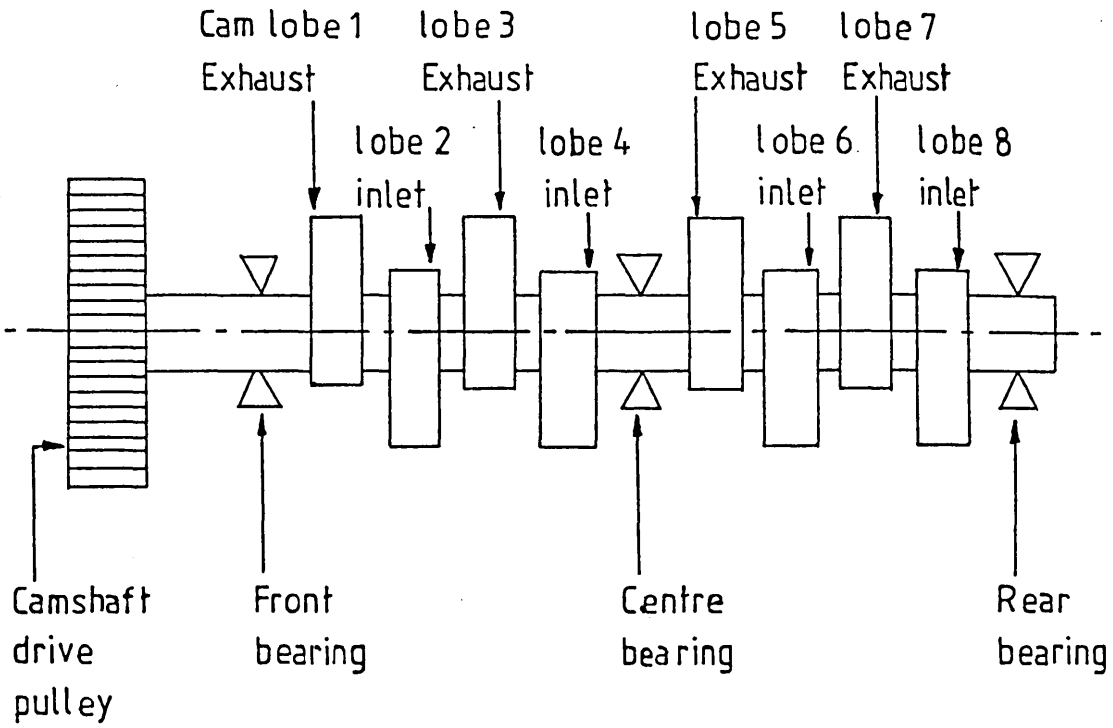

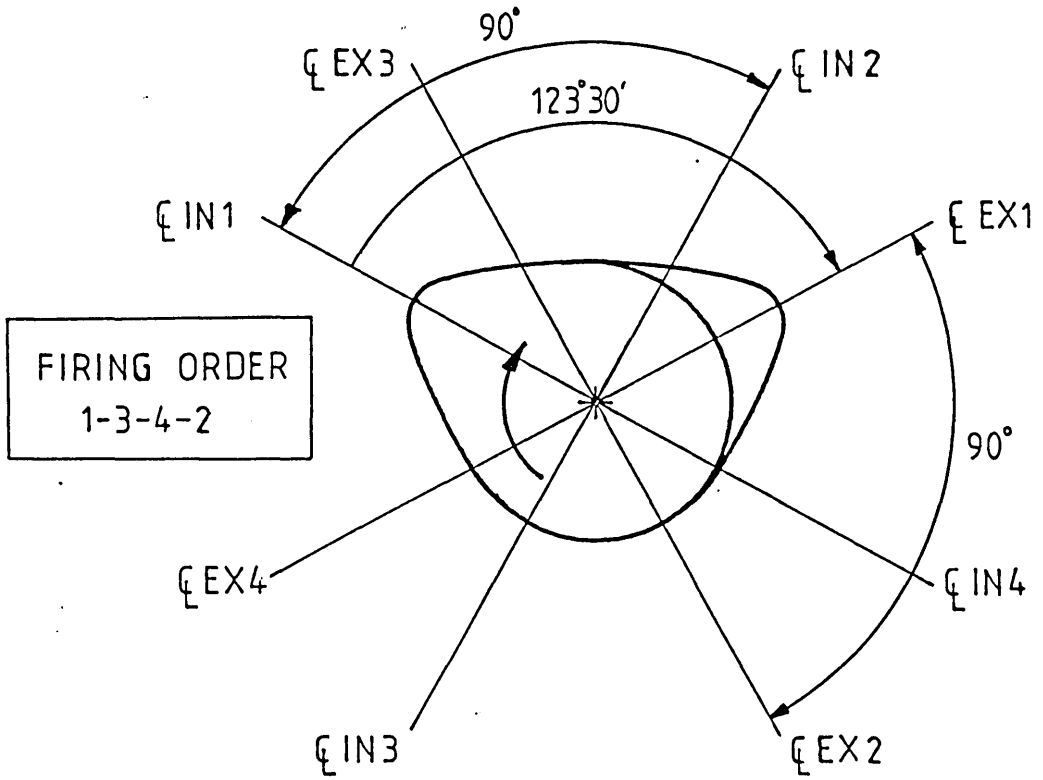

Figure (6.2) Schematic Representation of Ford 2.0 litre Pinto (Sierra) Camshaft.

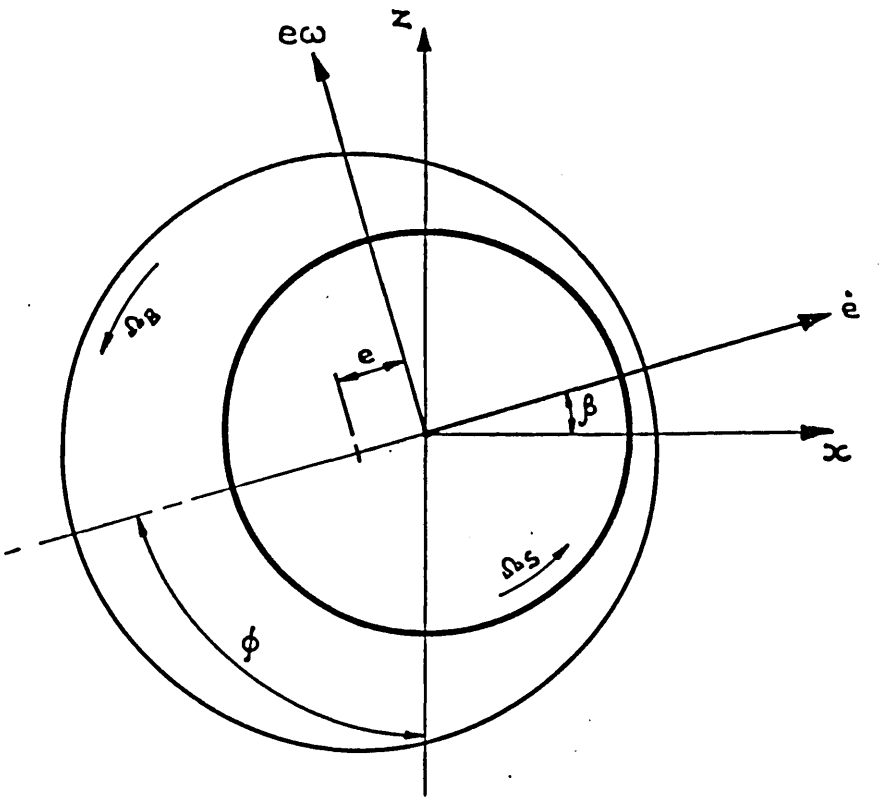

Figure (6.3) Journal Bearing Geometry.

in thus relies entirely upon the squeeze action. This phenomena is known as half speed whirl.

Film rupture, or cavitation, prevents the formation of significant negative gauge pressures. As a result the region of positive pressure is usually limited in extent to roughly half the bearing. The positive portion of the complete-film distribution lies between angles (θ_1) and (θ_2) where,

$$\theta_1, \theta_2 = fn\left[e, \frac{\partial e}{\partial t}, \bar{\omega}, \dot{\psi}\right] \qquad (6.1)$$

For the short bearing approximation,

$$\theta_2 = \theta_1 + \pi$$

i.e. the fluid film extends around half the bearing this is known as a π-film.

6.2.2 Calculation of Attitude Angle and Eccentricity Ratio.

The evaluation of the path of the journal centre during a loading cycle requires that the applied load is balanced by the load capacity of the bearing obtained by integrating the pressure distribution, (Equation (6.1)), around the extent of the positive portions of the pressure distribution. Shaft inertial effects are normally neglected.

Stone and Underwood (1947) introduced an equivalent speed concept. This assumed that the squeeze term was negligible (i.e. $\partial e/\partial t = 0$) in equation (6.1) over some parts of the cycle. It was then possible to evaluate the instantaneous eccentricity of the bearing and the attitude angle based upon a quasi-static constant load approach. This method, however, predicted zero film thickness at half speed whirl conditions. Around the position of half speed whirl it was possible to neglect the wedge term and thereby estimate the eccentricity change and attitude angle from squeeze film considerations alone.

Booker (1965) and Blok (1965) working independently developed graphical techniques to determine shaft orbits. Booker's method is described below.

Booker considered two velocity components:

(i) a velocity component for a stationary bearing with a non-rotating journal and load, and,

(ii) a velocity component taking into account the angular velocity of the load, bearing and journal. The graphical technique adopted a fixed load direction with the resultant shaft orbit being relative to this.

The equations of motion for the shaft journal are given by,

$$\frac{de}{dt} = \frac{P_c \left[\frac{C_d}{D}\right]^2}{\eta b D} \cdot M_\varepsilon \left[e,\ \psi,\ \frac{b}{D},\ \theta_1,\ \theta_2\right] \tag{6.3}$$

$$e(\dot{\psi} - \bar{\omega}) = \frac{P_c \left[\frac{C_d}{D}\right]^2}{\eta b D} \cdot M_\psi \left[e,\ \psi,\ \frac{b}{D},\ \theta_1,\ \theta_2\right]$$

where M_ε and M_ψ are the mobilities (dimensionless ratios of velocity to force) parallel and perpendicular to the line of centres.

These mobilities can be determined directly for a non-cavitating case or by iterating between Equations (6.2) and (6.3) for a ruptured film. The analysis is simplified further if M_ε and M_ψ are considered as components of a mobility vector (**M**), where,

$$\mathbf{M} = \left[M_\varepsilon^2 + M_\psi^2\right]^{\frac{1}{2}} \tag{6.4}$$

$$\tan \alpha = \frac{M_\psi}{M_\varepsilon} \tag{6.5}$$

$$\mathbf{M} = \mathbf{M}(e, b/D) \tag{6.6}$$

Therefore a mobility chart can constructed for the bearing (with a simple dependence upon length to diameter ratio (b/D)). Such a chart consists of lines of constant mobility number, (M), and squeeze paths relative to a fixed load line. Blok's method is similar to the above, only lines of constant impulse are considered.

To evaluate the orbit of the journal centre, an initial "guess"

is made as to the position of the journal centre upon the mobility diagram. The velocity of the journal along the squeeze line (de/dt) may be readily found from the determination of the mobility number. The angular velocity of the journal, the bearing and the load is taken into account by considering an additional component, a whirl ($e\bar{\omega}$) in a direction normal to the line of centres. The vectorial addition of these two vectors gives the resultant velocity vector. Knowing this it is possible to step to the next position for a time increment, (dt). By stepping the position of the journal centre in such a way, convergence of the journal orbit is readily attain in less than two cycles.

The mobility method is simply programmed on a digital computer and this approach still finds wide use in the analysis of engine bearings some twenty years after its development.

In general, analyses of dynamically loaded bearings make no allowance for elastic or thermal distortion of the journal or bearing. In addition, in choosing a lubricant viscosity for any analysis, an estimate of the effective lubricant temperature must therefore be made. This is normally made without reference to a thermal analysis.

6.2.3 Power Loss in Dynamically Loaded Bearings.

Martin (1985) showed that the power loss associated with the (Couette) shearing of the full width or complete film within the bearing gave a fair approximation to the total power loss.

This power loss for the 2π film is given by

$$H = \frac{\eta\, r^3\, b}{c} \cdot \frac{2\pi}{\sqrt{(1 - \varepsilon^2)}} \cdot \omega^2 \qquad (6.7)$$

By integrating around the complete orbit it is possible to calculate the average power loss per cycle.

6.3 Evaluation of the Camshaft Bearing Loads.

6.3.1 Evaluation of the Load Applied by the Cam Lobes.

The computer program described in Chapter (4) evaluates the load and frictional force at a cam/follower interface. It is possible to resolve the loads into components acting along, and perpendicular to, the axis of the cylinder bores. These components are F_Y and F_X respectively. The forces F_Y and F_X can be calculated at points around the lift cycle for each cam. Knowing the timing of the camshaft (the angular displacement between the maximum lift position of the opening cam lobe and that of the closing cam lobe), the distance between each of the lobes, and the firing order of the engine, it is possible to construct a loading diagram, such as is shown in Figure (6.4), for each of these points around the cam cycle.

6.3.2 Determination of the Bearing Loads.

The calculation of the loads upon each of the three camshaft bearings supporting the camshaft is a statically indeterminate problem. It is therefore necessary to apply a simplifying assumption to enable the loads to be calculated. In crankshaft bearing analysis, it is invariably assumed that each pair of adjacent bearings can be treated as a completely separate system. In the system shown in Figure (6.4) the rear and centre bearing loads are calculated assuming that the only forces acting upon them are those applied at the cam lobes between the two bearings. A similar exercise is undertaken for the front and centre bearing loads, treating the front and centre bearings as a separate system. The load on the central bearing is then assumed to be equal to the sum of the two loads obtained from the two separate systems. The pulley load is also added to the front bearing loading. Figure (6.5) shows the load evaluation process.

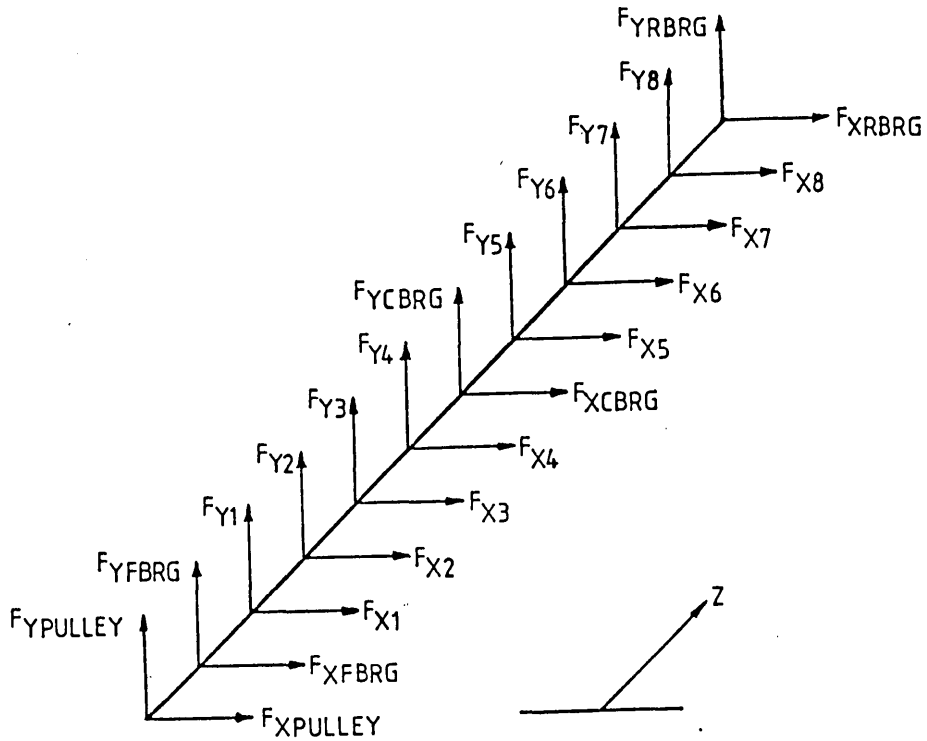

Figure (6.4) Loading Diagram.

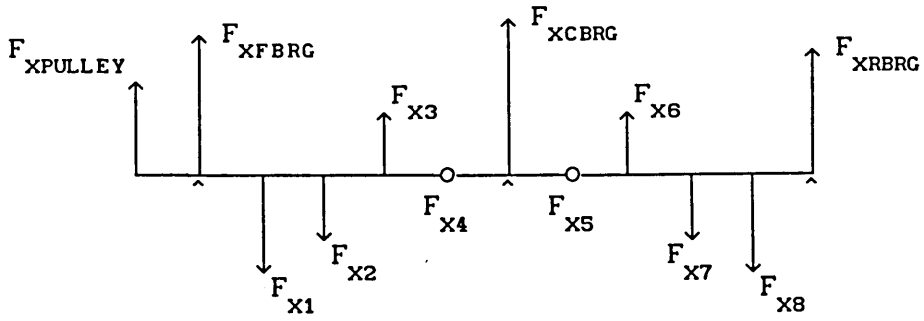

Is equivalent to:

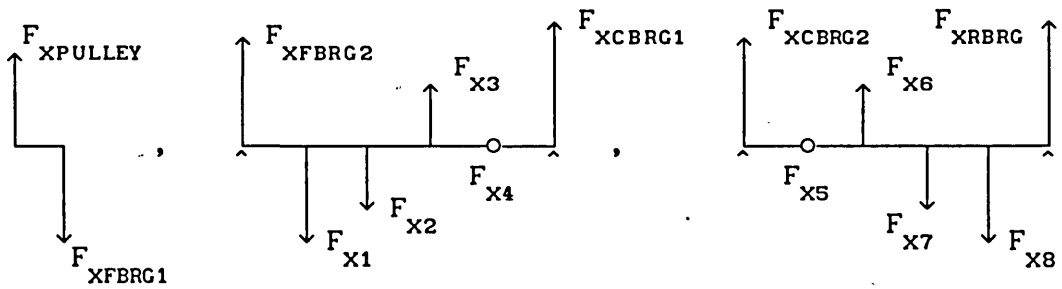

Where:

$$F_{XFBRG} = F_{XFBRG1} + F_{XFBRG2}$$

$$F_{XCBRG} = F_{XCBRG1} + F_{XCBRG2}$$

$$F_{XRBRG} = F_{XRBRG}$$

and similar for forces in the y-direction.

Figure (6.5) Load Equaluation Process For Camshaft Bearings.

6.4 Power Loss Predictions.

6.4.1 Description of the Input Data.

As mentioned previously, the camshaft used for this analysis was the 2.01 Pinto. The valve lift data and general valve train geometry has been described in Chapter (5). In order to carry out an analysis of the camshaft bearings other additional information was required. This is detailed below.

The timing of the camshaft was such that the inlet valve was at it's fully open position 123°30' of camshaft revolution before the inlet valve reached its maximum lift position. The engine firing order was 1-3-4-2 (i.e. the firing stroke of cylinder one was followed by cylinder three, etc), the engine and camshaft both rotating clockwise when viewed from the front. An approximate value for the load applied to the camshaft drive pulley was calculated using the pulley diameter and the power loss predictions for the cam/follower interface friction. This of course gave an underestimate of the pulley load as the bearing losses were neglected. The above information allowed the components represented in Figure (6.4) to be constructed.

The geometry of the three bearings is given in Table (6.1). A lubricant viscosity of 0.02 Pa s was used throughout the analysis. Figures (6.6), (6.7) and (6.8) show polar load diagrams for the front, centre and rear bearings respectively at a camshaft rotational speed of 25 Hz (1500 rpm).

6.4.2 Results of Analysis.

The bearing loads were introduced to a computer program written by Dunning (1980). The program is based upon the mobility method of orbit prediction, and uses the short bearing approximation for a π-film. The eccentricity ratios predicted by this program were then introduced to a second program which calculated the power loss due to fluid film shearing in the bearings.

Figure (6.9) shows the predictions of the analysis for the power

	Front	Centre	Rear
Bearing Diameter (mm)	42.19	44.81	45.19
Journal Diameter (mm)	42.00	44.62	45.00
Radial Clearance (mm)	0.0965	0.0965	0.0965
Bearing Width (mm)	20.00	17.00	16.00

Table (6.1) Camshaft Bearing Geometry Data.

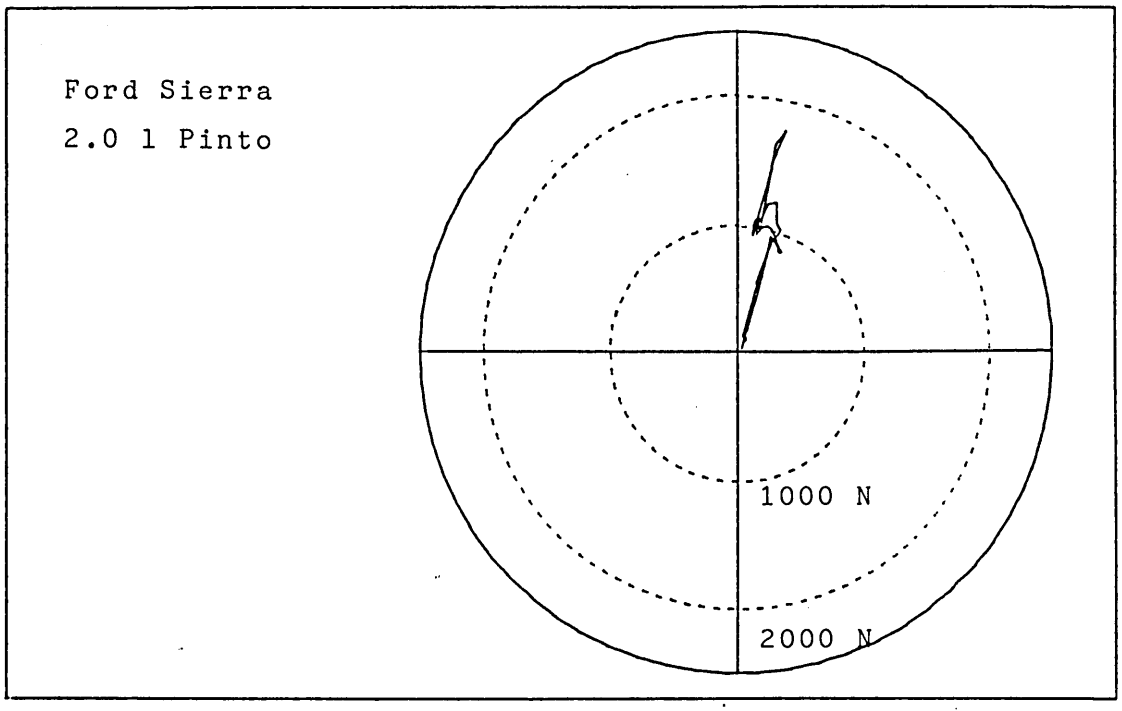

Figure (6.6) Polar Load Diagram for Front Camshaft Bearing at 25 Hz (1500 rpm).

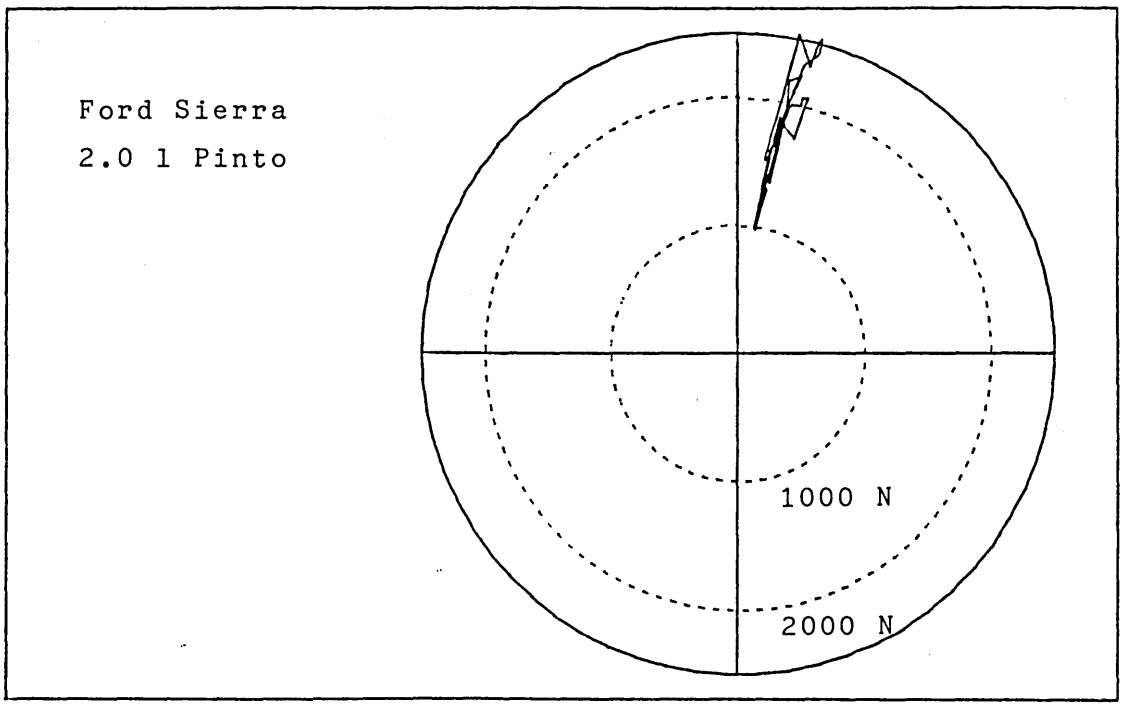

Figure (6.7) Polar Load Diagram for Centre Camshaft Bearing at 25 Hz (1500 rpm).

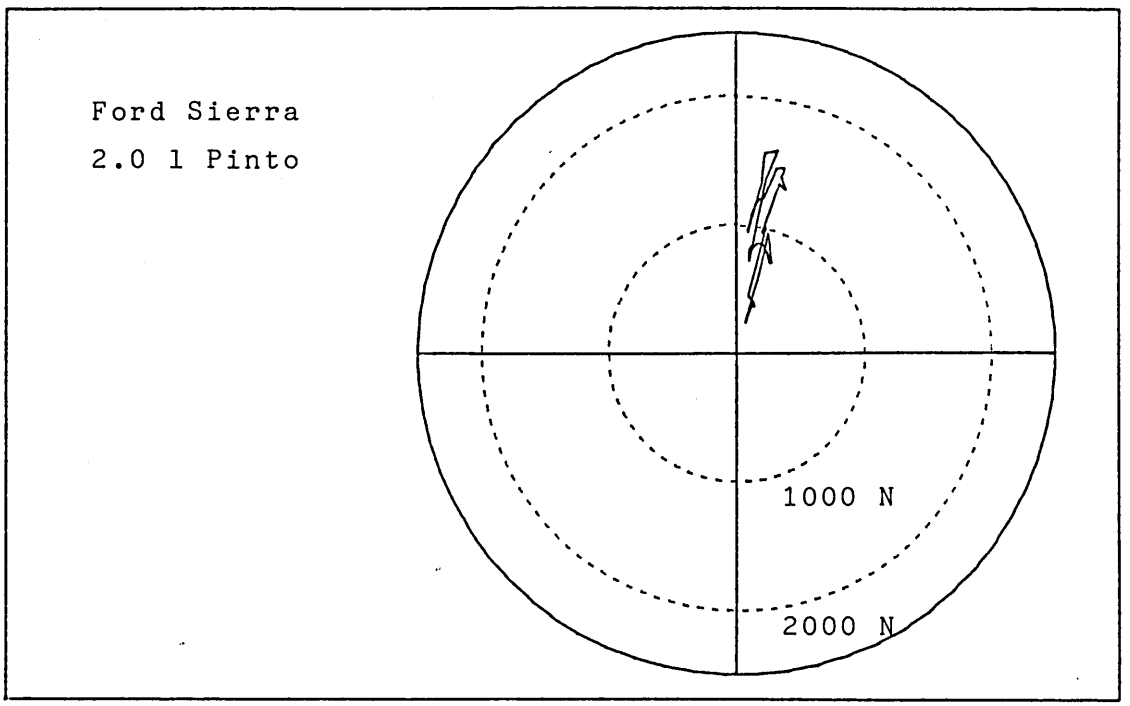

Figure (6.8) Polar Load Diagram for Rear Camshaft Bearing at 25 Hz (1500 rpm).

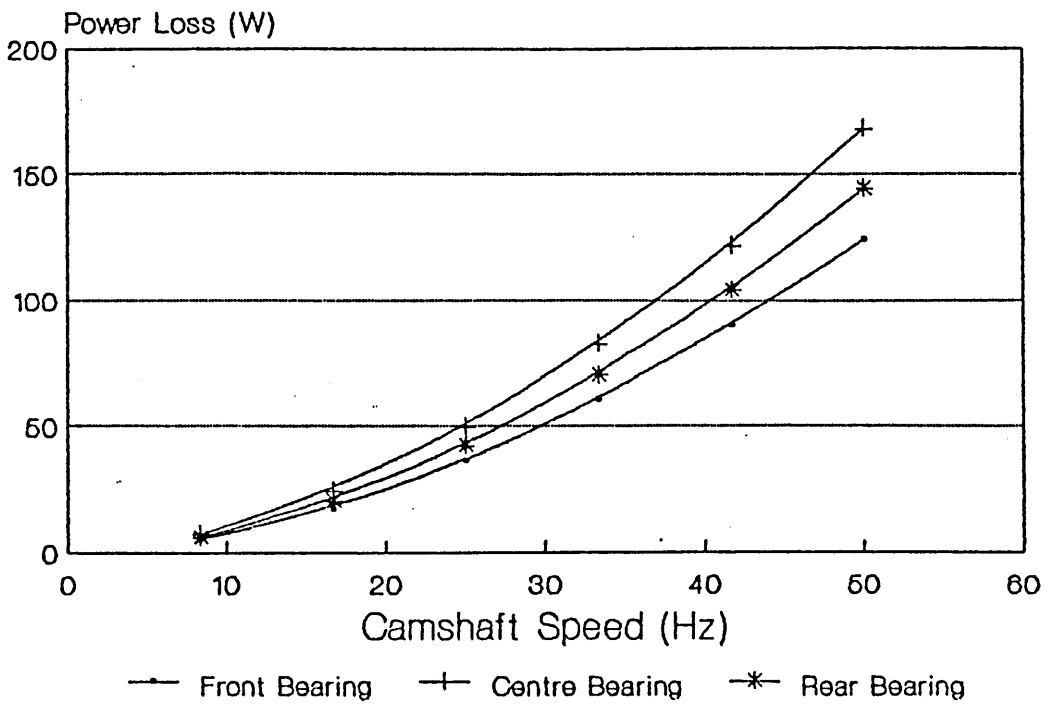

Figure (6.9) Camshaft Bearing Power Losses.

loss of the three bearings for camshaft speeds ranging from 8.3 Hz to 50 Hz (500 rpm to 3000 rpm). Figure (6.10) shows the total power loss of the three bearings compared with the frictional power loss at the cam/follower interface.

Figure (6.11) shows the minimum lubricant film thicknesses experienced by the three bearings, whilst Figures (6.12), (6.13) and (6.14) show the journal orbits of the front, centre, and rear bearings respectively at a camshaft speed of 25 Hz (1500 rpm).

6.5 Discussion.

It can be seen from Figure (6.10) that the power loss predicted for the three bearings is approximately one fifth of that predicted for the cam/follower interfaces.

The Ford 2.01 Pinto produces 77 kW of power at the fly wheel at an engine speed of 86.7 Hz (5200 rpm). If we estimate that the engine converts one quarter of the fuel energy input into brake energy, then the fuel energy input to the engine at 86.7 Hz is 308 kW. It can be seen from Figure (6.10) that the valve train requires about 1.6 kW to overcome the friction of the bearings and cam/follower interaction at a camshaft speed of 43.3 Hz (2600 rpm), which is equivalent to an engine speed of 86.7 Hz (5200 rpm). The valve train operation, therefore, from the above predictions, requires about 0.52% of the fuel energy input. Bearing in mind that this percentage relates to the engine with a fully open throttle, and equation (6.8) gives an overestimate of the power loss, it is in good agreement with values given elsewhere in the literature (e.g. Martin (1985) who quotes 0.48 - 0.6%).

6.6 Conclusions.

An analysis of the Ford 2.01 Pinto valve train friction losses has been made. Bearing loads were evaluated for each of the three camshaft bearings and a dynamically loaded journal bearing analysis was performed. Power loss predictions were made for the three bearings. These losses were then compared with the power losses

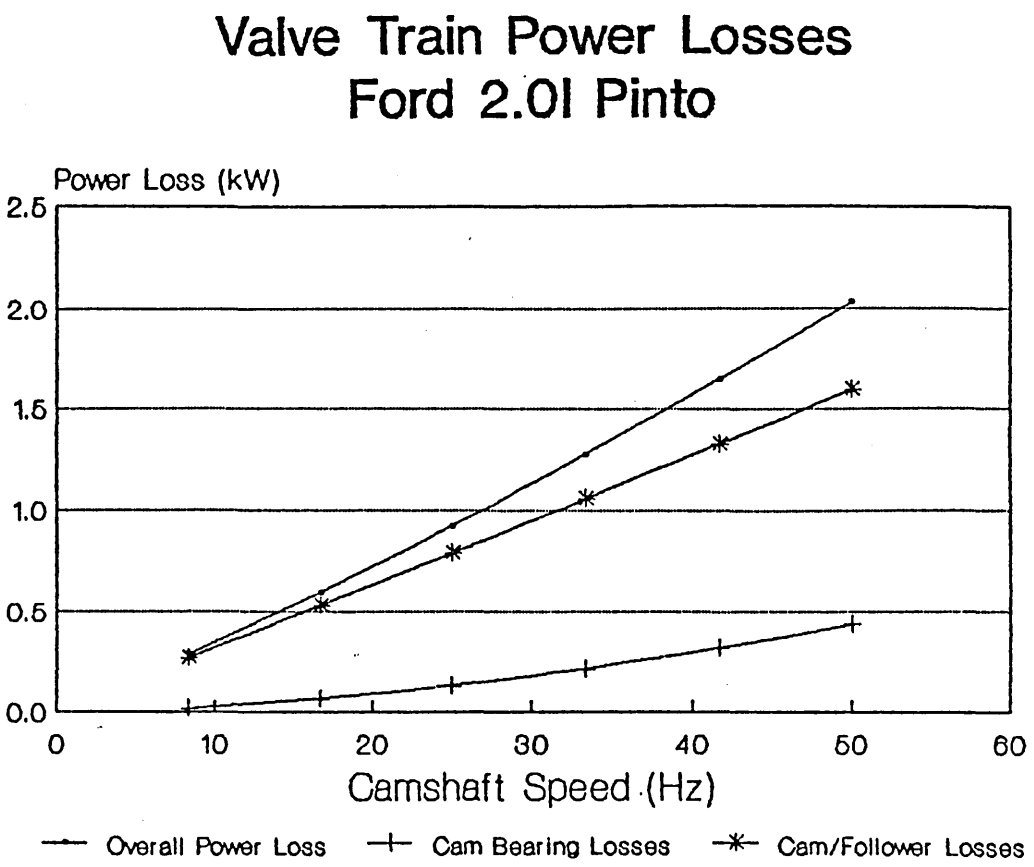

Figure (6.10) Valve Train Power Losses.

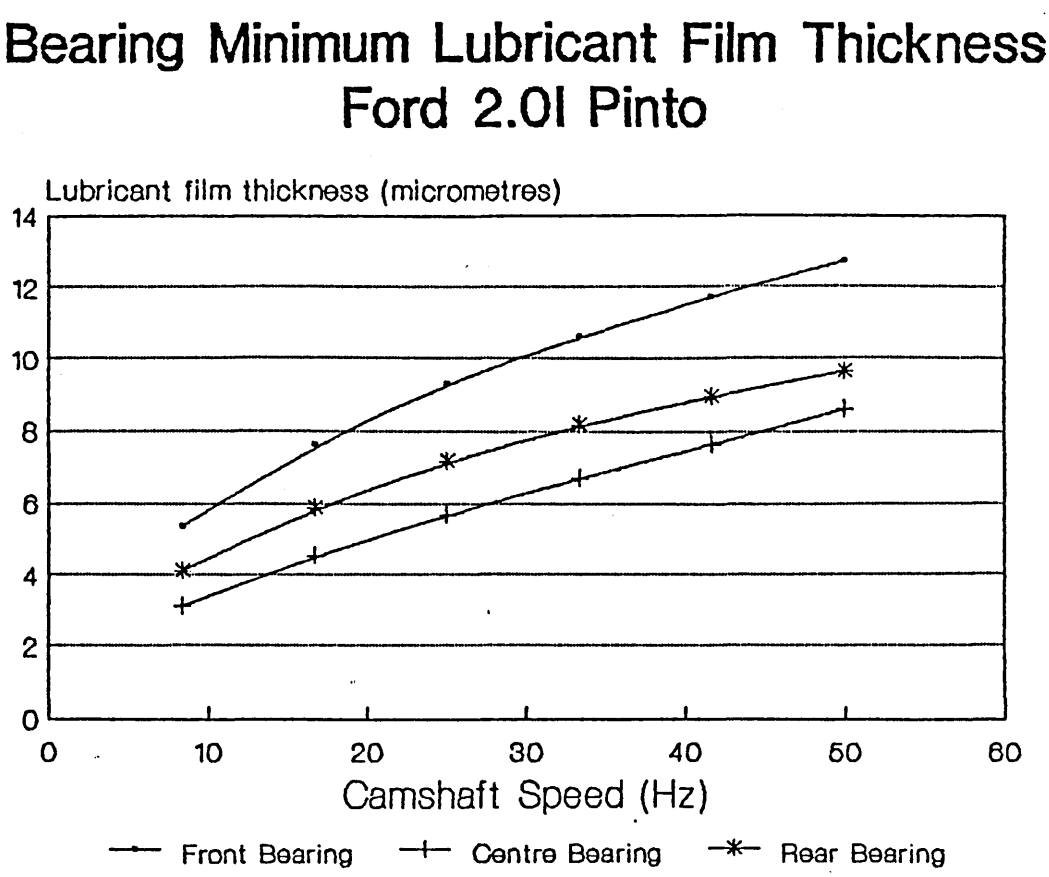

Figure (6.11) Camshaft Bearing Minimum Lubricant Film Thicknesses.

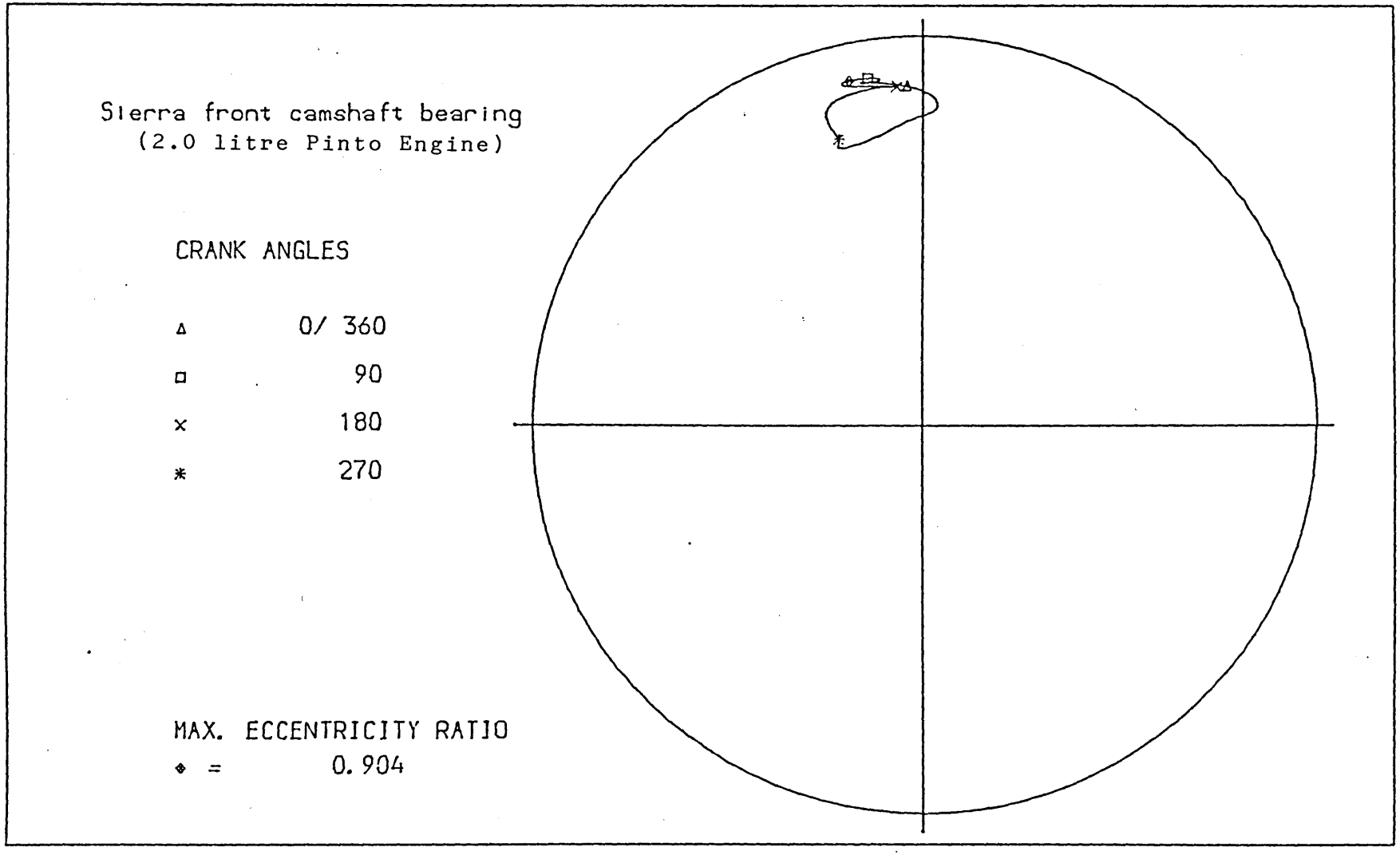

Figure (6.12) Journal Orbit for Front Camshaft Bearing at 25 Hz (1500 rpm)

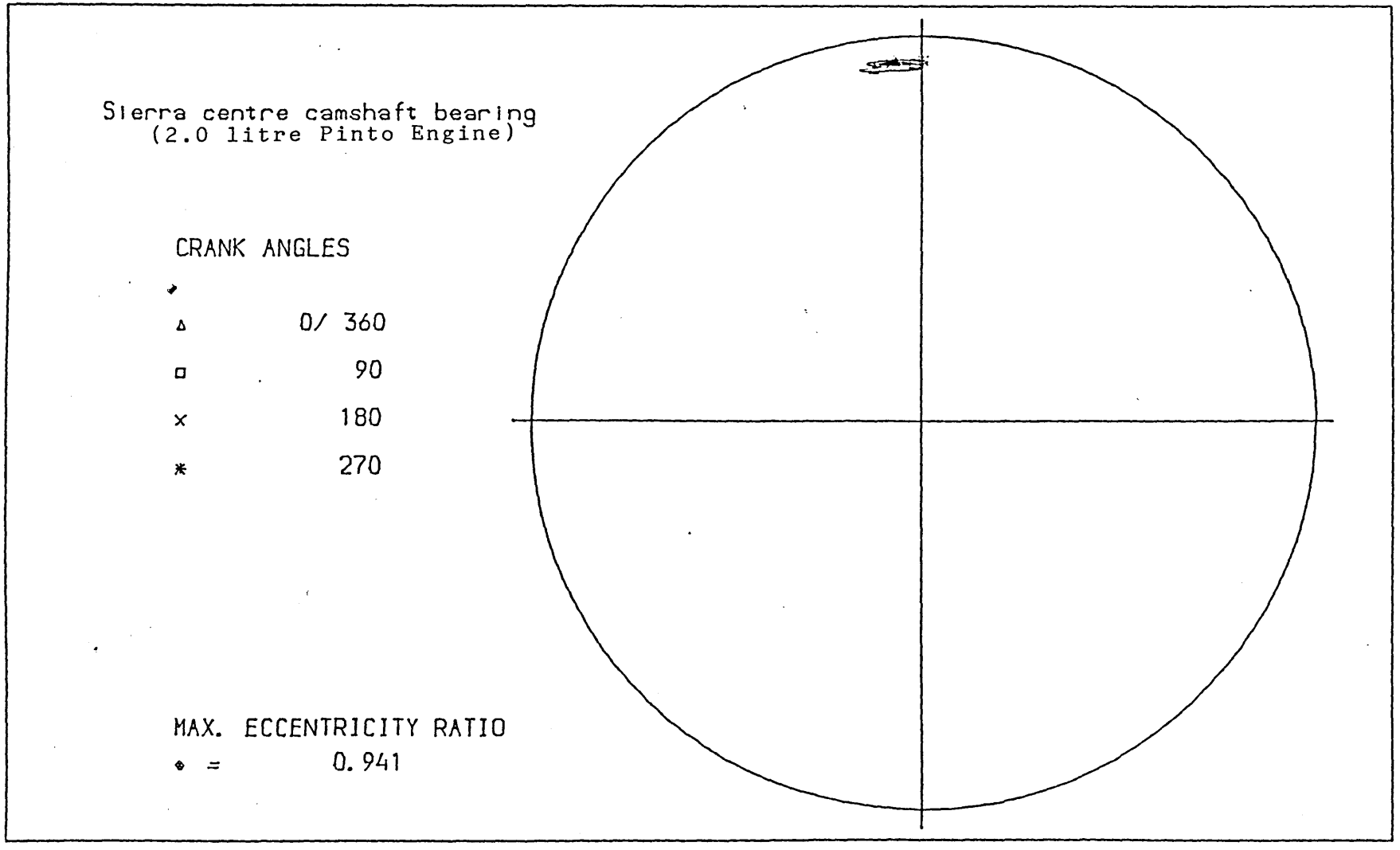

Figure (6.13) Journal Orbit for Centre Camshaft Bearing at 25 Hz (1500 rpm)

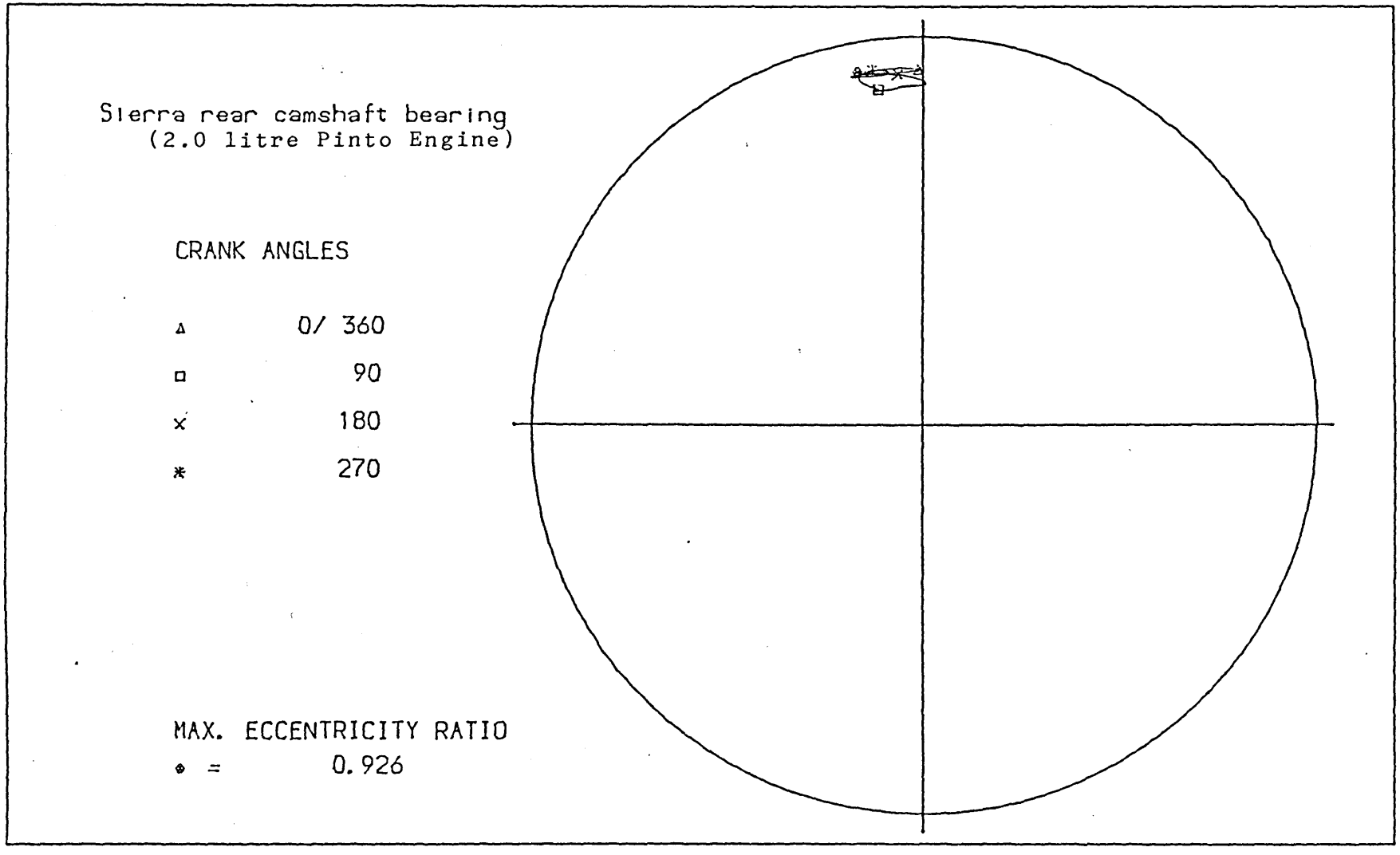

Figure (6.14) Journal Orbit for Rear Camshaft Bearing at 25 Hz (1500 rpm)

predicted for the cam/follower interfaces.

The predictions of power loss arising from the interaction of the cams and followers was found to be approximately five times greater than the predicted overall camshaft bearing losses. It was also found that the camshaft power losses increase with speed, accounting for approximately 0.5% of the total energy input to the engine.

It is believed that this is the first time that such results for camshaft bearings have been published. The results, although approximate, show a good agreement with experimental findings reported by other researchers.

CHAPTER 7

EXPERIMENTAL APPARATUS

7.1 Introduction

7.2 Past Experimental Investigations into Cam and Follower Lubrication

7.3 Aims of the Present Study

7.4 The Design of the Apparatus

7.5 Measurement Systems

7.6 Commissioning and Calibration

7.1 Introduction.

Today's internal combustion engine designer relies heavily upon computer aided design (CAD) techniques and other computer based analytical tools. The sophistication and complexity of these tools is growing rapidly. It is therefore important that the models, upon which these techniques are based, are validated and continually improved by experimental investigation.

This chapter will describe the development of an experimental apparatus used to investigate the interaction of cam and follower pairs. It will outline the steps involved, and the decisions taken, in its design. The chapter will also report upon the commissioning of the apparatus.

Firstly, there will be a brief discussion of the history of experimental investigations into cam and follower lubrication.

7.2 Past Experimental Investigations into Cam and Follower Lubrication.

There has been much experimental work carried out upon the effects of lubricant properties and additives with regard to the failure of cams and followers. Similarly, much has been reported upon investigations into the compatibility of the materials used in valve trains. Until relatively recently, however, very little literature had appeared that accounted for the frictional losses at the cam/follower interface. This is also true of studies relating to the correlation between theoretically predicted lubricant film thicknesses and experimental findings of either the film state or wear patterns upon the cam and follower.

7.2.1 Measurements of Cam/Follower Interface Friction.

Measuring the friction force at the cam/follower interface is very difficult. Firstly, it is not easy to separate the losses associated with components such as the cam journals and the valve guides. Secondly, the torque required to drive the camshaft can be

separated into two components; that due to the normal load on the cam (often known as the geometic torque), and that required to overcome the friction at the cam/follower contact. Isolating the frictional component has been the subject of several experimental projects which are described below.

Dyson and Naylor (1960-1961) were possibly the first to report upon attempts to measure the friction at the cam/follower interface. They utilised an apparatus incorporating a single cam acting against a nominally flat faced follower. The follower guide was suspended in a pair of flat springs; their deflection giving a measure of the cam/follower friction. They reported that this arrangement was unsatisfactory due to oscillatory problems associated with the flat springs.

Vichard and Godet (1966-1967) developed an apparatus in which an eccentric was driven against a follower. An indication of the frictional force at the interface was given by a strain gauged ring. This ring restrained the follower holder (in a similar manner to the flat springs used by Dyson and Naylor), the strain in the ring being related to the friction at the interface.

Armstrong and Buuck (1981) used a motored cylinder head with an in-line torque transducer to measure the driving torque and power requirements of several types of valve trains. The power loss associated with the oil seals and cam journals was evaluated by running the camshaft without the followers. This power loss was then subtracted from the overall power loss to give the power required to overcome the friction at the cam/follower interfaces, and to open the valves. No attempt was made to separate the frictional component from the geometric component.

Staron and Willermet (1983) carried out tests similar to the above. To reduce parasitic losses (losses in the journal bearings, seals, valve guides, etc) they replaced many of the bearings, for example, the rocker fulcrums, with rolling elements. The apparatus was eventually equipped with rolling element valve guides (Willermet (1987)).

Bair et al (1985) devised an ingenious arrangement to simulate the cam/follower contact. The follower remained stationary, except for rotation, whilst the cam was free to move through the lift cycle. The follower was located in a load frame with piezo-electric force transducers measuring the load in three mutually perpendicular directions. This allowed the friction force at the cam/follower contact to be evaluated.

Harrison (1985) and van Helden et al (1985) independently developed similar test apparatus in which the torque required to drive a single cam operating a flat faced follower was measured using an in-line torque transducer. Van Helden and his coworkers calculated the theoretical geometric torque to give the frictional torque at the cam/follower interface. Zhu (1988), utilised a similar technique in an extensive study that employed, and much improved, the apparatus used by Harrison.

7.2.2 Assessment of the Lubricant Film State at the Cam/Follower Interface.

The assessment of the lubricant film state in cam/follower contacts is not easy.

The correlation between theoretically predicted kinematic velocities (hence film thicknesses) and wear rates in valve train systems was reported by Coy and Dyson (1981), after experiments carried out on an Amsler machine adapted to simulate the kinematics of the cam/follower contact. This was followed by work carried out by Purmer and van den Berg (1981) on cams whose profiles were measured very accurately both before and after being run in a test apparatus.

The measurement of the lubricant film state during the operation of the cam within a test apparatus has been attempted by relatively few people. One reason is undoubtedly the difficulty in obtaining results in a harsh environment, where the load, radius of curvature, and surface velocities all change abruptly. Workers in this area have tended to concentrate on two methods, the global capacitance technique and the electrical resistivity technique. In the past two years other interesting methods have arisen. The following few

paragraphs briefly describe the major contributions to this field of study.

Vichard and Godet (1967-1968) used the global capacitance technique in an attempt to measure the minimum film thickness. The follower was electrically isolated from the cam so that the capacitance of the film formed between the two could be measured. Although the flux losses in the lubricant and the air surrounding the contact could be taken into account, difficulties arose in interpreting the results due to excessive electrical breakdown of the lubricant film.

Hamilton (1980) used a purpose built apparatus to measure the film thickness between a cam and flat faced follower. To overcome the problems of film breakdown he embedded a small electrically isolated capacitance gauge in the centre of a large flat faced follower. The apparatus allowed the follower to be moved so that the capacitance gauge could be subjected to different parts of the cam cycle. It was therefore possible to investigate the film thickness around many parts of the cam cycle. Hamilton's results appear to be very good over the cam base circle and the flanks. He reported that film breakdown was still a major problem across the nose of the cam.

Local film thickness measurements in an eccentric cam and flat faced follower system by means of miniature vapour deposited thin layer capacitance transducers were reported by van Leeuwen et al (1986). The results presented by the authors seem very encouraging. It is felt, however, that difficulties would arise with the durability of the transducers if they were to be used with actual cam forms, where the lubrication conditions would be much more severe, and film thicknesses much smaller, than those enjoyed by the eccentric used in the experimental apparatus.

The resistivity technique gives a measure of the amount of asperity contact during the operation of cams and followers (Watkins (1985)). It therefore gives a good indication of the degree of boundary versus elastohydrodynamic lubrication. The resistivity technique was employed by Ninomiya et al (1978) to investigate how engine oil viscosity affected the film state between a cam and follower in a motored engine. Harrison (1985) used the technique to

study the running in of cam and follower pairs. Harrison expressed concern over the effect that the potential difference across the contact might have upon the attraction of polar lubricant additives to the interacting surfaces. The formation of reaction layers would change the resistivity of the contact and cause problems in the interpretation of results.

Monteil et al (1987) used a variation of the resistivity technique to measure the film thickness at the cam/follower interface. No potential difference was applied across the contact, instead the electromotive force (emf) induced by the interaction of the cam and follower surfaces, was monitored. Smaller film thicknesses allowed more asperity contact causing a larger emf to be induced. Monteil and his co-workers used a base oil (without any additives) in their experiments, to prevent the formation of reaction layers which, they reported, would change the resistivity across the contact.

The technique developed by Monteil et al (1987) appears to be very promising (a more detailed explanation of the method can be obtained in Monteil's thesis (Monteil (1987)). The authors reported that the base circle clearance had to be set to zero as this affected the film thickness measurement system. This necessity, although a seemingly unimportant requirement, renders the technique impossible to use with some valve train systems. It also increases the amount of power required to drive the valve train.

7.3 Aims of the Present Study.

The present work is intended to validate (or otherwise) results obtained from a computer based model of a desmodromic valve train.

The valve train is described in Appendix (D). In the desmodromic arrangement a cam is used to close the valve instead of a spring, as is usually the case in conventional systems. The valve train was designed by Ricardo Consultant Engineers Ltd. for the Ford Motor Co. Ltd. as part of a large valve train evaluation programme. The original concept of the programme was to compare the operation of different valve trains under similar conditions. To this end, several

valve trains were designed using nominally the same lift characteristics. These designs are currently being tested at the Industrial Unit of Tribology (IUT) at the University of Leeds in a specially designed test apparatus. The desmodromic valve train was chosen for this study as the Ford Motor Co. Ltd. had shown a specific interest in this mechanism and also because very little was known about the tribology of such systems.

The apparatus is designed to take a single valve, and its operating mechanism, of any type of valve train design. This allows the power loss of various different designs of valve train to be compared, under similar conditions, with common cam drive train and valve guide losses. The tests consist of a series of measurements of the torque requirements of the valve train at different operating speeds.

The computer program (described in Chapter (4)) gives predictions of torque and power requirements, and Hertzian stress and lubricant film thickness at the cam/follower interface around the operating cycle. In order to validate the predictions, the experimental apparatus would have to be capable of:

(i) measuring the torque and power requirements to operate the valve train,

(ii) giving an indication of the film state at the contact, and

(iii) giving an indication of which cam and follower pair in the desmodromic arrangement was in control of the valve at any one time in the cycle.

In addition to these measurements, values of the cam and follower surface roughness and profile traces would be taken before and after the running of the valve train.

7.4 The Design of the Apparatus.

The major problem in designing an apparatus to study the tribological behaviour of cams and followers was seen as the difficulty in isolating the frictional torque, caused by the interaction of the cams and followers, from the parasitic torques

inherent in the system.

It was felt that apparatus that simulated the contacts at the cam/follower interfaces were too complex to work satisfactorily in practice, the complexity being further exaggerated, to almost unthinkable proportions, when desmodromic arrangements are considered. The decision was therefore made to build an apparatus that would, as far as possible, use standard valve train components.

As the apparatus designed by the IUT appeared to be working very satisfactorily, with few problems, it was decided that an apparatus should be built based upon the IUT design. Several changes were made to arrive at a solution that would satisfy the requirements of the project:

(i) The lubricant film state was to be measured using the resistivity technique as this was felt to be the most reliable technique, and there was experience of this technique within the Institute of Tribology at Leeds.

(ii) The temperature of the oil supply was to be thermostatically controlled to allow investigations to be carried out at oil temperatures experienced in engines. The temperature of the oil at inlet and outlet to the apparatus was also to be monitored using thermocouples.

(iii) Thermocouples were to be attached to the cams and followers to allow their temperatures to be monitored.

(iv) The torque transducer was to be linked to the analogue to digital converters (ADC's) on a VAX 8600 mainframe computer. Triggering of the ADC's and angular reference was to be gained using an optical shaft encoder.

The general layout of the apparatus is shown in Figure (7.1). A detailed drawing is given in Figure (7.2).

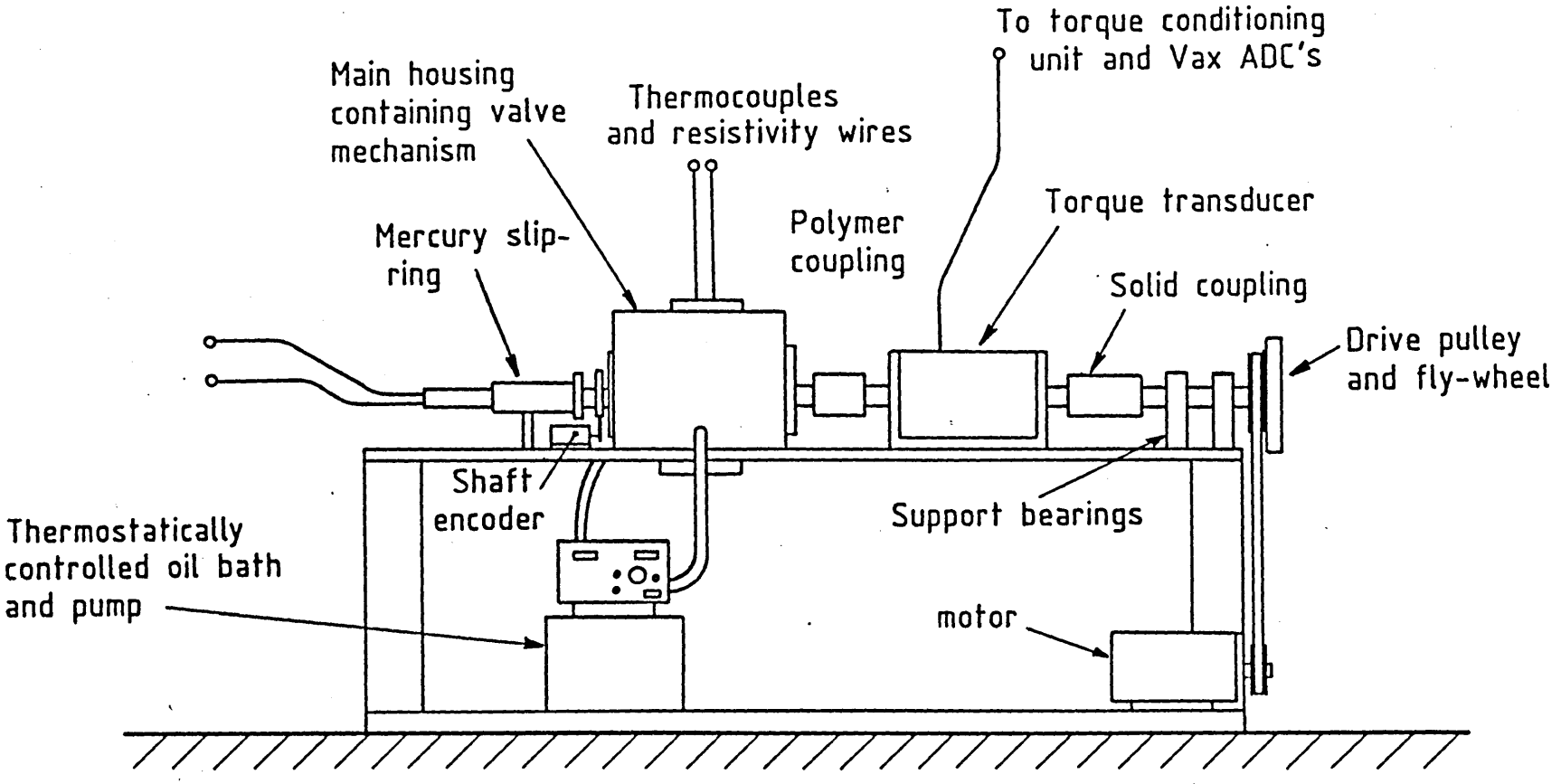

Figure (7.1) General Layout of Experimental Apparatus.

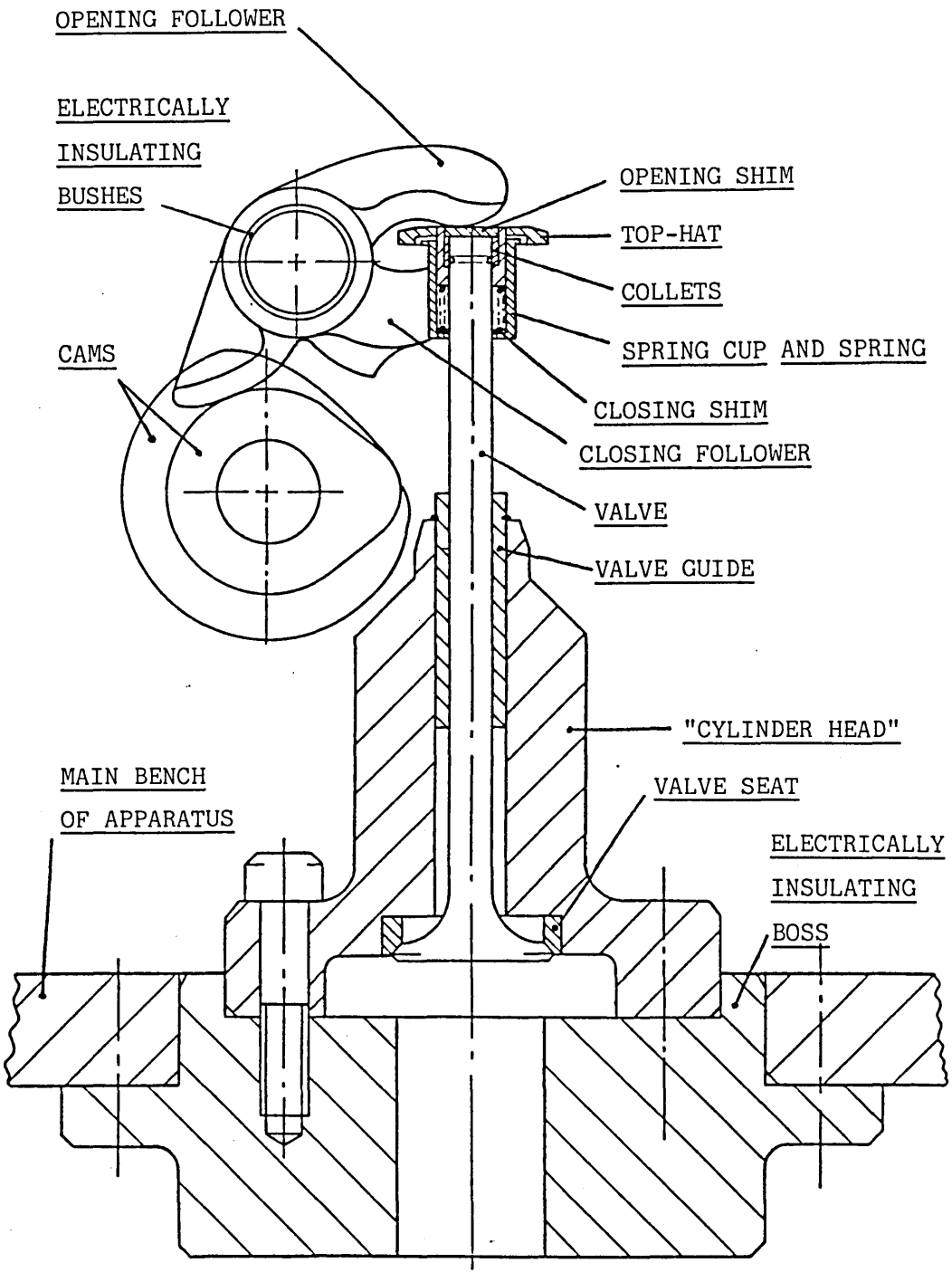

Figure (7.2) Detailed Drawing of Experimental Desmodromic Valve Train Test Apparatus.

7.5 Measurement Systems.

7.5.1 Torque Measurement.

The torque required to drive the valve mechanism was measured using an in-line torque transducer (Vibrometer TG2/BP). It was necessary to use a torque transducer with a high rating (20 Nm) as a high torsional natural frequency was required in order to minimise the torsional oscillations along the cam drive train.

The signal from the torque transducer was fed to a conditioning unit (Vibrometer TG P/N M) where it was amplified and passed to the ADC's attached to the mainframe computer. The signal to the ADC's was amplified such that the maximum possible torque requirement of the apparatus would pass an 8.0V signal. This gave an acceptable signal to noise ratio, and a workable maximum limit compared to the ADC saturation voltage of 10.0V.

The ADC's were programmed to capture the torque signal upon command from the operator. Two thousand data points were collected at equal angular increments over two camshaft revolutions. A one thousand pulse per revolution shaft encoder (Gaebridge 1000M/23/5/10) was used to clock the ADC's. The shaft encoder also gave a single datum pulse each revolution which was set to be synchronous with the valve maximum lift position.

The power required to drive the apparatus was obtained from the torque signal and the camshaft rotational speed. The rotational speed was obtained by measuring the elapsed time between the datum pulses emitted by the shaft encoder.

7.5.2 Resistivity Measurements.

The camshaft and the followers were electrically isolated from the rest of the apparatus by means of insulating bearing housings. The two followers were electrically isolated by means of a polymer separating shim and insulating bushes upon the rocker shaft. The shim between the valve tip and the opening follower was made of a ceramic material (partially stabilised zirconia). A potential difference was

applied between the camshaft and the followers via a slip-ring assembly on the end of the camshaft and insulated wires to each of the followers. This enabled the interaction of the cams and their respective followers to be studied separately.

The apparatus used for the resistivity measurements was the same as that employed by Harrison (1985), except that the contact pulses were captured by the VAX mainframe's ADCs. Figure (7.3) shows the circuit diagram of the resistivity curcuit. The variable resistors (R_3) and (R_4) represent the resistance of the oil films between the opening and closing cam and follower pairs respectively. A potential difference of 50mV across resistors (R_1) and (R_3), and (R_2) and (R_4) was maintained by a precision voltage source. It has been shown (Nimoniya et al (1978)) that this potential difference was sufficiently small to prevent arcing across the very thin films, which would obviously cause damage to the cam and follower. It was also felt to be high enough to give an adequate signal to noise ratio. Harrison (1985) showed that this potential difference was unlikely to cause electrical breakdown of the lubricant film for film thicknesses greater than 0.1μm.

The operation of the resistivity curcuit can be illustrated by considering just one cam and follower pair, for example the opening cam and follower. When the cam and follower are separated by an oil film the resistance (R_3) of the contact is large. When metal to metal contact of the cam and follower occurs the resistance (R_3) falls, allowing a current to flow across the contact, thus the potential difference across (R_3) falls. This drop in potential is registered by the VAX ADCs, angular reference being attained from the shaft encoder.

7.5.3 Cam/Follower Contact Measurements.

In order to validate the analytical model of the desmodromic valve train it was necessary to evaluate which cam and follower was controlling the valve at any one time during the lift cycle. To do this it was decided that a continuity test should be performed.

As the components were electrically isolated from the main part

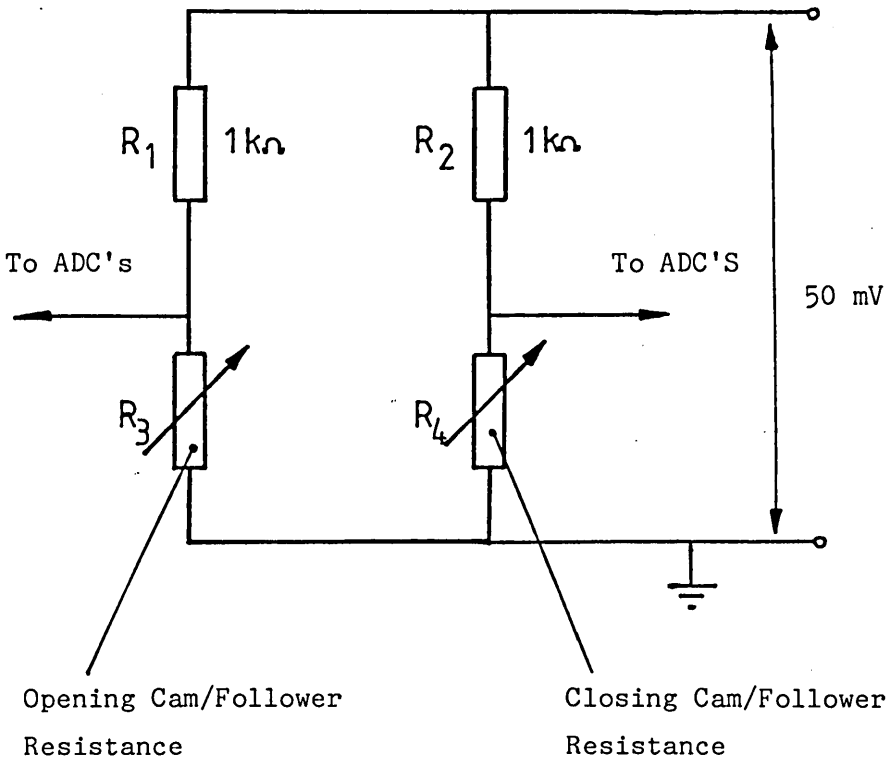

Figure (7.3) Curcuit Diagram of the Resistivity Apparatus.

of the apparatus, this was easily accomplished. Figure (7.4) shows a circuit diagram of the apparatus used. A potential difference of 15V was applied between the camshaft and the followers. This potential was deemed large enough to cause electrical break down of any lubricant between the cams and followers. As this eventually causes damage to the cams and followers due to arcing, old pairs of cams and followers were used for this test.

Resistors (R_3) and (R_4) represent the resistances between the two respective cam and follower pairs. When a cam and follower pair was in contact the resistance (R_3), say, would fall to zero and the potential difference across that contact would become zero. The potential difference across each contact was monitored by separate channels on the ADC's on the VAX mainframe computer. When a cam was not in control of it's follower, i.e. a clearance was present between the cam and follower, the ADC's would receive a signal of 15V which would cause them to saturate at 10V.

7.5.4 Temperature Measurements.

The temperatures of the nose of each cam, the centre of the contact patch of each follower, and the lubricant at entry to and exit from the main housing were measured. This was carried out using nickel-chromium thermocouples connected to a Comark electrical thermometer (type 1604-2). The thermocouples in the cams and followers were fixed within holes spark eroded parallel to the contacting faces. The thermocouples were thus located approximately 1.0mm from the contacting surfaces.

7.5.5 Torque Signal Filtration.

Upon initial testing of the apparatus it became apparent that there was considerable noise within the torque signal. This noise arose from three sources:

(i) From unwanted vibrations of the apparatus (mainly the camshaft and the torque transducer),

(ii) From noise generated by the torque transducer's conditioning unit, and,

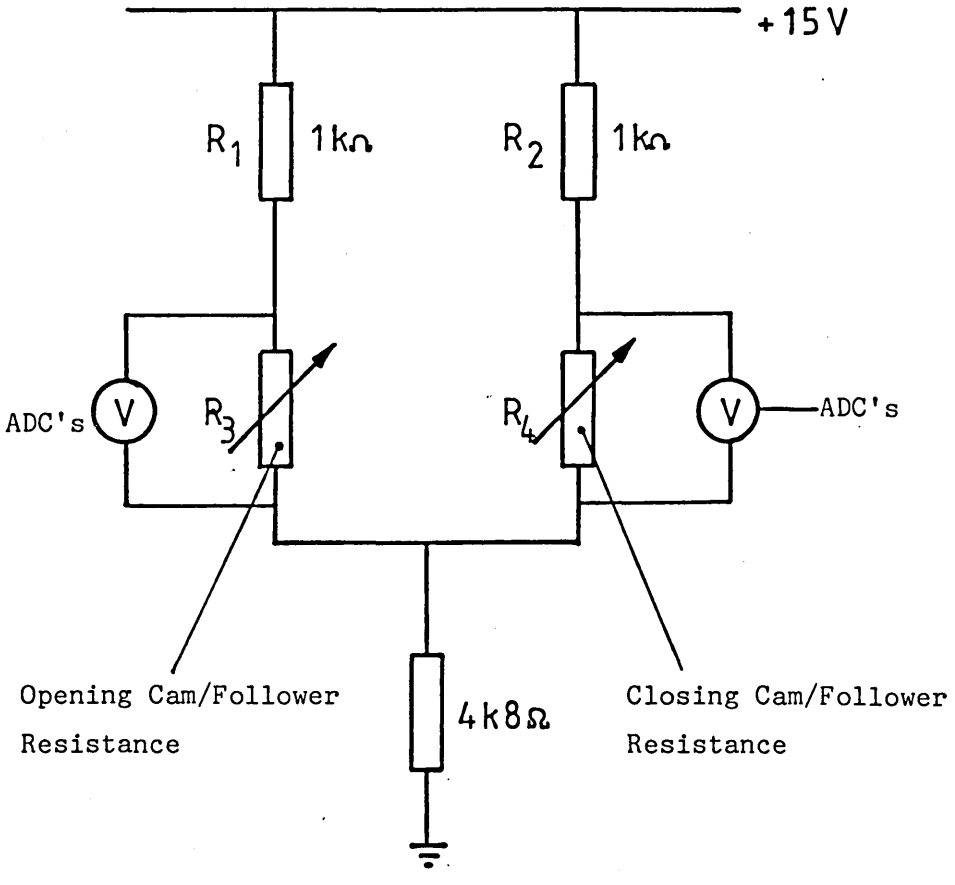

Figure (7.4) Electrical Curcuit Used For The Continuity Experiments.

(iii) From background noise such as mains frequency pick-up and other noise introduced along the lengthy cable joining the apparatus to the VAX mainframe.

Initially it was felt necessary to filter the signal in order to gain information regarding the variation of the torque requirement of the camshaft around the cycle. Tests were performed to investigate the effects of filtering the torque signal.

Firstly, the torque signal was filtered using an electrical Kemo Variable Filter (type VBF/24). This filter was an eighth order elliptic filter giving a slope attenuation of 135dB/octave (i.e. an 80dB attenuation would be gained at one and a half times the selected cut-off frequency in low pass filter mode). The filter was used in low-pass mode in order to reject frequencies around and above the resonant frequency of 400Hz. The cut-off frequency was selected using a spectrum analyser to ensure that the main part of the signal was not lost. It was found, however, that this filter caused severe attenuation and large phase shifts of the torque signal.

The torque signal was then filtered using an eighth order Butterworth lowpass digital filter designed by Zhu (Zhu (1988)). The filter uses an ingenious concept of filtering the data twice in order that any phase shifts of the data are eliminated. The raw data is passed through the filter and then the processed signal is filtered a second time, but in reverse order, thus negating any phase shifts that occurred on the first pass. It was found, however, that although this method of filtering the signal gave results with little or no phase shift of the original signal, it still considerably attenuated the signal around the positions of peak torque. Figure (7.5) shows the filtered and unfiltered torque signals at a camshaft speed of 16.7 Hz (1002 rpm) (the theoretical torque is also shown as it is part of the graphical output of the data processing program - its evaluation will be explained in the next chapter). The attenuation of the signal caused by the filter can be clearly seen, as can the resonant frequency of 400 Hz in the unfiltered signal.

It was therefore decided that the signal should be left unfiltered as this at least appeared to give an insight into the

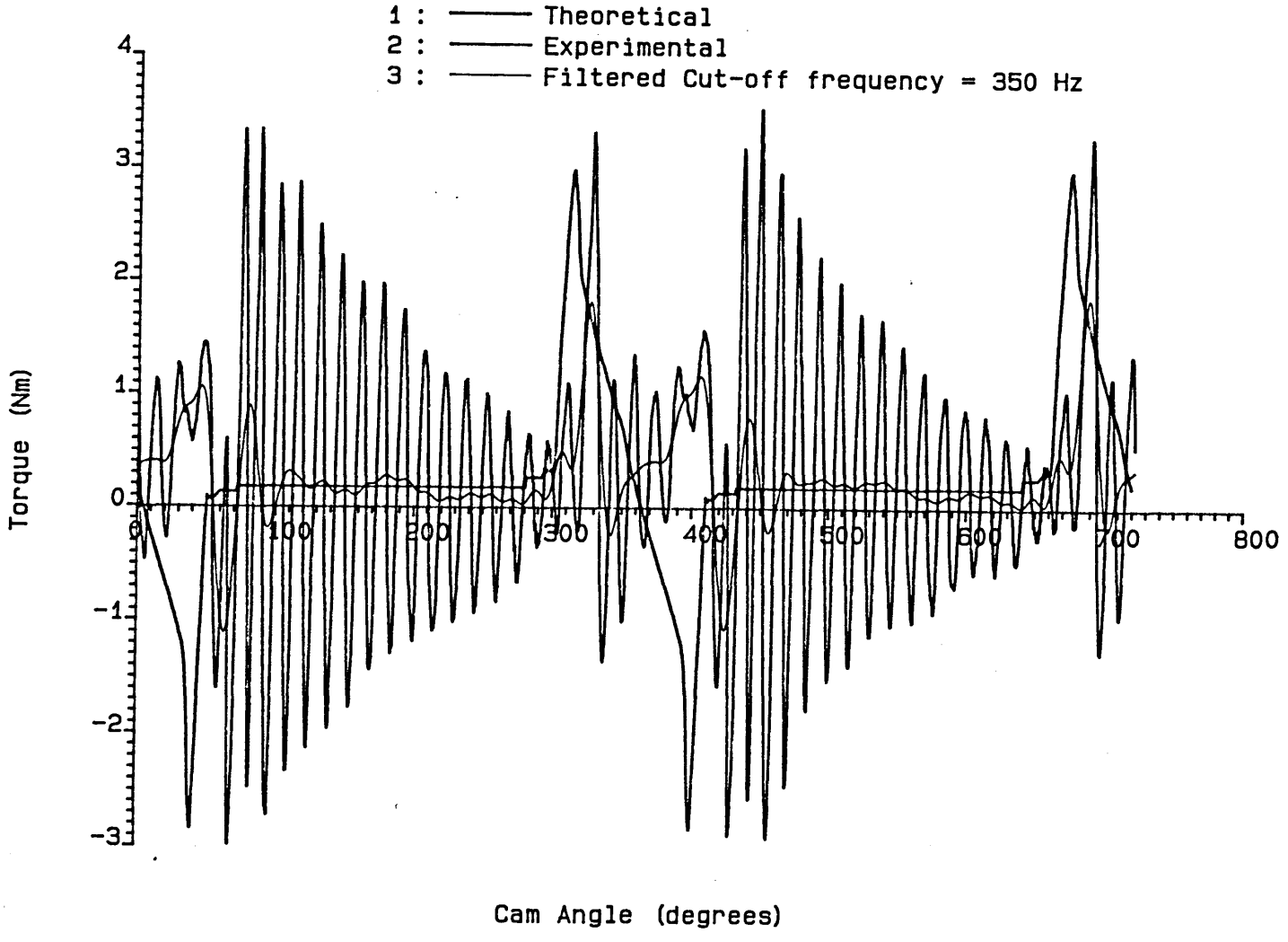

Theoretical and Experimentally Measured Torque Variation.
Camshaft Rotational Speed = 16.7 Hz. Oil Supply Temp = 60C.

Figure (7.5)

magnitude and position of the maximum torques around the valve lift cycle.

7.6 Commissioning and Calibration.

7.6.1 Commissioning.

The apparatus was built with great care to ensure that components were properly aligned. The valve gear was shimmed so that the valve stem and spring cup sat at the correct height to give the working clearances required along the base circle and at the maximum lift position.

Initial testing of the apparatus was used to identify the source of troublesome torsional vibrations. These vibrations were traced, using a spectrum analyser, and were found to be caused mainly by a flexible coupling placed between the camshaft and the torque transducer. The replacement of the flexible coupling, with a solid one, reduced the level of the noise substantially. By tracing such problems by spectrum analysis it was possible to raise the torsional natural frequency of the apparatus to 400 Hz, and to obtain a much 'cleaner' torque signal.

It was found that the spring cup was not strong enough and would break after only a few revolutions of the camshaft. A new spring cup of slightly larger dimensions was manufactured from EN30B nickel-chromium steel and hardened to 400 Brinell. This proved to be satisfactory.

Severe problems were encountered when the camshaft rotational speed was increased to values above 33.33 Hz (2000 r.p.m.). At this speed the operation of the valve train became very noisy, so much so that it was impossible, and very fool-hardy, to work near the apparatus without using ear-defenders. When operating at these higher speeds it was found that within a very short space of time the collet retainer would fracture, thus neccessitating the shutting down of the apparatus. The source of the problem, it is believed, was due to the offset between the closing cam/follower contact and the closing follower/collet retainer contact in the direction parallel to the

rocker shaft (see Figure (7.6)). This offset induced a moment causing the closing follower to twist on its bush. Evidence of this twisting was found when the closing rocker bushes and the closing cam/follower contact patches were inspected, wear was found not to be uniform across the contact patches. This twisting would caused only one side of the closing follower forks to contact with the collet retainer and spring cup. This would then give rise to significant bending moments in the collet retainer leading eventually to failure. The twisting would also reduced the operating clearance between the two pairs of cams and followers thus increasing the contact loads. It was therefore decided that the camshaft rotational speed should be restricted to 33.33 Hz (2000 r.p.m.).

It was also found during the commissioning tests that the life of the thermocouples attached to the followers was very limited due to failure by fatigue caused by their continual oscillation. As a partial solution to this problem, two thermocouple wires were embedded into each follower, to increase the probability of attaining a successful reading. As thermocouple failure was a very regular occurrence, it was deemed not to be grounds to stop a test, and experiments would be continued without the temperature measurement.

7.6.2 Calibration of the Torque Measurement System.

The torque transducer was calibrated by applying a series of loads at a known radius from the shaft's centre of rotation. During the calibration the torque transducer was disconnected from the camshaft. The part of the torque transducer attached to the driving pulley was locked whilst the loads were applied to the other end.

The series of known applied torques then gave a series of voltages at the ADC's which could be read from a computer terminal. A straight line fit to these points gave an rms residual of less than 0.1% of the maximum reading. A check was made to ensure that there were no hysterisis effects. The torque data acquisition program was then amended to convert the voltage applied to the ADC's to applied torque (Nm).

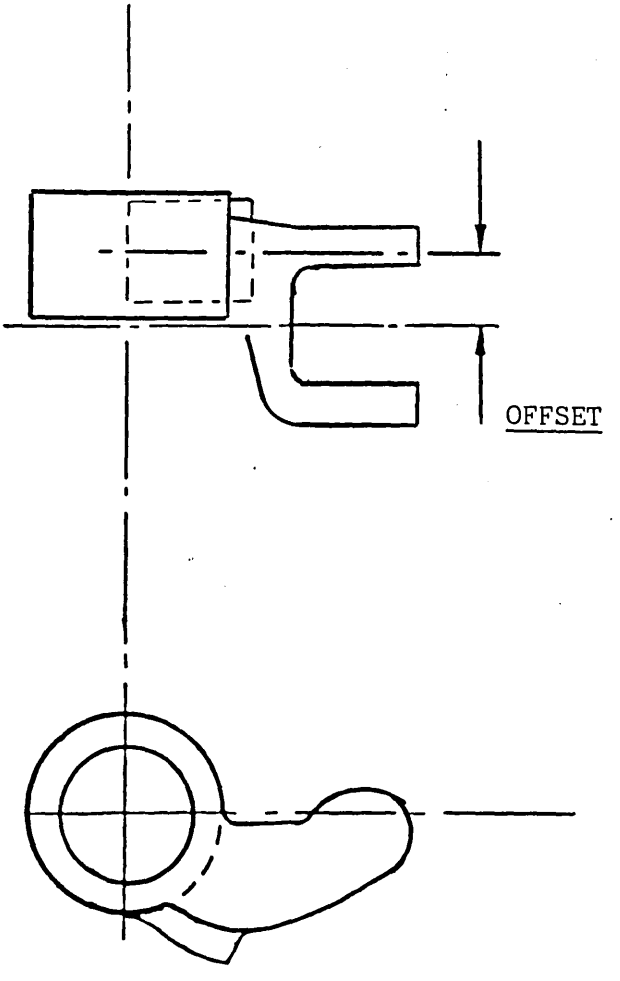

Figure (7.6) Desmodromic Closing Cam Follower.

7.6.3 Oil Characteristics.

The oil used was Texaco ETL 0671 E. This is the base oil of the 10W/30 lubricant normally specified by the Ford Motor Co. Ltd. A base oil was used as it contains no polar additives. These would create reaction layers upon the cam and follower surfaces. The presence of such reaction layers would significantly raise the resistivity of the contact area (see Monteil (1987)) and this, in turn would make the interpretation of the resistivity results very difficult. Even though the lubricant selected contained no polar additives it was felt unlikely that the formation of surface reaction layers would have been completely prohibited as the base oil would still contained some reactive species or polar species. By using a base oil the formation of reaction layers was kept to a minimum.

It was necessary to know the temperature/viscosity characteristics of the oil as this was an important parameter in the theoretical analysis. This was achieved by using a suspended level viscometer. The variation of dynamic viscosity of the lubricant with temperature is shown in Figure (7.7).

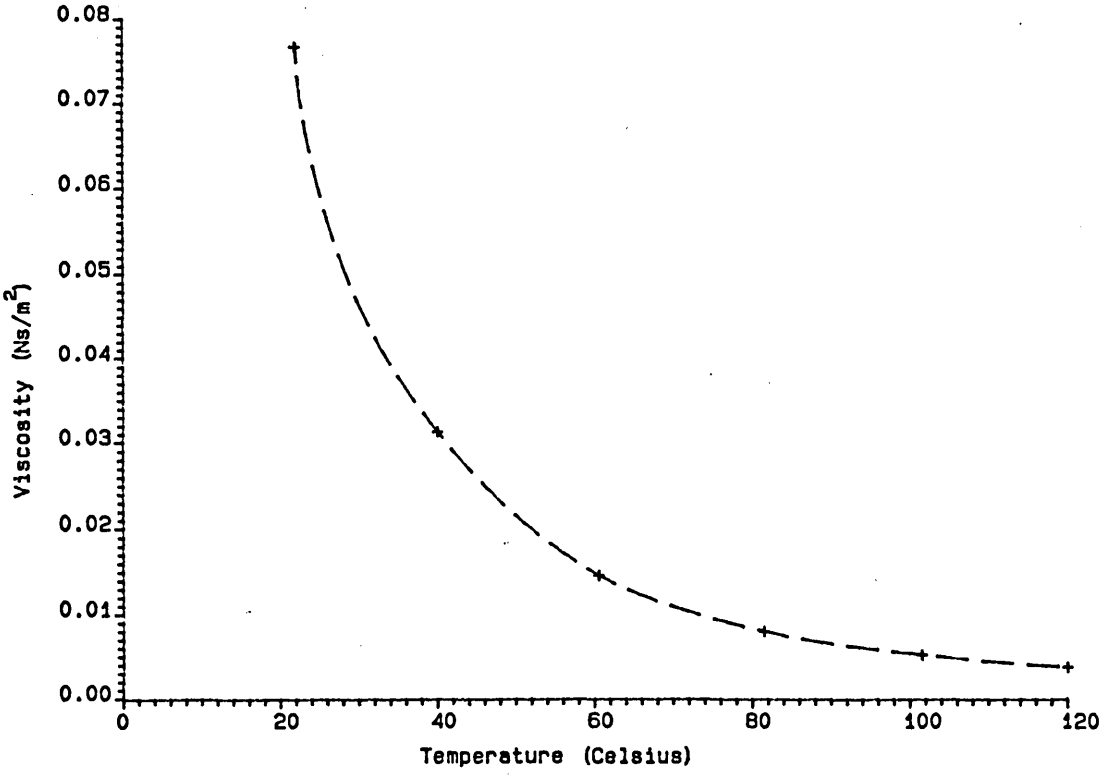

Figure (7.7) Variation of Lubricant Dynamic Viscosity with Temperature.

CHAPTER 8

EXPERIMENTAL RESULTS AND THEIR COMPARISON WITH THE PREDICTIONS OF THE THEORETICAL ANALYSIS

8.1 Introduction.

This chapter describes the experimental project carried out using the apparatus detailed in the previous section. It will define the experimental procedures adopted and will then report the findings and their comparisons with theoretical predictions.

8.2 Experimental Procedures.

It was felt important that a concise method be established prior to the commencement of any experiments. This ensured that clear aims could be attributed to the project. The aims of the work have been discussed in greater detail in the previous chapter, but to summarise, they were:

(i) to measure the torque and power requirements to drive the valve train,

(ii) to give an indication of the film state at the contact,

(iii) to discover which cam and follower pair in the desmodromic arrangement was in control of the valve at any one time in the valve lift cycle, and

(iv) to detect any changes in the cam and follower surface roughness.

These aims were drawn up so that the theoretical models detailed in previous chapters could be tested.

The experimental procedures adopted to realise these aims were:

(i) The surface roughnesses of the followers (in directions parallel and perpendicular to the direction of sliding) were measured before and after the tests. This was done using a using a Taylor Hobson Talysurf 5-120 - an instrument that accurately charts the movement of a stylus across the test piece, and can evaluate surface roughness parameters.

(ii) The valve train was run-in for a period of eight hours

continuous operation at a camshaft rotational speed of 16.67 Hz (1000 rpm). This speed was chosen arbitrarily, although it was felt to represent a reasonable average speed for an engine being run-in during normal operating conditions. The data aquisition program was run after fifteen minutes of operation, then after one hour of operation, and then subsequently at one hourly intervals. It was programmed to read data from the torque transducer and from the resistivity curcuits. The thermocouple readings were noted manually.

(iii) The apparatus was then run at camshaft rotational speeds ranging from 8.33 Hz (500 rpm) through to 33.33 Hz (2000 rpm) in steps of 4.17 Hz (250 rpm). At each speed setting the apparatus was allowed to reach a steady state (this was judged to have occurred when the readings from the thermocouples embedded within the cams and followers had stabilised). The data aquisition program was then used to capture data from the torque transducer. Again the thermocouple readings were noted manually.

The procedure was carried out using three different sets of cams and followers, each being used at a different operating temperature. The oil temperature at inlet to the apparatus was regulated and tests were performed with the lubricant inlet temperature at 40C, 60C, and 80C. For all of the tests the oil flow rate was fixed at 0.1 litres/minute.

A series of continuity tests, to establish which cam and follower pair was in control of the valve at any one point around the cam cycle, were performed using a separate set of cams and followers (those used to commission the apparatus). The lubricant inlet temperature was fixed at 40C for these tests. The tests were performed at camshaft rotational speeds of 8.33 Hz, 16.67 Hz, 25.00 Hz and 33.33 Hz (500 rpm, 1000 rpm, 1500 rpm, and 2000 rpm respectively).

8.3 Experimental Results.

8.3.1 Running-In of the Valve Train.

8.3.1.1 Variation of Mean Torque.

The variation in mean torque requirement during the running-in of the valve-trains operating at the three different temperatures is shown in Figure (8.1). It can be seen that in general the torque level declined to a fixed value. It can also be seen that the torque level reached a steady level quickest for the valve-train that operated with an oil inlet temperature of 80C, followed by that at 60C, and finally, that at 40C (which still showed signs of decreasing at the end of the eight hours running-in). This suggests that the cams and followers operating at the higher lubricant temperatures ran-in more quickly than those at lower temperatures. This could perhaps be explained by any of three phenomena (or perhaps a combination of the three):

(i) The lubricant viscosity was lower at the elevated temperatures (hence the lubricant film thicknesses separating the cams and followers would be smaller) and so the surfaces became more conforming at a higher rate due to the larger number of asperity contacts, or,

(ii) Surface reaction layers built up more quickly at the higher temperatures because the chemical species responsible for these reactions became more active when the temperature and amount of surface contact were increased, or,

(iii) The material properties of the cams and followers were changed as the temperature increased - the asperities becoming more plastic and hence more susceptible to permanent deformation.

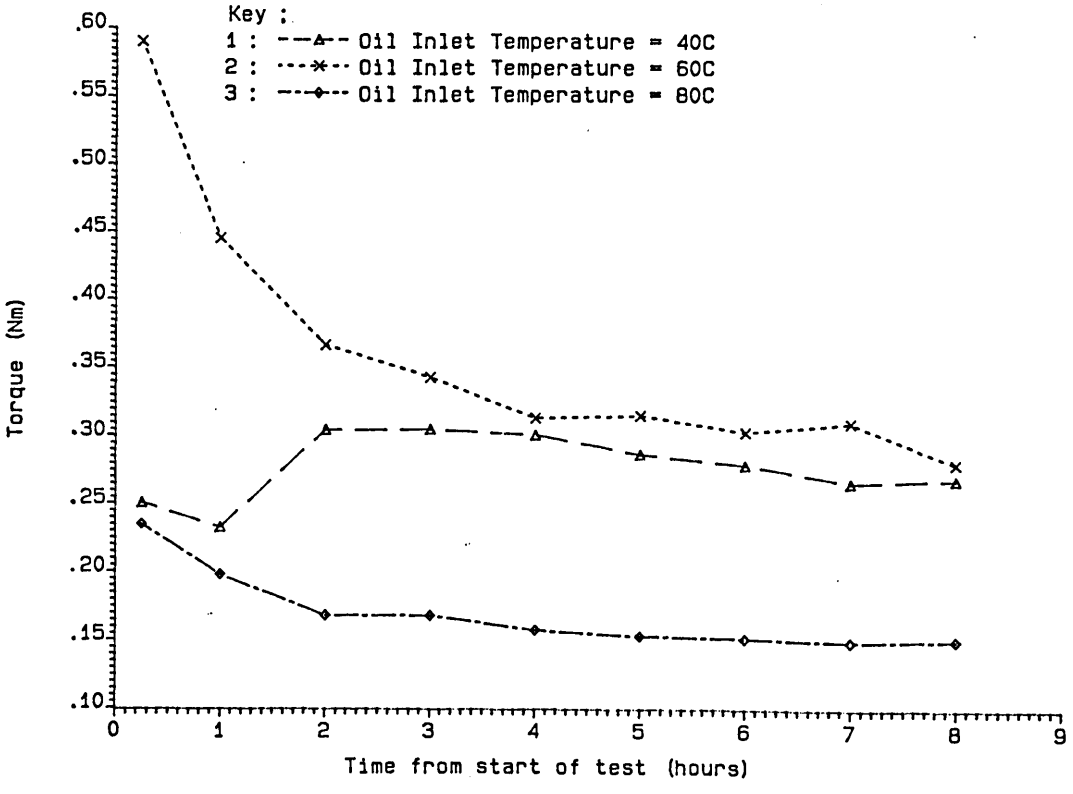

Graph Showing the Variation of the Mean Torque Levels During the Running-In of the Valve Trains

Figure (8.1)

8.3.1.2 Resistivity Measurements.

Figures (8.2), (8.3), (8.4), (8.5), (8.6) and (8.7) show the results of the resistivity measurements for the opening and closing cams at the different operating temperatures after fifteen minutes of running and after eight hours of running. It can be seen that the cams and followers operating at the higher temperatures were apparently suffering less surface interaction after eight hours of running-in than those at the lower temperatures. This again could be explained by either the surfaces becoming more conformal at a faster rate, or, by the more rapid growth of high resistivity surface layers at the higher temperatures.

It can be seen that the closing cams and followers operating at oil inlet temperatures of 60C and 80C (Figures (8.5) and (8.7) respectively) were initially suffering contact throughout almost all of the cam cycle. The closing cam/follower pair operating at 60C had a brief moment of separation at the end of the cam lift cycle, on the closing ramp, the separation probably being caused by the dynamic effects of the valve hitting the valve seat. After running for eight hours the amount of surface interaction had fallen dramatically, with evidence of full fluid films existing during parts of the cycle. The majority of the interactions can be seen to have occurred around the base circle radius portion of the cam. This is consistent with the predictions for lubricant film thickness around the cam cycle, which predict smaller lubricant film thicknesses (at a camshaft speed of 16.67 Hz) around the base circle radius than around the cam nose for the closing cam (see Figure (8.8) and also Appendix (F), where the output from the valve train lubrication analysis program for the opening and closing cam/follower pairs is presented). This is due to the lower lubricant entrainment velocities around the cam base circle radius than the cam nose caused by the larger radius of curvature of the nose. This is opposite to the findings in conventional cam and followers where the entrainment is very small around the nose and a clearance usually exists between the cam and follower around the base circle radius. (Also interesting are the four points of predicted zero lubricant film thickness, due to four points where the entrainment velocity falls to zero. These points occur in pairs at

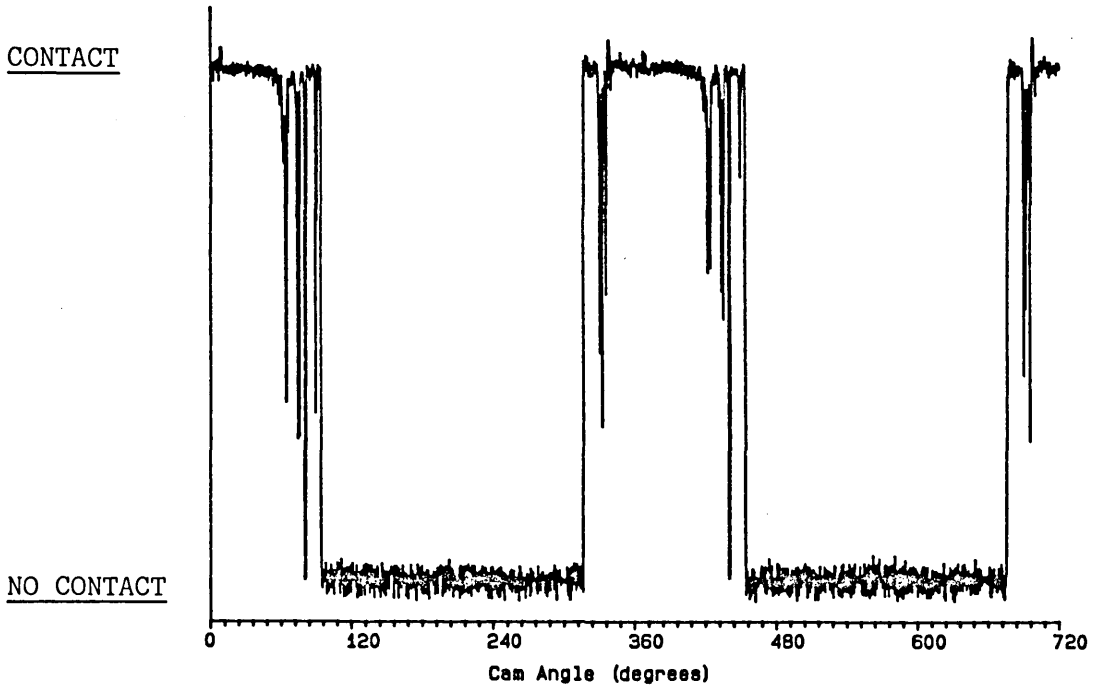

Resistivity Tests for Opening Cam and Follower.
Oil Supply Temp = 40C. Time = 0hrs 15mins.

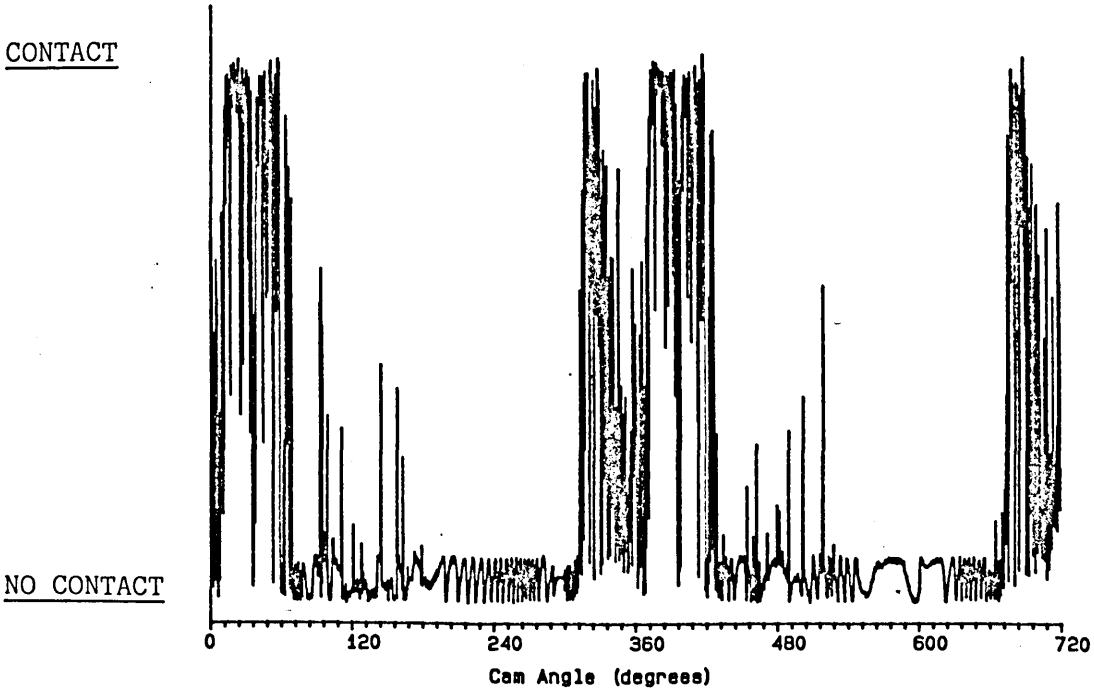

Resistivity Tests for Opening Cam and Follower.
Oil Supply Temp = 40C. Time = 8hrs 00mins.

Figure (8.2)

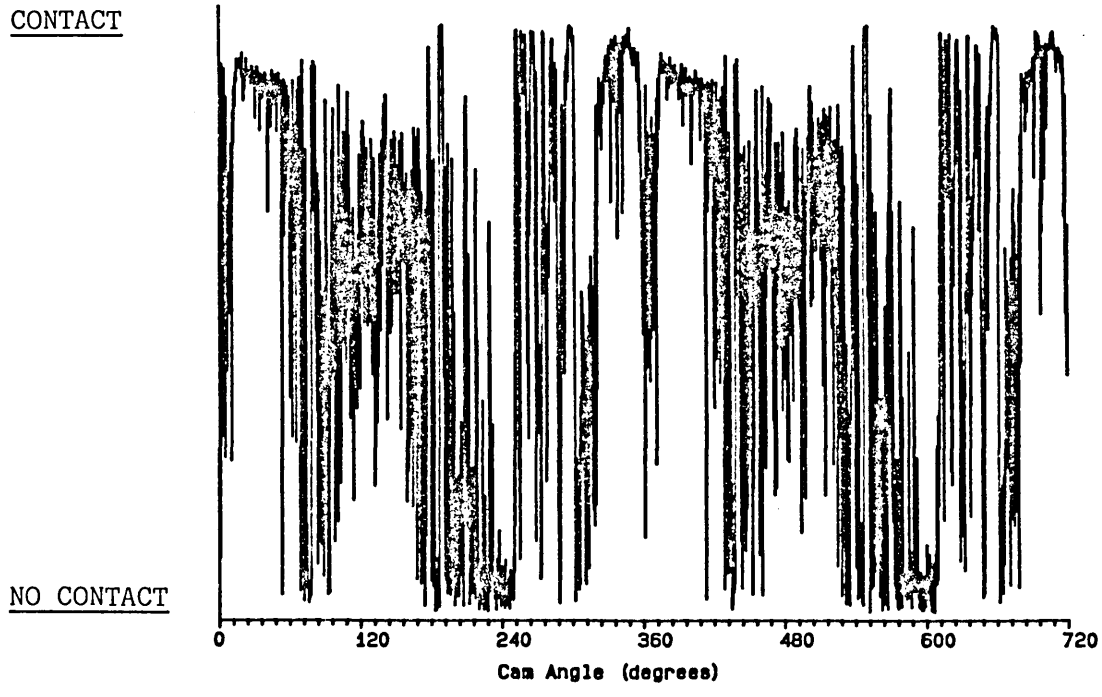

Resistivity Tests for Closing Cam and Follower.
Oil Supply Temp = 40C. Time = 0hrs 15mins.

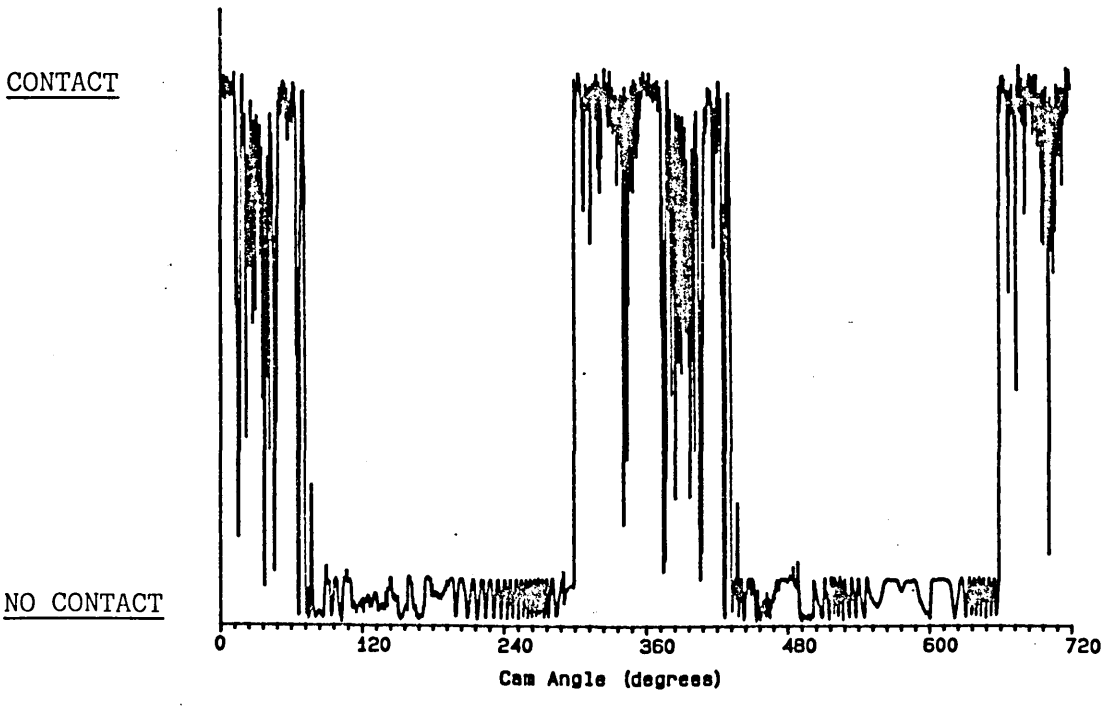

Resistivity Tests for Closing Cam and Follower.
Oil Supply Temp = 40C. Time = 8hrs 00mins.

Figure (8.3)

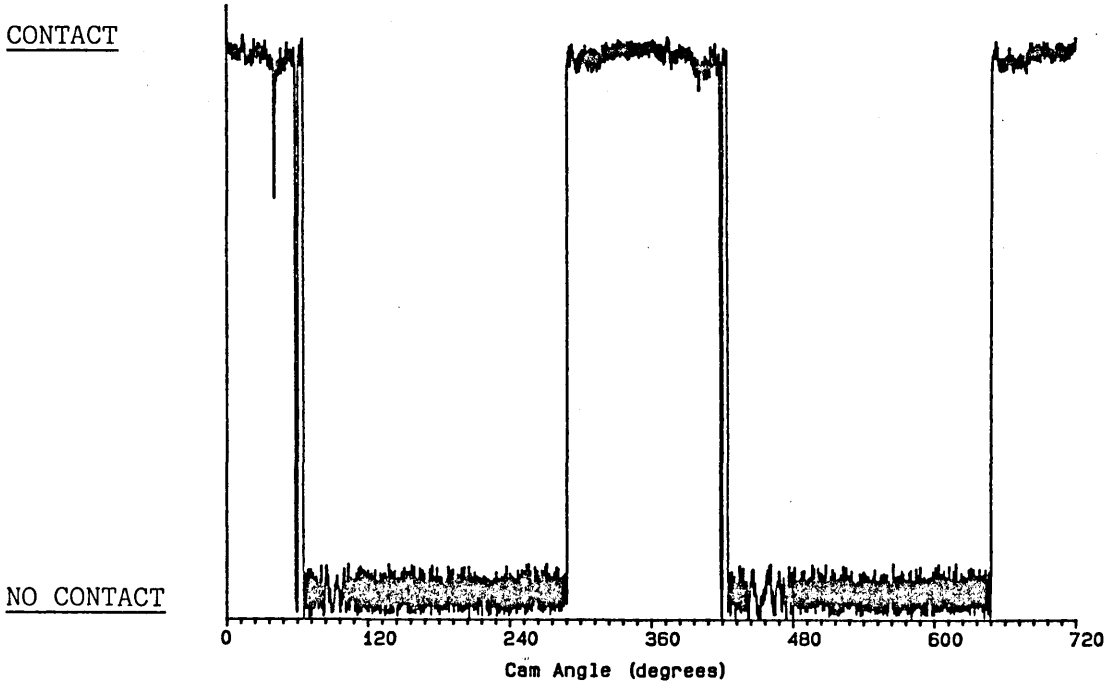

Resistivity Tests for Opening Cam and Follower.
Oil Supply Temp = 60C. Time = 0hrs 15mins.

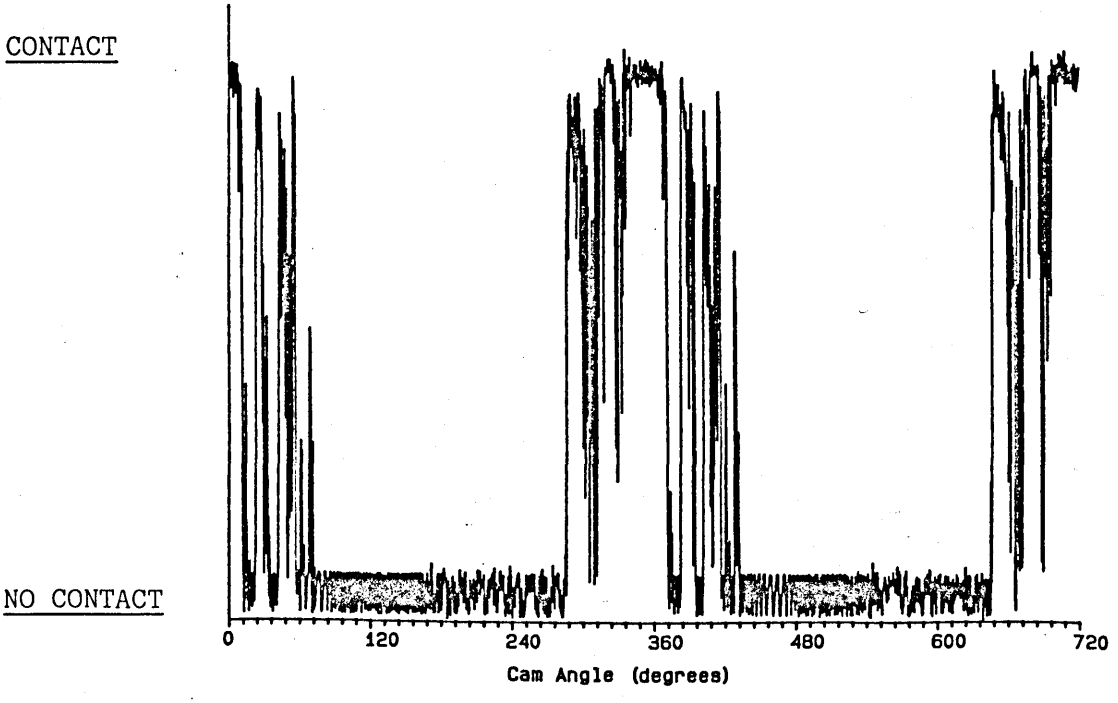

Resistivity Tests for Opening Cam and Follower.
Oil Supply Temp = 60C. Time = 8hrs 00mins.

Figure (8.4)

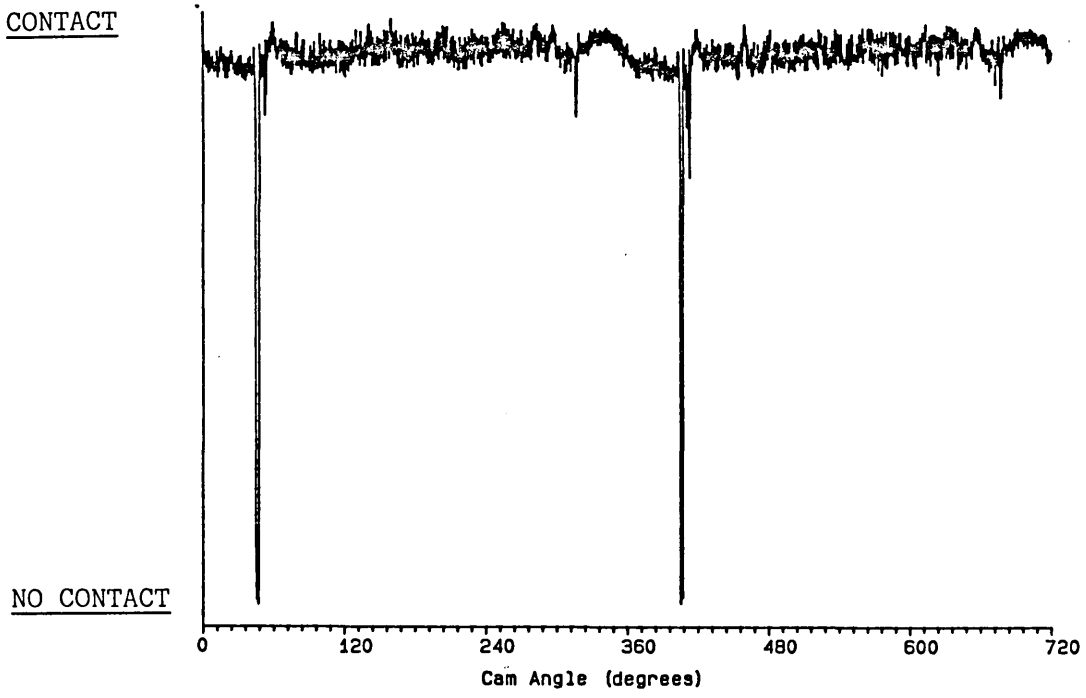

Resistivity Tests for Closing Cam and Follower.
Oil Supply Temp = 60C. Time = 0hrs 15mins.

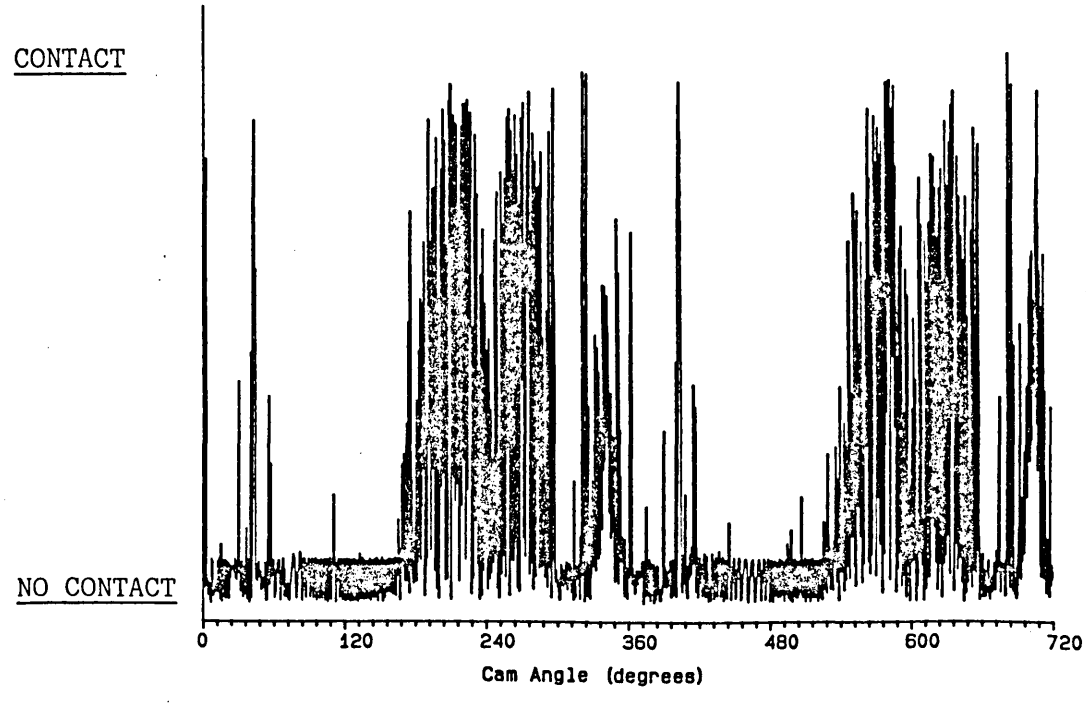

Resistivity Tests for Closing Cam and Follower.
Oil Supply Temp = 60C. Time = 8hrs 00mins.

Figure (8.5)

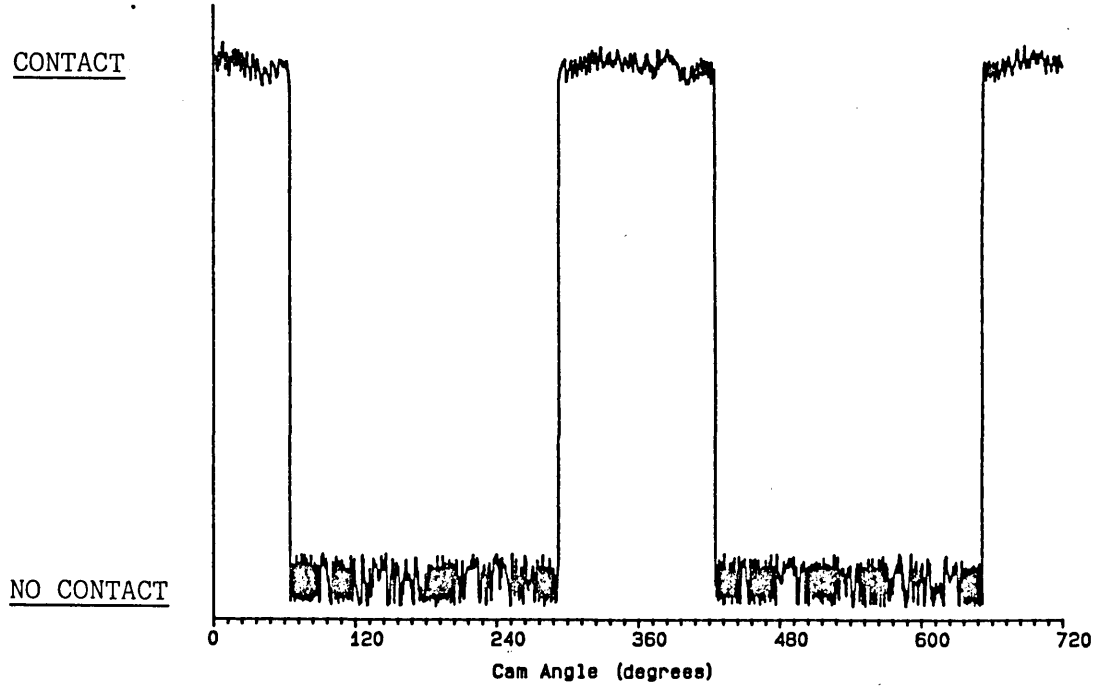

Resistivity Tests for Opening Cam and Follower.
Oil Supply Temp = 80C. Time = 0hrs 15mins.

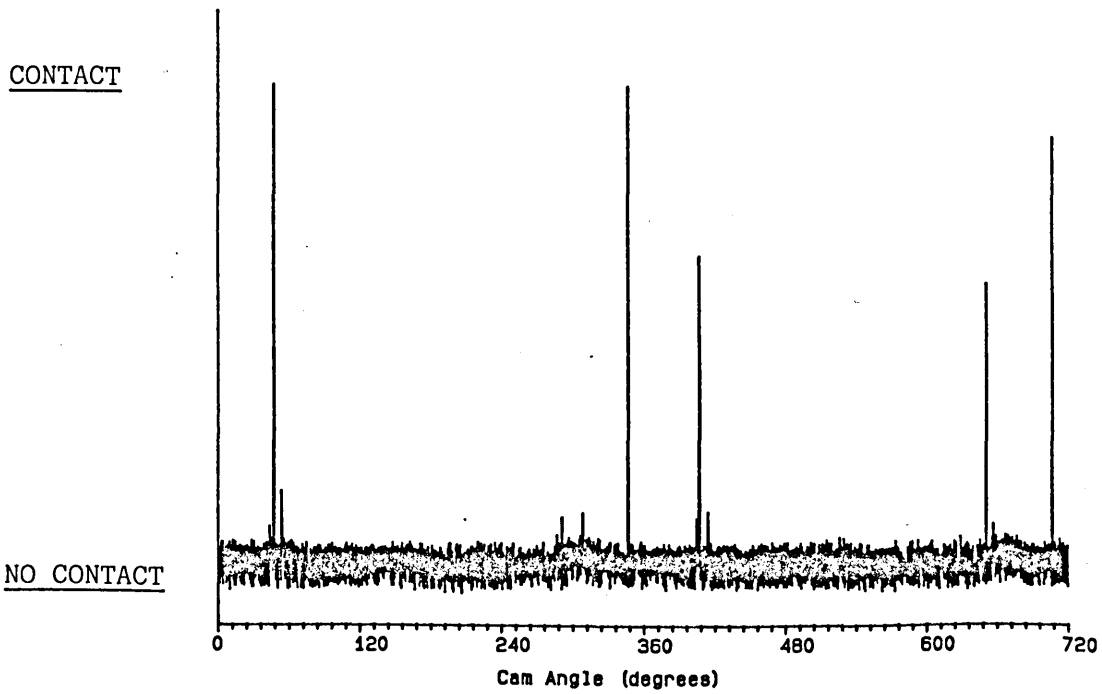

Resistivity Tests for Opening Cam and Follower.
Oil Supply Temp = 80C. Time = 8hrs 00mins.

Figure (8.6)

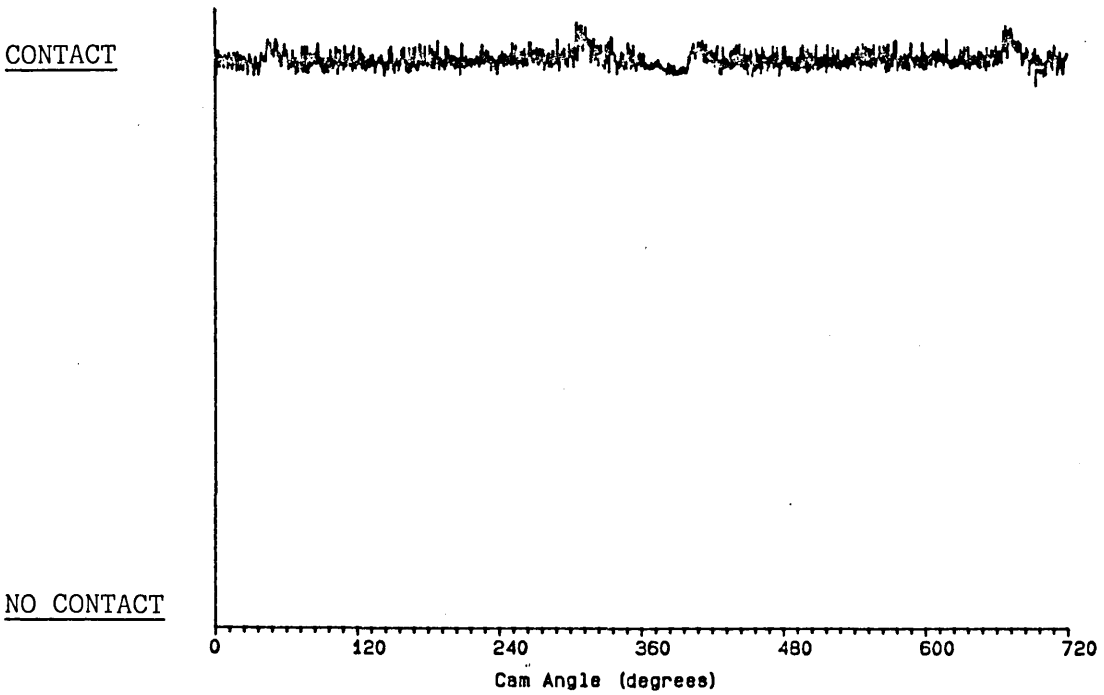

Resistivity Tests for Closing Cam and Follower.
Oil Supply Temp = 80C. Time = 0hrs 15mins.

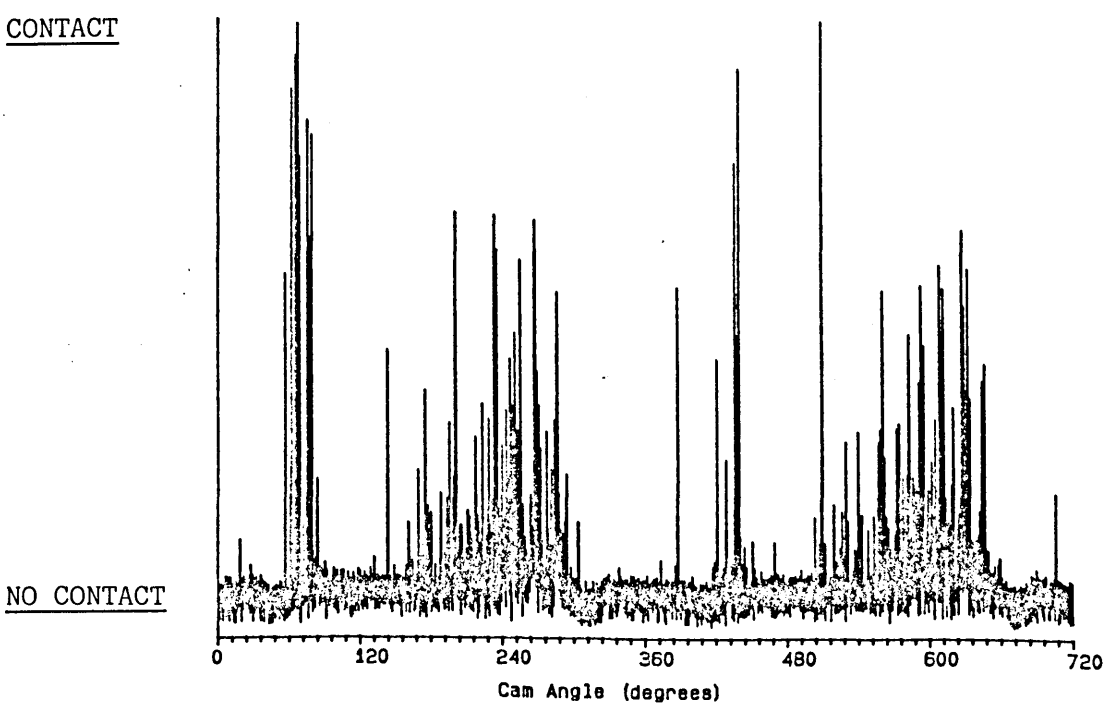

Resistivity Tests for Closing Cam and Follower.
Oil Supply Temp = 80C. Time = 8hrs 00mins.

Figure (8.7)

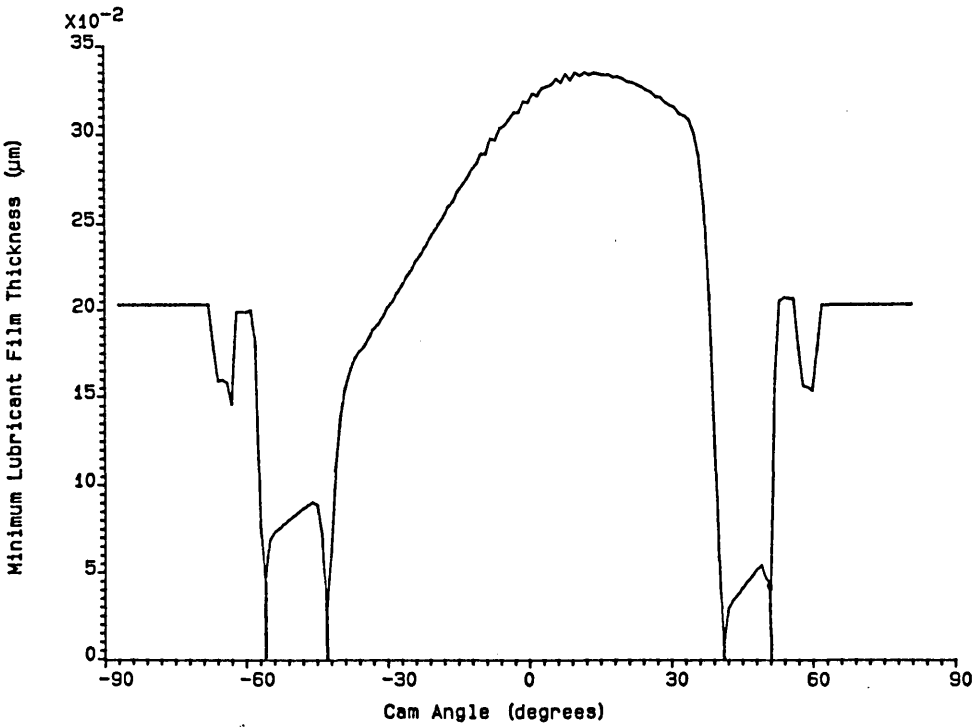

Figure (8.8) Lubricant Film Thickness Around Cam Cycle for Closing Cam Operating at a Camshaft Rotational Speed of 16.67 Hz.

the beginning of the opening flank and the end of the closing flank.) The findings are further substantiated by the surface profile traces (see section 8.3.1.3) where exaggerated wear was found to occur on the followers at the point of contact on the base circle radius.

Interestingly the closing cam and follower operating with an oil inlet temperature of 40C (Figure 8.3) suffered more surface contact around the lift portion of the cam than around the base circle region, wereas the opposite was found at the higher temperatures. It is not understood why this should occur (it may be due to an error in the labelling of the computer data files - Figure (8.3) may relate to an opening cam/follower pair).

The opening cam and follower pairs (Figures (8.2), (8.4) and (8.6)) enjoyed full separation over the cam base circle region. At the beginning of the tests there was evidence of much asperity contact during the lift portion of the cam cycle. The amount of this contact fell over the duration of the tests. The cam and follower pair operating at 80C (Figure (8.6)) showed signs of asperity contact only at the point where the opening follower relinquished control of the valve (just before maximum lift position at a camshaft angle of approximately 345°) and at the point where the valve seated (approximately 400°). For the other opening cam and follower pairs there was still evidence of surface interaction, although the mean drop in voltage fell considerably across the cam opening flanks, indicating an increase in conformity between the cam and follower surfaces. Again these findings are consistent with the predictions for lubricant film thickness around the cam cycle (Figure (8.9)), the contact, on the whole, enjoying larger film thicknesses than the closing cam and follower contact, but suffering two points on the cam nose where theoretically (ignoring squeeze effects), the lubricant film thickness falls to zero.

8.3.1.3 Surface Roughness and Surface Profile Measurements.

The surface roughness of a component may be described by many different parameters. One of the most widely adopted (certainly by

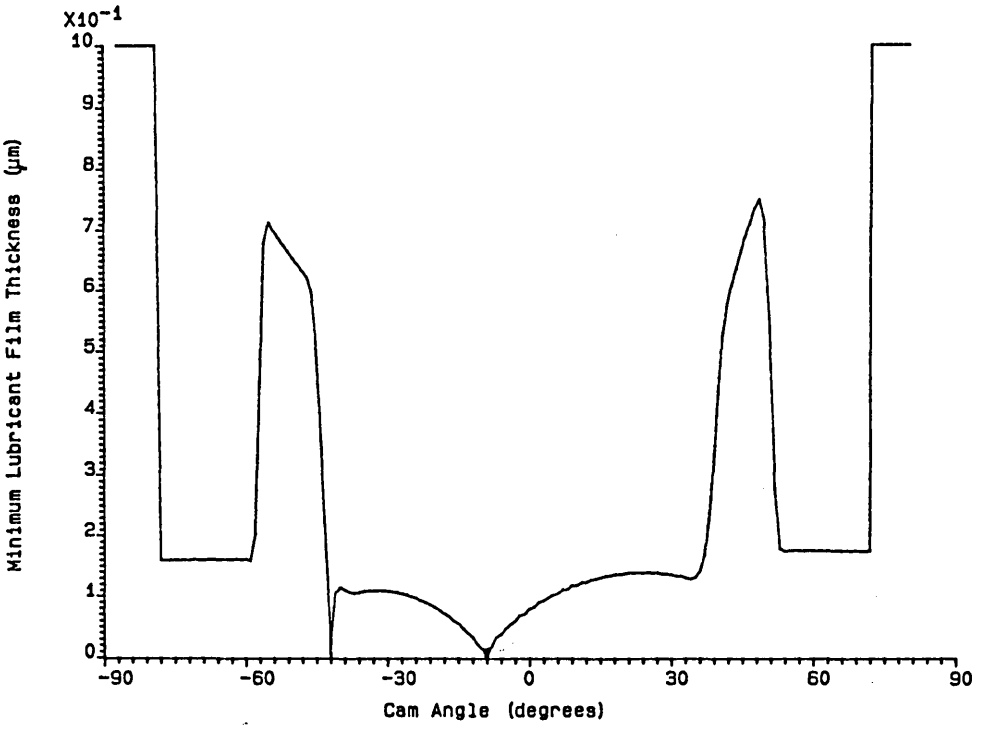

Figure (8.9) Lubricant Film Thickness Around Cam Cycle for Opening Cam Operating at a Camshaft Rotational Speed of 16.67 Hz.

the 'SI' engineer in Britain) is the roughness average (R_a). The roughness average is defined as the arithmetic mean of the departures of the roughness profile from the mean line. Table (8.1) shows the (R_a) values of the cam and follower surfaces before and after running. It also shows a pictorial definition of (R_a).

A jig was manufactured to ensure that the profile traces and roughness measurements were made in (as closely as possible) the same place on the components before and after their use in the test apparatus. The measurements across the components (perpendicular to the direction of sliding) were made at the points that the cams and followers would make contact at the maximum valve lift position. Caution should be urged in comparing profile traces as the repeatability of results is not high, indeed, two consecutive profile traces would undoubtedly give different results. Comparisons are therefore only qualitative, and restricted to comments regarding the overall appearance of the profile traces. Roughness average measurements were taken five times at each location and a mean taken of these.

It can be seen that in general the (R_a) of the surfaces decreased after the components had been run in the apparatus. In the two cases where the values increased, the changes were very small.

Figures (8.10), (8.11) and (8.12) show the surface profile traces along the surfaces of the followers in the direction of sliding and across the cams perpendicular to the direction of sliding for the three different sets of cams and followers. The labels A_1 and A_2 refer to the extremities of the cam travel on the follower surfaces, B refers to the base circle radius period position, and Z_1 and Z_2 refer to the points on the surfaces where the entrainment of lubricant into the contact falls to zero. It can be seen that the general appearance of all the profiles were changed. All of the surface profiles showed that the peaks had become more rounded after running. Wear scars on the closing followers are also clearly visible. These scars coincide with the point of contact on the follower during the whole of the cam (zero lift) base circle radius period. Figures (8.13) and (8.14) show the predicted lubricant film

Oil Inlet Temp (C)		40C		60C		80C	
Roughness (R_a)		Across	Along	Across	Along	Across	Along
Opening Follower	Before	0.969	0.770	0.991	0.740	1.548	1.093
	After	0.955	0.446	0.765	0.547	1.267	0.796
Opening Cam	Before	0.248	-	0.287	-	0.396	-
	After	0.232	-	0.156	-	0.363	-
Closing Follower	Before	0.637	0.548	0.497	0.497	0.538	0.432
	After	0.514	0.437	0.465	0.477	0.447	0.434
Closing Cam	Before	0.244	-	0.297	-	0.517	-
	After	0.212	-	0.310	-	0.293	-

Across = Perpendicular to sliding direction

Along = Parallel to sliding direction

$$R_a = \frac{1}{L}\int_0^L |y(x)| \cdot dx$$

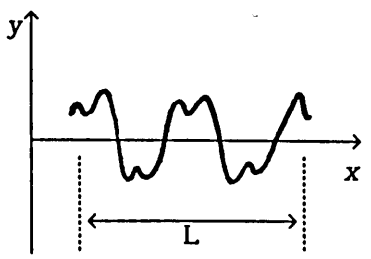

Table (8.1) Table Showing Surface Roughness (R_a) of the Cam and Follower Surfaces Before and After Running.

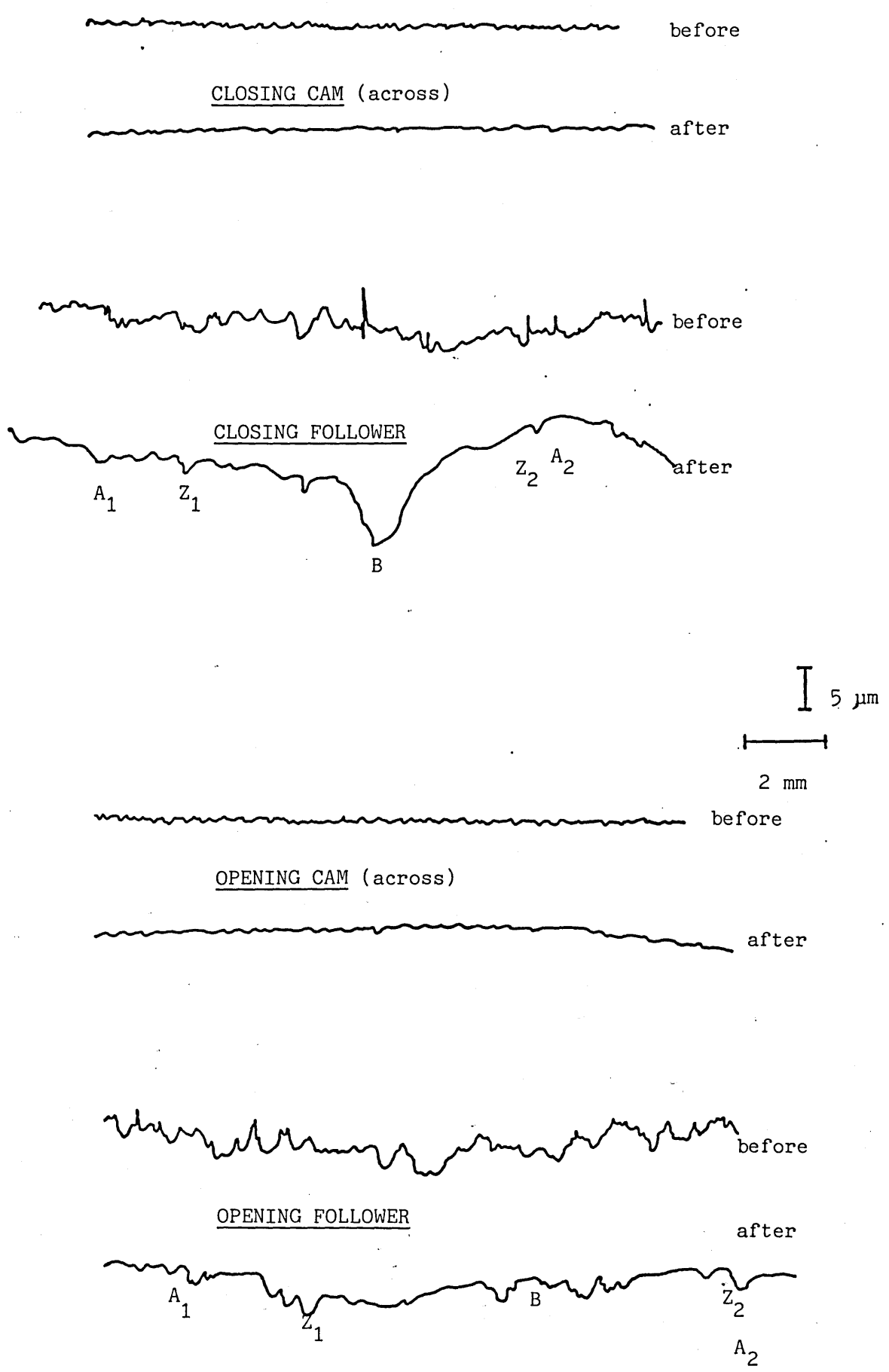

Figure (8.10) Surface Profile Traces for Cams and Followers Operating at 40 C.

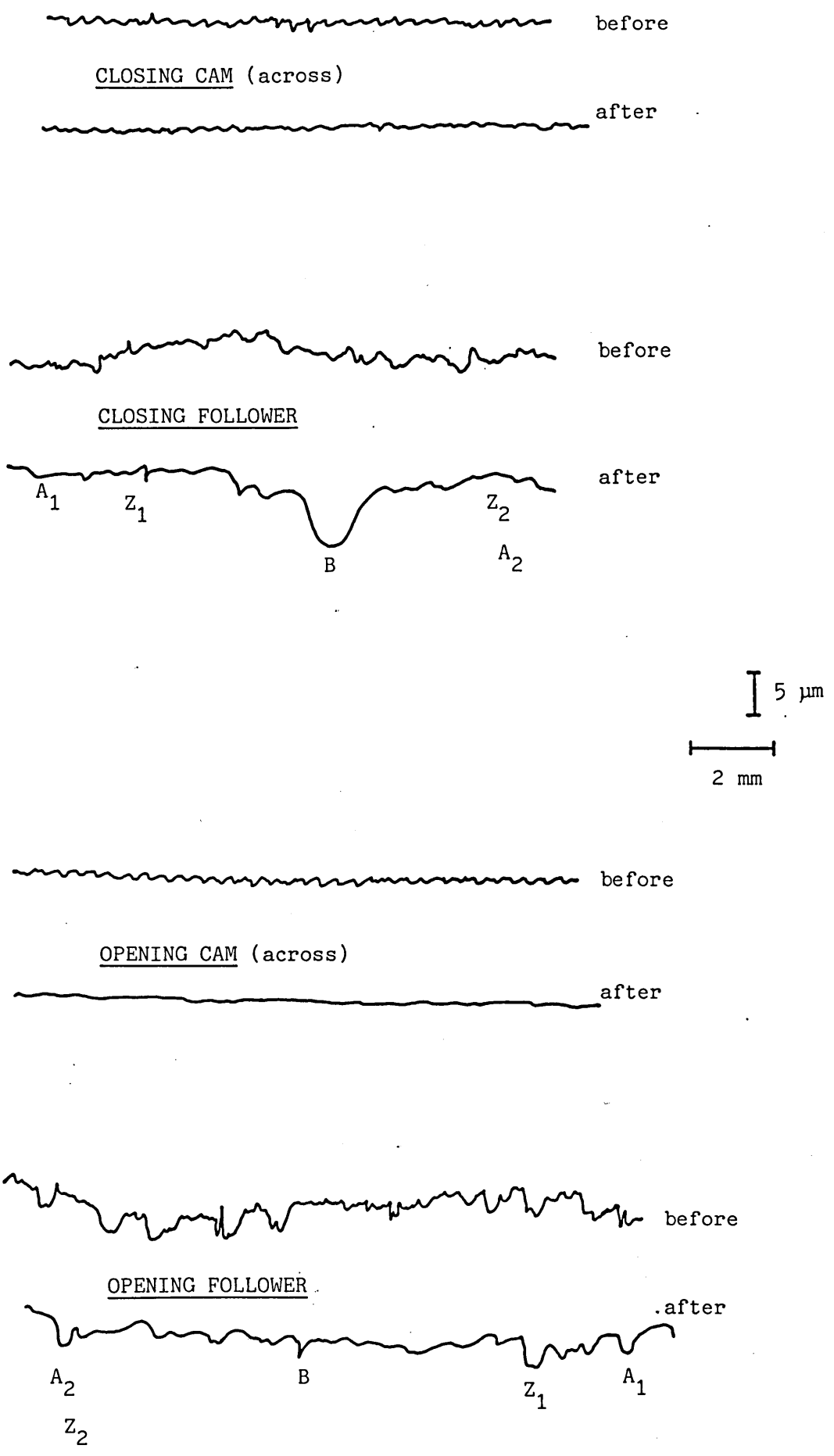

Figure (8.11) Surface Profile Traces for Cams and Followers Operating at 60 C.

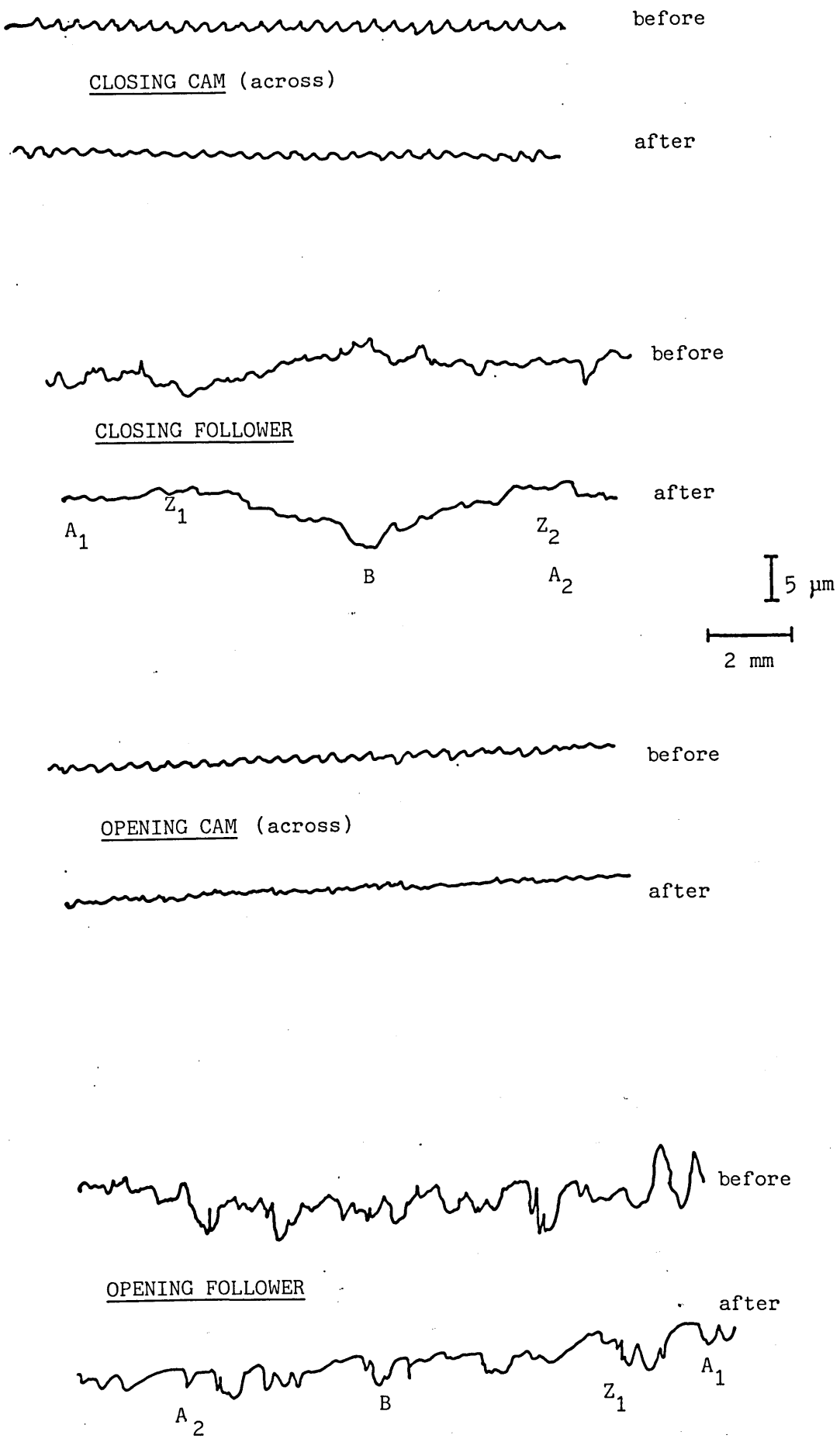

Figure (8.12) Surface Profile Traces for Cams and Followers Operating at 80 C.

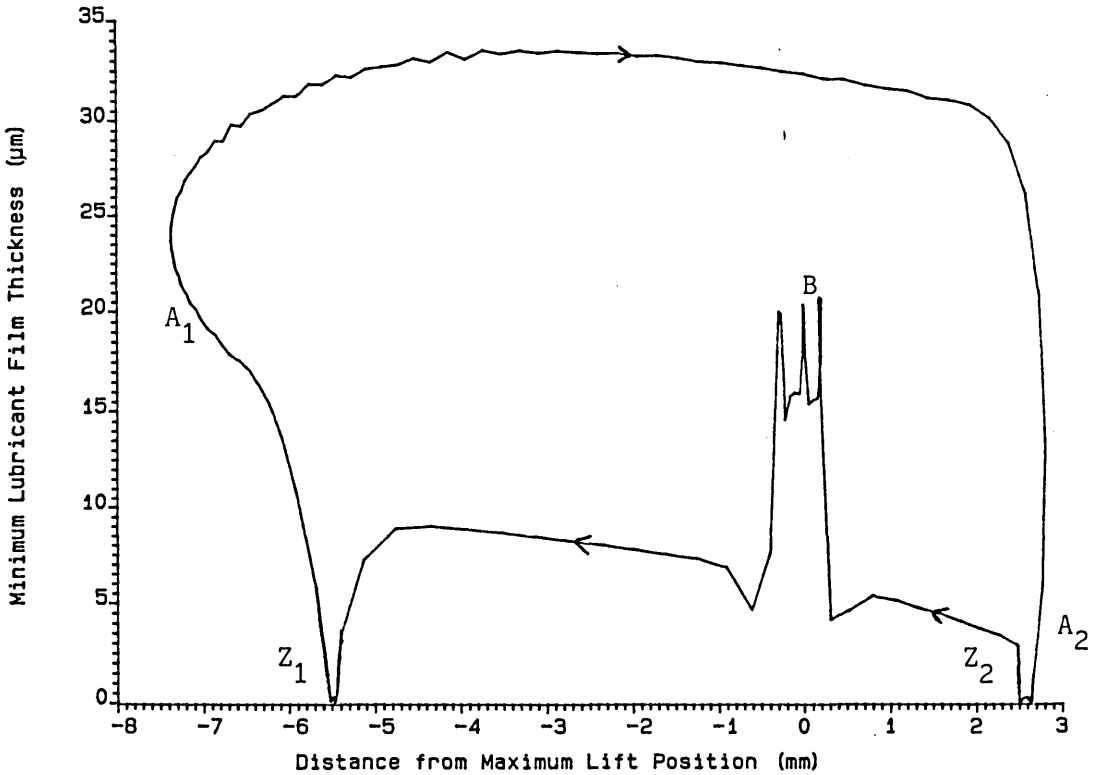

Variation of Lubricant Film Thickness Across
The Follower Surface.

Figure (8.13) Lubricant Film Thickness Across The Closing Follower Surface at a Camshaft Rotational Speed of 16.67 Hz and Oil Inlet Temperature of 60 C.

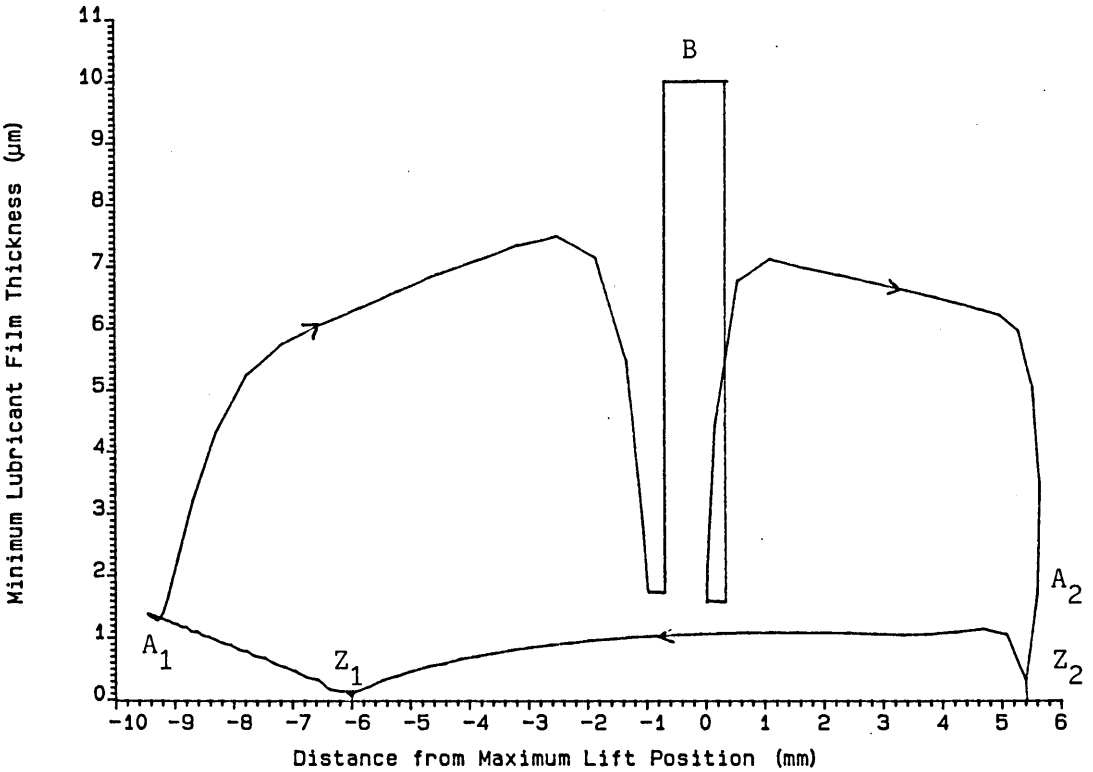

Variation of Lubricant Film Thickness Across
The Follower Surface.

Figure (8.14) Lubricant Film Thickness Across The Opening Follower Surface at a Camshaft Rotational Speed of 16.67 Hz and Oil Inlet Temperature of 60 C.

thicknesses along the follower surfaces at a camshaft rotational speed of 16.67 Hz (1000 rpm) with a lubricant temperature of 60 C. The Figures are labelled in a similar manner to the profile traces. It can be seen that the predicted lubricant film thickness for the closing cam and follower contact is not generous during the cam base circle radius period. This, combined with the 50 N spring force, used to ensure that the valve remains seated, and the large sliding distances seen by this one point, leads to the higher amounts of wear at this position on the follower surface. The opening cam and follower pair operate more like a conventional cam and centrally pivoted follower system. At a camshaft rotational speed of 16.67 Hz, the valve inertia is still small enough to cause the cam to be in contact during the whole of the period of cam lift. At higher speeds the cam and follower are in contact for a smaller portion of the lift period (this is discussed in more detail in section 8.3.2.3), and are less like conventional systems. A clearance always exists between the opening cam and follower during the base circle radius period. Although not deep, wear scars which were visible to the naked eye were starting to appear on all of the opening followers at points coinciding with the zero lubricant entrainment positions and the extremities of cam travel.

8.3.2 Variation of Torque and Power With Camshaft Rotational Speed.

After the cam and follower sets had been operating for eight hours they were considered to be run-in. They were then subjected to speed tests. These tests consisted of measuring the torque variation around two camshaft cycles at speeds of 8.33 Hz through to 33.33 Hz at 4.17 Hz intervals (500 rpm to 2000 rpm at 250 rpm intervals). The readings at each speed were taken when the temperatures indicated by the thermocouples in the cams and followers had stabilised. The signal from the torque transducer was sent directly to a VAX mainframe computer where the signal could be processed to give the instantaneous torque signal as a function of camshaft angle, the mean torque value, and the mean power loss associated with the running of the valve.

8.3.2.1 Power Loss.

Figures (8.15), (8.16) and (8.17) show comparisons of the experimentally measured power loss across the speed range at the three operating temperatures. They also show the theoretically predicted power loss across the speed range.

The theoretical power loss was calculated using the computer program described in Chapter (4). The program computed the power loss at the cam/follower interfaces and the loads at the contacts. The loads at the contacts were then resolved to give the loads applied to the support bearings. The power loss associated with the support bearings was then calculated using formulae and data supplied in the SKF bearing catalogue. The power loss associated with each of the follower (rocker) pivot bushes was calculated by evaluating the applied normal load at a number of intervals around the cam cycle (by considering the follower as a simply supported beam and resolving the forces) and then multiplying this by an assumed coefficient of friction and the velocity of the frictional force component. These instantaneous power losses were then averaged to give the mean power loss. The coefficient of friction adopted was 0.2 - that of PTFE sliding on EN38 steel. This was felt to reasonable as the bearing surfaces of the bushes were PTFE coated and the rocker shaft was steel.

Tests were performed upon the support bearings to validate the SKF formulae. This was done by applying a series of known loads at the test speeds to a cradle containing two bearings, identical to, and positioned midway betweeen, the camshaft support bearings. Thus the loads on each of the four bearings could be assumed to be equal. The torque and power loss were then measured and compared with the calculated values. Across the whole of the speed range the differences between the measured and theoretical values were less than 7% at an oil inlet temperature of 40C, and less than 5% at oil inlet temperatures of 60C and 80C. It should be noted, however, that these tests were carried out in conditions where the loads were not varying, unlike the conditions found in the operating apparatus.

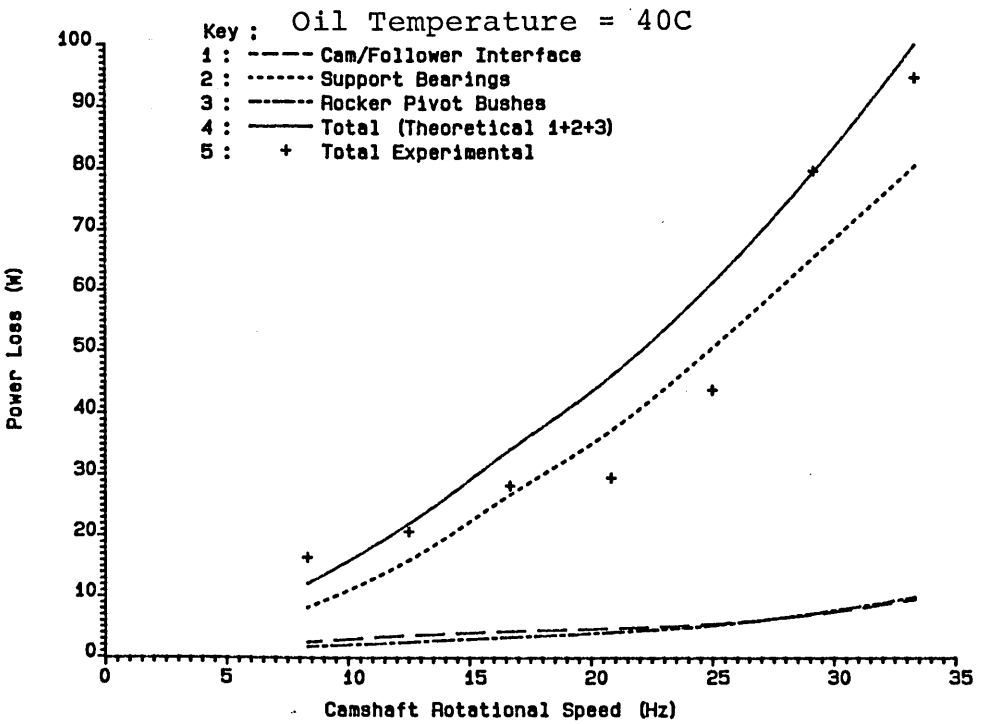

Comparison of Experimental and Theoretically Predicted Power Losses for the Desmodromic Valve Train Apparatus

Figure (8.15)

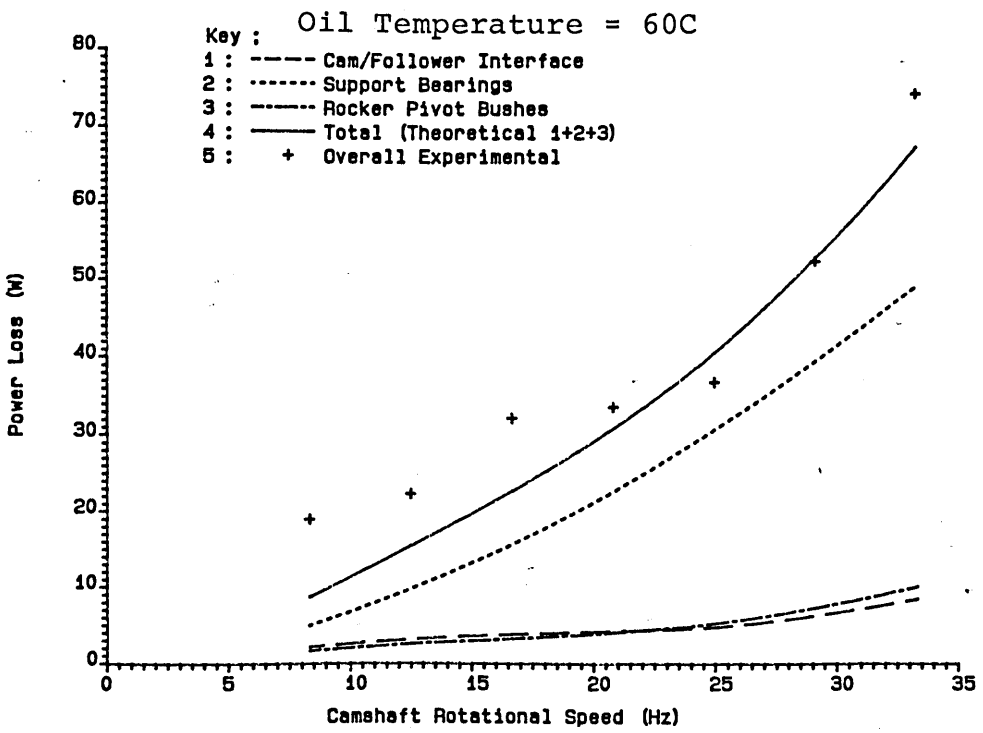

Comparison of Experimental and Theoretically Predicted Power Losses for the Desmodromic Valve Train Apparatus

Figure (8.16)

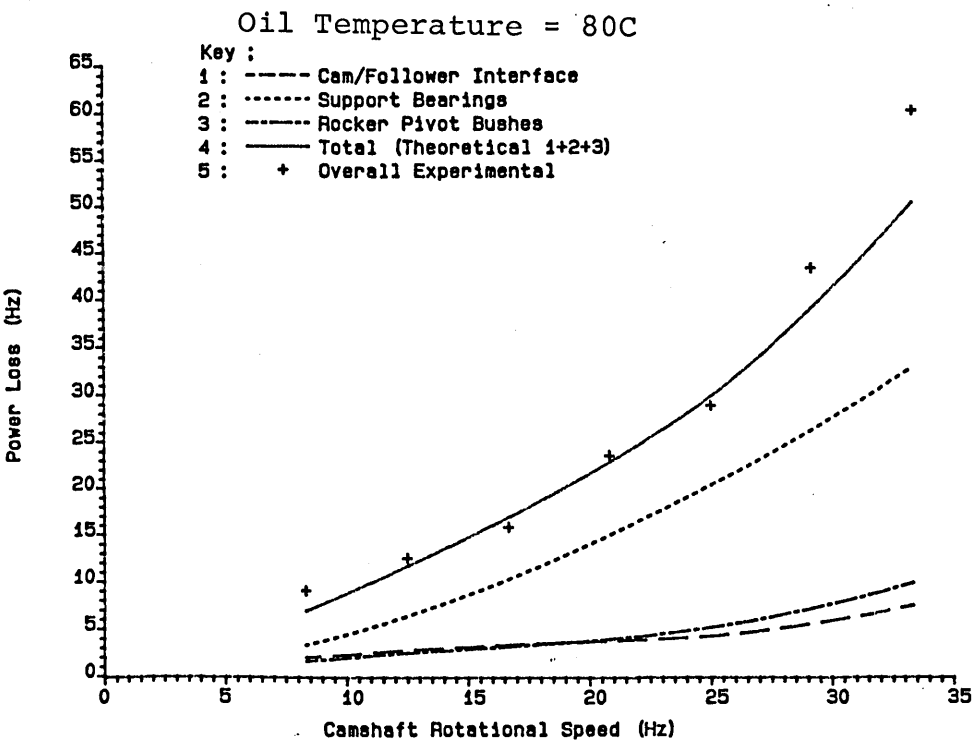

Comparison of Experimental and Theoretically Predicted Power Losses for the Desmodromic Valve Train Apparatus

Figure (8.17)

It can be seen from Figures (8.15), (8.16) and (8.17) that the agreement between the experimentally measured and the predicted frictional power losses is remarkably good. However, it can be seen that the frictional power loss arising from the cam/follower interfaces makes up only a very small proportion of the overall power loss figure. This really serves to amplify the problems associated with attempting to measure the friction at the cam/follower interface when the losses involved are low (such as in desmodromic and roller follower arrangements). Indeed a cynical view might be to state that such experiments are merely a good test of the SKF formula for bearing loss under dynamic conditions!

8.3.2.2 Instantaneous Torque.

Figures (8.18) to (8.21) inclusive, show the experimentally measured and theoretically predicted torque variations around the valve lift cycle for the apparatus operating at camshaft rotational speeds of 8.4 Hz, 16.7 Hz, 24.9 Hz and 33.4 Hz (504 rpm, 1002 rpm, 1498 rpm and 2004 rpm respectively) with an oil inlet temperature of 60C. The theoretical torque was calculated using the same method as adopted for the theoretical power loss.

The damped oscillations across the cams' base circle radii are clearly obvious in the experimental data. It is believed that the difference in the angular position of the maximum torque values for the theoretical and experimental cases was due to error in the positioning of the datum pulse at the maximum lift position. Again agreement between the theoretical predictions and experimental data is good if the oscillatory portions are ignored. The higher than predicted torque levels around the maximum lift positions (camshaft angles of 0°, 360°, and 720°) are believed to be caused by friction between the 'tophat' and spring cup and also due to twisting of the closing follower due a moment enduced by the offset between the position of the applied load and the valve inertia load in the direction parallel to the rocker shaft axis. It is believed that this twisting was also responsible for the problems incurred when attempts

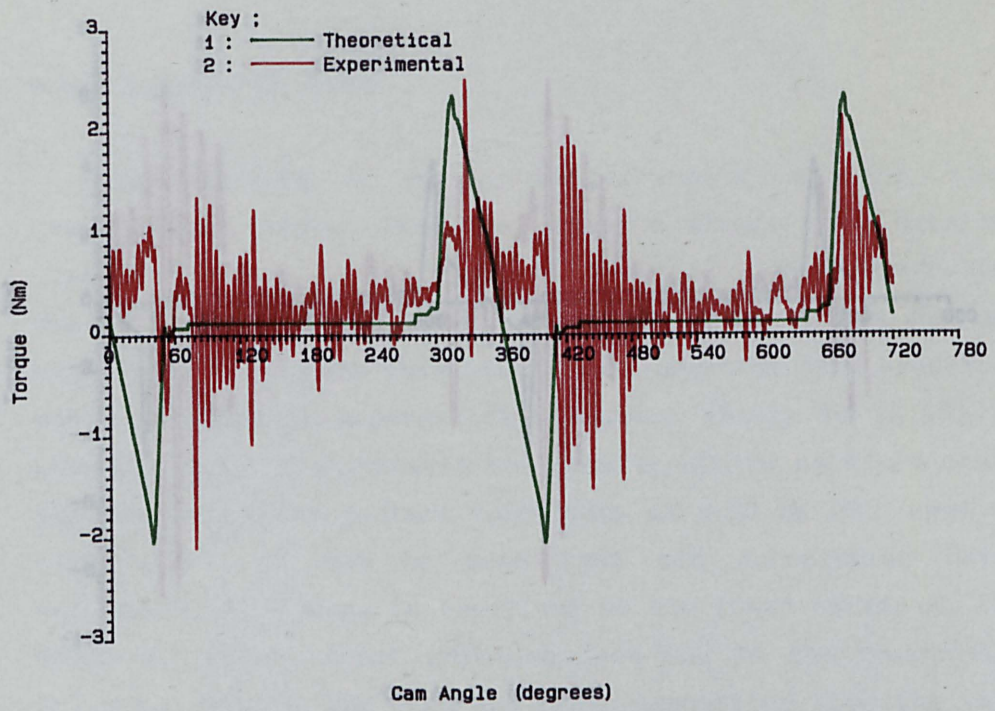

Theoretical and Experimentally Measured Torque Variation.
Camshaft Rotational Speed = 8.4 Hz. Oil Supply Temp = 60C.

Figure (8.18)

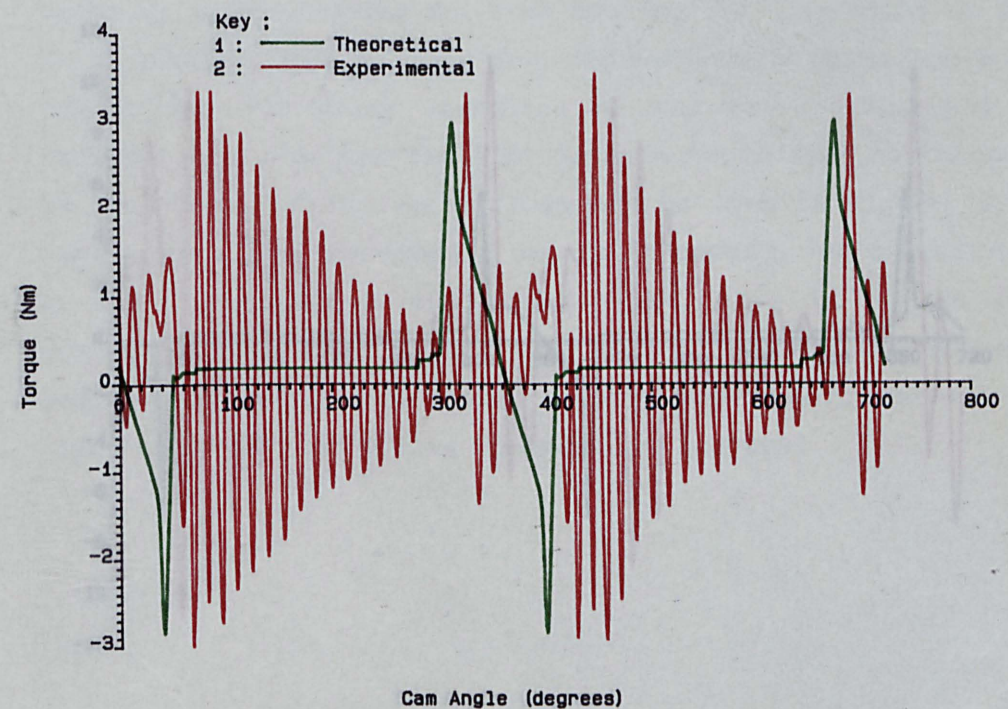

Theoretical and Experimentally Measured Torque Variation.
Camshaft Rotational Speed = 16.7 Hz. Oil Supply Temp = 60C.

Figure (8.19)

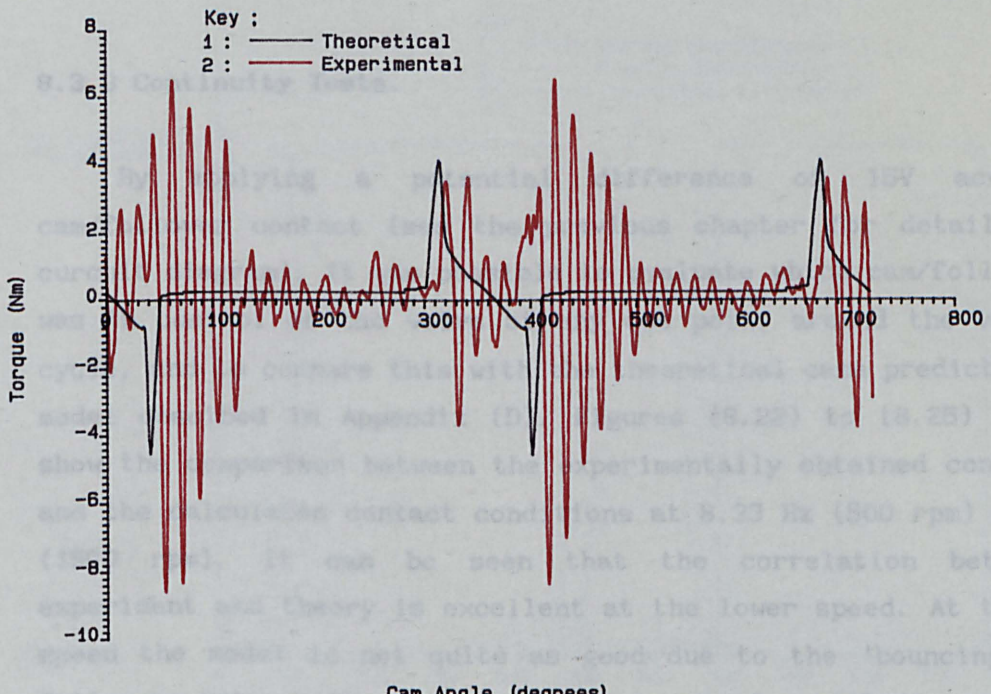

Theoretical and Experimentally Measured Torque Variation.
Camshaft Rotational Speed = 24.9 Hz. Oil Supply Temp = 60C.

Figure (8.20)

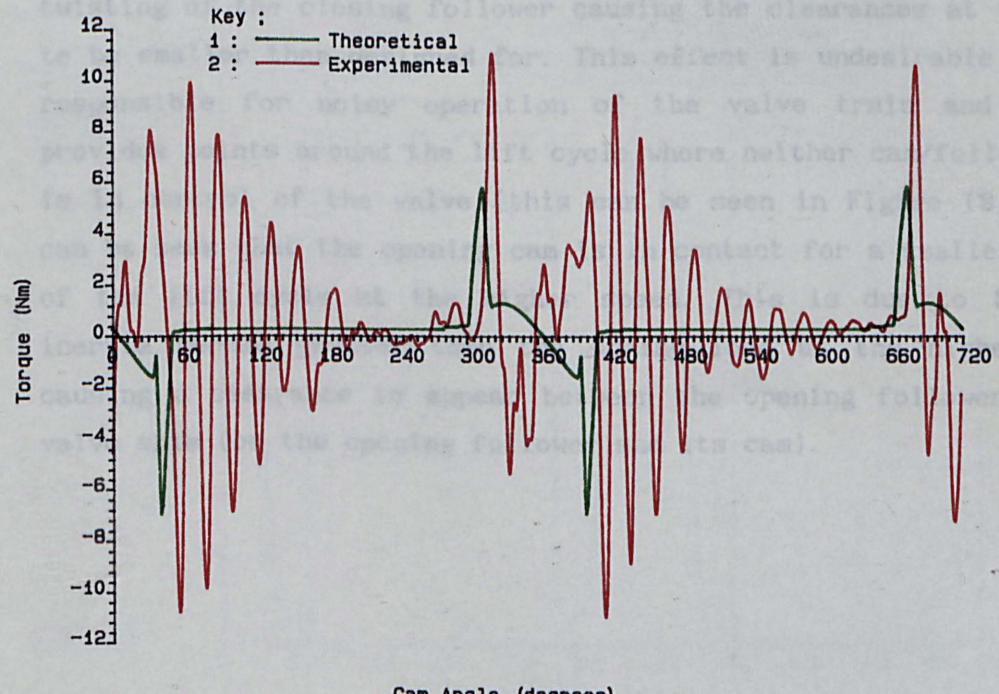

Theoretical and Experimentally Measured Torque Variation.
Camshaft Rotational Speed = 33.4 Hz. Oil Supply Temp = 60C.

Figure (8.21)

were made to run the apparatus at speeds greater than 33.33 Hz (2000 rpm), causing the eventual failure of the 'tophat'.

8.3.3 Continuity Tests.

By applying a potential difference of 15V across the cam/follower contact (see the previous chapter for details of the curcuit diagram), it was possible to evaluate which cam/follower pair was in control of the valve at any one point around the valve lift cycle, and to compare this with the theoretical case predicted by the model descibed in Appendix (D). Figures (8.22) to (8.25) inclusive show the comparison between the experimentally obtained contact data and the calculated contact conditions at 8.33 Hz (500 rpm) and 25 Hz (1500 rpm). It can be seen that the correlation between the experiment and theory is excellent at the lower speed. At the higher speed the model is not quite as good due to the 'bouncing' of the followers between the cams and their connection with the valve. This bouncing occurs at the points where the operation of the valve should be passed from one cam/follower pair to the other, and is due to dynamics of the small closing spring, and to imperfections in the cam lift profiles causing transient discontinuities in the valve acceleration. It is also believed, in this case, to be due to the twisting of the closing follower causing the clearances at the valve to be smaller than designed for. This effect is undesirable as it is responsible for noisy operation of the valve train and it also provides points around the lift cycle where neither cam/follower pair is in control of the valve (this can be seen in Figure (8.24)). It can be seen that the opening cam is in contact for a smaller portion of the lift cycle at the higher speed. This is due to the valve inertia become greater than the spring load at the higher speed, causing a clearance to appear between the opening follower and the valve shim (or the opening follower and its cam).

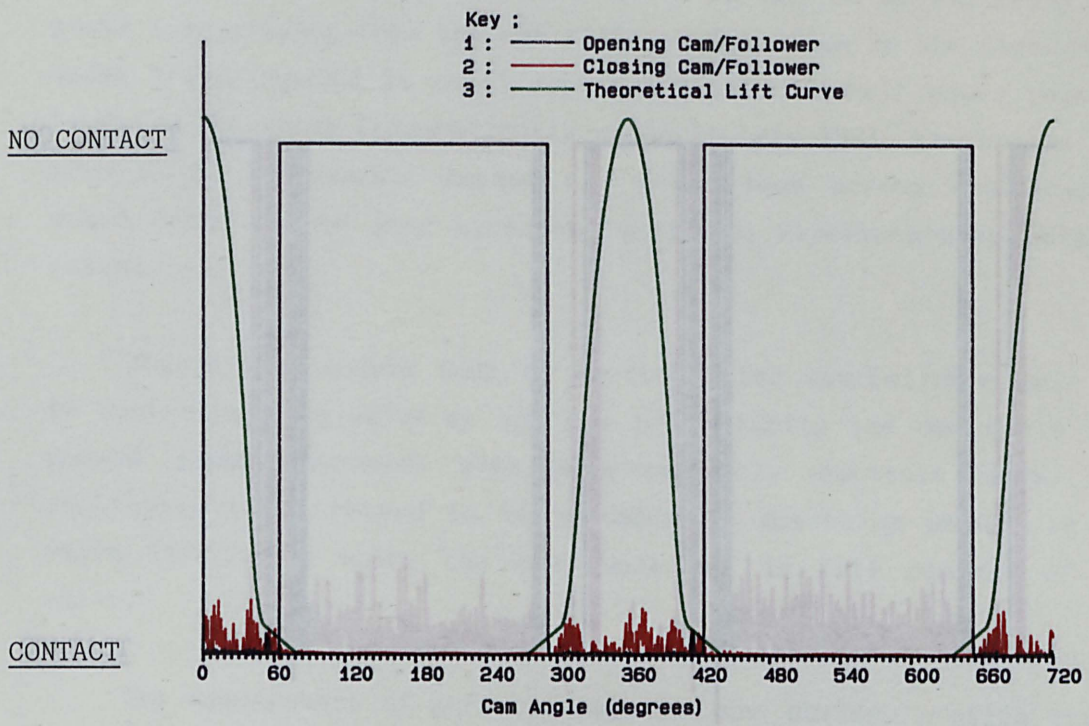

Cam/Follower Contact Test
8.33 Hz (500 rpm)

Figure (8.22)

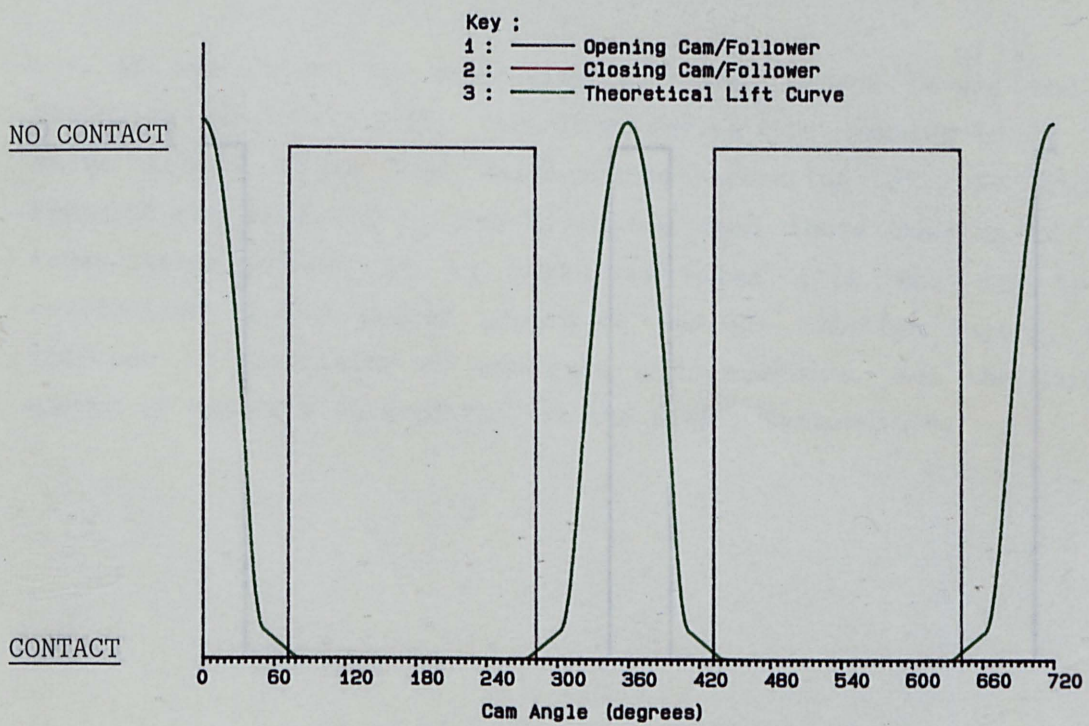

Theoretical Contact For Desmodromic Valve Train
8.33 Hz (500 rpm)

Figure (8.23)

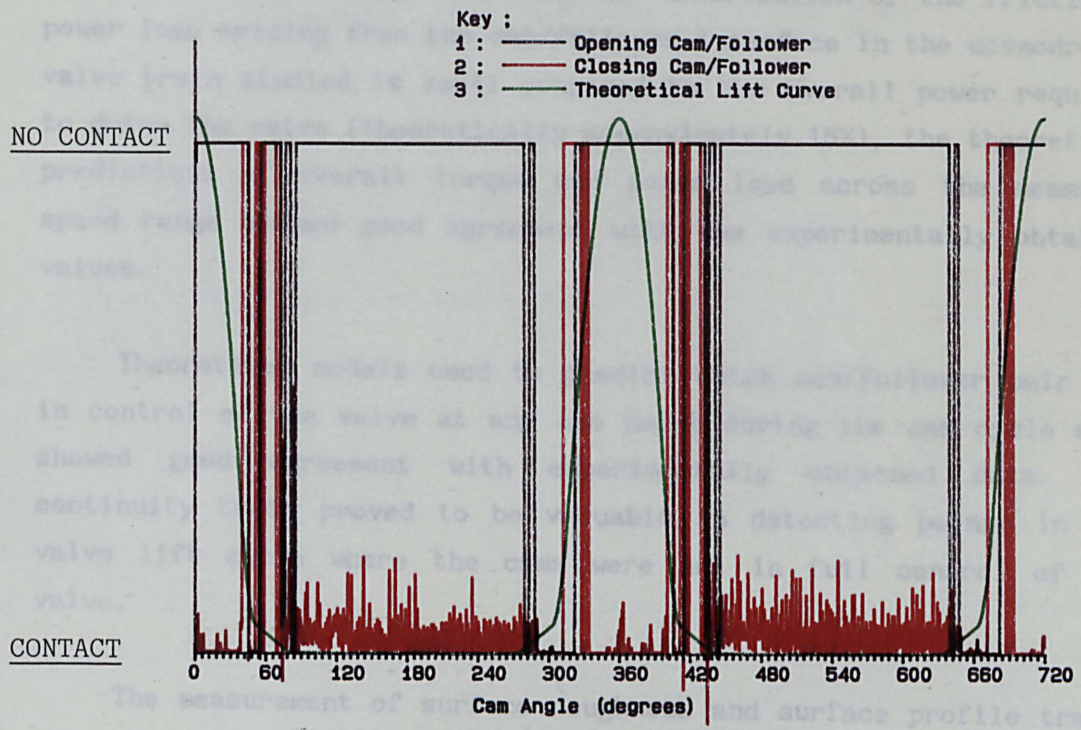

Cam/Follower Contact Test
25 Hz (1500 rpm)

Figure (8.24)

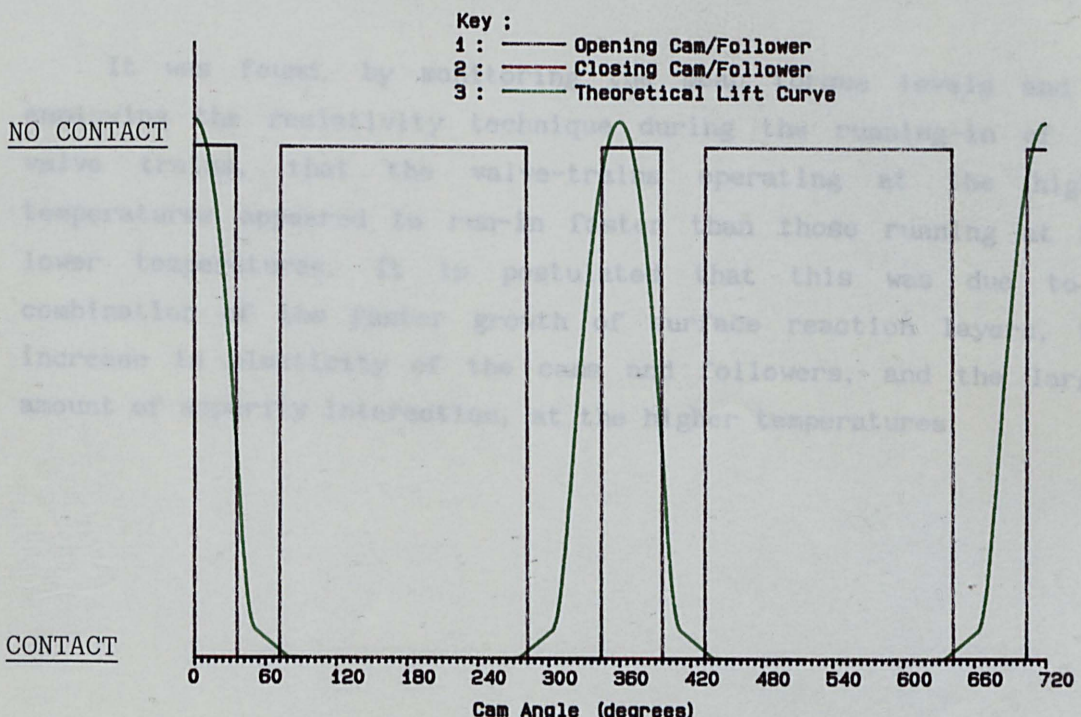

Theoretical Contact For Desmodromic Valve Train
25 Hz (1500 rpm)

Figure (8.25)

8.4 Conclusions.

Whilst it is recognised that the contribution of the frictional power loss arising from the cam/follower interface in the desmodromic valve train studied is small compared to the overall power required to drive the valve (theoretically approximately 15%), the theoretical predictions of overall torque and power loss across the measured speed range showed good agreement with the experimentally obtained values.

Theoretical models used to predict which cam/follower pair was in control of the valve at any one point during the cam cycle also showed good agreement with experimentally obtained data. The continuity tests proved to be valuable in detecting points in the valve lift cycle where the cams were not in full control of the valve.

The measurement of surface roughness and surface profile traces showed how the surfaces of the cams and followers changed once they had been used in the apparatus. It was found that the (R_a) value of the surfaces generally decreased from the manufactured value. Correlations were found between surface profile traces and lubrication film thickness predictions.

It was found, by monitoring the mean torque levels and by employing the resistivity technique during the running-in of the valve trains, that the valve-trains operating at the higher temperatures appeared to run-in faster than those running at the lower temperatures. It is postulated that this was due to a combination of the faster growth of surface reaction layers, the increase in plasticity of the cams and followers, and the larger amount of asperity interaction, at the higher temperatures.

CHAPTER 9

CONCLUSIONS AND SUGGESTIONS FOR FUTURE WORK

9.1 Main Contributions of This Study.

In this study techniques have been collated into a concise form applicable to the tribological design of cam and follower systems is a valuable contribution in itself. The models used to describe the kinematics, loading and tribological conditions at the cam/follower interface for any valve train system in common use today have been presented. Many of the models developed during this study have been written into computer code to form a robust, user friendly program which would in its present structure be a valuable tool to anyone wishing to design a valve train. To this end, the program is currently being introduced to the valve train design suite at the Ford Motor Co. Ltd..

Using the valve train tribological analysis computer program, parametric studies have been carried out on three different types of valve train, namely, a cam acting against a flat faced follower system, a cam acting against a centrally pivoted follower system and a cam acting against an end pivoted follower system. The results of these parametric studies have been clearly presented using graphics and tables, which it is hoped, could be referred to during design procedures.

A study of the orbits and power losses associated with the camshaft bearings of the Ford 2.0 litre Pinto engine have been presented. It is believed that this is the first time that dynamically loaded bearing analysis has been applied to camshaft bearings. Again, the valve train tribological computer program was an invaluable tool, helping to provide the loads applied to the bearings. The results of the study showed good agreement with the experimental findings of other workers.

An experimental programme was carried out to verify the models developed during the project. The experimental programme was carried out upon a desmodromic valve train apparatus at the specific request of the Ford Motor Co. Ltd.. It was found that the losses at the cam/follower interface for this particular valve train arrangement attributed for approximately 15% of the overall mechanism friction. Theoretical predictions of the overall frictional power loss showed

good agreement with experimental findings. It is felt that the experimental project gives grounds for confidence to be attached to the analytical models.

9.2 Suggestions for Future Work.

Whenever anything is put under close scrutiny, one always tends to find that the number of questions arising from the study by far outweigh the number of answers. Many questions still remain to be answered regarding the tribological operation of valve trains, but it is hoped that the present study has extended considerably our understanding of the operation of such mechanisms.

During this study the effects of the make-up of the lubricant have been totally ignored, as have most of the metallurgical properties of the cam and follower. Many workers have observed the effects of differing lubricants and metallurgies during experimental projects, but very few have offered predictive analytical techniques.

Another area that has been neglected during this study is that of the dynamics of the valve train. The components of the valve train are not rigid, flexures and torsions are bound to occur. These will undoubtedly affect the kinematics and loading of the contact and hence its lubrication. Many models have been put forward to predict the dynamics of valve trains, none interact with the kinematics - for example, if a camshaft is subject to a torsional deflection this will cause its rotational speed to change, thus altering the surface velocities of importance to lubrication.

As a continuation of the present study, the valve train tribological analysis program needs to be extended in several ways. The use of hydraulic elements has become very popular with automobile manufacturers as they automatically compensate for wear in the valve train system and thus cut down the amount of servicing required. The program can cope, to some extent, with this type of valve train by setting the valve clearance to zero, it cannot however model the effects that hydraulic elements have upon the loading of the contact. An obvious method of cutting down frictional losses within the valve train, which many designers are now exploring, is to incorporate

rolling element followers into the design. Whilst these are costly, if they can prove to be reliable and to offer significant reductions in frictional losses, they may well become a common component within the automobile engine. The addition of such a model would have to include analytical techniques to study the traction between the cam and the rolling element, as pure rolling cannot be assumed at high camshaft speeds around the cam flanks where accelerations are very high. The addition of a model to incorporate the effects of lubricant squeeze at the points of zero lubricant entrainment velocity would be desirable, although at present the techniques available are very costly in computing time and would render the computer program useless as an interactive tool.

A great deal of long term experimental work still remains to be carried out. Analytical expressions are available to the designer of machine elements to allow predictions (by adopting certain assumptions) of the oil film thickness existing between interacting lubricated parts, if the kinematics and loading of the contact are known along with the lubricant properties. Similarly, the designer can predict Hertzian stress levels in the components, and sliding speeds and distances during the design life. What is still unknown to a great extent is the correlation between these predictions and the guaranteed survival of the components in service. By a series of comprehensive experimental tests with accompanying analytical predictions the analytical tools could be tested and some degree of certainty attached to them.

Some reservations are still held regarding the experimental project. During the project much thought was put into ways of trying to eliminate frictional forces arising from sources other than the cam/follower interface. Many ideas were thought of, but very few were practical as the apparatus conceived bore very little similarity to real systems. One possible solution would perhaps be to carry out the equivalent of a morse test on a driven cylinder head by removing a single follower and studying the change in friction levels. The main problem with this method is that by removing one of the contacts, the whole loading of the system is changed and hence the frictional losses of the system are also changed. Maybe a very long, very stiff camshaft with many cam lobes and followers is the solution, minimising the disturbance to the system by removing one

contact.

It can be seen that there are still many avenues left unexplored and there remains a great deal of work to be done before the tribological operation of valve trains can be fully understood.

REFERENCES

AKIBA, K., SHIMIZU, A., SAKAI, H. (1981). "A Comprehensive Simulation of High Speed Driven Valve Trains", S.A.E. 810865.

ARMSTRONG, W.B., BUUCK, B.A. (1981). "Valve Gear Energy Consumption: Effect of Design and Operation Parameters", S.A.E. 810787.

BAIR, S., GRIFFIOEN, J.A., WINER, W.O. (1985). "The Tribological Behavior of an Automotive Cam and Flat Lifter System", Trans. A.S.M.E. J.Trib., vol. 108, No. 3, pp 478-486.

BARKEN, P. (1953). "Calculation of High-Speed Valve Motion with a Flexible Overhead Linkage", S.A.E. National Passenger Car, Body, and Materials Meeting, Detroit.

BELL, A.G. (1981). "Performance Tuning in Theory and Practice", Haynes.

BELL, J.C., DAVIES, P.T., FU, W.B. (1985). "Prediction of Automobile Valve Train Wear Patterns With a Simple Mathematical Model", Mechanisms and Surface Distress, 12th Leeds-Lyon Symposium on Tribology, pp 323-333, Butterworths.

BEARD, C.A., HEMPSON, J.G.G. (1962). "Problems in Valve Gear Design and Instrumentation", S.A.E. National Power Plant Meeting, Philadelphia.

BLOK, H. (1965). Unpublished work.

BOOKER, J.F. (1965). "Dynamically Loaded Journal Bearings: Mobility Method of Solution", Journal of Basic Egineering, Trans A.S.M.E., September 1965, pp 537-546.

BUUCK, B.A. (1982). "Elementary Design Considerations for Valve Gears", S.A.E. 821574.

CHEN, F.Y. (1982). "Mechanics and Design of Cam Mechanisms", Permagon Press.

COY, R.C., DYSON, A. (1981). "A Rig to Simulate the Kinematics of the Contact Between a Cam and Finger Follower", A.S.L.E./A.S.M.E. Conf. as 81-LC-2B-1.

DOWSON, D., DUNN, J.F., TAYLOR, C.M. (1983). "The Peizo-viscous Fluid, Rigid Solid Regime of Lubrication", Proc. I. Mech. E. Vol 197C, pp 43-52.

DOWSON, D., HARRISON, P., TAYLOR C.M., (1985). "The Lubrication of Automotive Cams and Followers", Mechanisms and Surface Distress, 12th Leeds-Lyon Symposium on Tribology, pp 305-322, Butterworths.

DOWSON, D., HIGGINSON, G.R., (1977). "Elastohydrodynamic Lubrication", SI Edition, Pergamon Press.

DOWSON, D., TOYODA, S. (1978). "A Central Film Thickness Formula for Elastohydrodynamic Line Contacts", Elastohydrodynamics and Related Topics, Proc. 5th Leeds-Lyon Symposium on Tribology, Inst of Tribology, Dept. Mech. Eng., University of Leeds, p 60.

DUNNING, S.W. (1980). "A Study of Cavitation Erosion Under Conditions of Hydrodynamic Lubrication", Ph.D. thesis, Dept. of Mech. Eng., Univ. of Leeds.

DYSON, A., NAYLOR H. (1960). "Application of the Flash Temperature Concept to Cam And Tappet Wear Problems", I. Mech. E., Proc. Auto. Div. No. 8, pp 225-280.

DYSON, A. (1977). "Elastohydrodynamic Lubrication and Wear of Cams Bearing Against Cylindrical Tappets", S.A.E. 770018.

DYSON, A. (1980). "Kinematics and Wear Patterns of Cam and Follower Automotive Valve Gear", Tribology International, June 1980, pp 121-132.

E.S.D.U. Item No. 66002, (1966). "Contact Stresses Between a Cam and Follower", I. Mech. E..

E.S.D.U. Item No. ME2, (1981). "Design of Disc Cams With Various Followers: Derivation of Kinematic Equations.", I. Mech. E..

HAMILTON, G.M. (1980). "The Hydrodynamics of a Cam Follower", Trib. Intl., June 1980, pp 113-119.

HARRISON P. (1985). "A Study of the Lubrication of Automotive Cams", Ph.D. thesis, Dept. of Mechanical Engineering., Univ. of Leeds.

van HELDEN, A.K., van der-MEER, R.J., van SFAADEN, J.J., van GELDEREREN, E. (1985). "Dynamic Friction in Cam/Tappet Lubrication", S.A.E. 850441.

HERTZ, M., (1882). "Uber die Berührung Fester Elastischer Körper" ("On the Contact of Elastic Solids"), J. reine und angewandte Mathematik, Vol 92, pp 156-171.

HOSHI, M. (1984). "Reducing Friction Losses in Automobile Engines", Trib. Int., Vol. 17, No. 4, pp 185-189.

KANESA, H., AKIBA, K., SAKAI, H. (1977). "A New Method of Valve Cam Design - HYSDYNE Cam", S.A.E. 770777.

LANG, O.R. (1981). "Reibungsverluste in Verbrennungsmotoren" ("Friction Losses in Combustion Engines"), Schmiertechnik und Tribologie, 29, January 1982, presented at 'Limits of Lubrication' conference, London, July 1981.

van LEEUWEN, H., MEIJER, H, SCHOMTEN, M. (1986). "Elastohydrodynamic Film Thickness and Temperature Measurements in Dynamically Loaded Concentrated Contacts: Eccentric Cam - Flat Follower", Fluid Film Lubrication - Osborne Reynold Centenary, 13th Leeds-Lyon Symposium on Tribology, pp 611-625, Elsevier.

LIM, C.E., EVANS, H.P., SNIDLE, R.W. (1983). "Kinematics and Lubrication Conditions at Cam Contact in a Centrally Pivoted Cam-Finger Follower", S.A.E. 830309.

MARTIN, F.A. (1985). "Friction in Internal Combustion Engine Bearings" in Combustion Engines - Reduction of Friction and Wear, Paper C67/85, I. Mech. E. Conference Publication, pp 1-7.

MONTEIL, G. (1987). "Etude Tribologique D'un System Came-Poussoir", Ph.D. thesis, Faculte Des Sciences et Des Techniques De L'Universite De Franche-Comte.

MONTEIL, G., LONCHAMPT, J., ROQUES-CARMES, C., GODET, M. (1987). "Interface Composition in Hertzian Contacts. Application to the Cam-Tappet System.", Interface Dynamics, 14th Leeds-Lyon Symposium on Tribology, pp 355-365, Elsevier.

MULLER, R. (1966). "The Effect of Lubrication on Cam and Tappet Performance", Motor Tech. Z, Vol 27, Pt 2, pp 58-61. MIRA Translation, No 27/66.

MUNDAY, H. (1961). "Merecedes 300 SLR Type M196", The Autocar Magazine, January 13th and January 20th, 1961.

NINOMIYA, K., KAWAMORA, M., FUJI, K. (1978). "Electrical Observation of Lubricant Film Between a Cam and Lifter of an O.H.V. Engine", S.A.E. 780093.

PARKER, D.A., ADAMS, D.R. (1982). "Friction Losses in the Reciprocating Internal Combustion Engine" in Tribology - Key to the Efficient Engine, Paper C5/82, I. Mech. E. Conference Publication, pp 31-39.

POLAK, T.A., LETTS A. (1987). "When Did You Last Change Your Camshaft?", Automobile Engineer. Vol 12, No 3, June/July 1987, pp6-8.

PURMER, P.D., van den BERG, W. (1985). "Measurements of Camshaft Wear - Wear and Kinematics of Overhead Camshafts", S.A.E. 850442.

SAKAI, H., TSUDA, K., (1970). "Analysis of Valve Motion In Overhead Linkages", Bulletin of J.S.M.E. Vol. 13, No 55 p 120.

STARON, J.T., WILLERMET, P.A. (1983). "An Analysis of Valve Train Friction in Terms of Lubrication Principles", S.A.E. 830165.

STONE, J.M., UNDERWOOD, A.F. (1947). "Load Carrying Capacity of Journal Bearings", Quart. Trans. S.A.E. vol. 1, pp 56-57.

VICHARD, J.P., GODET, M. (1966-67). "Simultaneous Measurement of Load, Friction and Film Thickness in a Cam and Tappet System", Symposium on Experimental Methods in Tribology, Proc. I. Mech. E., vol. 182, pt 3G, pp 109-113.

WATKINS, R.C. (1985). "A New Approach to the Derivation of Viscosity in Lubricated Contacts", Proc. 4th European Tribology Congress, Eurotrib. Elsevier, Amsterdam.

WILLERMET, P.A. (1987). Private Communication.

ZHU, G. (1988). "A Theoretical and Experimental Study of the Tribology of a Cam and Follower", Ph.D. thesis, Dept. of Mechanical Engineering, Univ. of Leeds.

APPENDIX A

THE KINEMATICS OF PIVOTED FOLLOWER SYSTEMS

(a) The Kinematics of a Cam and End Pivoted Follower System.

The geometry of the system is shown in Figure (A.1). An axis system, (Oxy), rotates at cam speed, its y-axis passes through the nose of the cam and the origin, O, is coincident with the cam centre of rotation. The follower is pivoted at the point U and touches the cam at the point P. The angle between the common tangent to the cam/follower and the x-axis is (ψ). The centre of curvature of the face of the follower in contact with the cam is is at Q and has radius of curvature (r_f). The centre of curvature of the face of the follower in contact with the valve is at V. The angle between the x-axis and the line OU is (ϕ'). The fixed distances are (A) = UQ, (B) = UV, and (D) = UO. The fixed angles are (κ), the angle between OU and the direction of valve motion and (λ) = $\angle$VUQ. The important variable angles are (ψ) and (γ) (= $\angle$OUV).

It is assumed that the angular velocity of the camshaft, (ω), (which is half that of the crankshaft) is constant, and so the angle (ϕ') varies linearly with time, such that

$$\phi' = \phi'_o + \phi$$

$$= \phi'_o + \omega t$$

where (ϕ'_o) is the value of (ϕ') at maximum lift, and (ϕ) is measured from the top of lift. It is also assumed that the cam and follower are always in contact, i.e. the clearance on the cam base circle radius is neglected.

It can be seen from Figure (A.1) that the point of contact between the cam and follower, $P(x_1,y_1)$, has coordinates in the rotating coordinate system, (Oxy), of

$$x_1 = - D \cos\phi' - A \cos(\pi-\phi'-\lambda-\gamma) + r_f \sin\psi \qquad (A.1)$$

$$y_1 = - D \sin\phi' + A \sin(\pi-\phi'-\lambda-\gamma) - r_f \cos\psi \qquad (A.2)$$

Referring to Figure (A.2) (after Lim et al (1983)), (r_c) is the local radius of curvature of the cam (= PG) and G the centre of

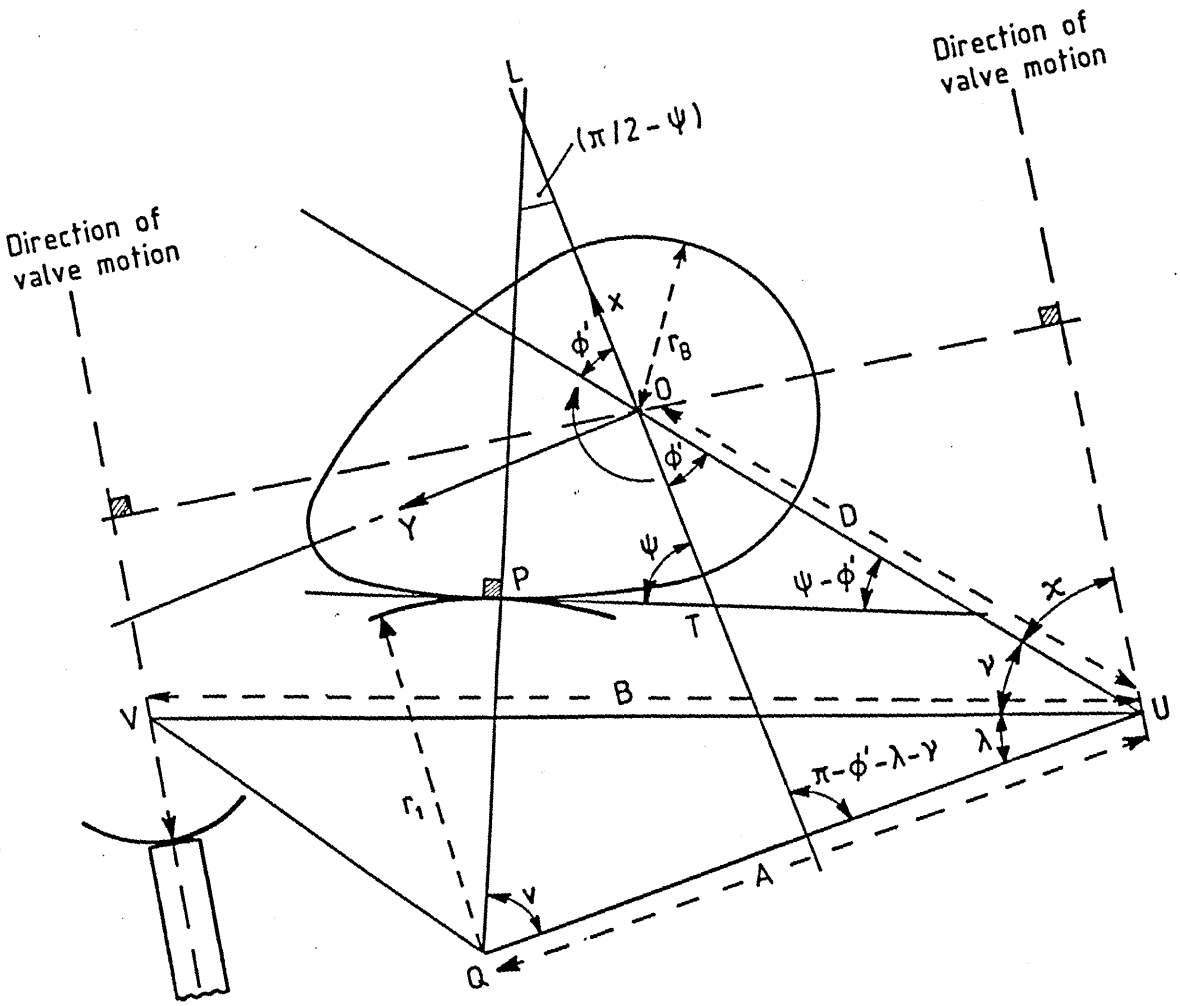

Figure (A.1) Geometry of a Cam Acting Against an End Pivoted Follower.

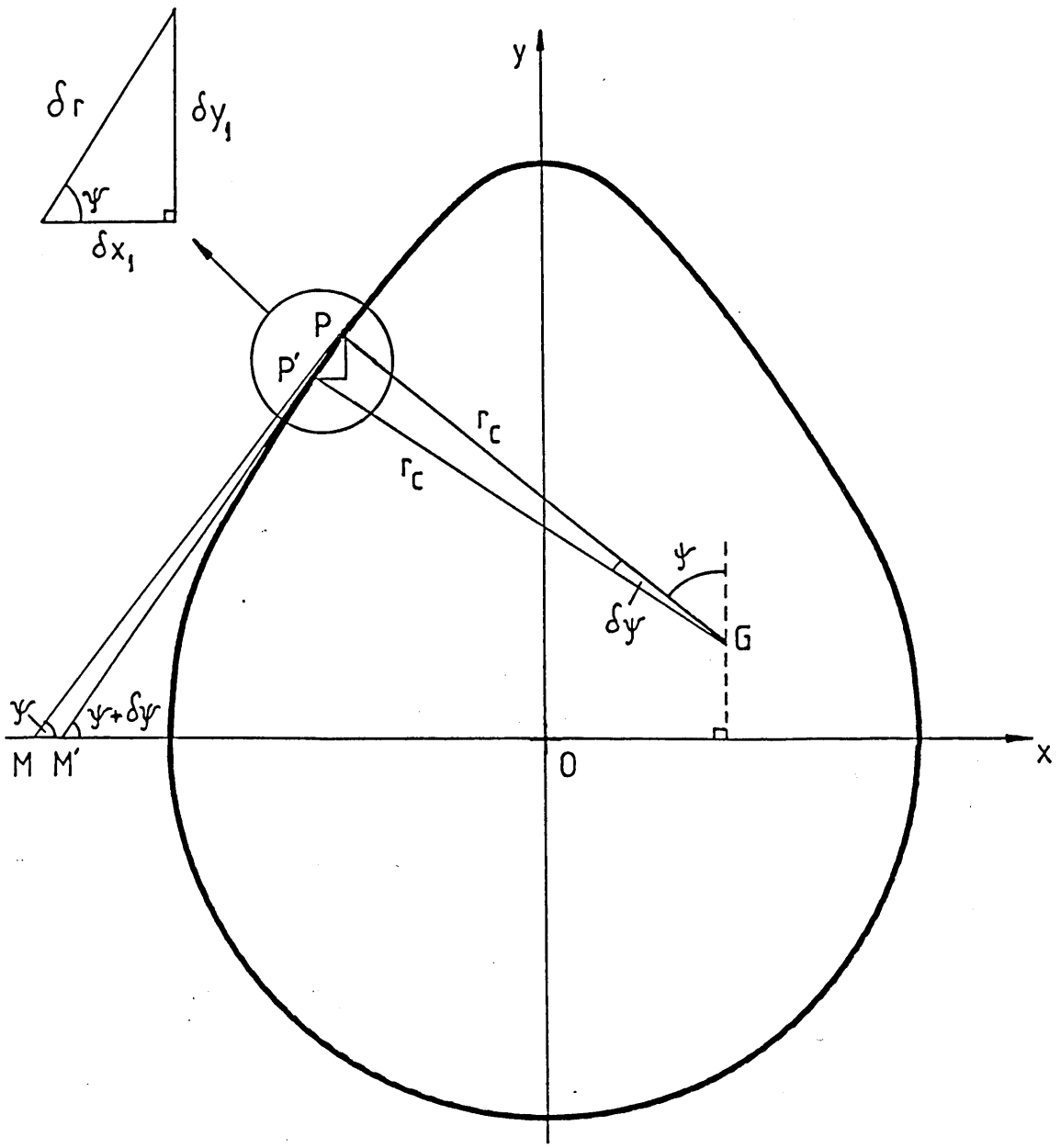

Figure (A.2) Successive Points of Contact on the Cam Surface.

curvature of the cam at the instant when the point of contact of the cam and follower is at P. When the cam is rotated through a small angle ($\delta\phi'$), with corresponding change in (ψ), ($\delta\psi$), the point of contact is displaced by a distance (δr) along the cam surface to point P'. If we consider ($\delta\psi$) to be small then the centre of curvature, G, can be assumed to remain in the same position. PM and P'M' are the tangents to the cam surface at P and P' respectively. As ($\delta\psi$) is small

$$\delta r = r_c \, \delta\psi$$

It can be seen that the displacement of P in the y_1 direction is

$$\delta y_1 = - \delta r \sin\psi$$

and in the x_1 direction is

$$\delta x_1 = - \delta r \cos\psi$$

Differentiating (x_1) with respect to (ψ)

$$\lim_{\delta\psi\to 0}\left[\frac{\delta x_1}{\delta\psi}\right] = \lim_{\delta\psi\to 0}\left[\frac{\delta r \cos\psi}{\delta\psi}\right]$$

$$= \lim_{\delta\psi\to 0}\left[\frac{r_c \, \delta\psi \cos\psi}{\delta\psi}\right]$$

Thus

$$\frac{dx_1}{d\psi} = - r_c\cos\psi \qquad (A.3)$$

and similarly,

$$\frac{dy_1}{d\psi} = - r_c\sin\psi \qquad (A.4)$$

Differentiating Equations (A.1) and (A.2) with respect to (ψ) and substituting Equations (A.3) and (A.4) gives

$$(r_f+r_c)\cos\psi = \left[A\left(1+\frac{d\gamma}{d\phi'}\right)\sin(\phi'+\lambda+\gamma)-D\sin\phi'\right]\frac{d\phi'}{d\psi} \qquad (A.5)$$

$$(r_f+r_c)\sin\psi = \left[-A\left(1+\frac{d\gamma}{d\phi'}\right)\cos(\phi'+\lambda+\gamma)+D\cos\phi'\right]\frac{d\phi'}{d\psi} \qquad (A.6)$$

Hence

$$\tan\psi = \frac{-A\left(1+\frac{d\gamma}{d\phi'}\right)\cos(\phi'+\lambda+\gamma)+D\cos\phi}{A\left(1+\frac{d\gamma}{d\phi'}\right)\sin(\phi'+\lambda+\gamma)-D\sin\phi'} \qquad (A.7)$$

and

$$(r_f + r_c) = M\,\frac{d\phi'}{d\psi} \qquad (A.8)$$

where

$$M^2 = A^2\left[1+\frac{d\gamma}{d\phi'}\right]^2 - 2AD\left[1+\frac{d\gamma}{d\phi'}\right]\cos(\lambda+\gamma) + D^2 \qquad (A.9)$$

Differentiating Equation (A.7) with respect to (ϕ') gives

$$\sec^2\psi \frac{d\psi}{d\phi'} = L^2\left[A\left[1+\frac{d\gamma}{d\phi'}\right]\sin(\phi'+\lambda+\gamma)-D\sin\phi'\right]^{-2} \qquad (A.10)$$

where

$$L^2 = -A^2\left[1+\frac{d\gamma}{d\phi'}\right]^3 + AD\frac{d^2\gamma}{d\phi'^2}\sin(\lambda+\gamma) - D^2 +$$

$$AD\left[1+\frac{d\gamma}{d\phi'}\right]\left[2+\frac{d\gamma}{d\phi'}\right]\cos(\lambda+\gamma) \qquad (A.11)$$

It should be noted that (L^2) may take negative values (it is defined as a square as it has dimensions of the square of a length).

Using the relationship

$$\sec^2\psi = 1 + \tan^2\psi$$

Equation (A.7), (A.9) and (A.11) yield

$$\frac{d\psi}{d\phi'} = \frac{L^2}{M^2} \qquad (A.12)$$

Equations (A.8) and (A.12) then give

$$r_c = \frac{M^3}{L^2} - r_f \qquad (A.13)$$

The equivalent radius of curvature at the contact (R) is given by

$$\frac{1}{R} = \frac{1}{r_c} + \frac{1}{r_f}$$

Hence using (A.13)

$$R = r_f - \frac{r_f^2 L^2}{M^3} \qquad (A.14)$$

The velocity of the point of contact along the cam surface, (V_c), is defined as being positive and may be only in that direction - that opposite to the rotation of the cam. It can be shown that (see Dyson (1977))

$$V_c = \omega r_c \frac{d\psi}{d\phi'}$$

which on substituting (A.12) and (A.13) gives

$$V_c = \omega\left[M - \frac{L^2}{M^2}\right] \qquad (A.15)$$

The velocity of the point of contact along the follower surface may take positive (i.e. in the same direction as (V_c)) or negative values. From Figure (A.1):

$$V_f = - \omega \frac{ds}{d\phi'} = - \omega r_f \frac{d\nu}{d\phi'}$$

and

$$\nu = \frac{\pi}{2} - \phi' - \gamma - \lambda + \psi \qquad (A.16)$$

therefore

$$V_f = \omega r_f \left[1 + \frac{d\gamma}{d\phi'} - \frac{d\psi}{d\phi'}\right]$$

Substituting (A.12) gives

$$V_f = \omega r_f \left[1 + \frac{d\gamma}{d\phi'} + \frac{L^2}{M^2}\right] \qquad (A.17)$$

The displacement of the point of contact from its position at maximum lift, (s), is given by

$$s = r_f (\nu - \nu_o)$$

so from (A.16)

$$s = r_f(\phi + \psi + \gamma + \gamma_o) \qquad (A.18)$$

The angle (γ) and its derivatives with respect to (ϕ') may be found by considering the lift of the valve (l_v). From Figure (A.1):

$$l_v = B \cos(\gamma_B + \kappa) - B \cos(\gamma + \kappa) \qquad (A.19)$$

which on differentiating with respect to (ϕ') gives

$$\frac{dl_v}{d\phi'} = B \sin(\gamma + \kappa) \frac{d\gamma}{d\phi'}$$

so

$$\frac{d\gamma}{d\phi'} = [B \sin(\gamma + \kappa)]^{-1} \frac{dl_v}{d\phi'} \qquad (A.20)$$

and

$$\frac{d^2\gamma}{d\phi'^2} = [B \sin(\gamma + \kappa)]^{-2} \frac{d^2 l_v}{d\phi'^2} -$$

$$[B^2 \sin^3(\gamma + \kappa)]^{-1} \left[\frac{dl_v}{d\phi'}\right]^2 \cos(\gamma + \kappa) \qquad (A.21)$$

(γ_B) may be found by considering the system in the base circle position ($OQ = r_f + r_B$) and applying the cosine rule:

$$\cos(\gamma_B + \lambda) = \frac{A^2 + D^2 - (r_f + r_B)^2}{2AD}$$

(b) The Kinematics of a Cam and Centrally Pivoted Follower System.

Lim et al (1983) showed that the analysis presented above was also valid for a cam acting against a centrally pivoted follower. Such a system is shown in Figure (A.3). The only difference to the analysis is in the expressions for the position of the point of contact between the cam and follower:

$$x_1 = - D \cos\phi' + A \cos(\phi' + \lambda + \gamma) + r_f \sin\psi$$

$$y_1 = - D \sin\phi' + A \sin(\phi' + \lambda + \gamma) - r_f \cos\psi$$

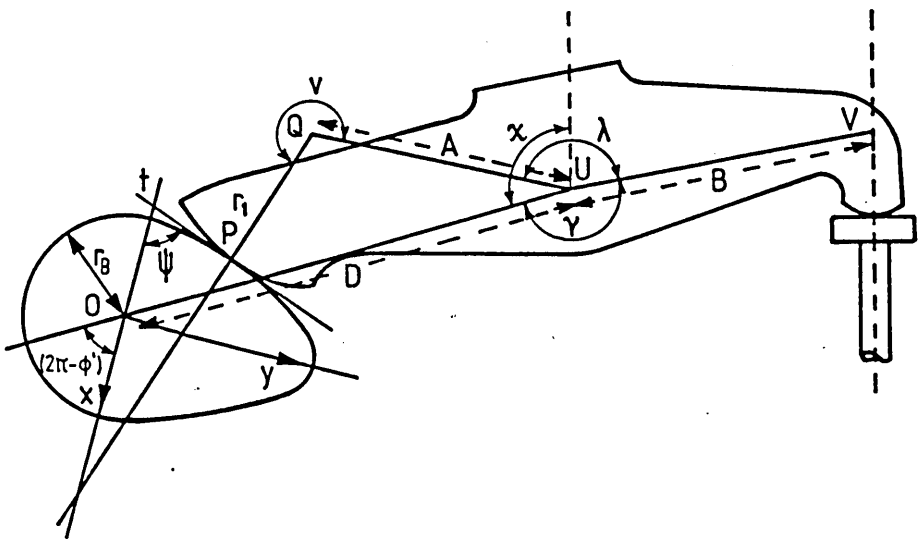

Figure (A.3) Geometry of a Cam Acting Against a Centrally Pivoted Follower.

APPENDIX B

THE LOADING AT THE CAM/FOLLOWER INTERFACE FOR CAMS ACTING AGAINST TRANSLATING FOLLOWERS

(a) The Load at the Cam/Follower Interface for a Cam Acting Against a Flat Faced Follower.

The forces associated with the operation of a cam mechanism are: the inertia force, the spring force, the forces created by the dynamic deflections and damping effects of the parts and the friction between the moving parts. It is assumed that the valve train is rigid and therefore the dynamic deflections and damping characteristics of the system are neglected. Figure (B.1) shows a free-body diagram of the cam/follower system, where (S) is the spring force, (I_f) is the inertia force, (F_v) and (F_f) are the friction at the valve and follower guides respectively and (Mg) is the gravitational force.

Applying D'Alembert's principle and resolving forces in the direction of valve motion we obtain:

$$W = I_f + S + F_v + F_f - Mg$$

The forces (Mg), (F_v) and (F_f) are small when compared to (I_f) and (S) and can be safely neglected.

The inertia force (I_f) is equal to the product of the equivalent mass of the reciprocating parts and the acceleration of these parts and is given by:

$$I_f = M \frac{d^2 l_v}{d\phi'^2} \omega^2$$

The equivalent reciprocating mass of the system (M) can be shown to be equal to the sum of the masses of the follower, valve and spring retainers plus one third of the spring mass (Harrison (1985)).

The spring force (S) is equal to the product of the spring constant and the deflection of the spring from its free length:

$$S = k(l_v + \delta)$$

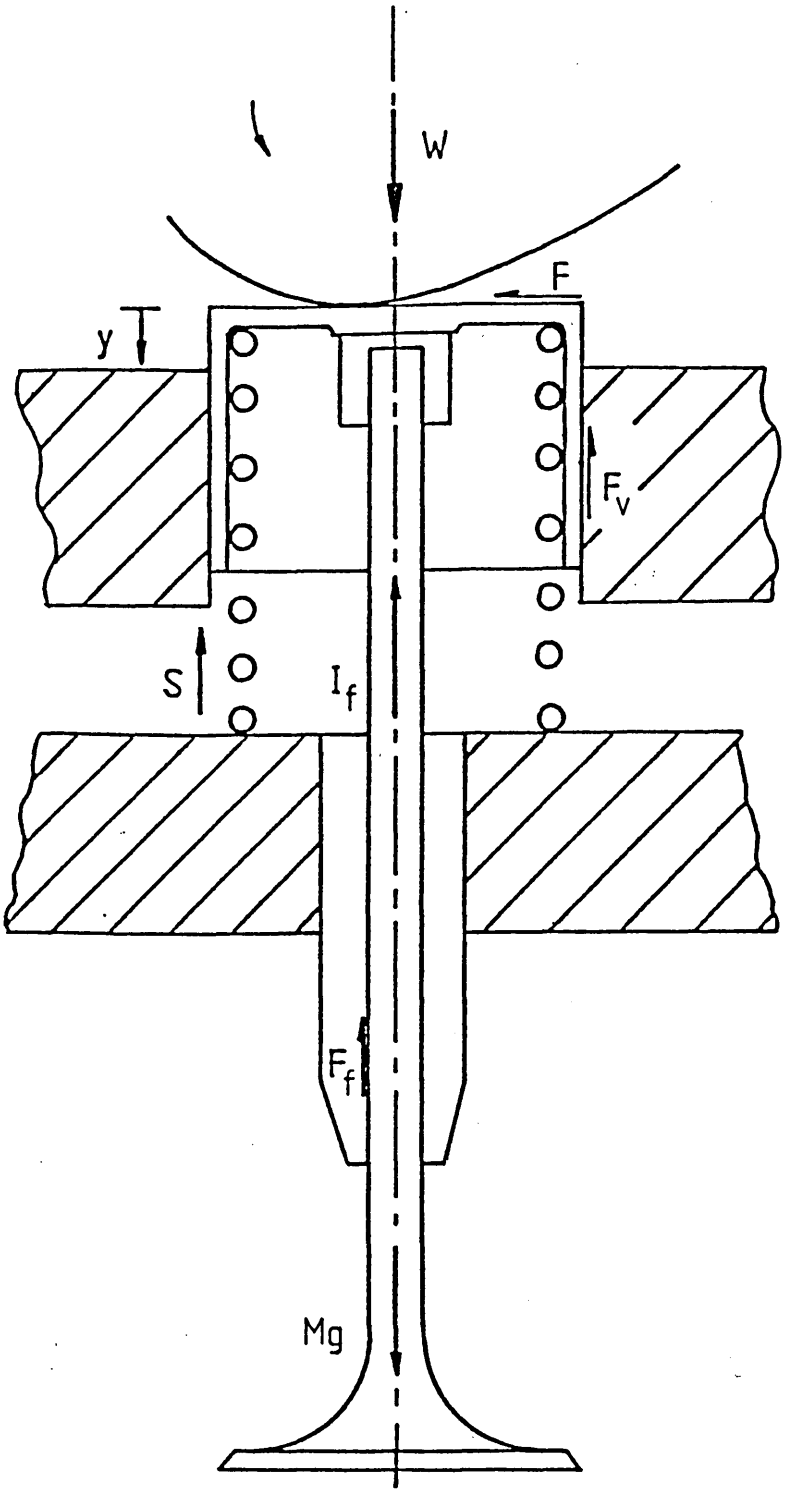

Figure (B.1) Free Body Diagram of a Cam and Flat Faced Follower System.

Therefore the load (W) at the cam/follower interface for a cam acting against a flat faced follower is given by:

$$W = k(l_v + \delta) + M\omega^2 \frac{d^2 l_v}{d\phi'^2} \qquad (B.1)$$

(b) The Loading at the Cam/Follower Interface for a Cam Against a Domed Follower.

Figure (B.2) shows the general arrangement of a cam acting on a domed follower operating a rocker to open the valve. The rocker ratio (RR) is equal to (b/a) and the masses (M_1) and (M_2) are the equivalent masses at the follower end of the rocker and the valve end of the rocker respectively. The lift at the valve (l_v) is equal to the lift at the follower (l_c) multiplied by the rocker ratio (RR). Neglecting the effects of gravity, friction and the rocker inertia and assuming the valve train to be rigid we are left with the free-body diagram as shown in Figure (B.3). Applying D'Alembert's principle and resolving in the direction perpendicular to the cam/follower common tangent we obtain:

$$W = \frac{M_1\omega^2 \frac{d^2 l_c}{d\phi'^2} + M_2 RR^2\omega^2 \frac{d^2 l_c}{d\phi'^2} + RR.k(l_c RR + \delta)}{\cos\beta}$$

where

$$\beta = \cos^{-1}\left[\frac{\left\{r_f^2 + \left[\frac{dl_c}{d\phi'}\right]^2\right\}^{\frac{1}{2}}}{r_f}\right]$$

thus

$$W = \frac{r_f}{\left[r_f^2 + \left[\frac{dl_c}{d\phi'}\right]^2\right]^{\frac{1}{2}}} \cdot \left[M_1\omega^2 \frac{d^2 l_c}{d\phi'^2} + M_2 RR^2\omega^2 \frac{d^2 l_c}{d\phi'^2} + RR.k(l_c + \delta)\right] \qquad (B.2)$$

If we take the case of a domed follower acting directly against the valve then the rocker ratio (RR) is equal to unity and Equation

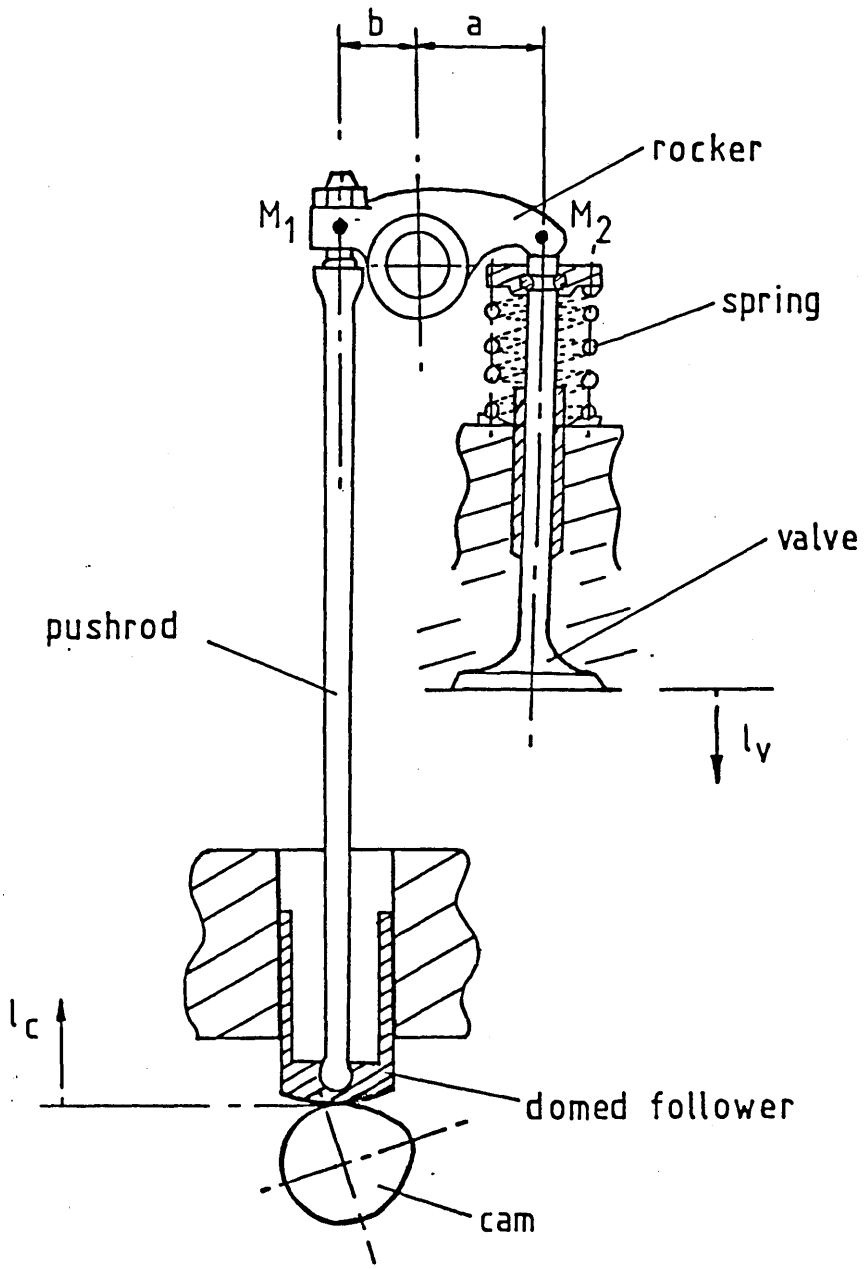

Figure (B.2) Cam Acting Against a Domed Follower
In a Pushrod Operated System.

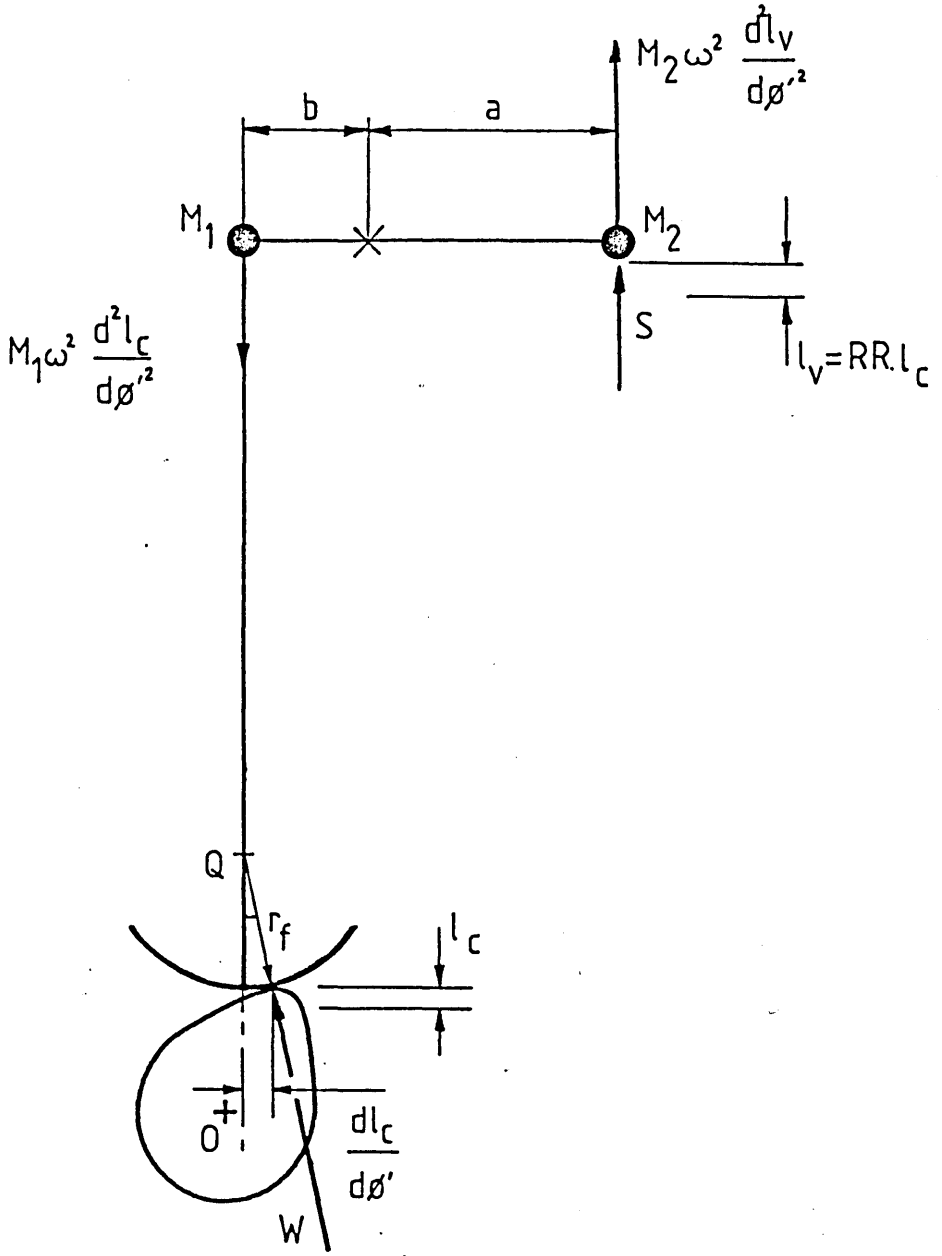

Figure (B.3) Free Body Diagram for a Cam Acting Against a Domed Follower in a Pushrod Operated System.

(B.2) reduces to

$$W = \frac{r_f}{\left[r_f^2 + \left[\frac{dl_v}{d\phi'}\right]^2\right]^{\frac{1}{2}}} \cdot \left[M\,\omega^2 \frac{d^2 l_v}{d\phi'^2} + k(l_v + \delta)\right] \qquad (B.3)$$

If we now consider a direct acting flat faced follower system where the radius of the follower, (r_f), is infinity then Equation (B.3) reduces to

$$W = M\,\omega^2 \frac{d^2 l_v}{d\phi'^2} + k(l_v + \delta) \qquad (B.4)$$

which is the same as that given in Equation (B.1).

APPENDIX C

THE LOADING AT THE CAM/FOLLOWER INTERFACE FOR A CAM ACTING AGAINST A PIVOTED FOLLOWER

(a) Cam and Centrally Pivoted Follower.

Figure (C.1) shows a cam acting against a centrally pivoted follower. The forces shown are the spring force, (S), the valve assembly inertia force, (F_v), the frictional force at the cam/follower interface, (F_{frict}), the follower inertia force, (F_f), and the load exerted on the follower by the cam, (W). The frictional forces at the valve/follower interface and at the follower pivot point have been neglected as have gravitational and dynamic forces.

The moments caused by each of the above forces about the follower pivot point, (U), defining a clockwise moment as positive, are:

$$\text{Spring force moment} = - S\ B \cos\left[-\frac{3.\pi}{2} + \kappa + \gamma\right] \qquad (C.1)$$

$$\text{Valve inertia moment} = - F_v\ B \cos\left[-\frac{3.\pi}{2} + \kappa + \gamma\right] \qquad (C.2)$$

$$\text{Cam load moment} = W\ A \cos\left[\frac{3.\pi}{2} - \nu\right] \qquad (C.3)$$

$$\text{Frictional force moment} = - F_{frict}\left[r_f - A \cos\left[\frac{3.\pi}{2} - \nu\right]\right] \qquad (C.4)$$

$$= - \mu\ W\left[r_f - A \cos\left[\frac{3.\pi}{2} - \nu\right]\right] \qquad (C.5)$$

$$\text{Follower inertial moment} = - M_f\ B^2\omega^2\ \frac{d^2\gamma}{d\phi'^2} \qquad (C.6)$$

where (M_f) is the equivalent mass of the follower at a distance (B) from the follower pivot point (U). Summing the moments and substituting:

$$S = k\ (l_v + \delta) \qquad (C.7)$$

and

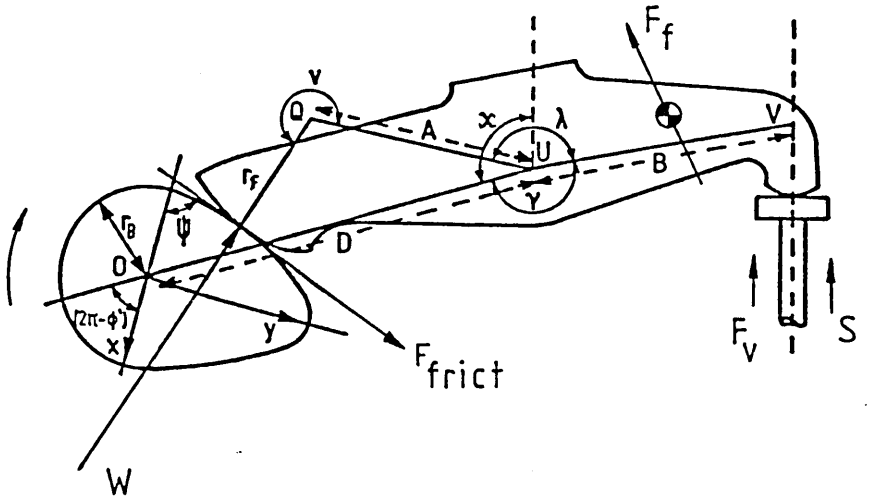

Figure (C.1) The Loads in a Cam and Centrally Pivoted Follower System.

$$F_v = M \omega^2 \frac{d^2 l_v}{d\phi'^2} \tag{C.8}$$

gives:

$$W = \frac{\left[M \frac{d^2 l_v}{d\phi'^2} \omega^2 + k(\delta + l_v) \right] B \cos \left[\frac{-3.\pi}{2} + \kappa + \gamma \right] + M_f \frac{d^2\gamma}{d\phi'^2} \omega^2 B^2}{A \cos \left[\frac{3.\pi}{2} - \nu \right] - \mu \left[r_f + A \sin \left[\frac{3.\pi}{2} - \nu \right] \right]} \tag{C.9}$$

where (M) is equal to one third of the valve spring mass plus the mass of the valve and any retainers.

(b) Cam and End Pivoted Follower.

Figure (C.2) shows a cam acting against an end pivoted follower. The forces shown are the spring force, (S), the valve assembly inertia force, (F_v), the frictional force at the cam/follower interface, (F_{frict}), the follower inertia force, (F_f), and the load exerted on the follower by the cam, (W). The frictional forces at the valve/follower interface and at the follower pivot point have been neglected as have gravitational and dynamic forces. The moments caused by each of the above forces about the follower pivot point, (U), defining a clockwise moment as positive, are:

$$\text{Spring force moment} = - S B \cos \left[\frac{\pi}{2} - \kappa - \gamma \right] \tag{C.10}$$

$$\text{Valve inertia moment} = - F_v B \cos \left[\frac{\pi}{2} - \kappa - \gamma \right] \tag{C.11}$$

$$\text{Cam load moment} = W A \sin \nu \tag{C.12}$$

$$\text{Frictional force moment} = F_{frict} (r_f - A \cos \nu) \tag{C.13}$$

$$= \mu W (r_f - A \cos \nu) \tag{C.14}$$

$$\text{Follower inertia moment} = - M_f B^2 \omega^2 \frac{d^2\gamma}{d\phi'^2} \tag{C.15}$$

where (M_f) is the equivalent mass of the follower at a distance (B) from the follower pivot point U. Summing the moments and substituting:

$$S = k(l_v + \delta) \tag{C.16}$$

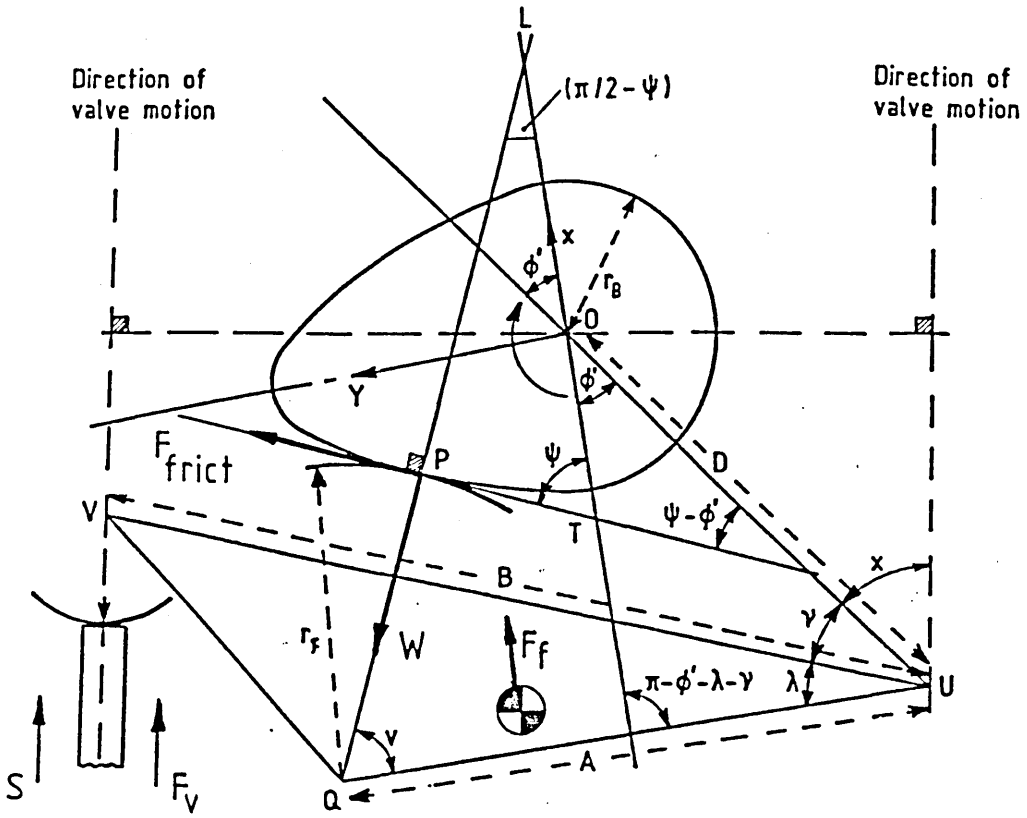

Figure (C.2) The Loads in a Cam and End Pivoted Follower System.

and

$$F_v = M\,\omega^2\,\frac{d^2 l_v}{d\phi'^2} \qquad (C.17)$$

gives:

$$W = \frac{\left[M\,\frac{d^2 l_v}{d\phi'^2}\,\omega^2 + k(\delta + l_v)\right] B \cos\left(\frac{\pi}{2} - \kappa - \gamma\right) + M_f\,\frac{d^2\gamma}{d\phi'^2}\,\omega^2 B^2}{A \sin\nu + \mu\left(r_f - A\cos\nu\right)} \qquad (C.18)$$

where (M) is equal to one third of the valve spring mass plus the mass of the valve and any retainers.

APPENDIX D

THE LOADING AT THE CAM/FOLLOWER INTERFACE FOR A DESMODROMIC VALVE TRAIN SYSTEM

The system to be analysed is shown in Figure (D.1). The opening cam operates a centrally pivoted follower operating the valve directly via a shim. The closing cam operates an end pivoted follower via a spring cup. The position of the valve is defined by (x_{v1}). The light spring ensures that the closing follower is always in contact with the cam and provides the valve seating force when both of the cams are contacting their respective followers on their base circles. When the acceleration of the closing rocker is large enough the clearance between the spring cup and the 'top-hat' (see Figure (D.1)) disappears and the closing follower acts directly upon the valve via the 'top-hat'.

This analysis ignores the effects of the rocker inertia and neglects gravitational and frictional forces. The valve spring has a high fitted load but very low spring constant, and the travel of the spring is very small, therefore it is reasonable to ignore the extra small load introduced by the spring deflection from its fitted length, i.e.

$$S = \text{fitted spring load} = \text{constant}.$$

Each portion of the valve lift curve will now be examined in turn and the loads at each of the cam/follower interfaces investigated. The portions of the valve lift curve discussed below are shown in Figure (D.2). The results are summarised in Table (D.1).

(a) Base Circle (Zero Valve Lift).

At the zero lift position their is a clearance between the opening follower and its cam. The clearance (C_{oc}) is at its maximum. The load on the opening follower is, therefore, zero, and the load on the closing follower is given by:

$$W_c = RR_c S \qquad (D.1)$$

where (RR_c) is the rocker ratio of the closing cam.

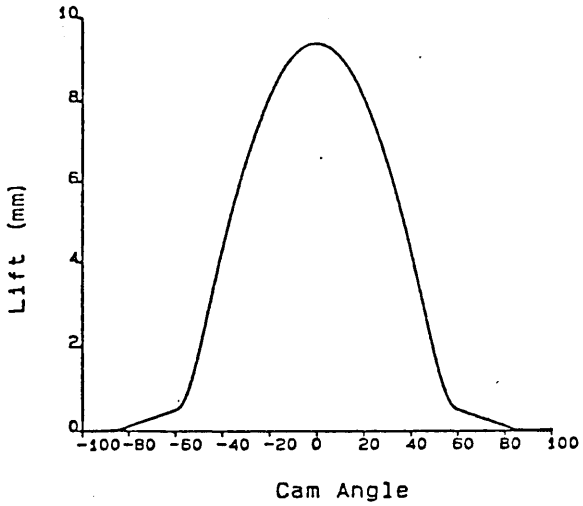

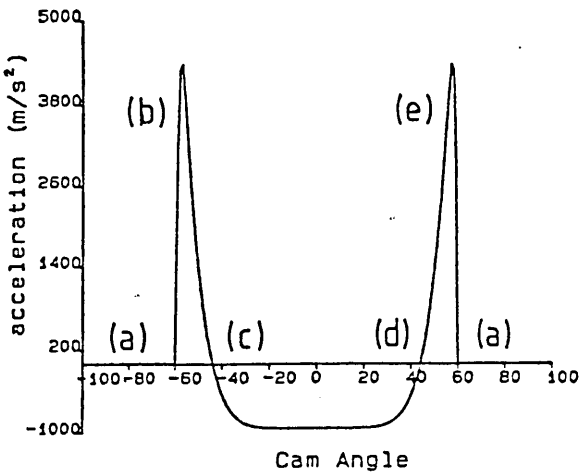

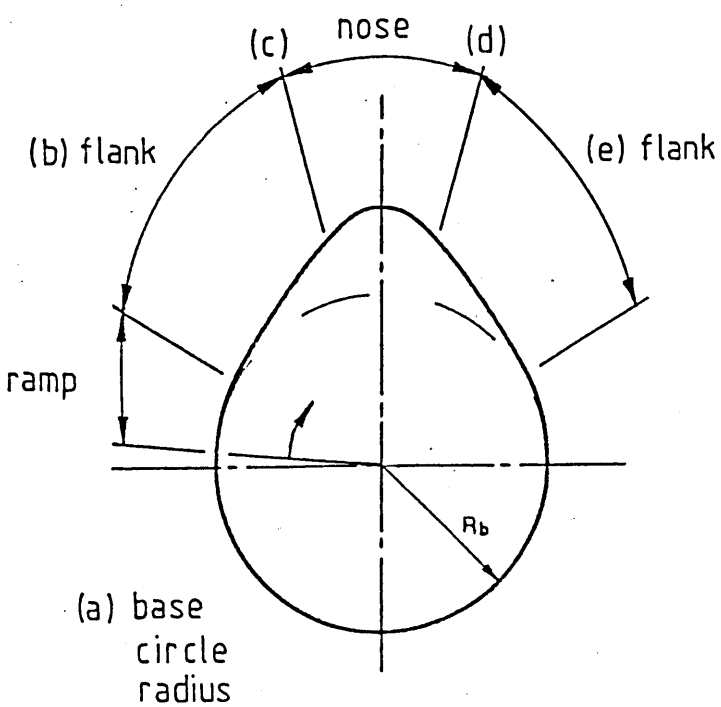

Figure (D.2) Valve Lift Curve.

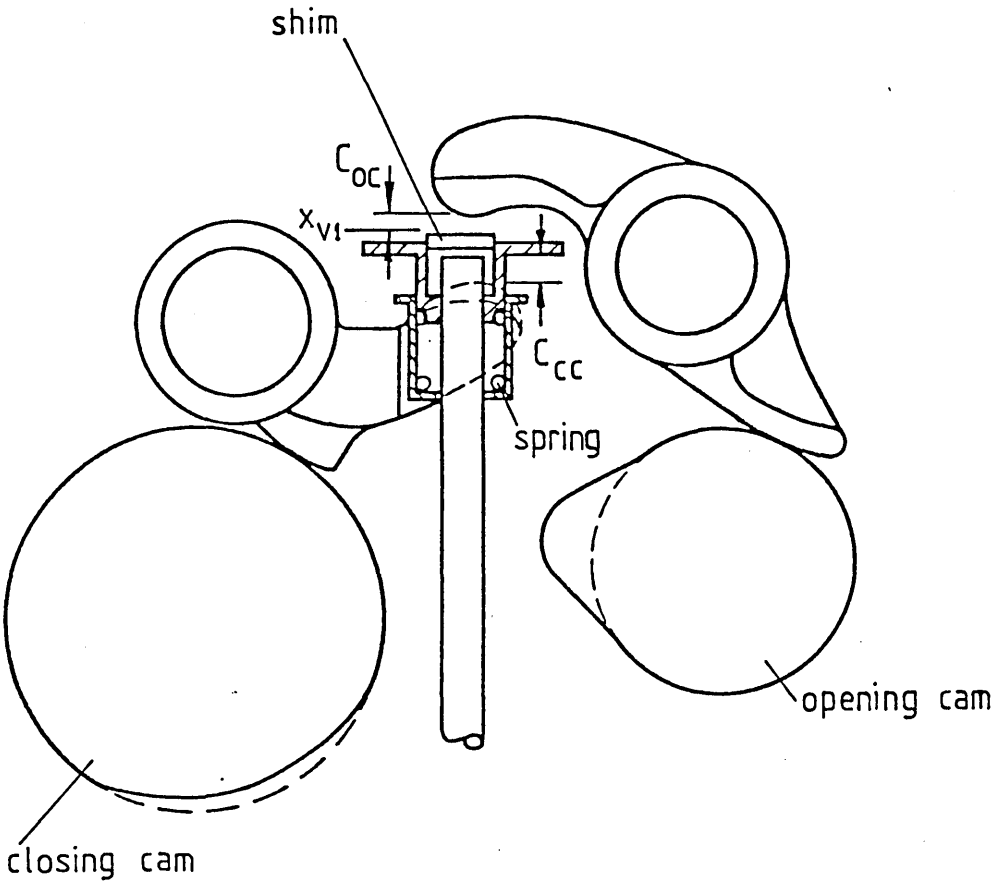

Figure (D.1) Desmodromic Valve Train.

	Load	
	Opening Cam/Follower	Closing Cam/Follower
Base Circle Radius	0	$RR_C.S$
Action Period: $\ddot{Mx}_{V1} + S > 0$	$(\ddot{Mx}_{V1} + S).RR_O$	$RR_C.S$
Action Period: $\ddot{Mx}_{V1} + S < 0$	0	$\ddot{Mx}_{V1}.RR_C$

Table (D.1) Summary Of Cam/Follower Loads For Desmodromic System.

(b) Flank (Valve Acceleration Period).

Figure (D.3) shows the free body diagram for the system during the flank period, where the opening cam is accelerating the valve and the closing cam is following the motion of the opening cam, with the clearance (C_{cc}) still existing.

The force at the top of the valve (F_{vo}) is given by

$$F_{vo} = M.\ddot{x}_{v1} + S \qquad (D.2)$$

Taking moments about the opening follower pivot gives:

$$W_o = (M.\ddot{x}_{v1} + S).RR_o \qquad (D.3)$$

where (RR_o) is the rocker ratio of the opening follower. Taking moments about the closing follower pivot gives:

$$W_c = S.RR_c \qquad (D.4)$$

(c) Flank to Nose Transition.

At the point where the opening cam stops accelerating the valve, the valve has no inertia. From Equations (D.3) and (D.4) this gives:

$$W_o = S.RR_o \qquad (D.5)$$

and

$$W_c = S.RR_c \qquad (D.6)$$

As the valve acceleration becomes negative across the cam nose the valve inertia force becomes negative and eventually greater in magnitude than the spring force. At this point the load at the opening cam/follower interface becomes zero. Also, the spring begins to compress in order to provide the inertia force necessary to decelerate the valve. The clearance (C_{cc}) is eventually taken up and the closing rocker operates the valve directly via the 'top-hat'. The free body diagram of the system in this state is shown in Figure (D.4).

The force at the valve (F_{vc}) is given by:

$$F_{vc} = M.\ddot{x}_{v1} - S \qquad (D.7)$$

such that the force required to decelerate the valve mass is provided

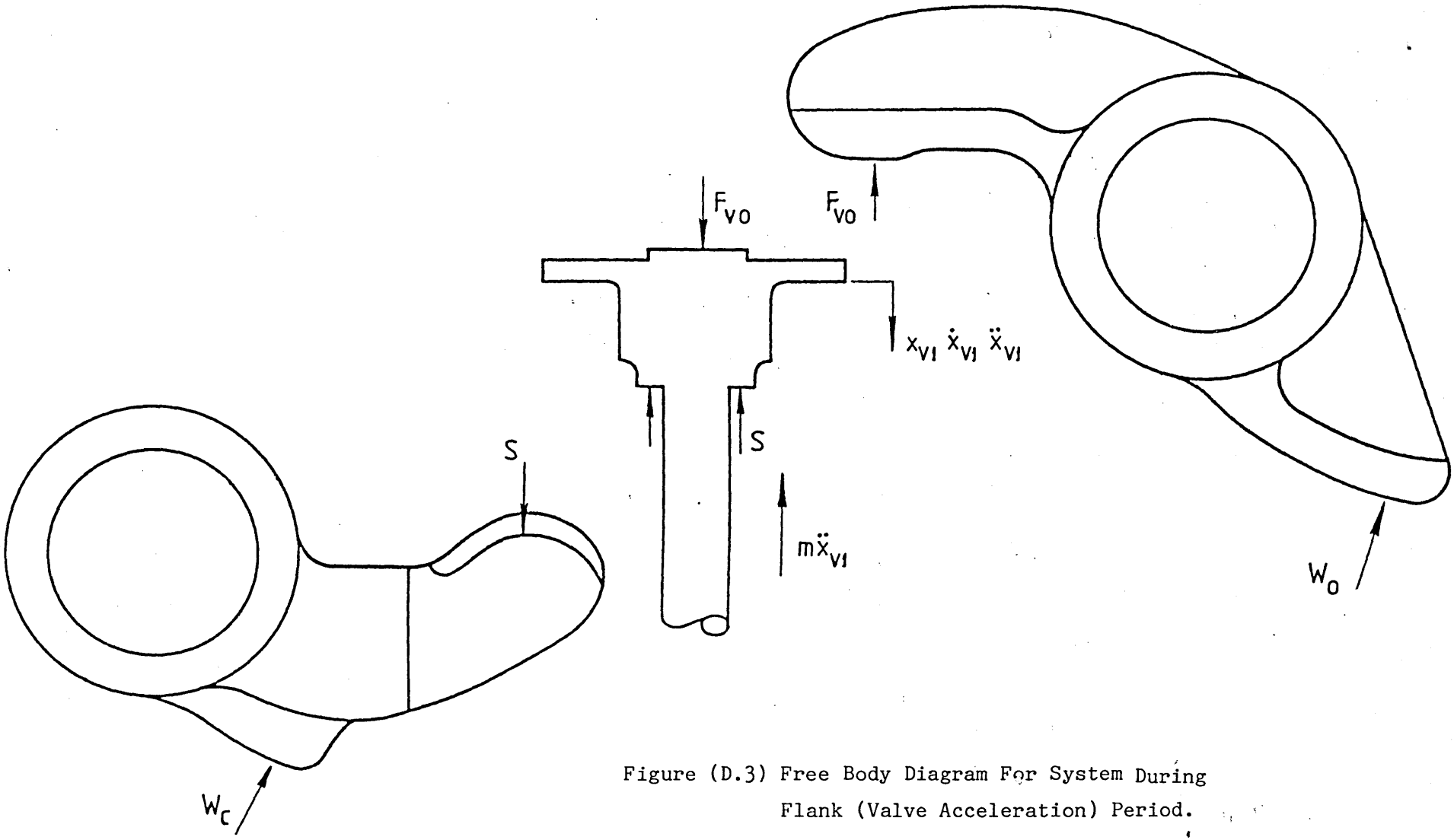

Figure (D.3) Free Body Diagram For System During Flank (Valve Acceleration) Period.

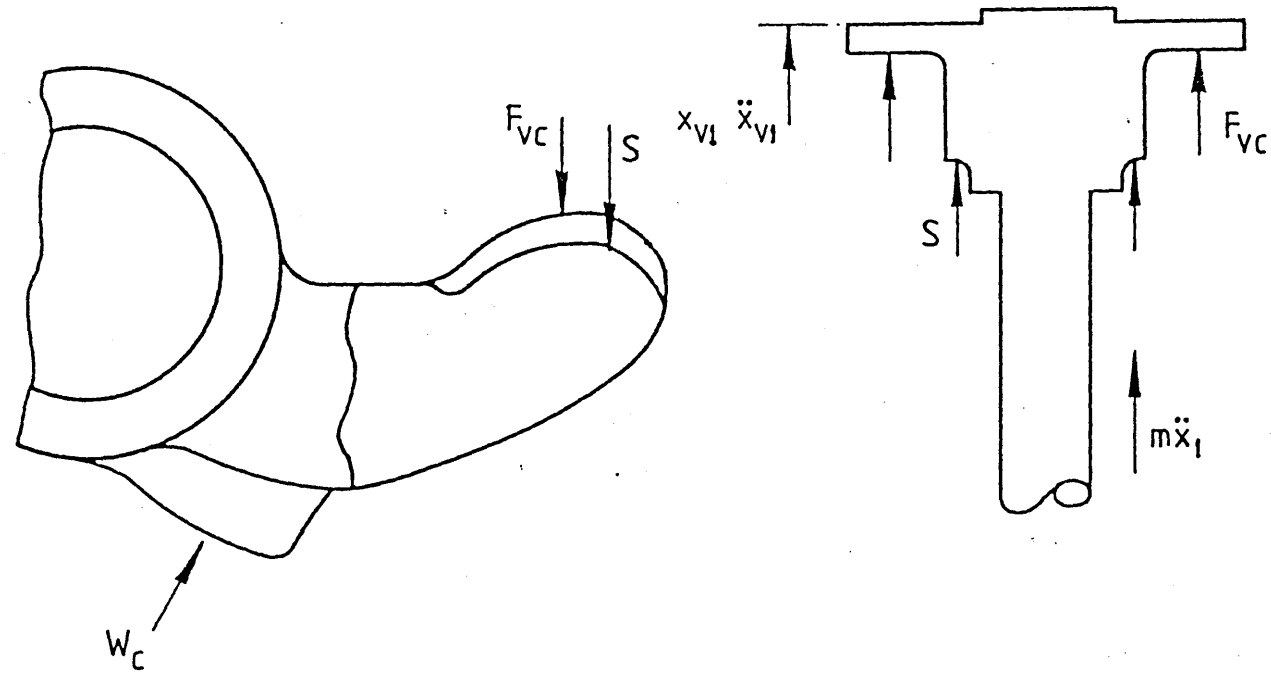

Figure (D.4) Free Body Diagram for System During Nose Period.

by the spring plus the direct action of the closing follower on the valve. Taking moments about the closing follower pivot point we obtain:

$$W_c = (F_{vc} + S).RR_c \qquad (D.8)$$

therefore

$$W_c = M.\ddot{x}_{v1}.RR_c \qquad (D.9)$$

(d) Nose to Flank Transition.

The valve acceleration starts to become positive in this region and a point is reached at which the valve inertia is equal to the spring force. The valve motion being given by:

$$M.\ddot{x}_{v1} = S \qquad (D.10)$$

The valve then moves across the clearance between the opening and closing followers until it hits the opening follower. The motion of the valve then follows that prescribed by the opening cam and follower pair (as in section (b)).

(e) Closing Flank.

The loads at the two cam/follower interfaces are as given in section (b) above.

APPENDIX E

LIFT CURVE DEFINITION FOR 2.01 PINTO (SIERRA) INLET VALVE

Lift At Cam As Seen By A Roller Follower Of Radius 44.0mm

CAM ANGLE(degrees)	LIFT(mm)	CAM ANGLE(degrees)	LIFT(mm)
-87.0	0.0000	15.0	5.9109
-86.0	0.0008	16.0	5.8542
-85.0	0.0038	17.0	5.7940
-84.0	0.0094	18.0	5.7305
-83.0	0.0174	19.0	5.6635
-82.0	0.0275	20.0	5.5932
-81.0	0.0386	21.0	5.5196
-80.0	0.0495	22.0	5.4426
-79.0	0.0604	23.0	5.3623
-78.0	0.0713	24.0	5.2787
-77.0	0.0822	25.0	5.1919
-76.0	0.0931	26.0	5.1018
-75.0	0.1040	27.0	5.0084
-74.0	0.1149	28.0	4.9119
-73.0	0.1258	29.0	4.8121
-72.0	0.1367	30.0	4.7091
-71.0	0.1476	31.0	4.6029
-70.0	0.1585	32.0	4.4935
-69.0	0.1694	33.0	4.3810
-68.0	0.1803	34.0	4.2654
-67.0	0.1912	35.0	4.1468
-66.0	0.2021	36.0	4.0251
-65.0	0.2129	37.0	3.9005
-64.0	0.2238	38.0	3.7731
-63.0	0.2347	39.0	3.6430
-62.0	0.2457	40.0	3.5102
-61.0	0.2569	41.0	3.3750
-60.0	0.2688	42.0	3.2375
-59.0	0.2825	43.0	3.0979
-58.0	0.2990	44.0	2.9565
-57.0	0.3208	45.0	2.8134
-56.0	0.3509	46.0	2.6690
-55.0	0.3922	47.0	2.5236

CAM ANGLE(degrees)	LIFT(mm)	CAM ANGLE(degrees)	LIFT(mm)
-54.0	0.4472	48.0	2.3777
-53.0	0.5176	49.0	2.2316
-52.0	0.6046	50.0	2.0857
-51.0	0.7085	51.0	1.9408
-50.0	0.8290	52.0	1.7974
-49.0	0.9653	53.0	1.6562
-48.0	1.1158	54.0	1.5181
-47.0	1.2788	55.0	1.3837
-46.0	1.4521	56.0	1.2540
-45.0	1.6332	57.0	1.1296
-44.0	1.8203	58.0	1.0115
-43.0	2.0116	59.0	0.9007
-42.0	2.2055	60.0	0.7982
-41.0	2.4005	61.0	0.7050
-40.0	2.5950	62.0	0.6220
-39.0	2.7877	63.0	0.5499
-38.0	2.9776	64.0	0.4893
-37.0	3.1637	65.0	0.4402
-36.0	3.3454	66.0	0.4022
-35.0	3.5221	67.0	0.3742
-34.0	3.6934	68.0	0.3547
-33.0	3.8590	69.0	0.3414
-32.0	4.0188	70.0	0.3319
-31.0	4.1727	71.0	0.3238
-30.0	4.3205	72.0	0.3158
-29.0	4.4624	73.0	0.3079
-28.0	4.5983	74.0	0.2999
-27.0	4.7282	75.0	0.2920
-26.0	4.8524	76.0	0.2840
-25.0	4.9709	77.0	0.2761
-24.0	5.0838	78.0	0.2681
-23.0	5.1913	79.0	0.2601
-22.0	5.2933	80.0	0.2522
-21.0	5.3901	81.0	0.2442
-20.0	5.4816	82.0	0.2363
-19.0	5.5681	83.0	0.2283
-18.0	5.6495	84.0	0.2203
-17.0	5.7259	85.0	0.2124
-16.0	5.7975	86.0	0.2044

CAM ANGLE(degrees)	LIFT(mm)	CAM ANGLE(degrees)	LIFT(mm)
-15.0	5.8643	87.0	0.1964
-14.0	5.9264	88.0	0.1885
-13.0	5.9838	89.0	0.1805
-12.0	6.0365	90.0	0.1725
-11.0	6.0848	91.0	0.1645
-10.0	6.1286	92.0	0.1566
-9.0	6.1679	93.0	0.1486
-8.0	6.2029	94.0	0.1406
-7.0	6.2336	95.0	0.1326
-6.0	6.2601	96.0	0.1247
-5.0	6.2823	97.0	0.1167
-4.0	6.3004	98.0	0.1086
-3.0	6.3144	99.0	0.1015
-2.0	6.3244	100.0	0.0948
-1.0	6.3303	101.0	0.0882
0.0	6.3323	102.0	0.0815
1.0	6.3303	103.0	0.0748
2.0	6.3245	104.0	0.0681
3.0	6.3148	105.0	0.0614
4.0	6.3013	106.0	0.0547
5.0	6.2840	107.0	0.0480
6.0	6.2630	108.0	0.0414
7.0	6.2383	109.0	0.0347
8.0	6.2099	110.0	0.0280
9.0	6.1779	111.0	0.0213
10.0	6.1422	112.0	0.0146
11.0	6.1030	113.0	0.0081
12.0	6.0603	114.0	0.0030
13.0	6.0140	115.0	0.0004
14.0	5.9642	116.0	0.0000

APPENDIX F

LUBRICATION ANALYSIS OF A DESMODROMIC VALVE TRAIN SYSTEM

This appendix presents the output from the valve train analysis program which was discussed in Chapter 4. The desmodromic valve train described was also used in the experimental project described in Chapter 8.

F.1 Input Data.

F.1.1 Valve Lift.

The valve lift may be described by a multipol of the form:

$$l_v = l_{vs} + C_1\left[\frac{\theta}{\theta_T}\right] + C_2\left[\frac{\theta}{\theta_T}\right]^2 + C_3\left[\frac{\theta}{\theta_T}\right]^3 + C_4\left[\frac{\theta}{\theta_T}\right]^4 + C_5\left[\frac{\theta}{\theta_T}\right]^5$$

where

l_v is the valve lift in mm,

l_{vs} is the valve lift at the start of the segment (= 0.3333 mm for the first segment, i.e. the ramp height),

θ is the cam angle from the start of the segment,

θ_T is the period of the segment,

and the coefficients C_1 to C_5 are:

Segment	1	2	3	4	5
θ_T	3.0	8.0	5.0	5.0	34.0
C_1	.03700	.35969	.87736	1.10212	7.06324
C_2	.00000	.52204	.20392	.00000	-2.07447
C_3	.04894	.00000	.00000	-.04167	-1.44115
C_4	-.01224	.00000	.08113	.02153	.34428
C_5	.00000	.00000	.02828	-.00490	.00640

F.1.2 Geometry, Lubricant, Material and Loading Data.

	Opening Cam/Follower	Closing Cam/Follower
Cam width (mm)	12.00	12.00
A (mm)	26.23	17.32
B (mm)	33.29	32.39
D (mm)	39.32	39.32
r_f (mm)	35.00	20.00
r_B (mm)	17.50	25.00
κ (degrees)	172.69	-7.31
λ (degrees)	125.28	9.41
δ (mm)	5.00	5.00
$E_{follower}$ (GN/m^2)	207.0	207.0
E_{cam} (GN/m^2)	207.0	207.0
$\nu_{follower}$	0.29	0.29
ν_{cam}	0.29	0.29
k (kN/m)	10.00	10.00
M (kg)	.0745	0.0745
α (x 10^{-9} m^2/N)	15.00	15.00
η_0 (Ns/m^2)	.0147	.0147
ω (Hz)	33.33	33.33

The graphical output from the valve train lubrication analysis program is shown in Figures (F.1) and (F.2).

CAM OPERATING CHARACTERISTICS
1995 DESMO OPENING CAM

Cam Base Radius (mm)	=	17.50
Maximum Valve Lift (mm)	=	10.50
Cam Width (mm)	=	12.00
Rotational Speed (rpm)	=	2000.0
Spring Stiffness (kN/m)	=	10.000
Initial Spring Disp. (mm)	=	5.0
Equiv. Mass At Valve (kg)	=	.074
Lubricant Viscosity (Ns/m^2)	=	.015
Press. Visc. Coeff. (/Pa)	=	15.0E-9
Youngs Mod. (Cam) (GPa)	=	207.0
Youngs Mod. (Foll.) (GPa)	=	207.0
Poissons Ratio (Cam)	=	.30
Poissons Ratio (Foll.)	=	.30
Frictional Power Loss (W)	=	1.82

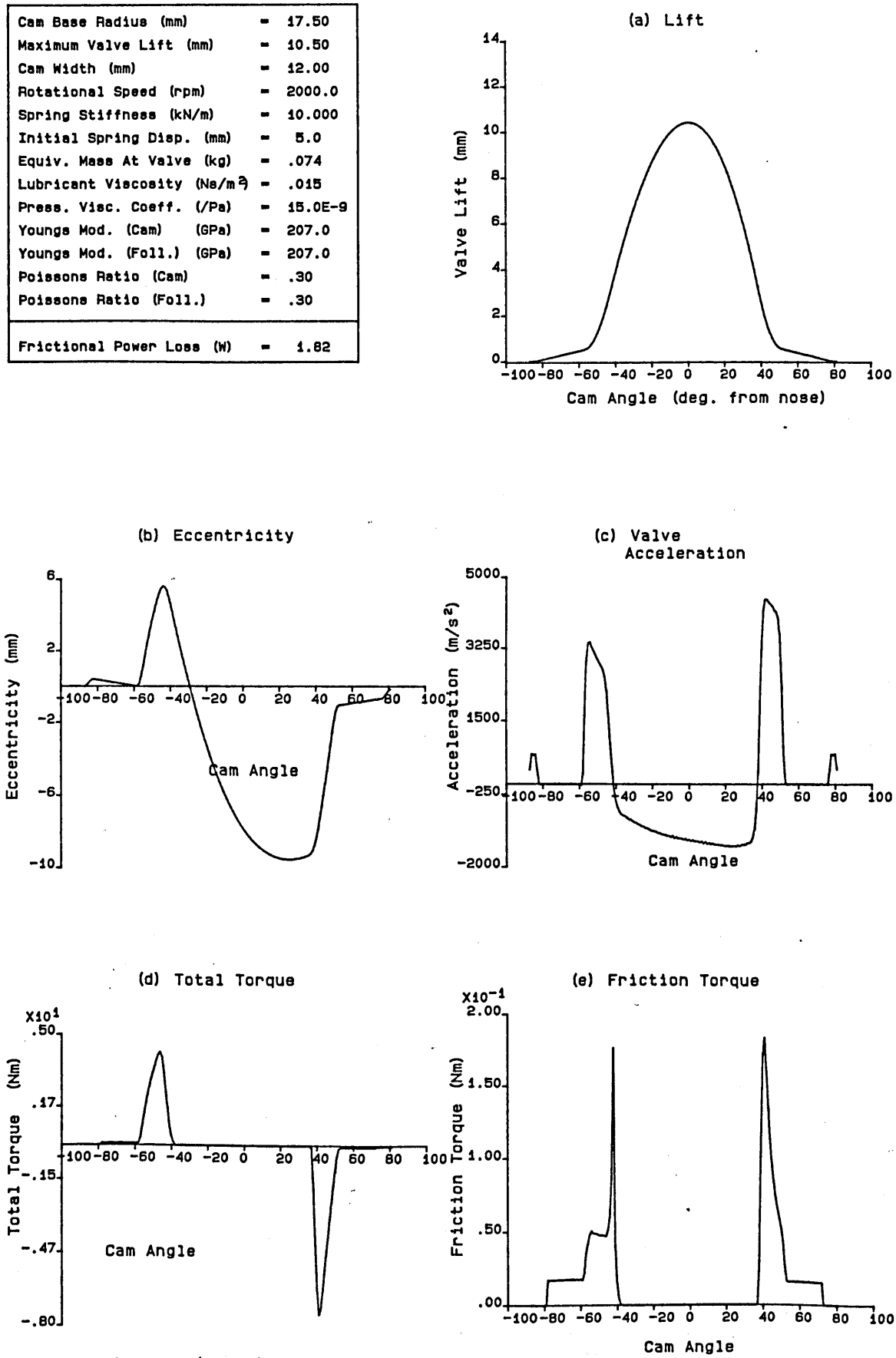

Figure (F.1a) Graphical Output from the Valve Train Lubrication Analysis Program for the Desmodromic Opening Cam and Follower.

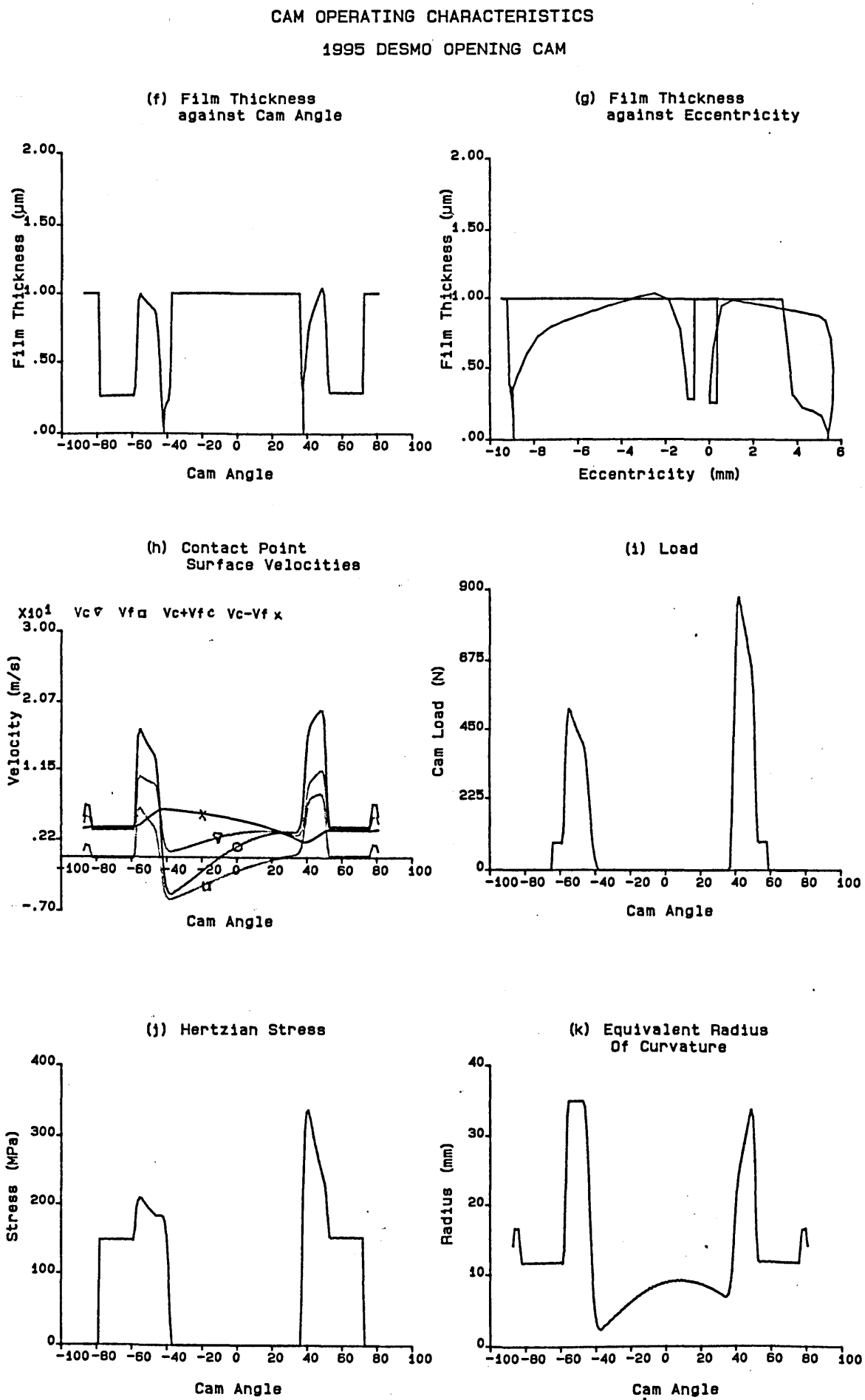

Figure (F.1b) Graphical Output from the Valve Train Lubrication Analysis Program.

CAM OPERATING CHARACTERISTICS
1995 DESMO OPENING CAM

(l) Film thickness around cam periphery

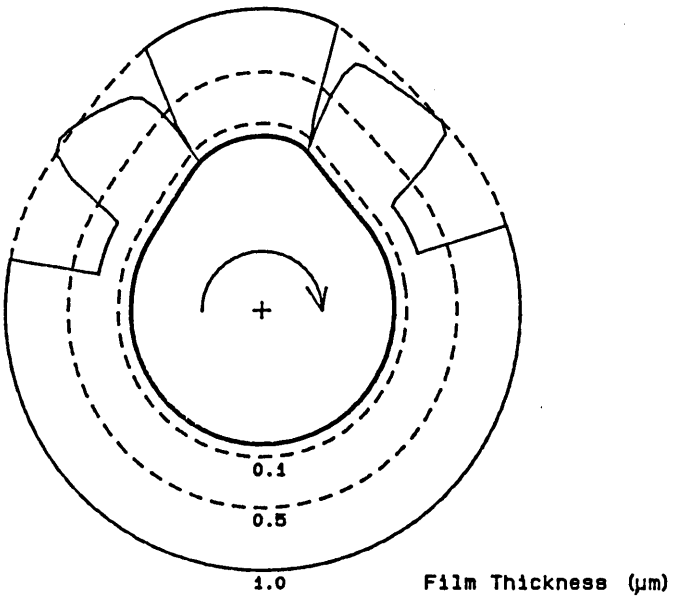

(m) Hertzian stress around cam periphery

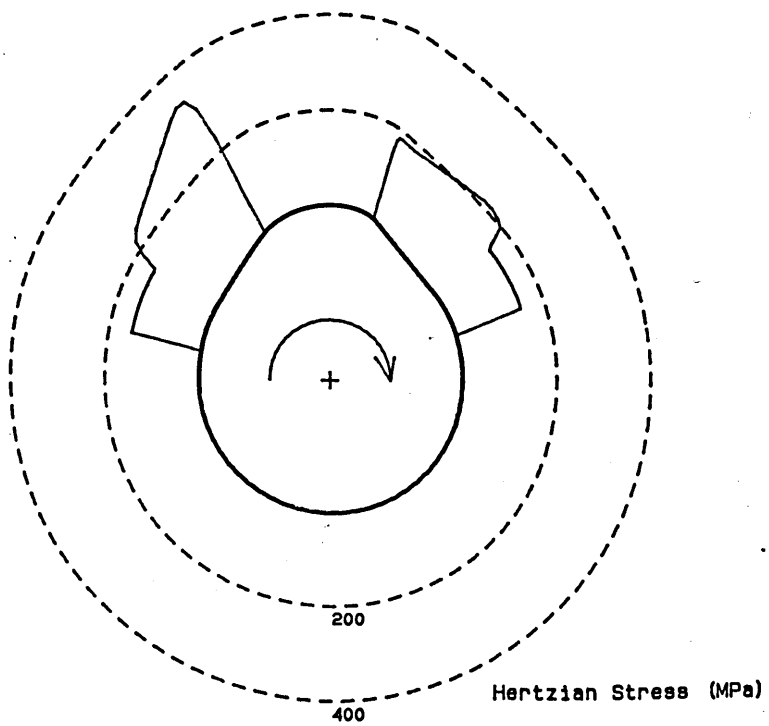

Figure (F.1c) Graphical Output from the Valve Train Lubrication Analysis Program.

CAM OPERATING CHARACTERISTICS

1995 DESMO CLOSING CAM

Cam Base Radius (mm)	=	25.00
Maximum Valve Lift (mm)	=	-10.10
Cam Width (mm)	=	12.00
Rotational Speed (rpm)	=	2000.0
Spring Stiffness (kN/m)	=	10.000
Initial Spring Disp. (mm)	=	5.0
Equiv. Mass At Valve (kg)	=	.074
Lubricant Viscosity (Ns/m^2)	=	.015
Press. Visc. Coeff. (/Pa)	=	15.0E-9
Youngs Mod. (Cam) (GPa)	=	207.0
Youngs Mod. (Foll.) (GPa)	=	207.0
Poissons Ratio (Cam)	=	.30
Poissons Ratio (Foll.)	=	.30
Frictional Power Loss (W)	=	6.46

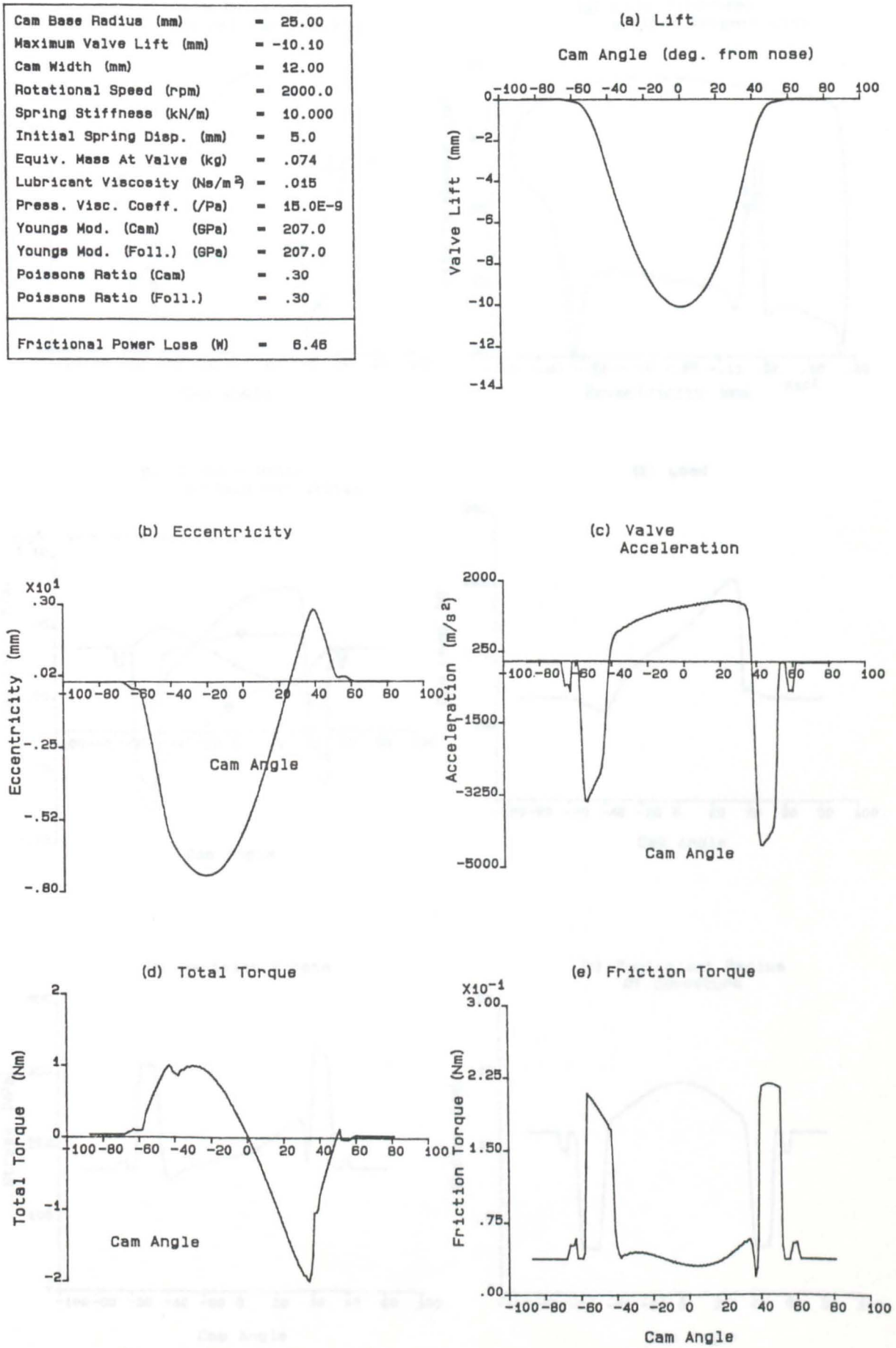

Figure (F.2a) Graphical Output from the Valve Train Lubrication Analysis Program for the Desmodromic Closing Cam and Follower.

CAM OPERATING CHARACTERISTICS

1995 DESMO CLOSING CAM

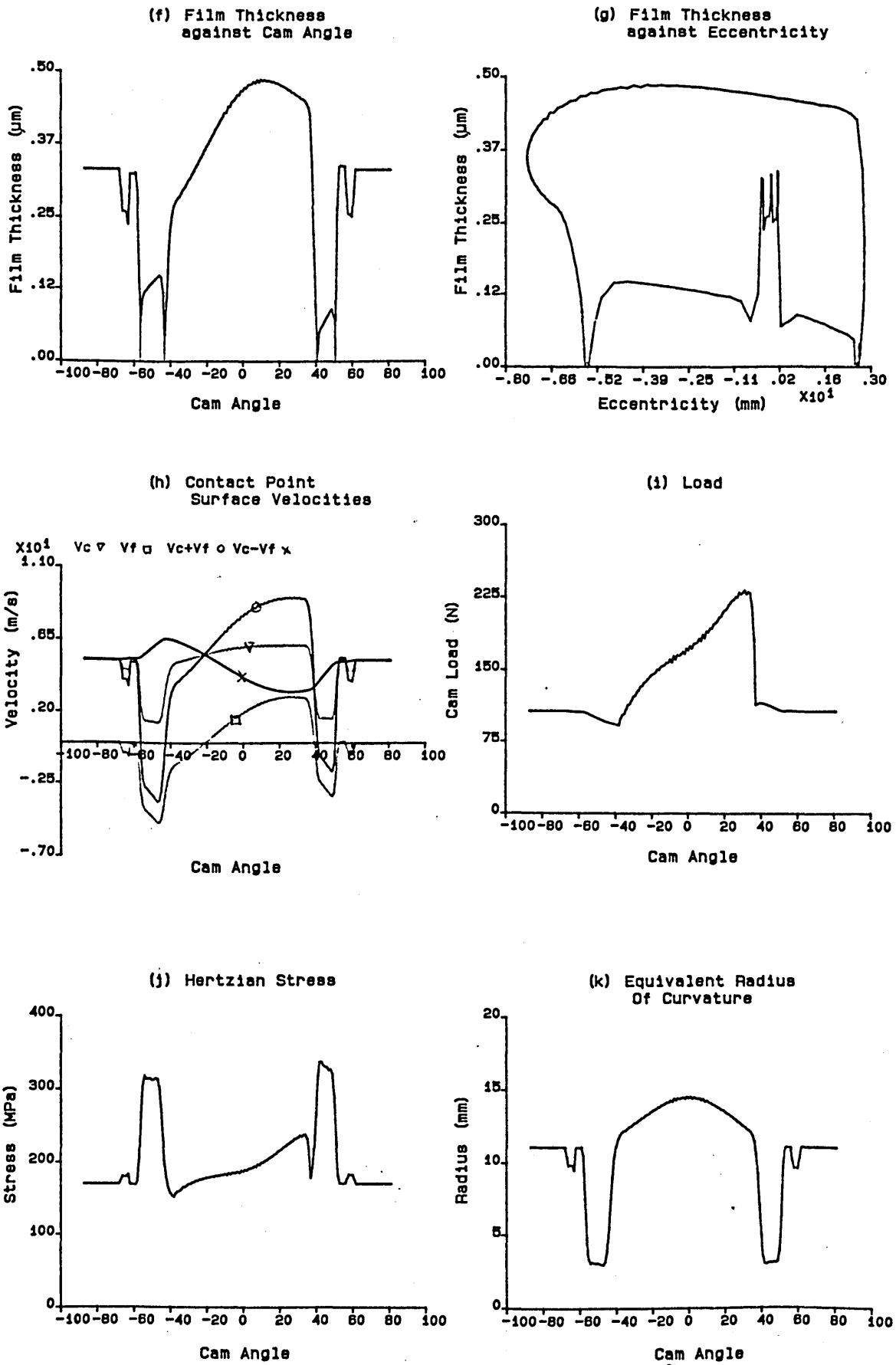

Figure (F.2b) Graphical Output from the Valve Train Lubrication Analysis Program.

CAM OPERATING CHARACTERISTICS
1995 DESMO CLOSING CAM

(l) Film thickness around cam periphery

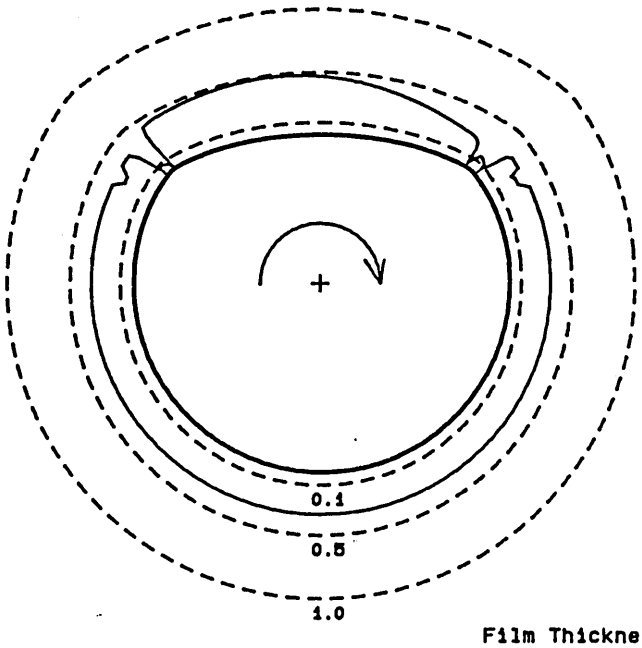

(m) Hertzian stress around cam periphery

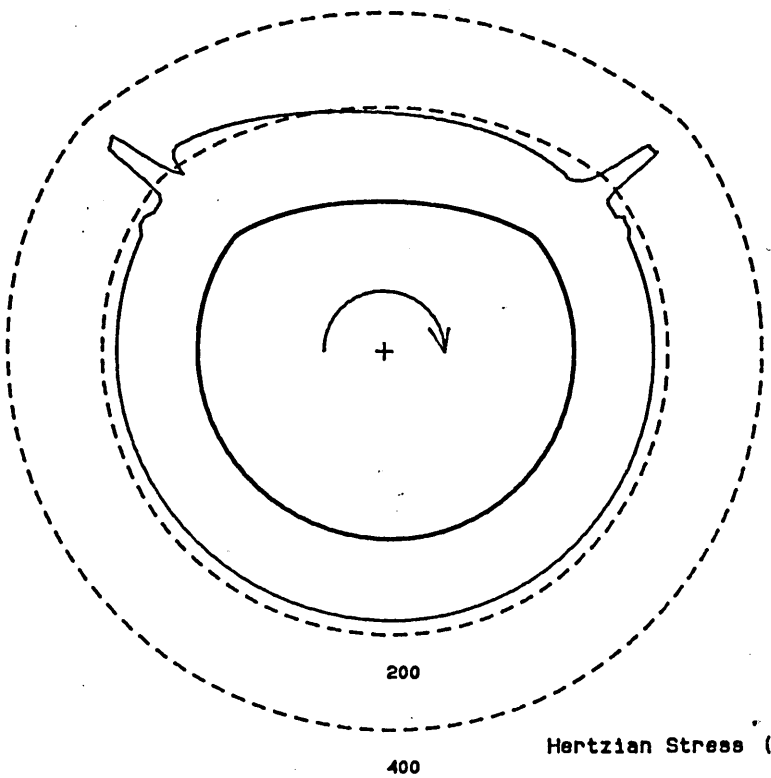

Figure (F.2c) Graphical Output from the Valve Train Lubrication Analysis Program.